



Cardiff University

Mechanistic action of Death Associated Protein-3 (DAP-3) in breast cancer progression

Michal Uhercik

**Thesis submitted to Cardiff University for the degree of
Doctor of Medicine (MD)
October 2021**

Declarations

This thesis is hereby submitted to Cardiff University for fulfilment of the degree of Medical Doctorate by Research. The works compiled here have been conducted and presented solely by myself.

I have not made use of other people's work (published, presented or otherwise) without acknowledging the source of all such work.

Michal Uhercik

Student no. 1560582

Acknowledgements

I would like to express my gratitude to my main supervisor Prof. Wenguo Jiang for his guidance and mentorship throughout this research project. I would like to thank my co-supervisors Dr. Andrew Sanders for his invaluable support and advice, also Dr. Tracy Martin along with external supervisors Mr. Anup Sharma and Prof. Kefah Mokbel for their support.

I am grateful to St. George's University Hospital Charity and Breast Cancer Hope Charity for funding this project along with my university fees.

Presentations

Uharcik M, Sanders AJ, Sharma AK, Mokbel K, Jiang WG. Death Associated Protein 3 influences Heat Shock Protein 90 expression in Breast cancer cell lines. Presented at 11th European Breast Cancer Conference 3/2018, Barcelona Spain

Uharcik M, Sanders AJ, Sharma AK, Mokbel K, Jiang WG. Identification of DAP-3 and HSP90 interaction and potential clinical implications in Breast cancer. Presented at Association of Breast Surgery Conference 15-16/05/2017, Belfast UK

Publications

Uharcik M, Sanders AJ, Sharma AK, Mokbel K, Jiang WG. Death Associated Protein 3 influences Heat Shock Protein 90 expression in Breast cancer cell lines. ABSTRACT European Journal of Cancer April 2018, Volume 92, S124

Uharcik M, Sanders AJ, Sharma AK, Mokbel K, Jiang WG. Identification of DAP-3 and HSP90 interaction and potential clinical implications in Breast cancer. ABSTRACT EJSO. 2017 May, Volume 43, Issue 5, S14

Summary

Breast cancer is the most common cancer in the UK and places a substantial burden on health care systems. Despite advances in breast cancer treatments, it still causes substantial morbidity and mortality. Metastatic dissemination significantly influences patient outlooks, with the development of treatment resistance being a significant factor.

This MD study aims to further explore the role of Death Associated Protein 3 (DAP-3) in breast cancer progression and therapy response and to shed light on the mechanisms of action involved in these processes.

DAP-3 was targeted in MCF-7 and MDA-MD-231 breast cancer cell lines. Furthermore, potential interacting and mechanistic partners of DAP-3 were explored in clinical paired normal and breast cancer protein samples following immunoprecipitation with DAP-3 and protein micro-array analysis to identify differential expression patterns. This identified the Heat Shock Protein 90 (HSP90) molecule as a key player of a number of associated differential pathways. The relationship between DAP-3 and HSP90 was subsequently explored in *in vitro* functional tests utilising individual and collective DAP-3 knockdown and HSP90 inhibitor systems. This demonstrated DAP-3 KD reduced HSP90 expression, although HSP90 inhibition did not affect DAP-3 expression levels.

In functional assays, DAP-3 knockdown led to nonsignificant increases in adhesion (MCF-7) and invasion (MDA-MD-231), and decreased migration (MDA-MD-231). HSP90 inhibition showed a significant increase in adhesion (MCF-7), and a nonsignificant increase in growth (MDA-MD-231) and invasion (both cell lines). The combined effect of HSP90 inhibition and DAP-3 KD was inhibition of adhesion and invasion.

Furthermore, the DAP-3-HSP90 relationship was assessed in clinical samples and suggest high levels of these molecules result in longer overall survival.

With regards to DAP-3 – HSP90 impact on response to chemotherapy, although we recorded significant increases in expression of both molecules in certain receptor variants of breast cancer in online datasets, there were no obvious patterns observed either from online datasets or *in vitro* models.

Collectively this work has expanded the current knowledge on DAP-3 and interacting partners role in breast cancer, providing insights into novel mechanisms related to breast cancer progression and acquisition of therapy resistance.

Table of contents

1. Introduction	13
1.1. Breast cancer and history of its treatment	14
1.2. Modern breast cancer treatment	18
1.3. Radiotherapy	21
1.4. Endocrine treatment	27
1.4.1. Tamoxifen	29
1.4.2. Aromatase inhibitors (AIs)	30
1.4.3. Progesterone receptor (PR) importance in breast cancer	34
1.5. Chemotherapy	34
1.6. Human epidermal growth factor 2 (HER2)	36
1.7. Nottingham Prognostic Index (NPI)	38
1.8. Breast cancer staging	39
1.9. Breast cancer treatment outcomes	42
1.10. Molecular subtypes of breast cancer	43
1.11. Triple negative breast cancer (TNBC)	43
1.11.1. Chemoresistance in TNBC	44
1.11.1.1. ATP-binding cassette (ABC) transporters	44
1.11.1.2. Breast cancer stem cells (BCSCs)	45
1.11.1.2.1. Signalling pathways vital for BCSCs renewal	45
1.11.1.2.1.1. Transforming growth factor beta (TGF- β) pathway	45
1.11.1.2.1.2. Notch pathway	46
1.11.1.2.1.3. WNT and Hedgehog (HH) pathway	47
1.11.1.3. Further processes involved in chemoresistance development	47
1.11.1.4. Signalling pathways in TNBC chemotherapy resistance development	48
1.12. Programmed cell death	49
1.13. Death associated proteins (DAP)	50
1.13.1. Death associated protein 3 (DAP-3)	56
1.13.1.1. Discovery and expression profile in normal tissues	56
1.13.1.2. Role of DAP-3 in normal physiological processes	56
1.13.1.3. Implications in human disease and cancer	57
1.13.1.3.1. Relation of DAP-3 to cancer treatment response	58
1.14. Heat shock protein (HSP) family	60
1.14.1. Heat shock protein 90 (HSP90)	61
1.14.1.1. JAK2/STAT3 pathway	62
1.14.1.2. PI3K/AKT/mTOR pathway	63

1.14.1.3. MAPK pathway	63
1.15. Aims and objectives	63
2. Materials and methods	66
2.1. Chemical and plastic ware	66
2.1.1. Standard solutions used in cell culture works	66
2.1.1.1. 0.05M EDTA	66
2.1.1.2. Trypsin	66
2.1.1.3. Antibiotic solution	66
2.1.2. Solutions used for RNA and DNA molecular biology	67
2.1.2.1. PCR water	67
2.1.2.2. DEPC water	67
2.1.2.3. TBE (5X Tris, Boric acid, EDTA)	67
2.1.3. Solutions used for protein molecular biology	67
2.1.3.1. Lysis buffer	67
2.1.3.2. 10X TBS	68
2.1.3.3. Running buffer	68
2.1.3.4. Transfer buffer	68
2.1.3.5. Washing buffer	68
2.1.3.6. Blocking buffer	68
2.2. Cell cultures	70
2.2.1. Cell subculture and maintenance	71
2.2.2. Cell preservation and storage	71
2.3. RNA extraction and cDNA synthesis by reverse transcription	73
2.4. Polymerase chain reaction (PCR)	77
2.5. RT-qPCR	80
2.6. Protein extraction and protein quantification	81
2.6.1. Breast tissue cohort	83
2.7. Kinexus and paired tissue samples	84
2.8. Sodium dodecyl sulphate-polyacrylamide gel electrophoresis (SDS-PAGE) and western blotting	85
2.9. Co-immunoprecipitation	91
2.10. Reamplification of DAP-3 knock-down plasmids	91
2.11. Transfection of anti-DAP-3 ribozyme transgene into breast cancer cell lines	96
2.12. Functional assays	97
2.12.1. Growth assay	97
2.12.2. Adhesion assay	97
2.12.3. Invasion assay	99
2.12.4. Scratch wounding assay	101
2.13. Small molecule inhibitors	101

2.14.	Statistical analysis	102
3.	Screening and establishment of DAP-3 modified breast cancer cell lines	104
3.1.	Introduction	105
3.2.	Methods	106
3.2.1.	Cells and cell culture	106
3.2.2.	RNA extraction, quantification and cDNA synthesis	106
3.2.3.	Polymerase Chain Reaction (PCR)	107
3.2.4.	Protein extraction and quantification	107
3.2.5.	SDS-polyacrylamide gel electrophoresis (SDS-PAGE) and Western blotting	108
3.2.6.	Reamplification of plasmid, plasmid extraction and confirmation of ribozyme insert orientation	108
3.2.7.	Transfection of pEF6/V5-HIS TOPO TA vector containing DAP-3 ribozyme into breast cancer cell lines	108
3.2.8.	RT-qPCR	109
3.3.	Results	109
3.3.1.	PCR screening of DAP-3/GAPDH expression in 9 Breast cell lines	109
3.3.2.	Western blot screening of DAP-3/GAPDH expression in chosen MCF-7 and MDA-231 cell lines	111
3.3.3.	Reamplification of DAP-3 ribozyme plasmids, plasmid purification and orientation checking	111
3.3.4.	Quantitative PCR confirmation of DAP-3 knockdown in MCF-7 and MDA-231 cell line models (qPCR)	114
3.4.	Discussion	116
4.	Potential interaction and mechanistic actions of DAP-3 in Breast cancer	118
4.1.	Introduction	119
4.2.	Material and methods	119
4.2.1.	Cells and Cell Cultures	119
4.2.2.	RNA extraction, quantification and cDNA synthesis	120
4.2.3.	Protein extraction and quantification	120
4.2.4.	Co-Immunoprecipitation	121
4.2.5.	Kinexus antibody microarray	121
4.2.6.	Polymerase Chain Reaction	122
4.2.7.	Pathway mapping by Reactome	123
4.2.8.	SDS-polyacrylamide gel electrophoresis (SDS-PAGE) and Western blotting	123
4.3.	Results	123

4.3.1. Kinexus protein microarray - Identification of potential DAP-3 interacting partners	123
4.3.2. DAP-3 Pathway analysis	129
4.3.3. Expression of Heat shock protein 90 in breast cancer cells lines	152
4.3.3.1. PCR screen for expression of HSP90 gene transcript	152
4.3.3.2. Expression of HSP90 proteins as detected by Western Blot	152
4.4. Discussion	155
5. Relationship between DAP-3 and HSP90 in breast cancer	157
5.1. Introduction	158
5.2. Methods	160
5.2.1. Cell lines	160
5.2.1.1. MCF-7	160
5.2.1.2. MD-MB-231	161
5.2.2. RT-qPCR	161
5.2.3. Functional Assays	161
5.2.3.1. Growth assay	161
5.2.3.2. Adhesion assay	162
5.2.3.3. Invasion assay	162
5.2.3.4. Scratch assay	163
5.2.4. HSP90 Inhibitor	163
5.2.5. Statistical analysis	163
5.3. Results	164
5.3.1. Expression analysis of HSP90 a/b in DAP-3 KD MDA-MB-231 and MCF-7 cells	164
5.3.2. Expression profile of DAP-3 following HSP90 inhibition	164
5.3.3. Functional implications of the DAP-3 - HSP90 relationship	169
5.3.3.1. Growth Assay	169
5.3.3.1.1. MCF-7	169
5.3.3.1.2. MDA-MB-231	171
5.3.3.2. Adhesion Assay	173
5.3.3.2.1. MCF-7	173
5.3.3.2.2. MDA-MB-231	175
5.3.3.3. Invasion Assay	177
5.3.3.3.1. MCF-7	177
5.3.3.3.2. MDA-MB-231	179
5.3.3.4. Scratch migration assay	181
5.3.3.4.1. MCF-7	181
5.3.3.4.2. MDA-MB-231	183
5.4. Discussion	185

6. Clinical implications of DAP-3 and HSP90 in breast cancer progression and chemoresistance	189
6.1. Introduction	190
6.2. Materials and Methods	191
6.2.1. Cell lines and cell cultures	191
6.2.2. RNA extraction, quantification and cDNA synthesis	192
6.2.3. RT-qPCR	192
6.2.4. Clinical cohort	192
6.2.5. HSP90, DAP-3 and sensitivity to chemotherapy in patients with breast cancer.	193
6.2.6. Chemotherapy agents and Chemotherapy resistance assessment in cell models	193
6.2.7. Growth assay	194
6.2.8. HSP90 inhibitor	194
6.2.9. Statistical analysis	195
6.3. Results	195
6.3.1. Clinical cohort analysis (HSP90A & HSP90B)	195
6.3.2. HSP90 survival analysis (OS & DFS for HSP90A, HSP90B, HSP90A & DAP-3 combined and HSP90B & DAP-3 combined)	199
6.3.2.1. OS and DFS for HSP90A	199
6.3.2.2. OS and DFS HSP90B	199
6.3.2.3. Correlations between DAP-3 and HSP90 in breast cancer	205
6.3.2.4. OS and DSF for DAP-3 and HSP90A/HSP90B combined	207
6.3.2.4.1. OS and DSF for DAP-3 and HSP90A combined	207
6.3.2.4.2. OS and DFS for DAP-3 and HSP90B combined	210
6.3.2.4.3. Survival analysis with the expression patterns of DAP-3, HSP90A and HSP90B combined	213
6.3.2.4.4. Multivariate survival analysis for the combined expression pattern of DAP-3, HSP90A and HSP90B	216
6.3.3. Implications in therapy resistance using online datasets – (DAP-3/HSP90A/HSP90B relationship to responsiveness to chemo therapy)	217
6.3.3.1. DAP-3 expression	218
6.3.3.1.1. Oestrogen receptor positive breast cancer	218
6.3.3.1.2. Oestrogen receptor negative breast cancer	219
6.3.3.1.3. HER2 positive breast cancer	220
6.3.3.1.4. HER2 negative breast cancer	221
6.3.3.1.5. Triple negative breast cancer (ER-, PR-, HER2-)	222
6.3.3.2. HSP90A expression	223
6.3.3.2.1. Oestrogen receptor positive breast cancer	223
6.3.3.2.2. Oestrogen receptor negative breast cancer	224
6.3.3.2.3. HER2 positive breast cancer	225

6.3.3.2.4.	HER2 negative breast cancer	226
6.3.3.2.5.	Triple negative breast cancer (ER-, PR-, HER2-)	227
6.3.3.3.	HSP90B expression	228
6.3.3.3.1.	Oestrogen receptor positive breast cancer	228
6.3.3.3.2.	Oestrogen receptor negative breast cancer	229
6.3.3.3.3.	HER2 positive breast cancer	230
6.3.3.3.4.	HER2 negative breast cancer	231
6.3.3.3.5.	Triple negative breast cancer (ER-, PR-, HER2-)	232
6.3.4.	Impact on chemoresistance	233
6.3.4.1.	MCF-7	233
6.3.4.1.1.	Paclitaxel	233
6.3.4.1.2.	Docetaxel	235
6.3.4.2.	MDA-MB-231	238
6.3.4.2.1.	Paclitaxel	238
6.3.4.2.2.	Docetaxel	240
6.4.	Discussion	243
7.	General Discussion	246
	References	255
	Abbreviations	278

Chapter-1

Introduction

1. Introduction

1.1. Breast cancer and history of its treatment

The first documented case of Breast cancer was found in the Edwin Smith Surgical Papyrus and dates back to around 1700 BC but the original manuscript is thought to be dated back to the Pyramid Age 3000 BC - 2600 BC. It describes bulging tumours of breast which come from a disease rather than injury, are cool to touch, with no granulation tissue and not forming any secretions or fluid. The translation describes examination findings as like touching a ball of wrappings and a comparison to green hemat-fruit is made. The treatment part of this text states 'There is nothing' or 'There is no treatment'. Explanations of this document suggest that prognosis of this diagnosis was deemed fatal (1) (Fig. 1.1.).



Fig. 1.1. Edwin Smith Surgical Papyrus, Vol 2, Column XV. Fascimile plate and it's hieroglyphic transliteration (1). Case 45 'Bulging tumor on the breast'.

In the Hyppocratic era in ancient Greece (from 5th century BC) the term “cancer” came to being. It originated from the word karkinos (Greek word for crab or crayfish) and was used to describe nonhealing swellings. Hippocrates’ theory of the cause of the disease was based on the imbalance of 4 humors or body fluids which were blood, phlegm, yellow bile and black bile (Humoral theory). He believed that cancer was caused by the accumulation of black bile in a particular organ.

Galen (200AD) also supported the theory of black bile accumulation as the cause of cancer and the term ‘oncos’ meaning swelling is attributed to him. He proposed treatment of breast cancer should only happen in the early phases of disease and later should not take place. As means of treatment, he suggested excision with cauterisation of the roots of the cancer. Approximately in the same era, Leonides of Alexandria described breast cancer treatment as amputation of breast utilising alternation between incision and cautery with hot irons as means of stopping haemorrhage (Fig. 1.2.). Cauterisation is also used at the end of the procedure to ‘burn the roots of the tumour’. He as well advised against surgery in late stages, once the tumour has taken over the whole breast and invaded the chest wall (2-5).

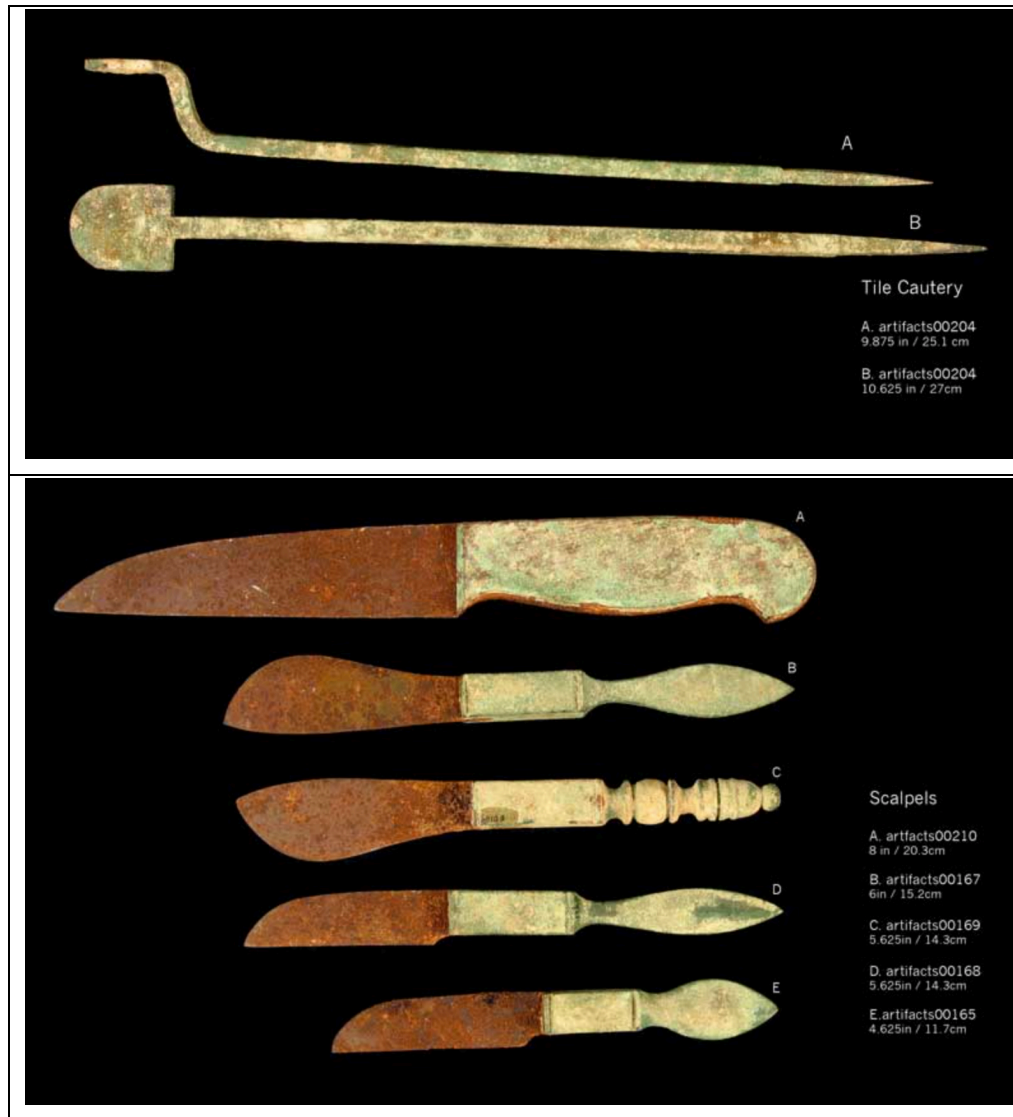


Fig. 1.2. Roman Era surgical instruments (granted permission of reproduction of images from dmc7be@virginia.edu 9/2/21)

Further progress in medicine in Europe was hindered by early Christian views which attributed the cause of diseases to God. Rather than surgery and medicines, the treatments were similarly based on faith and divine miracles. Furthermore, due to the religious traditions, autopsy or dissection of the human body in this era also remained forbidden, although this has weakened over time. It was from the 10th century with the rise of the Islamic empire that physicians like Avicenna and Albucasis expanded the medical knowledge. It was Avicenna's 'Al-Oanun fi al-Tibb' known as 'The Canon of Medicine' (Fig.1.3.) that was one of the most influential medical books up to the 1700s (6).

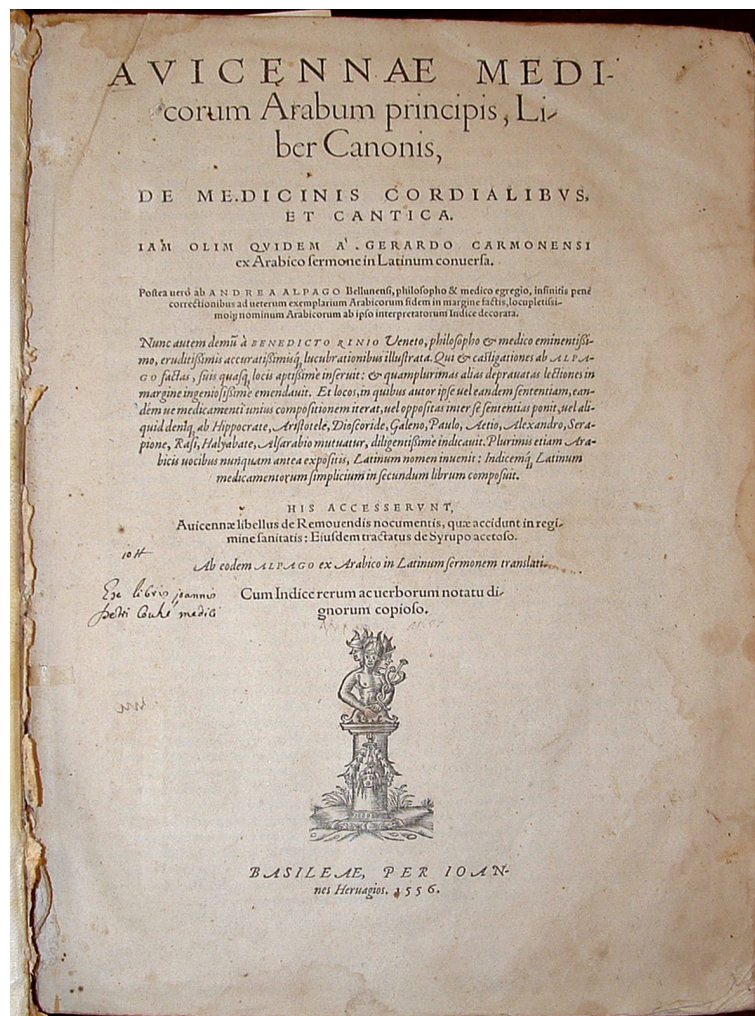


Fig.1.3. The title page of the 1556 edition of Avicenna's The Canon of Medicine (7)

1.2. Modern breast cancer treatment

The modern breast cancer approach started with William Steward Halsted in the 1880s. In 1894, he published 'The Results of Operations of the Cure of Cancer of the Breast Performed at the Johns Hopkins Hospital from June 1889 to January 1894' in *Annals of Surgery*. Here he described the outcomes of 50 women who have undergone surgery for breast cancer. The 'complete' method Halsted described as radical mastectomy which involved removal of all breast tissue with a large area of skin, at least part of pectoralis major muscle, axillary lymph nodes and commonly infra and supraclavicular lymph nodes together. In his patient group, he described only 3 cases of local recurrence. This has effectively proven to be a curative approach in an age where there was no other option available (8). This approach remained the standard of care for most of the 20th century.

In the 1970s B Fisher published a study that promoted more conservative methods of surgical treatment of breast cancer. He compared 'simple' and radical mastectomy outcomes that showed no significant difference after a follow up of 2-5 years. He also showed that postoperative regional radiotherapy applied to clinically axillary node-positive versus negative patients resulted in no significant differences either (9). D H Patey described that preservation of pectoralis muscles provided equally satisfactory results in breast cancer treatment (10). J L Madden then published an article 'Modified Radical Mastectomy' describing that preservation of both Pectoralis Major and Minor Muscles is as satisfactory as the radical operation described by Halsted (11).

Despite these advances, there was an appetite for more conservative approaches in the surgical treatment of breast cancer. The hallmark paper from Veronesi *et al.* from 1981 evaluated treatment of women with breast cancer smaller than 2 cm with no axillary lymphadenopathy. He

compared the 'radical' Halsted mastectomy to 'quadrantectomy' with axillary node dissection and radiotherapy to remaining breast tissue. There was no difference in overall survival (OS) or disease-free survival (DFS) and these results were a significant step in the de-escalation of breast cancer surgery (12). In 2002, Fisher *et al.* published a 25 year follow up of the NSABP B-04 trial further validating these results (13). Veronesi *et al.* later evaluated that even more conservative approach than quadrantectomy – a lumpectomy, provided the same outcomes in terms of distant metastasis and survival, although this approach carried a higher recurrence rate (14). Radiotherapy to the remaining breast tissue of the surgically treated ipsilateral breast played a vital role in controlling local recurrence rate (15). Breast-conserving surgery became the new standard approach for early breast cancer across the globe and mastectomy rates started falling dramatically as this approach was, in 2002, confirmed to have the same long-term outcomes when compared to radical mastectomy (16).

The next big step in the de-escalation of breast cancer treatment was the development of Axillary Sentinel Node Biopsy. From at least the late 1970s there were efforts to show that Axillary lymph node dissection, which was the standard axillary procedure at the time, might be avoidable in node-negative patients. Axillary node dissection was initially deemed as part of the treatment of breast cancer but became an aspect of staging of breast cancer in clinically node-negative patients and a key prognostic indicator with treatment decisions dependent on axillary lymph node status (17). It has although carried a burden of significant morbidity (18).

The concept of sentinel node was initially described for staging melanoma. It describes the primary draining lymph node of melanoma identified by technetium labelled dextran. This lymph node was then localised utilising a gamma probe and excised for histological evaluation, identifying patients that would benefit from immediate regional lymph node dissection (19). Krag *et al.* have described this technique in 1993 in

their pilot study in the context of breast cancer (20). Following this, further clinical trials validated this approach and confirmed that this approach stages axilla as well as complete axillary node dissection is safe, reduces morbidity and length of patients' postoperative hospitalisation (21, 22). This approach is currently the gold standard in staging axilla in early breast cancer where there is no evidence of lymph node involvement and is part of NICE Guidelines (23). The technology has since evolved to sophisticated wireless devices which are easier to use (Fig 1.4.).



Fig. 1.4. Neoprobe® Gamma Detection System
(<https://www.mammotome.com/neoprobe/>)

1.3. Radiotherapy

A German Physics professor W.C. Röntgen (Fig. 1.5.) studied cathode radiation, which occurs when an electrical charge is applied to two metal plates inside a glass tube filled with rarefied gas. Although this device ('Crookes tube'; Fig. 1.6.) was initially invented by an English physicist William Crookes around 1870, the concept of X-rays was described by Röntgen 1896 and has won him the first-ever Nobel Prize in physics in 1901 (24). At the point he was associated with Munich University in Germany.



Fig. 1.5. Wilhelm Conrad Röntgen, Born: 27 March 1845, Lennep (now Remscheid), Prussia (now Germany), Died: 10 February 1923, Munich, Germany.
<https://www.nobelprize.org>



Fig.1.6. Crookes tube, Victorian Collections,
<https://victoriancollections.net.au/items/5a66957321ea6a0d1872565e>, Accessed 18 March 2021

However, it wasn't until the 1930s that radiotherapy was introduced as part of breast cancer treatment, with the utilisation of radium needles and also external beam radiation (25).

It was a welcomed substitute for the mutilating radical mastectomy, in spite of its side effects. Although the benefits were more obvious when it was combined with surgical treatment.

Radiotherapy was initially combined with mastectomy but later has established itself as part of breast conserving-surgery, being applied to the remaining breast tissue after a tumour has been excised. The initial trials were evaluating radiotherapy of the whole breast after breast conserving surgery with regimes split into 25 fractions giving 2 Gray (Gy) in one session, amounting to a total dose of 50Gy. They have confirmed a reduction of risk of local recurrence and that this treatment regimen may

help to avoid a mastectomy which has significantly helped the adoption breast conserving-therapy (15, 26). Further to this, radiotherapy as an adjuvant treatment to breast conserving surgery has also been shown to decrease mortality from breast cancer (27).

Alongside the advancement in used equipment (Fig. 1.7.), the focus after this was to examine different radiotherapy regimes and see if the change of daily dose and decreasing number of fractions would still have same benefits. Whelan *et al.* confirmed in their study that an accelerated schedule with number of fractions reduced from 25 to 16 and total dose from 50Gy to 42.5Gy was not inferior (28). This was a significant step forward as it also had major effects on freeing up the capacity of radiotherapy centres and also shorter treatment being better accepted by patients. Further positive aspect of this approach was increased cost-effectiveness in improved resource utilisation (29). This 15-fraction regime of adjuvant radiotherapy for early breast cancer has been the standard schedule up till recently. The FAST forward trial evaluated a 5-fraction regime with just 26Gy delivered and was found non-inferior to the standard 15 fraction 40Gy regimen currently widely used (30). The unprecedented circumstances of the COVID-19 pandemic led to a very rapid adoption of this new radiotherapy protocol in order to decrease the exposure of the vulnerable patients undergoing this treatment.

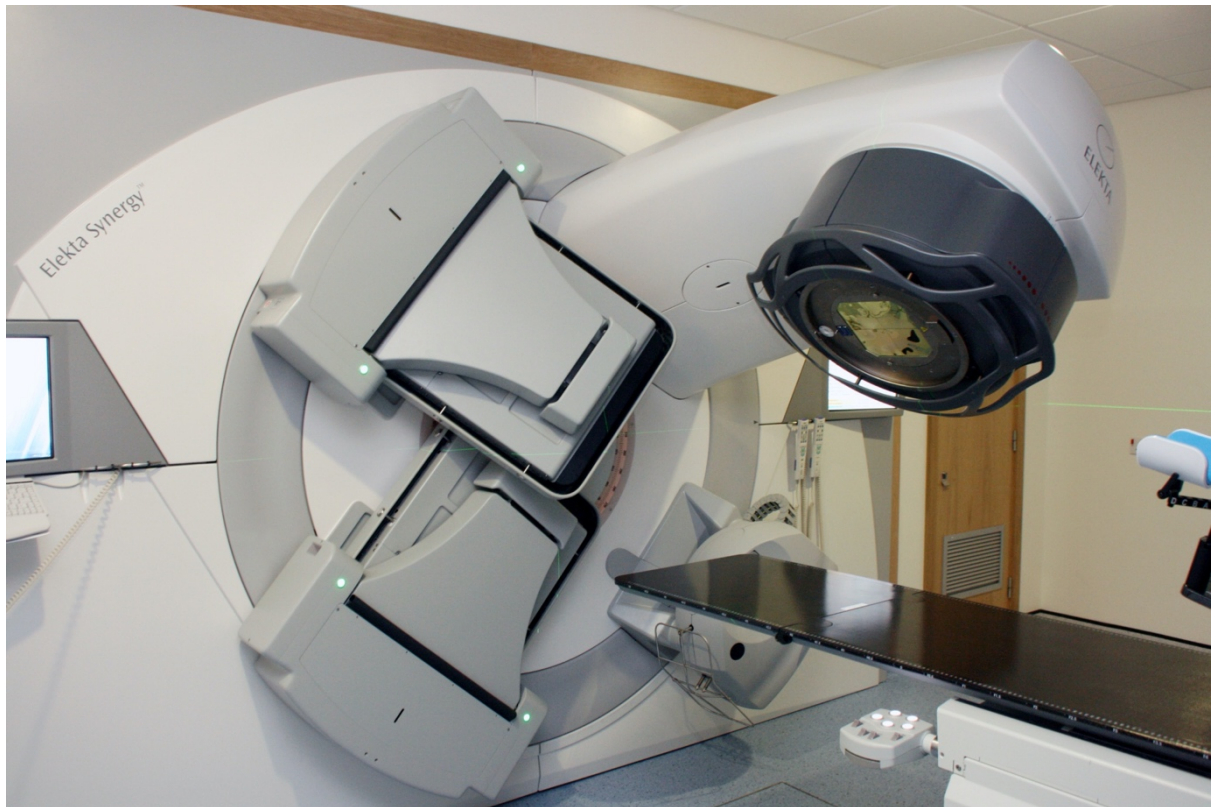


Fig. 1.7. *Modern Radiotherapy Suite. Elekta Synergy.*

Further approaches in adjuvant radiotherapy have been evaluated. Accelerated partial breast irradiation (APBI) (Fig. 1.8), irradiating only the tumour-bearing quadrant of the breast, appears to lead to a higher rate of local recurrence (31). Although in another study by Meattini *et al.*, APBI was compared to whole breast irradiation (WBI) (Fig. 1.9.) and showed no significant difference in the rate of local recurrence (32). A different approach, in the form of Intraoperative radiotherapy (21Gy single intraoperative dose as APBI), were evaluated and the outcomes were reported in the ELIOT trial. These were in favour of WBI in terms of local recurrence although no difference in OS was observed (33). Albeit the worse local recurrence rates, APBI has a significantly better toxicity profile.

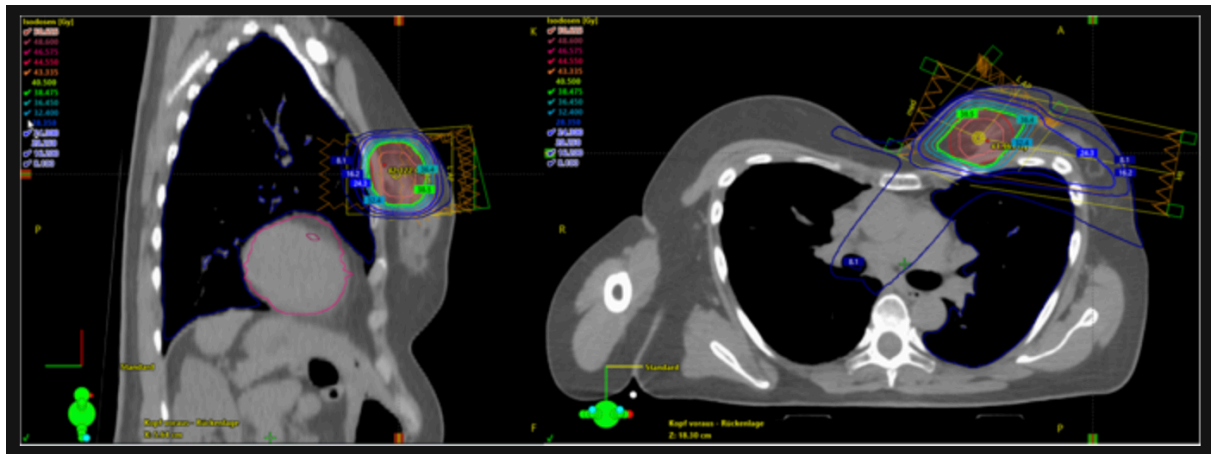


Fig.1.8. Partial Breast Irradiation (PBI), planning scout images for left breast PBI.

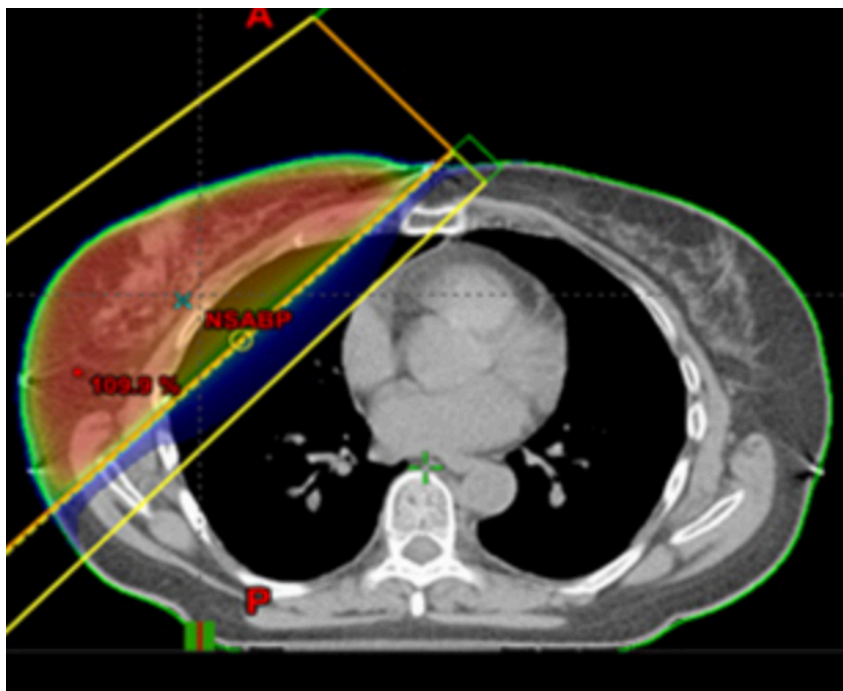


Fig. 1.9. Whole breast irradiation (WBI) -scout planning image for right breast WBI

Despite all the advances in radiotherapy, side effects remain an important aspect when planning adjuvant treatment. In particular irradiation of organs like lungs and, in left-sided tumours, the heart. Protocols incorporating breathing control resulted in a significantly lower cardiac dose of radiation (34) (Fig. 1.10). Further side effects include radiation dermatitis and there have been better outcomes observed with hypofractionated schedules and those with lower overall radiation dose

(35). Tumour bed boost has been associated with worse cosmetic outcome and also adverse effects on the function of the shoulder joint (36) (Fig. 1.11.). In addition to these, the prevalence of fatigue has been associated with receipt of radiotherapy and higher stages of the disease (37).

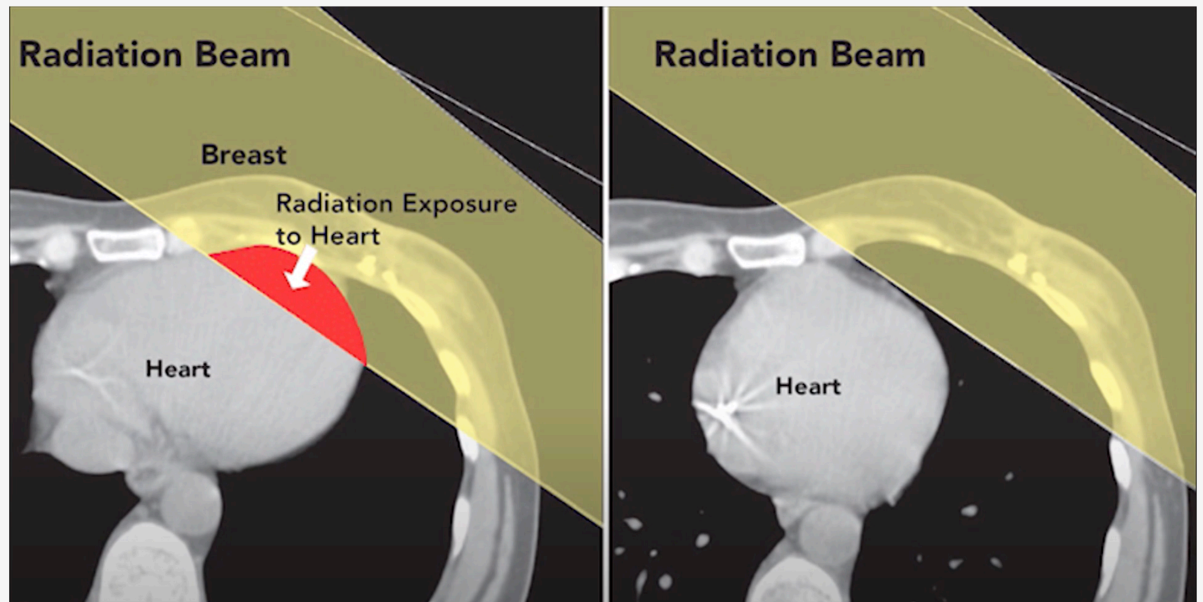


Fig. 1.10. Deep inspiration breath hold (DIBH) radiotherapy technique lowering cardiac radiation dose.

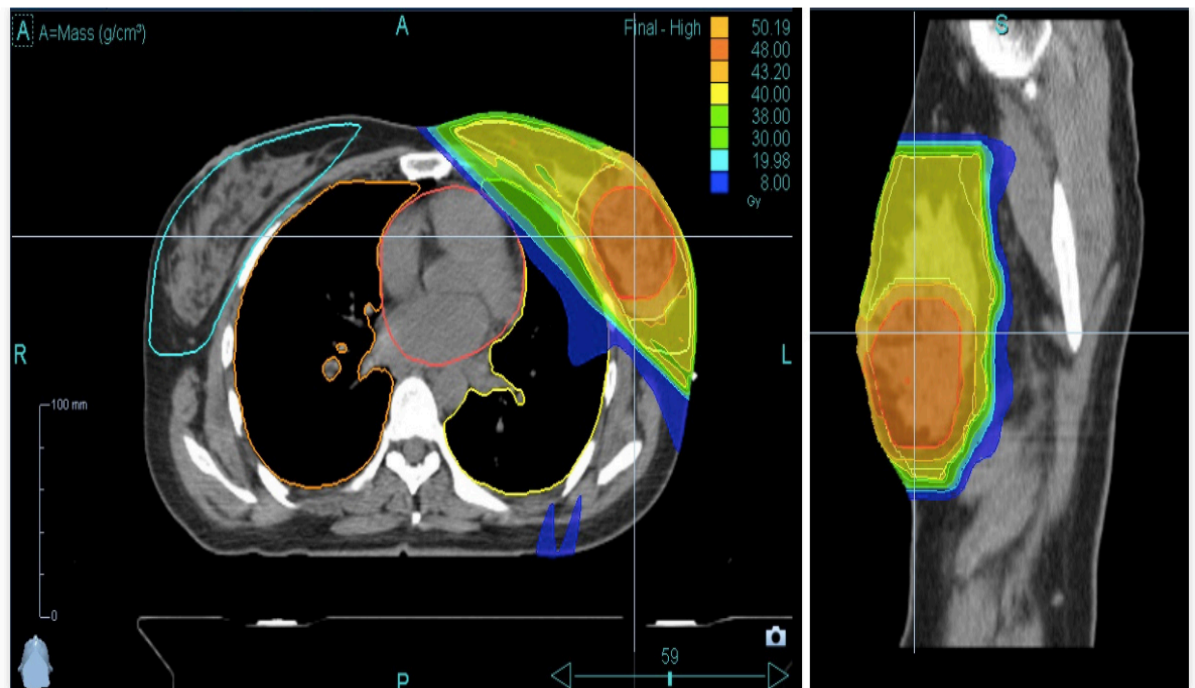


Fig. 1.11. Simultaneous integrated boost (SIB) providing extra radiation dose to tumour bed.

Advances in technology further allowed to precisely map the planned area to be irradiated and hence significantly decrease the dose of radiation to surrounding tissues. These techniques involve Conformal Radiation Therapy (CRT) and Intensity- Modulated Radiation Therapy (IMRT). Both these techniques show similar outcomes with regards to loco-regional tumour control although IMRT can lead to significantly smaller mean lung dose and also resulting in a lower incidence of radiation dermatitis (38).

Further application of radiotherapy is in the metastatic breast cancer setting. Application of this non-invasive strategy is aimed at oligometastatic disease, wherein selected cases targeted intracranial and extracranial metastatic deposits can be effectively ablated. This approach utilises sophisticated advanced imaging modalities for disease visualisation and ablation planning (39).

1.4. Endocrine treatment

Thomas Beatson in 1896 reported, in 2 patients, a temporary regression of metastatic breast cancer after being treated by oophorectomy. He suggested that the internal secretory function of ovaries in some cases promoted the growth of cancer. He also stipulated that after menopause the ovaries did not appear to have any effects on the cancer (40). However, it was only in the 1930s that hormonal therapy was introduced to treat men with prostate cancer. Charles B Huggins (Fig.1.12.) reported the effects of oestrogen that was given to men with prostate cancer. He observed that carcinoma of the prostate was inhibited either by castration causing elimination of androgen hormones or by injecting oestrogens neutralising the activity of androgens (41). Huggins also explored the effects of adrenalectomy on certain tumours. This has, in some patients with advanced breast cancer caused significant remission and he again observed similar effects on patients with prostate cancer. He

deducted that elimination of certain sex hormones was responsible for the observed tumour regression (42). For his work on hormonal treatment of prostatic cancer he was awarded a Nobel Prize in Physiology or Medicine in 1966 (43).

A big milestone was the discovery of the oestrogen receptor by Jensen who described very strong reversible affinity of these receptors to oestradiol in oestrogen dependent tissues (44). This has opened up the path for development of endocrine therapies and abandoning ablative surgeries for this purpose.

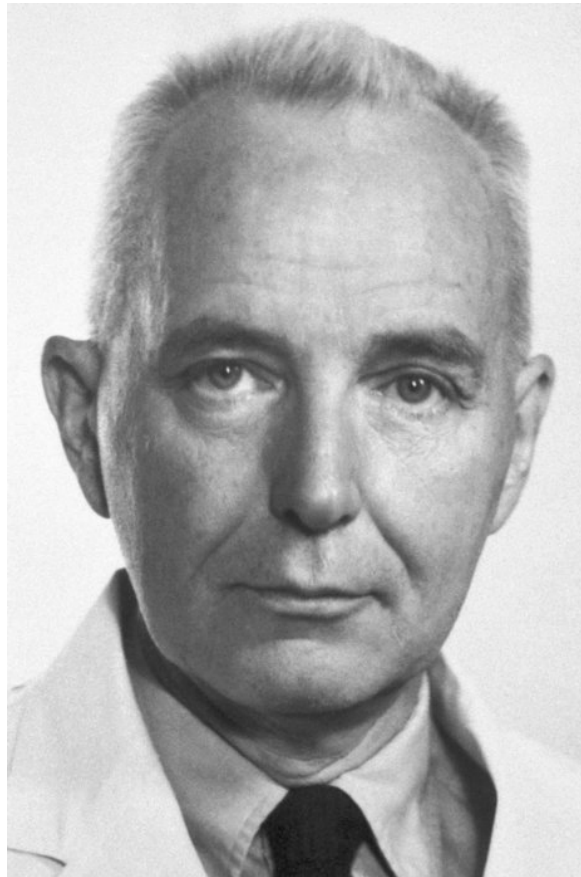


Fig. 1.12. Charles B Huggins, Born: 22 September 1901, Halifax, Canada
Died: 12 January 1997, Chicago, IL, USA.
<https://www.nobelprize.org/prizes/medicine/1966/huggins/facts/>

There are 2 forms of oestrogen receptors (ER)– ER α and ER β . Both are expressed in numerous human tissue types, with ER α predominantly being present in breast tissue, uterus, ovaries and bones. The distribution of ER β on the other hand is different and is mainly found in prostate, ovary and colon (45). It is believed that activation of ER α leads to increased proliferation whereas ER β is thought to counteract this with antiproliferative effect (46). ER α is the target for breast cancer treatment and its status is an important element of breast cancer staging.

1.4.1. Tamoxifen

Anti-oestrogen drugs were first developed in the 1950s as contraceptives. Tamoxifen (Fig.1.13.) being one of them, was synthesised in 1962, among other derivatives of triphenylethylenes and fall into the group of Selective Oestrogen Receptor Modulators (SERMs). It had rather a tortuous journey of development and it was only in 1973 that it became available in UK for clinical practice. Since then, Tamoxifen has been evaluated in a number of clinical trials, initially for the use in advanced metastatic breast cancer. It has been found that the response to Tamoxifen was dependent on the expression of cytoplasmic oestrogen receptor (47-49). It didn't take long, till Tamoxifen benefits were evaluated in the adjuvant setting of early breast cancer, showing highly significant prolongation of disease-free interval as well as significant decrease in death rate (50-52).

The low toxicity profile of Tamoxifen is far outweighed by the benefits, which also include the decrease in incidence of contralateral breast cancer and local recurrence after breast conserving therapy. Tamoxifen was becoming the benchmark for adjuvant treatment (53, 54).

Further application of Tamoxifen is chemoprevention and this has been evaluated in the IBIS I trial. The initial results from 2002

show that Tamoxifen, given over a 5-year period to women in high-risk category, reduces the risk of breast cancer by approximately one third. The overall risk to benefit ratio remained unclear as the increase in incidence of thromboembolic events reached significance (55). This was further validated after extended follow up (median 16 years) and confirmed a significant risk reduction in ER positive invasive breast cancer and DCIS even after a long period following cessation of Tamoxifen treatment, which greatly improves the risk-benefit ratio (56).

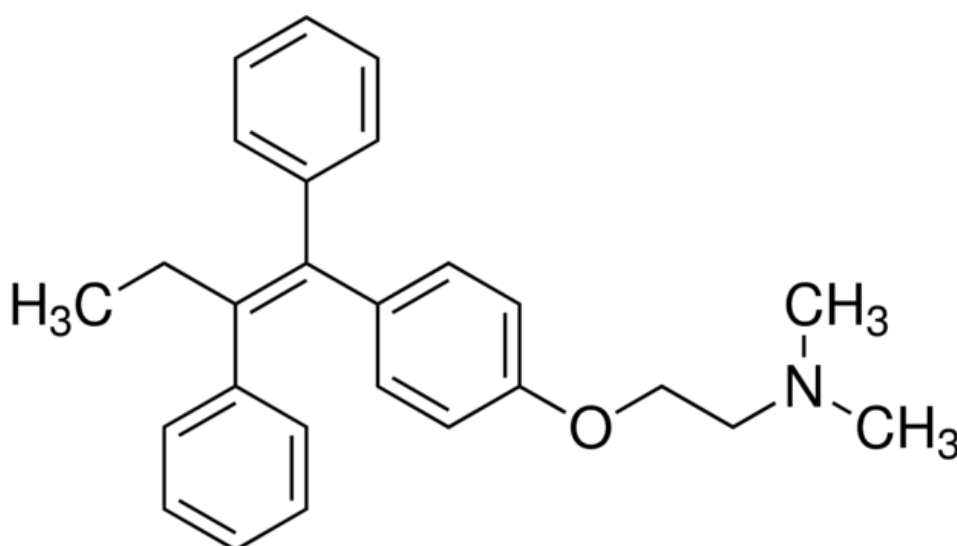


Fig.1.13. *Tamoxifen. (Z)-1-(p-Dimethylaminoethoxyphenyl)-1,2-diphenyl-1-butene, trans-2-[4-(1,2-Diphenyl-1-butenyl)phenoxy]-N,N-dimethylethylamine, C₂₆H₂₉NO*

1.4.2. Aromatase inhibitors (AIs)

A different approach to oestrogen blocking is demonstrated by another developed drug group, the aromatase inhibitors (AIs). Rather than blocking the ER, they function on a different principle, by decreasing the levels of ER's ligand, which is oestradiol, through targeting an enzyme which converts adrenal androgens to

oestrogen in peripheral tissues like muscles, fat and breast tissue. AIs have shown to be effective in suppressing the production of peripheral oestrogen in postmenopausal women (57).

Compared to Tamoxifen, AIs don't have a partial agonistic oestrogen effect and hence don't have the bone protective effect in postmenopausal women (58). On the other hand, the lack of this partial agonistic oestrogen effect causes that AIs are not associated with increased incidence of endometrial cancer and venous thromboembolism (59, 60).

The first AI that was originally used as an anticonvulsant was Aminoglutethimide and after reports of adrenal insufficiency it was consequently withdrawn. It was for these effects of aromatase inhibition in postmenopausal women (61) that it was later redeveloped in the 1970s for advanced breast cancer (62). This has subsequently triggered the generation of further molecules throughout the 1980s and 1990s that fall in to categories of 1st to 3rd generation of AIs, with a better side-effect profile. These molecules have 2 mechanisms of action which is either irreversibly binding to the aromatase molecule (androstenedione analogues i.e. exemestane) or reversibly binding to the aromatase molecule (nonsteroidal i.e. letrozole, anastrozole) Fig. 1.14.

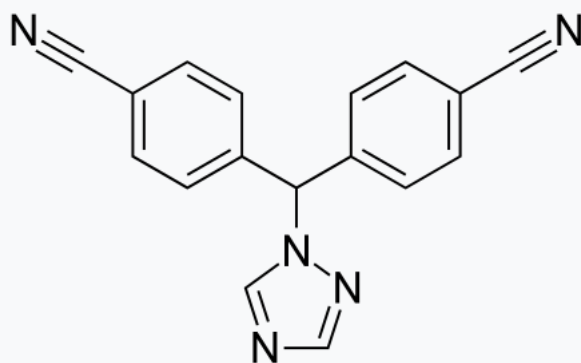
The 3rd generation of AIs (Letrozole, Anastrozole and Exemastane) have significantly improved potency compared to previous generations and almost completely block peripheral aromatase, hence reducing circulating oestrogen levels to almost undetectable levels (63). AIs have become the preferred drugs of choice in postmenopausal women and a significant advantage over tamoxifen has been described showing approximately 30% reduction in recurrence rates as well as decreased mortality (64). This benefit of AIs over Tamoxifen has been further confirmed by the BIG 1-98 study and also examining sequential treatments with Tamoxifen

and Letrozole not yielding improved outcomes over Letrozole monotherapy (65, 66). These adjuvant treatment regimens were routinely planned for a 5-year period. A further benefit of these treatments was explored by extending the length to 10 years and demonstrated a significantly higher disease-free survival with associated lower incidence of contralateral breast cancer although overall survival remained unaffected (67). The use of AIs was further extended to the pre-menopausal setting in the SOFT (Suppression of Ovarian Function Trial) and TEXT (Tamoxifen and Exemestane Trial) trial where ovarian suppression with AI (Exemastane) resulted in lower recurrence rates compared to Tamoxifen alone (68).

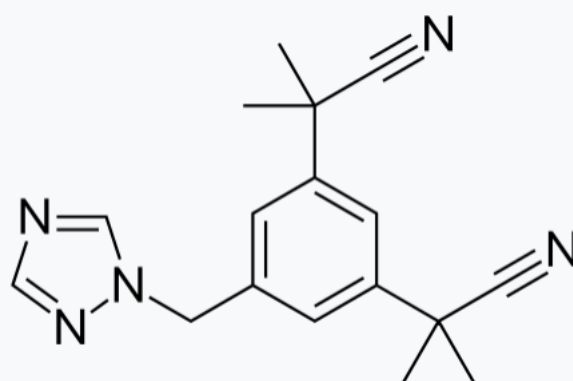
Further application of AIs is in elderly patients which would be considered unfit for surgery or those preferring to avoid surgical treatment. In this setting, the primary endocrine treatment provides reasonable control of the disease with relatively low number of patients actually dying from breast cancer although long term control is poor (69, 70).

Rather than an alternative to surgery, endocrine treatment in its neoadjuvant application is proving to be a viable option to neoadjuvant chemotherapy for women with similar response rates but better side-effect profile (71).

A.



B.



C.

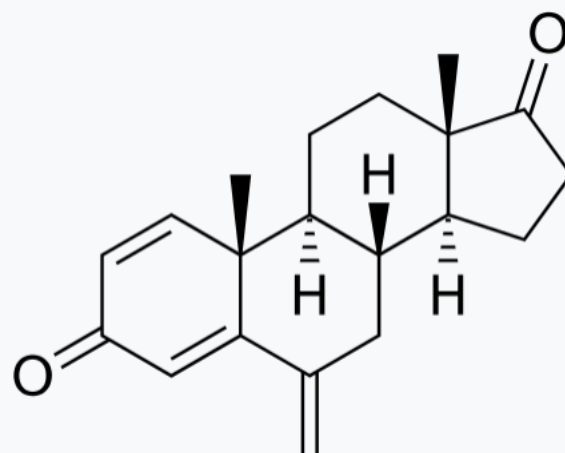


Fig. 1.14. 3rd Generation Aromatase Inhibitors. **A. Letrozole**, 4,4'-((1h-1,2,4-triazol-1-yl)methylene)dibenzonitrile, C₁₇H₁₁N₅, **B. Anastrozole**, 2-[3-(2-cyanopropan-2-yl)-5-(1,2,4-triazol-1-ylmethyl)phenyl]-2-methylpropanenitrile, C₁₇H₁₉N₅, **C. Exemestane**, (8R,9S,10R,13S,14S)-10,13-dimethyl-6-methylidene-7,8,9,11,12,14,15,16-octahydrocyclopenta[a]phenanthrene-3,17-dione, C₂₀H₂₄O₂

1.4.3. Progesterone receptor (PR) importance in breast cancer

Progesterone receptor has 2 isoforms (PR-A and PR-B) (72), and its status is routinely recorded in breast cancer as part of disease staging. PR status is mainly being utilised for its prognostic value aiding the choice of antioestrogen therapy (73). Bardou *et al.* described significantly better outcome prediction when ER and PR status is jointly evaluated compared to ER status alone for adjuvant endocrine treatment (74). The positive expression of PR indicates a good function of ER alpha pathway(75) .

1.5. Chemotherapy

The desire to identify compounds that could treat cancer was significant in the first decades of the 20th century. The challenge of testing and the difficulties of screening vast number of substances was making this elusive.

The interest in alkylating compounds was initially triggered by the effects of vesicant war gases. Nitrogen mustard, a war gas used in WWI, drew attention with its effects on lymphomas (76, 77).

Further identified compound of significances was folic acid and particularly its antagonists. Aminopterin (a synthetic compound with antifolate actions) caused remission in paediatric leukaemia patients (78). Another compound from this group is Amethopterin, which is now better known as Methotrexate.

More compounds of significance shortly followed. Purine analogues were used for acute leukaemia (78). However, the first agent to have effects outside of haematological malignancies with impact on solid tumours was 5-flourouracil, which was found to have a wide-spectrum effect on a number of solid tumours (79).

Vinca alkaloids were another group of agents discovered. Vincristine and Vinblastine caused remissions in paediatric leukaemia patients (80).

The combination of vinca alkaloids with other agents in repeated treatment cycles formed the VAMP treatment programme which set the path for modern chemotherapy regimens (81). Following this, a number of further protocols were developed.

In the 1970s, combination chemotherapy regimens were evaluated in the advanced metastatic breast cancer setting. With CMF regimen (combination of cyclophosphamide, methotrexate, 5-fluorouracil and prednisone) results were encouraging, with >25% achieving complete remission.

The concept of chemotherapy as adjuvant treatment after breast cancer surgery with number of regimes was evaluated and proven effective (82, 83).

Since then, a number of new compounds and treatment regimens have been developed including Herceptin (84). Although, there has been a change of direction in the last few decades to try to de-escalate the systemic treatments as has been observed in the surgical and radiotherapy treatments. A drive to identify patients into subgroups that would benefit from adjuvant systemic therapy was apparent, trying to decrease treatment-related toxicity and this was also in the context of decreasing costs.

Gene expression profiling was developed to aid de-escalation of systemic treatment and decision making by dividing patients with ER+ early breast cancer into categories with different risk of cancer recurrence (85, 86). There has been a number of commercial products available which have now become routinely used.

Among the new avenues of treatments of breast cancer are targeted therapies, such as (CDK4/6 inhibitors) (87) and immune-checkpoint inhibition therapies (PD-1, PD-L1) (88, 89).

This is a fast-changing arena and there is no lack of newly developed drugs and new treatment regimes. It is imperative to find the right balance and escalate treatments for patients that would benefit from it and on the other hand to de-escalate often very toxic and expensive treatments in patients who already have a very good prognosis.

1.6. Human epidermal growth factor 2 (HER2)

The HER family consists of 4 members – Epidermal growth factor receptor (EGFR), HER2, HER3 and HER4. Each one consists of 3 functional sections - extracellular (which is formed of 4 subdomains), transmembrane and intracellular.

HER2 was described as a tyrosine kinase receptor, which was initially identified in 1987 by Slamon *et al.* Correlation of HER2 gene amplification with a number of breast cancer parameters revealed it being a significant predictor of OS and DFS. HER2 overexpression was linked to more aggressive phenotype and worse prognosis (90). HER2 is found to be overexpressed in 14.2% of diagnosed primary breast cancers and 18% in metastatic breast cancers cases. There also appears to be lower incidence of HER2 overexpression identified in screening detected breast cancers compared to symptomatic ones (91).

HER2 overexpression leads to activation of Ras-Raf-MEK-Erk1/2 pathway, involved in regulation of cell proliferation and PI3K-Akt-mTOR pathway which is being associated with cell survival. Activation of these pathways leads to tumour growth and proliferation secondary to neoangiogenesis, invasion, increased cell proliferation and avoidance of apoptosis (92) (Fig.1.15.).

The generation of a recombinant monoclonal antibody Trastuzumab (human IgG fused with antigen-binding segment of murine HER2 antibody) (93) targeting the HER2, has significantly changed the

outcomes of patients with HER2 positive breast cancer. The benefits of this treatment were observed also as monotherapy, but maximum effect was reported in conjunction with chemotherapeutic agents which acted synergically (94-96). Enhanced sensitivity to radiotherapy of breast cancer cells overexpressing HER2 was also observed with this antibody treatment (97). The side effect profile of Trastuzumab includes cardiac dysfunction which varied depending on the choice of chemotherapeutic agents and reached incidence of up to 27% when used with anthracycline and cyclophosphamide, while the combination with Paclitaxel reduced this to 13% (96).

In the Herceptin Adjuvant (HERA) trial, after median follow up of 11 years, it was demonstrated that long term disease-free survival significantly improved following adjuvant 1-year treatment with trastuzumab after chemotherapy, albeit treatment with 2 years of trastuzumab had no added benefit for patients with HER2 positive breast cancer (84).

Trastuzumab with chemotherapy is used in the neoadjuvant as well in adjuvant setting in HER2 positive, either early or metastatic breast cancer. The recent addition of pertuzumab, which is another recombinant humanised monoclonal HER2 antibody, to the treatment regimens, has further significantly improved disease-free survival (98, 99).

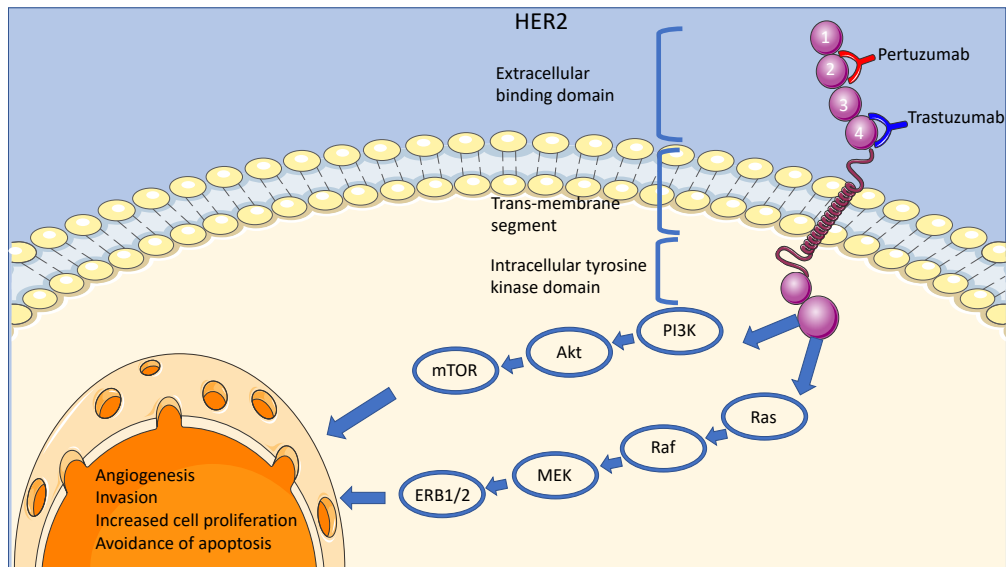


Fig. 1.15. HER2 receptor comprising of 3 domains: the extracellular binding domain, transmembrane segment and intracellular tyrosine kinase domain. Extracellular domain consists of 4 subdomains. Trastuzumab binds to domain 4 and pertuzumab to domain 2. Ras-Raf-MEK-Erk1/2 pathway, PI3K-Akt-mTOR pathway. PI3K, Phosphoinositide 3-kinase; Akt -AKT serine/threonine kinase; mTOR, mammalian Target of Rapamycin; Ras, rat sarcoma; Raf, proto-oncogene serine/threonine-protein kinase; MEK, MAPK/ERK kinase; ERB1/2 extracellular signal-regulated kinase. (100)

1.7. Nottingham Prognostic Index (NPI)

A prognostic index predicting survival in breast cancer (NPI), was developed in 1982. It combined time-dependent factors with biological factors. These factors were primary tumour size, lymph node involvement and histological grade.

NPI= Size in cm x 0.2 lymph node involvement (level 1-2-3 involvement) + Histological Grade (1-3).

The higher the calculated index, the worse is the prognosis. For simplicity, authors divided patients into 3 prognostic groups – good (<3.4), moderate (3.4-5.4) and poor (>5.4). It was developed as a tool to predict prognosis and to help with indication for adjuvant therapy, identifying patients with

high risk for locoregional recurrence. They also stipulate the utilisation of NPI score with regards to follow up interval planning (101, 102).

Currently though, the use of NPI has faded and given way to more elaborate methods like genetic profiling tests including Prosigna, Endopredict and OncotypeDX, all of which have been recommended by NICE (Diagnostic Guidance DG34, published 19 December 2018) to guide the decisions of offering adjuvant chemotherapy to patients with ER+, HER2 negative and node negative early breast cancer. These tests are now becoming part of the pre-treatment staging regimen providing valuable prognostic data (see section 1.8.).

1.8. Breast Cancer Staging

Staging is a way to determine tumour burden regardless of origin and outline its location. This provides prognostic data, allowing further patient stratification and therapy planning. The most widely used anatomical staging tool is TNM (Tumour, Node and Metastasis) classification developed in 1977 and updated by the American Joint Committee on Cancer (AJCC) and the Union for International Cancer Control (UICC), currently in the 8th Edition, published in 2018 (Table 1.1.-1.3.). It newly incorporates biomarkers such as Oestrogen receptor (ER), Progesteron receptor (PR) and HER2 receptor status, Tumour Grade and genomic profiling (21-gene assay Oncotype DX[®], with further multigene panels being evaluated and considered for future addition), although marker for proliferation Ki67 was omitted. The addition of these new components of staging allows more accurate outcome prediction and treatment planning. Prefix 'p' is used for post-operative pathology staging and prefix 'yp' for pathology staging post neoadjuvant chemotherapy. (103)

Table 1.1. *TNM staging in breast cancer, Tumour 'T' pathological classification.*

Tumour (T)	
pTX	cannot be assessed
pT0	no tumour
pTis	in situ malignancy
pT1mi	tumour ≤ 1 mm
pT1a	tumour > 1 mm but ≤ 5 mm
pT1b	tumour > 5 mm but ≤ 10 mm
pT1c	tumour > 10 mm but ≤ 20 mm
pT2	tumour > 20 mm but ≤ 50 mm
pT3	tumour > 50 mm
pT4a	extension to chest wall
pT4b	extension to skin
pT4c	extension to chest wall and skin
pT4d	inflammatory breast cancer

Table 1.2. TNM staging of breast cancer. Node 'N' pathological classification

Node (N)	
pNX	cannot be assessed
pN0	no nodal involvement
pN0(i+)	isolated tumour cells (≤ 0.2 mm)
pN1mi	micrometastasis (> 0.2 mm and ≤ 2.0 mm)
pN1a	metastasis in 1 - 3 axillary lymph nodes
pN1b	metastasis in internal mammary lymph node (Sentinel)
pN1c	pN1a and pN1b
pN2a	metastasis in 4 - 9 axillary lymph nodes
pN2b	metastasis in internal mammary nodes (clinically detected) with negative axillary nodes
pN3a	metastasis in ≥ 10 axillary lymph nodes or metastasis to infraclavicular lymph node
pN3b	imaging positive internal mammary node with pN1a or pN1b
pN3c	metastasis in supraclavicular lymph node (ipsilateral)

Table 1.3. TNM staging of breast cancer. Metastasis 'M' classification based on staging imaging.

Metastasis (M)	
Mx	cannot be assessed
M0	no distant metastatic deposits
M0(i+)	distant metastatic deposits < 2 mm
M1	distant metastatic deposits > 2 mm

ER and PR status is determined using immunohistochemistry (IHC) with a semiquantitative approach with the pathologist determining intensity of staining and the proportion of stained cancer cells on microscopy. Subsequently a score out of 8 is obtained, with 0/8 being negative and 8/8 strongly positive (104).

HER2 receptor status is as well routinely determined by IHC which is again a semiquantitative method. Using this method, a score of 0 and 1+ is considered negative, 2+ borderline and 3+ positive. Borderline results are further evaluated with Fluorescent In Situ Hybridisation (FISH) determining HER2 gene amplification (104).

Grading of breast cancer assesses the differentiation or aggressiveness of the tumour with a score G1-G3, G1 being least aggressive. This is obtained by assessing tubule formation, nuclear pleomorphism and mitotic count. The combined value determines a grading score (Table 1.4.).

Table 1.4. *Grading of breast cancer. Grade 1-3, determined by the combined value of assessed tubule formation, pleomorphism and mitotic count (each given score 1-3).*

G1	score 3 - 5
G2	score 6 - 7
G3	score 8 - 9

1.9. Breast cancer treatment outcomes

There has been significant progress made in terms of diagnosis and treatment of breast cancer although this occurred mainly in the last few decades. Since the early 1970s, breast cancer mortality rates have decreased by almost two-fifths (39%) in the UK. But despite all the advances, Breast cancer is still responsible for 11,400 breast cancer related deaths every year with about 55,200 new breast cancer cases

every year in UK alone. It is the most common cancer in UK and 1 in 7 UK females will be diagnosed with breast cancer in their lifetime. This creates a particularly important challenge in developing new more effective treatments for breast cancer (105). Despite these good advances in new treatment development, there are still sub-groups of breast cancer that pose a particular challenge and the patient outcomes remain poor. The most obvious example is triple negative breast cancer.

1.10. Molecular subtypes of breast cancer

There are 5 molecular subtypes of breast cancer described: Luminal A, Luminal B, HER2 enriched, Normal-like and Basal-like (106). Luminal A is the most common subtype representing up to 50% and mostly represents low grade cancers. In comparison Luminal B cancers tend to be higher grade with variable expression of HER2. About 15% of invasive cancers represent the HER2 overexpressing variant which is mostly high grade and lacking the expression of ER and PR. Although this is an aggressive variant anti-HER2 significantly improved prognosis of this cancer. Normal-like group share the hormone receptor profile with Luminal A but have worse outcomes. The Basal-like group is mostly described by the lack of expression of ER/PR and HER2 – triple negative breast cancer (107).

1.11. Triple negative breast cancer (TNBC)

The gene-expression profiling of TNBC falls mostly into basal-like phenotype (70-80% of TNBC) (108).

TNBC remains the most aggressive, highly diverse, with higher incidence of distant metastasis and with the highest mortality rate. It is diagnosed by IHC and the lack of expression of ER, PR and HER2 limits treatment alternatives and leaves chemotherapy as standard therapeutic option, but resistance development occurs frequently.

Neoadjuvant chemotherapy is increasingly an important approach in the treatment of early TNBC and its response is often assessed by rates of pathologic complete response (pCR). Cortazar *et al.* reported that patients with established pCR had significantly improved outcomes and this was predominantly observed in aggressive subtypes of breast cancer like TNBC (109). In a recent meta-analysis by Huang *et al.*, authors report that 5-year Event free survival (EFS) in TNBC patients with pCR was 86% while in patients without pCR was just 50%. 5-year OS in the presence of pCR was 92% and in the patient category without pCR only 58%. Authors also suggest that patients with early TNBC who received neoadjuvant treatment may benefit from further adjuvant therapy, irrespective of pCR status (110). TNBC patients who continue to be in remission after initial 5-year period have comparable prognosis to hormone receptor positive breast cancer.

1.11.1. Chemoresistance in TNBC

It is thought that TNBC either develops resistance to chemotherapy during treatment or is inherently less susceptible. There is variability in response to chemotherapy, which is thought to be as a result of the molecular diversity of this breast cancer subgroup.

There are several mechanisms thought to be involved in the development of chemoresistance.

1.11.1.1. ATP-binding cassette (ABC) transporters

ABC transporters are ATP dependent and efflux various substances across cell membrane. Among these substances are also cancer treatment drugs, hence leading to chemoresistance. Most commonly mentioned representatives of this family of molecules are ABCC1, ABCC11, ABCG2, ABCB1 (111, 112).

Targeted treatments aim to either focus to inhibit their expression or activity, although a new approach of identifying treatment molecules that are poor substrates for transporters appears to be promising (113).

1.11.1.2. Breast cancer stem cells (BCSCs)

BCSCs are a small subpopulation of cells present in breast tumours. Conventional therapies target fast dividing cells and complete response can be partially hindered by the presence of BCSCs. This may be as a result of the stem cells being most of the time in dormant state making them less susceptible to the treatments. Lee *et al.* report that following neoadjuvant chemotherapy, an increased proportion of stem cells in the tumour is associated with worse prognosis (114). The post treatment residual BCSCs have the capability to re-establish the tumour leading to disease relapse. Furthermore, BCSCs exhibit increased levels of ATP-binding cassette (ABC) transporters (115). Targeting these is one of the new treatment development strategies. Further options include targeting BCSCs surface antigens or signalling pathways vital for BCSCs renewal.

1.11.1.2.1. Signalling pathways vital for BCSCs renewal

1.11.1.2.1.1. Transforming growth factor beta (TGF- β) pathway

TGF- β binds to TGF- β receptor (TGF- β R) forming a receptor complex which phosphorylates Smad2 and Smad3 (principal effectors in this pathway). This Smad2/3 complex further link with Smad4 and subsequently once transferred to nucleus modulates expression of number of

target genes. Inhibition of this pathway augment chemotherapy effects in TNBC and prevent forming of treatment-resistant BCSCs (116). Fig.1.16.

1.11.1.2.1.2. Notch pathway

Cell-cell interaction is required for Notch receptor activation via the canonical pathway. Ligands including Delta like ligand (DLL) 1,3,4 and Serrate like ligand JAGGED 1 and 2 interact with Notch receptor extracellular domain (NECD) allowing the cleavage of metalloprotease 10 or 17 (Adam 10 or 17) and TNF α converting enzyme (TACE) and further cleavage of γ -secretase. γ -secretase releases the Notch receptor intracellular domain (NICD) into cytoplasm which is then transferred to nucleus where it leads to transcription of Notch target genes. The self-renewal of BCSCs has been linked to Notch receptor (117). Fig.1.16.

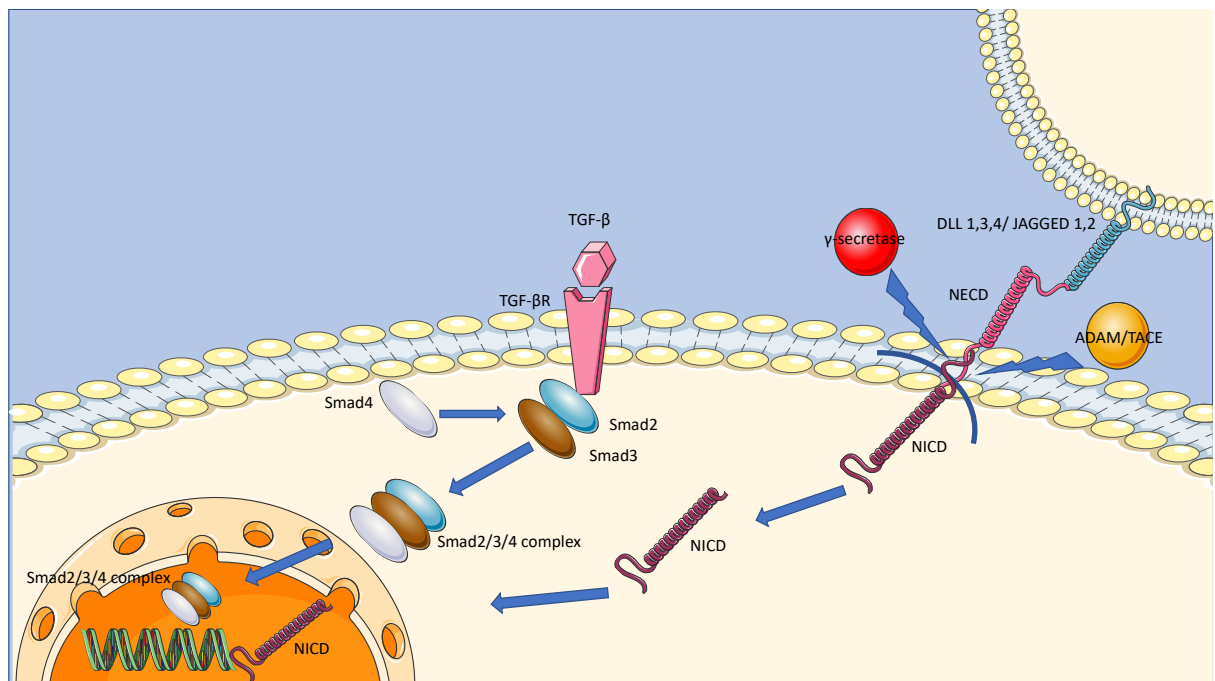


Fig. 1.16. TGF- β and Notch pathways. Transforming growth factor beta (TGF- β) binding to Transforming growth factor beta receptor (TGF- β R),

forming complex Smad2/3 which further binds Smad4 and effects transcription of target genes in nucleus. Delta like ligand (DLL)1,3,4 and serrate like ligand JAGGED 1 and 2 interact with Notch receptor extracellular domain (NECD) from which Notch receptor intracellular domain (NICD) is separated by the action of γ -secretase, metalloprotease (ADAM) and TNF α converting enzyme (TACE). NICD in nucleus triggers transcription of target genes.(100)

1.11.1.2.1.3. WNT and Hedgehog (HH) Pathway

Receptors of WNT are Frizzled (FZD) and low-density lipoprotein receptor-related proteins (LRP). Once bound with WNT, Destruction complex degradation is triggered which leads to β -catenin preservation. β -catenin then transfers to nucleus leading to transcription of target genes. This pathway is important for cell migration and is associated with metastatic spread. (118)

HH pathway is involved in regulation of cell growth and cell differentiation. A disrupted HH signalling pathway contributes to development of more aggressive forms of cancer. The pathway is activated by transmembrane receptor Patched 1 (PTCH1), once HH ligands bind to it. Once this occurs, the suppression of Smoothened (SMO), transmembrane G protein coupled receptor, ceases. The resulting activation of SMO leads to the release of glioma-associated oncogene homolog 1 (GLI1) by suppressor of fused (SUFU) triggering transport of GLI1 to nucleus, where it regulates targeted gene expression (119).

1.11.1.3. Further processes involved in chemoresistance development

Hypoxia (inadequate oxygen supply to tissues) is a factor in chemoresistance development. There is a number of

mechanisms that lead to it, among them is the acidity secondary to hypoxia affecting the cellular uptake of chemotherapy drugs (120). It also triggers cell adjustments that lead to resistance, i.e. enhanced expression of ABC transporters, and leads to modulation of apoptosis (121).

Evasion of apoptosis is considered a hallmark of cancer and is associated with resistance to number of chemotherapeutic agents. Elevated expression of bcl-2 (an apoptosis regulator) has been shown to be an independent prognostic factor of poor OS in TNBC (122).

1.11.1.4. Signalling pathways in TNBC chemotherapy resistance development

A variety of pathways, which often cross-link, have been identified with regards to TNBC chemoresistance.

Very important pathway is PI3K-AKT-mTOR which regulates cell motility, proliferation and cell growth. Following binding of growth factors to PI3K, which subsequently activates AKT, then leads to activation of mTOR, which results in increased cell growth and escalated protein synthesis. This pathway is also involved in overexpression of HER2 (section 1.6., Fig 1.16.).

JAK/STAT (janus kinase/ signal transducer and activator of transcription) pathway is involved in metastasis of breast cancer and tumorigenesis.

Cytokines binding to JAK cause its activation and phosphorylate STAT, which transfers to nucleus influencing transcription of target genes (123).

Further important pathway is NF- κ B (nuclear factor kappa-light-chain-enhancer of activated B cells) which plays an important role in regulating programmed cell death. (124, 125)

1.12. Programmed cell death

Apoptosis is a process with an important role in embryogenesis, teratogenesis, tumour response and normal tissue turnover in response to hormonal factors (126). Apoptosis, or Type I programmed cell death (PCD) is one of many mechanisms, which may occur in response to irreparable damage to DNA, or when induced by inflammatory cells. It is an ATP dependent process, contrary to necrosis, which is a passive process of cell destruction. Necrosis may also be referred to as accidental cell death (ACD) and is characterized by karyolysis and cell swelling. Apoptosis signs include shrinkage of the nucleus (pyknosis) and cytosol without triggering the inflammation process (127, 128).

Type II programmed cell death or Autophagy, is a catabolic process in which cells self-digest their intracellular content, and once completed, leads to cell death. Autophagy is a genetically controlled and evolutionarily well conserved process that leads to targeting of cellular proteins and organelles by lysosomes for degradation. This may facilitate normal turnover of organelles and the removal of defective to help maintain homeostasis. Autophagy is also considered a survival mechanism where self-digesting provides alternative source of energy for the cell during periods of starvation. On the other hand, the catabolic function provided by autophagy is suppressed when the external supply of nutrients is sufficient (129-132).

1.13. Death associated proteins (DAP)

Death Associated Proteins are a group of functionally related proteins with biochemical functions involved in programmed cell death, primarily in response to interferon gamma and consists of DAP1, DAP kinase, DAP-3, DAP4 and DAP5. This group of proteins, which are structurally and genetically unrelated (Figure 1.17), have been investigated in recent years for their role in physiological and pathological conditions.

DAP1, also referred to as DAP, is a small 15kDa protein, encoded by the *DAP* gene located 5p15.2. The DAP1 protein is believed to be involved in autophagy by providing inhibitory control. It has also been shown that DAP1 is a substrate of mTOR and is deactivated by phosphorylation (133). Study from our laboratories suggest that it may have a tumour suppressive function and that there might be an overlap between autophagy and apoptosis pathways. In breast cancer, DAP1 expression decreased in relation to TNM staging and there was a strong inverse correlation between qPCR confirmed DAP1 copy number and survival. (134)

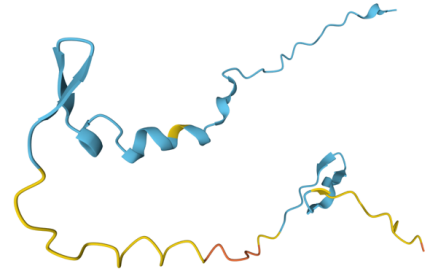

DAP2, initially referred to as Death Associated Protein Kinase DAPK1, is now known as a member of a small group of calmodulin-reliant serine/threonine kinases that have three members, DAPK1, DAP2, DAPK3, respectively encoded by the *DAPK1* (located at 9q21.33), *DAPK2* (located at 15q22.31), and *DAPK3* (located at 9p13.3) gene. The three DAPK proteins have a molecule weight of 160kDa, 42.9kDa and 52.5kDa respectively. DAPK1 was suggested that it is localised with the cytoskeleton's microfilament system and an essential regulator of autophagy. It is thought, that it is capable of influencing a number of different stages within the autophagy cascade, although it is not clear what triggers these. Due to the ability to emphasize several steps in this process it is potentially a "super activator" of autophagy. (135).



DAP-3, encoded by the *DAP-3* gene, is the main subject of the present study and is discussed in details in the next section.


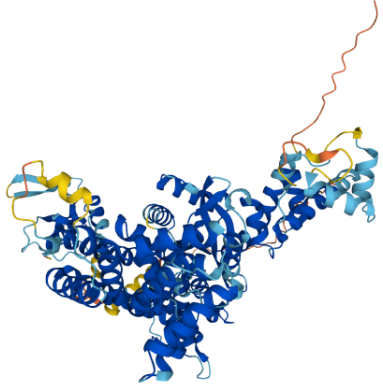
DAP4, also known as THAP Domain Containing 12 (THAP12) and PRKRIR (Protein-Kinase, Interferon-Inducible Double Stranded RNA Dependent Inhibitor, Repressor Of (P58 Repressor)), is an 88kDa protein encoded by the *THAP12* gene, which located at 11q13.5. The DAP4/THAP12 protein is widely expressed, constitutively nuclear polypeptide, which's overexpression does not appear to cause apoptosis alone, but seems to promote protein kinase MST1 induced apoptosis (136). It has also been described as a possible contributor in interferon gamma induced apoptosis (137). However, its overall role in cells and disease remain poorly understood.

DAP5, also known as Eukaryotic Translation Initiation Factor 4 Gamma 2 (EIF4G2) is a 95kDa protein, encoded by the *EIF4G2* gene, located at 11p15.4. The protein is thought to regulate protein translation and is implicated in cell survival during mitosis. It is also involved in stress related cell death (138).

Whilst these DAPs are subject to intensive research for their role in cancer and cancer cells, past work within the host laboratories has highlighted the role of DAP-3 as a key member of this family involved in cancer progression and therapy resistance.

Molecule name	Alternative names	Gene name and coding region	Size of protein	3 D structure
DAP1	DAP	<i>DAP</i> (5p15.2)	15kDa	
DAPK family DAPK1	DAPK ROCO3 EC 2.7.11	<i>DAPK1</i> (9q21.33),	160kDa	

DAPK2	<p>DRP-1 DAP-Kinase-Related Protein 1</p> <p>EC 2.7.11.1</p>	<i>DAPK2</i> (15q22.31),	42.9kDa	
DAPK3	<p>ZIPK Zipper-Interacting Protein Kinase</p> <p>DLK</p> <p>DAP-Like Kinase</p> <p>MYPT1 Kinase</p>	<i>DAPK3</i> (9p13.3)	52.5kDa	

DAP-3	<p>MRP-S29 S29mt Mitochondrial 28S Ribosomal Protein S29</p> <p>BMRP-10 Ionizing Radiation Resistance Conferring Protein</p>	<i>DAP-3</i> (1q22)	46 kDa	
DAP4	<p>THAP12 THAP Domain Containing 12</p> <p>PRPRIR Protein-Kinase, Interferon- Inducible Double Stranded RNA Dependent Inhibitor, Repressor Of (P58 Repressor)</p> <p>P58IPK-Interacting Protein</p>	<i>THAP12</i> (11q13.5).	88kDa	

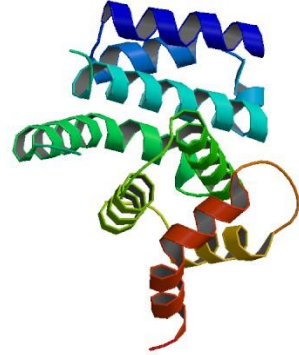
DAP5	<p>EIF4G2 Eukaryotic Translation Initiation Factor 4 Gamma 2</p> <p>AAG1 Aging-Associated Protein 1</p>	<i>EIF4G2</i> (11p15.4)	95kDa	
-------------	---	-------------------------	-------	---

Fig.1.17. The summary information and three-dimensional structure of the DAP proteins (www.uniprot.org).

1.13.1. Death Associated Protein 3 (DAP-3)

1.13.1.1. Discovery and expression profile in normal tissues

DAP-3 is a 46 KDa protein, initially described by Kissil *et al.* in 1995 (139). It is a GTP binding protein (or G protein) that is encoded by the *DAP-3* gene situated in chromosome 1 q22 (140).

It has been shown for DAP-3 to be localised in mitochondria (141), and proteomic analysis revealed for it to be part of small subunit of mitochondrial ribosome 28s (142), although it has been found to be also in cytosol albeit in smaller quantities.

The protein expression of DAP-3 appears ubiquitous and present in almost all human tissues but in variable levels (Figure 1.18). The highest expression protein levels appear to be within glandular cells of the gastrointestinal tract and high levels of mRNA seen in skeletal muscle, myocardium, lung, adipose tissue, and spleen. Breast tissue tend to have modest levels of expression (143, 144)

1.13.1.2. Role of DAP-3 in normal physiological processes

DAP-3 has been characterised as an integral component of the external apoptotic pathway.

The pro-apoptotic effects of DAP-3 in mitochondria are thought to modulate mitochondrial fragmentation (145).

Effects of protein kinase B (AKT/PKB) maintain DAP-3 in inactive phosphoprotein state. Once activated, it is engaged in the creation of Death Induced Signalling Complex (DISC) and co-localises with Fas associated Death Domain (FADD) (146). Actions of DAP-3

within the external apoptotic pathway are thought to be facilitated by binding with Death Ligand Signal Enhancer (DELE), knockdown of which has shown to inhibit apoptosis (147).

DAP-3 is also a factor in *anoikis*, where it is involved with IFN- β promoter stimulator 1 (IPS1) alongside with FADD. Caspase 8 inhibition results in prevention of Focal Adhesion Kinase (FAK) cleavage and cell detachment (148). By modulating activation of caspase 8 via IPS1, DAP-3 plays a vital role in cell detachment associated apoptosis (149) (Fig.1.19).

1.13.1.3. Implications in human disease and cancer

In Humans, the expression of DAP-3 is varied across the different spectrum of cancers and is detected in almost all tissues. Varied prognosis has been observed with different expression levels of DAP-3. In some cancers (i.e liver, head and neck and pancreatic cancer) decreased survival is associated with increased DAP-3 expression and although urothelial and cervical cancer it causes opposite effect on survival (143, 144). In a study by Han *et al.* it was reported that DAP-3 overexpression was observed in 17 cancer types and knockdown of DAP-3 would be a tumour suppressing phenotype, further indicating that DAP-3 is a strong oncogene (150). This relationship was further supported by a recent study by Sui in 2021 where in human pancreatic cancer, high levels of DAP-3 both at protein and message levels were linked to a shorter survival and poor clinical outcomes (151).

The expression of DAP-3 has been previously investigated in our laboratories and it was revealed that increasing Nottingham Prognostic Index (NPI) as well as TNM stage and tumour grade

was associated with decreased DAP-3 expression (152). In addition to this, *in vitro* studies have been conducted to examine the effects of DAP-3 knockdown in MCF-7 and MDA-MB-231 breast cancer cell lines. Results of these experiments suggested that silencing of DAP-3 led to increased cell adhesion, migration and invasion, indicating that DAP-3 is involved in breast carcinogenesis (153). Further study from our laboratories revealed that better prognosis in gastric cancer was associated with increased DAP-3 expression. This was evaluated *in vitro* in breast cancer cell lines, as well as a clinical cohort, where it was associated with local recurrence and distant metastasis. (154).

1.13.1.3.1. Relation of DAP-3 to cancer treatment response

DAP-3 has also been evaluated in the context of resistance to chemotherapy in gastric cancer. It was observed, that increased DAP-3 expression correlated with enhanced effectiveness to neoadjuvant chemotherapy. DAP-3 knockdown in gastric cancer cell lines resulted in slower growth rate and these cells showed signs of lower sensitivity to 5-FU and oxiplatin. These effects were explained that downregulation of DAP-3 might prevent chemotherapy induced apoptosis and thus may be a factor in increased chemoresistance (154).

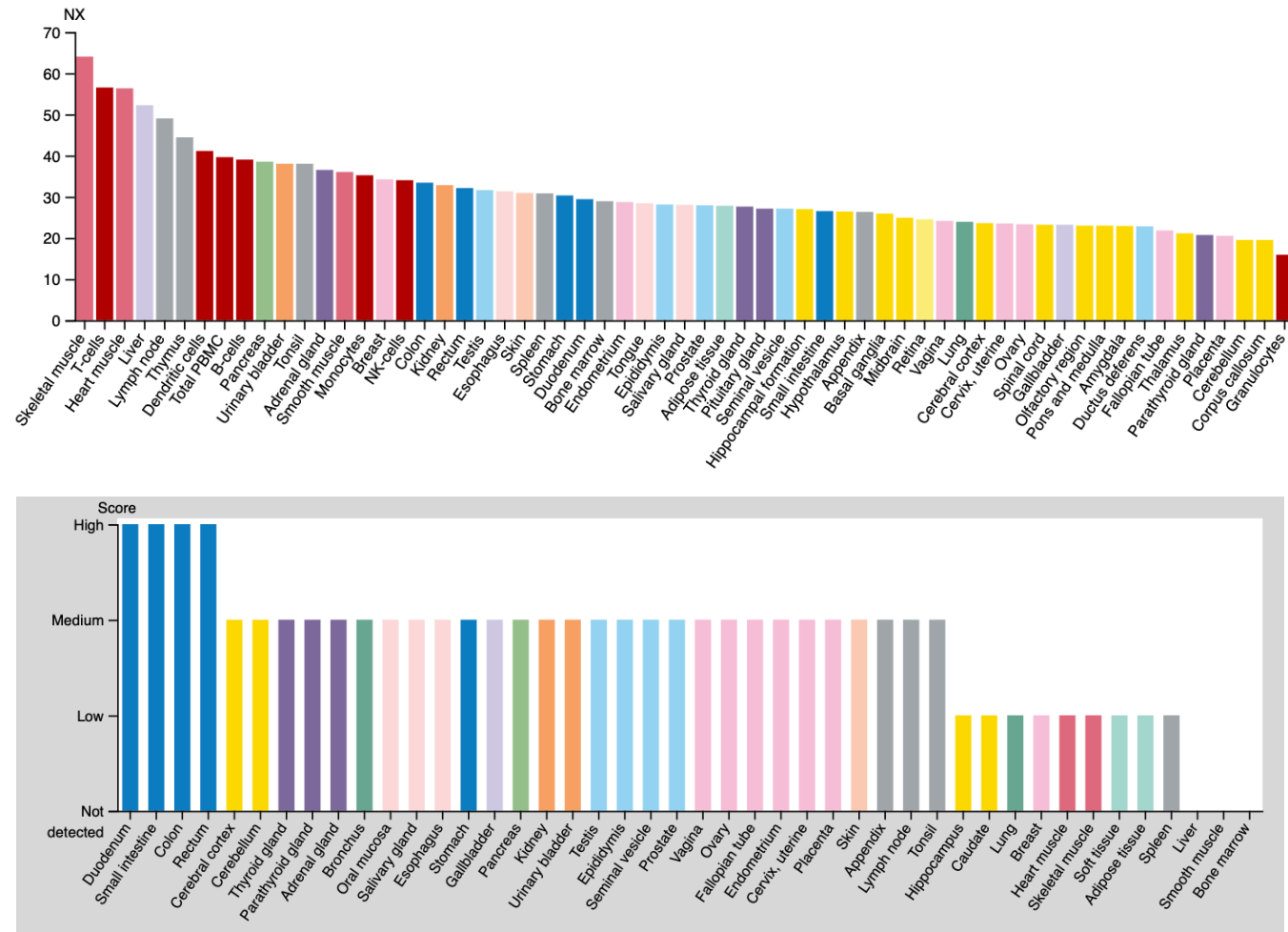


Fig. 1.18. Expression levels of DAP-3 in human tissues. Top: levels of RNA expression; Bottom: protein levels. (www.proteinatlas.org).

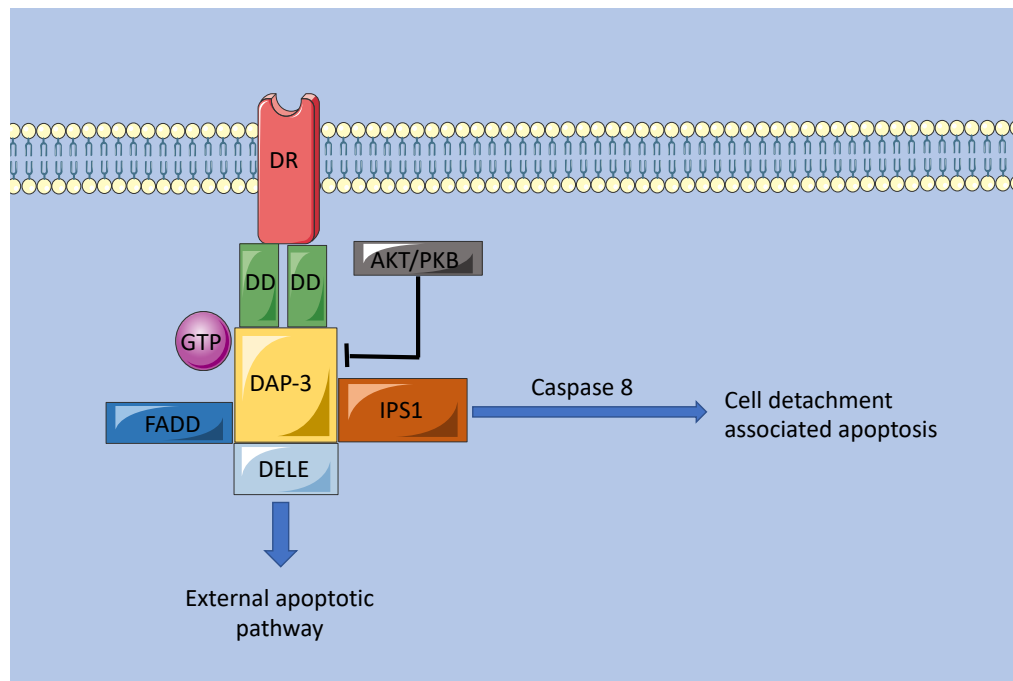


Fig. 1.19. Scheme of relations of DAP-3 with Fas receptor related DISC. AKT/PKB: protein kinase B, DAP-3: death-associated protein 3, DD: death domain, DELE: death ligand signal enhancer, DR: death receptor, DISC: death inducing signalling complex, FADD: Fas Associated Death Domain.

1.14. Heat Shock Protein (HSP) family

HSP family is a group of highly conserved mammalian chaperone proteins that have an important role in assisting of correct folding of newly created proteins or the refolding of denatured proteins under an array of extracellular or intracellular stress conditions i.e., hyperthermia, oxidative stress, cellular harm, ionising radiation and starvation, subsequently causing their upregulation (155).

The HSP family consists of large number of proteins which are classified based on their molecular weight. Among the more studied ones are HSP27, HSP40, HSP60, HSP70, HSP90 and Heat Shock Transcription Factor 1 (HSF1).

HSPs are located intracellularly in cytosol and also within various organelles including mitochondria. Further, they reside in nucleus and plasma membrane. Besides these locations, they are also found in extracellular space (156, 157).

1.14.1. Heat Shock Protein 90 (HSP90)

HSP90 and its 4 isoforms (HSP90a and HSP90b found in cytosol, GRP94 in endoplasmic reticulum and Trap1 in mitochondria) is thought to be the most abundant member of the Heat Shock Protein family and is an ubiquitously expressed chaperone protein that interacts with a great number of other proteins called clients (158). In normal cells, HSP90 is a vital regulator of the cell cycle, proliferation, signal transduction and transcriptional regulation. Under stress conditions, HSP90 induction is markedly upregulated to promote the misfolding and overexpression of client proteins (159).

HSP90 was shown to interact with unsaturated phospholipids and with a higher affinity to negatively charged molecules with further increased affinity in the presence of certain level of cholesterol (160).

Increased expression of HSP90 contributes to activation of protein kinases with oncogenic effect in particular PI3K/AKT/mTOR, JAK2/STAT3 and MAPK and inhibition of these via HSP90 inhibitor decreased cancer cell proliferation in pancreatic cell line models (161). Some of these pathways have been identified to play part in oxidative stress (162).

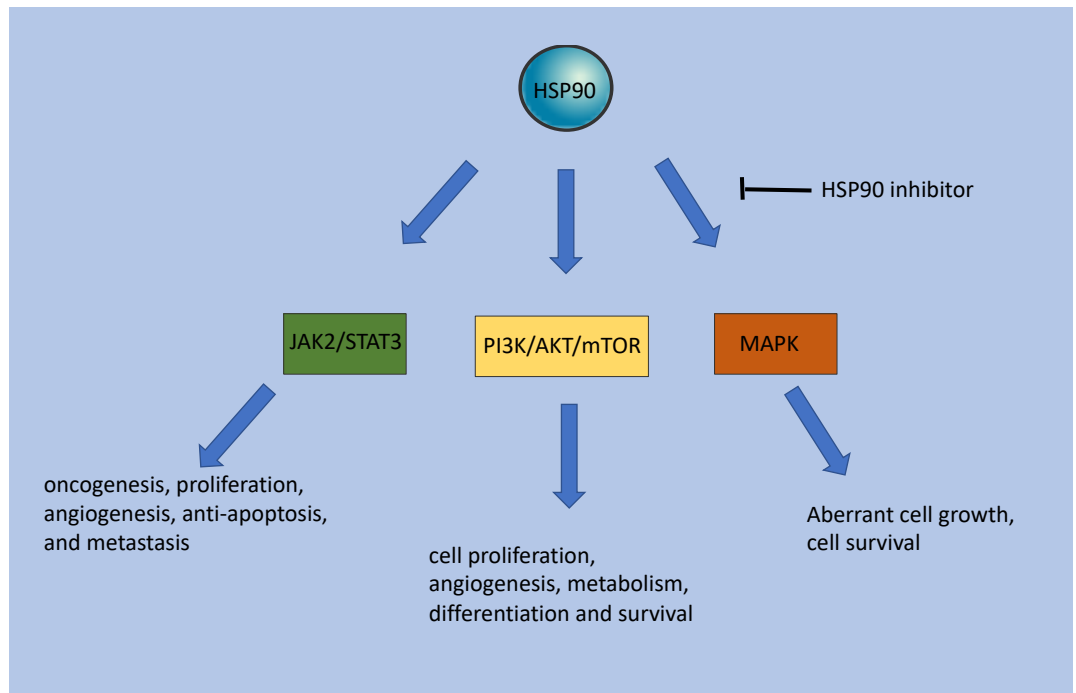


Fig.1.20. *HSP90 involved signalling pathways. JAK2 Janus-activated kinase 2; STAT3 signal transducer and activator of transcription 3; PI3K Phosphoinositide 3-kinase; AKT protein kinase B; mTOR mammalian Target of Rapamycin, MAPK mitogen-activated protein kinase*

1.14.1.1. JAK2/STAT3 pathway

JAK2, a non-receptor tyrosine kinase, combines extracellular signals from interleukin receptors and oncogenic receptor tyrosine kinases to an oncogenic transcription factor STAT3.

Activation of JAK2/STAT3 pathway results in oncogenesis, cell proliferation, angiogenesis, antiapoptotic effects and metastasis. Dysregulation of this pathway is associated with poor clinical outcomes (163).

Increased expression of HSP90 and PKM2 in hepatocellular carcinoma was correlated with poor clinicopathological features and shown to be strong predictive factor of poor prognosis of HCC patients (164).

1.14.1.2. PI3K/AKT/mTOR pathway

This pathway plays an integral role in cell proliferation, angiogenesis, cell metabolism, differentiation and cell survival. Giulino-Roth *et al.* found that HSP90 inhibition targets multiple elements of PI3K/AKT/mTOR pathway. The HSP90 inhibition was synergistic with inhibition of PI3K/AKT/mTOR pathway. For this pathway to retain expression of its proteins it requires HSP90 chaperoning. (165)

1.14.1.3. MAPK pathway

One of the 3 known MAPK pathways is previously described Ras-Raf-MEK-ERK pathway in section 1.7. Fig.1.16. triggered by growth factors in that example HER2.

This pathway influences cell survival and causes aberrant cell growth. HSP90 inhibition has been shown to have a disruptive effect on this pathway (166, 167).

Overexpression of oestrogen receptors is observed in most of breast cancer patients and they are also a class of clients of HSP90. These steroid receptors are HSP90 dependent clients that activate their target genes after binding to HSP90. As HSP90 is a significant target in cancer, HSP90 inhibitors have attracted great amount of research attention with many currently ongoing clinical trials (159).

1.15. Aims and objectives

The aim of the current study is to identify mechanisms and partners of DAP-3 and investigate their relevance in breast cancer progression and therapy response.

The central hypothesis is that DAP-3 is implicated in breast cancer progression and therapy response through interactions with downstream signalling pathways and associated effector proteins. Furthermore, we hypothesise that targeting such pathways or interactions in combination with DAP-3 may be useful as novel therapies.

Specific aims of the project are:

- 1) Investigate DAP-3 expression levels in selected group of breast cancer cell lines and Establish DAP3-KD cell models (Chapter 3.)
- 2) Identify interacting partners of DAP-3 in breast cancer clinical tissues (Chapter 4.)
- 3) Investigate implications of DAP-3 and combination with interacting partners in breast cancer progression and therapy response *in vitro* (Chapter 5.)
- 4) Explore the clinical significance of DAP-3 and/or interacting partner in breast cancer progression, survival and therapy response using in house and online breast cancer cohort datasets (Chapter 6.)

CHAPTER 2

Material and Methods

2. Materials and Methods

2.1. Chemical and plastic ware

All the chemicals for general use were purchased from Sigma-Aldrich (Poole, Dorset, England) and Melford Chemicals (Chelworth, Ipswich, Suffolk, England) unless otherwise state. A full list is provided in Table 2.1. Other specific compounds or reagents are stated in the respective chapters

2.1.1. Standard solutions used in cell culture works

2.1.1.1. 0.05M EDTA

The following were dissolved in distilled water:

- 1 g of monopotassium phosphate (KH_2PO_4)
- 5.72 g of disodium phosphate (Na_2HPO_4)
- 1 g of potassium chloride (KCl),
- 1.4 g of EDTA

2.1.1.2. Trypsin

500mg of trypsin was dissolved in 20ml 0.05M EDTA and aliquoted to 250 μ l samples. For the use of cell detachment, one aliquot of 250 μ l was diluted in 10 ml of 0.05M EDTA.

2.1.1.3. Antibiotic solution

Stock solution consists of:

- 12.5 mg Amphotericin B
- 5 g streptomycin
- 3.3 g penicillin

5ml of the stock solution added to 500ml of culture medium gives the following final concentrations of active agents:

- 0.25 µg/ml amphotericin B
- 0.1 mg/ml streptomycin
- 100 U/ml penicillin

2.1.2. Solutions used for RNA and DNA molecular biology

2.1.2.1. PCR water

Filtered distilled water exposed to ultra-violet light.

2.1.2.2. DEPC water

Solution of 250 µl of diethyl pyroncarbonate (DEPC) with 4750 µl distilled water was autoclaved before use.

2.1.2.3. TBE (5X Tris, Boric acid, EDTA)

- 275 g Boric acid
- 540 g of tris-Cl
- 46.5 g of disodium EDTA
- Distilled water up to volume of 10l

2.1.3. Solutions used for Protein Molecular Biology

2.1.3.1. Lysis Buffer

- 0.5% Triton X-100
- 1 mg/ml leupeptin
- 10 mM sodium orthovanadate
- 2 mM of calcium chloride (CaCl₂)

These components were dissolved in distilled water and stored at 4°C.

2.1.3.2. 10x TBS

- 121 g TRIS
- 400.3g NaCl
- Distilled water up to volume of 5l

2.1.3.3. Running buffer

- 303g TRIS
- 1.44 Kg Glycine
- 100g SDS
- Distilled water up to volume of 10l

2.1.3.4. Transfer buffer

- 15.15g TRIS
- 72g glycine
- 1l Methanol
- Distilled water up to volume of 5l

2.1.3.5. Washing buffer

- 500 µl Tween (polysorbate 20)
- 1X TBS up to volume of 500 ml

2.1.3.6. Blocking buffer

- 500 µl Tween (polysorbate 20)
- 1 g Marvel (condensed milk)
- 1X TBS up to volume of 500 ml

Table 2.1. General chemical and reagent (in alphabetic order) and their source

Material name	Source, selected product numbers
1 Bromo-3-chloro-propane	Sigma-Aldrich Co, Poole, Dorset, UK, T204005
1% Crystal violet solution	Sigma-Aldrich Co. Poole, Dorset, UK, V5265
100X antibiotic antimycotic Solution	Sigma-Aldrich Co, Poole, Dorset, UK, A5955
10X Phosphate Buffered Saline (PBS)	Sigma-Aldrich Co. Poole, Dorset, UK, P7059
10X Tris Glycine buffer	Sigma-Aldrich Co. Poole, Dorset, UK, T4904
10X Tris Glycine SDS buffer	Sigma-Aldrich Co. Poole, Dorset, UK, T7777
2X Lammeli loading buffer	Sigma-Aldrich Co. Poole, Dorset, UK, S3401
2X Precision qPCR Mastermix	Primerdesign Ltd., Southampton, Uk, oasing-standard-150
A/G protein agarose beads	Santa-Cruz Biotechnology, Santa-Cruz, CA, USA, sc-2003
Acetic acid	Fisher Scientific, Leicestershire, UK
Acrylamide mix (30%)	Sigma-Aldrich Co, Poole, Dorset, UK, 1.00639
Agarose	Melford Laboratories Ltd, Suffolk, UK
Ammonium persulfate (APS)	Sigma-Aldrich Co, Poole, Dorset, UK, A3678
Bio-RadDC Protein Colourimic Assay	Bio-Rad Laboratories, Hercules, CA, USA
Boric acid	Duchefa Biochemie, Haarlem, Netherlands
Broad Range Molecular weight Marker	Insight Biotechnologies, Middlesex, UK
Bromophenol Blue	Sigma-Aldrich Co, Poole, Dorset, UK, 114391
CaCl ₂	Sigma-Aldrich Co, Poole, Dorset, UK
DEPC (Diethylpyrocarbonate)	Sigma-Aldrich Co, Poole, Dorset, UK, D5758
Dimethylsulphoxide (DMSO)	Fisons Scientific Equipment, Loughborough, UK
DMEM/Ham's F12 with L-Glutamine medium	Sigma-Aldrich Co, Poole, Dorset, UK, D9785
EDTA (Ethylenediaminetetraacetic acid)	Duchefa Biochemie, Haarlem, Netherlands, E0511
Ethanol (molecular biology grade)	Fisher Scientific, Leicestershire, UK
EZ ECL	Geneflow, Litchfield, UK
Formalin	Fisher Scientific, Leicestershire, UK
Glycine	Melford Laboratories Ltd, Suffolk, UK
GoScript RT kit	Promega, Southampton, UK, A5001
GoTaq Green PCR Mastermix	Promega, Southampton, UK, M7123
HCL	Sigma-Aldrich Co, Poole, Dorset, UK
Immobilon P Polyvinylidene fluoride (PVDF) membrane	Merk-Millipore - Fisher Scientific, Leicestershire, UK, 10344661
Isopropanol	Sigma-Aldrich Co, Poole, Dorset, UK
KCl	Fisons Scientific Equipment, Loughborough, UK
KH ₂ PO ₄	BDH Chemicals Ltd, Poole, England, UK
Matrigel	Corning, Flintshire, UK, 354234
Mayers Htx	Sigma-Aldrich Co, Poole, Dorset, UK
Methanol	Fisher Scientific, Leicestershire, UK
Na ₂ HPO ₄	BDH Chemicals Ltd., Poole, Dorset, UK
NaCl	Sigma-Aldrich Co, Poole, Dorset, UK
NaN ₃	Sigma-Aldrich Co, Poole, Dorset, UK
NaOH	Sigma-Aldrich Co, Poole, Dorset, UK
PCR High Ranger PCR ladder	Geneflow, Litchfield, UK
PCR Ranger, PCR ladder	Geneflow, Litchfield, UK
Peroxidase conjugated secondary antibodies IgG	Sigma-Aldrich Co, Poole, Dorset, UK
Ponceau S Stain	Sigma-Aldrich Co, Poole, Dorset, UK
SDS (Sodium dodecyl sulphate)	Melford Laboratories Ltd, Suffolk, UK
Serum bovine albumin	Sigma-Aldrich Co, Poole, Dorset, UK
Supersignal TM West Dura system	Pierce Biotechnology Inc., Rockford, IL, USA

Sybr Safe	Fisher Scientific, Leicestershire, UK, 10328162
TBS Automation Wash Buffer	Biocare Medical, Concord, CA, USA, TWB945M
Tetramethylethylenediamine (TEMED)	Sigma-Aldrich Co, Poole, Dorset, UK, T9281
TRI Reagent	Sigma-Aldrich Co, Poole, Dorset, UK, 93289
Trion	Sigma-Aldrich Co, Poole, Dorset, UK
Tris-HCl	Melford Laboratories Ltd, Suffolk, UK
Trypsin	Sigma-Aldrich Co, Poole, Dorset, UK
Tween 20	Melford Laboratories Ltd, Suffolk, UK

2.2. Cell Cultures

Eight human breast cancer cell lines and 1 benign breast cell line (supplied by ATCC, via LGC Standard, Queens Road Teddington Middlesex, England) were selected for the current study (Table 2.2).

Selected cell lines (MCF-7 and MDA-MB-231) were grown in Dulbecco Modified Eagle Medium (DMEM) with L- glutamine and phenol supplemented with 10% foetal calf serum (FCS, Sigma-Aldrich, Poole, Dorset, England) and a stock antibiotic solution (Sigma-Aldrich). Twenty five cm² or 75 cm² tissue flasks (Greiner) were used for growing and maintaining cell cultures.

DMEM medium supplemented with 5 µg/ml blasticidin S (Melford Laboratories) was used for the selection of newly transfected cells for 5-10 days. Following successful selection, the cells were maintained in a solution of DMEM supplemented with 0.5 µg/ml blasticidin S.

All cell manipulation was performed in class II laminar flow hoods (SafeF ST Classisc) (Fig.2.1).

2.2.1. Cell subculture and maintenance

Cells were routinely subcultured to maintain cultures, prevent over-confluence, or when required for cellular assays. Cell medium was aspirated from the tissue culture flask using a disposable glass pipette attached to a vacuum and waste container (Fisher Scientific, Leicestershire, UK). Following this the cell monolayer was washed with 2 – 5 ml of phosphate buffered saline (PBS; Sigma-Aldrich, Dorset, UK) before removing the PBS and adding 1 – 3 ml of trypsin (Sigma-Aldrich, Dorset, UK) and incubating to detach adherent cells from the tissue culture vessel. Following detachment, cells were collected in a universal container and centrifuged at 1600 rpm for 5 minutes. The cell pellet was then resuspended in fresh medium and either used to seed appropriate vessels for either continued maintenance or experimental protocols following determination of cell density using a haemocytometer.

2.2.2. Cell preservation and storage

Low passage stocks were prepared for both wild type and transfected cell lines. Cells were detached from the tissue culture flask and quantified as described in section 2.2.1. Cells were resuspended in growth medium containing 10% Dimethyl Sulphoxide (DMSO) to aid in survival of the preservation process. Cells were prepared at a concentration of 1 million cells/ml and aliquoted into pre-labelled cryovials (Griener). Subsequently, cryovials were wrapped in tissue paper and initially stored in the -80°C freezer. For longer term storage cryovials were transferred to liquid nitrogen stock facilities.

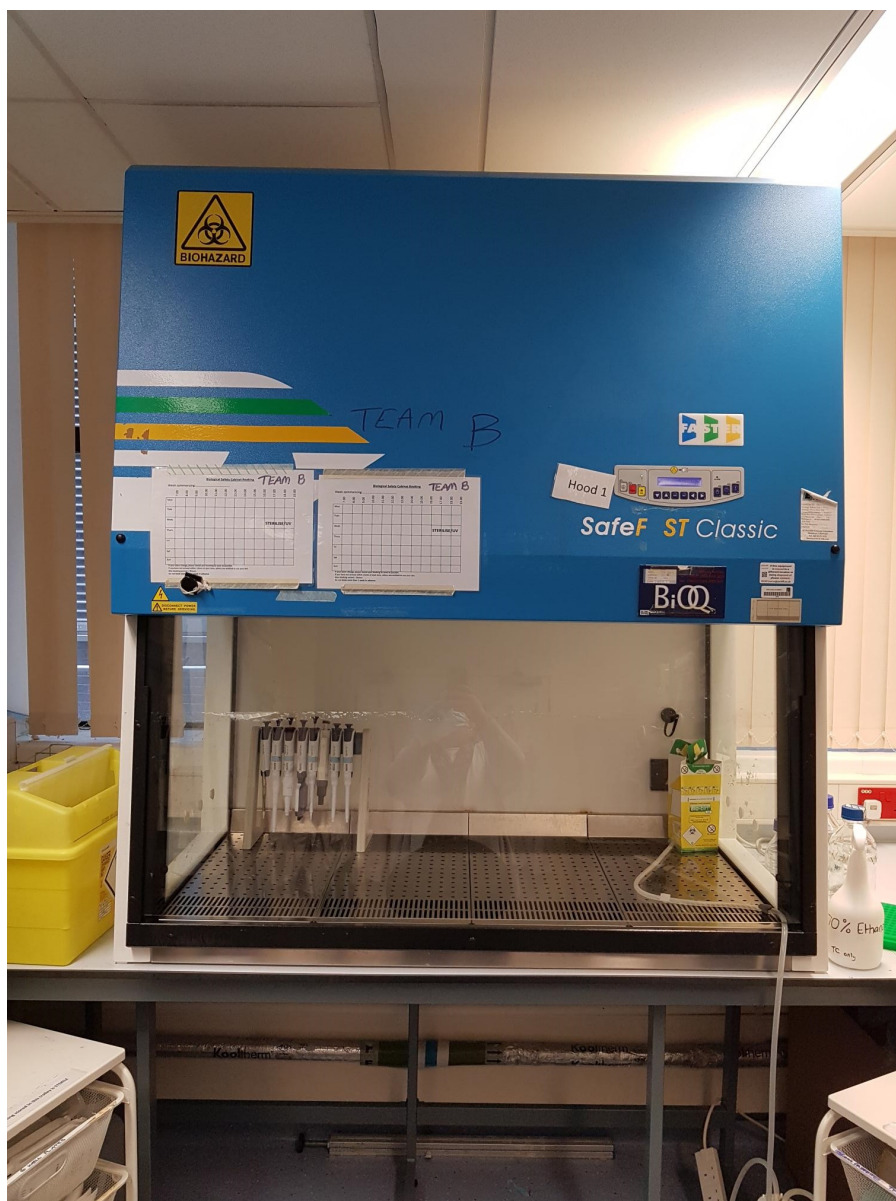


Fig.2.1 Laminar flow cabinet, SafeF ST Classic

Table 2.2. Breast cancer cell lines used in study with their stated origin, where they were derived from, adherence, age of patient and ethnicity

Cell line name	Type	Characteristics
BT-20	Human, Breast AdenoCa,	ER –ve, adherent, 74 F Caucasian
BT-483	Human, Breast AdenoCa	IDC,adherent , 23F Caucasian
BT-549	Human, Breast AdenoCa	IDC pappilary, LN 3/7, adherent 72F Caucasian
ZR-75-1	Human, Breast AdenoCa	IDC derived from Mts site – ascites, ER +ve, adherent, 63F Caucasian
MDA-MB-361	Human, Breast AdenoCa	derived from Mts site – brain, loosely adherent, 40F Caucasian
MDA-MB-436	Human, Breast AdenoCa	derived from Mts site – pleural effusion, adherent, 43F Caucasian
MCF 10A	Human, Breast, Fibrocystic disease,	adherent, 36F Caucasian
MCF-7	Human, Breast AdenoCa	derived from Mts site- pleural effusion, ER/PR +ve, adherent, 69F Caucasian
MDA-MB-231	Human, Breast AdenoCa	derived from Mts site – pleural effusion, triple negative, adherent, 51F Caucasian

2.3. RNA Extraction and cDNA synthesis by Reverse Transcription

Total RNA extraction from cells and tissues was carried out with TRI Reagent (Sigma-Aldrich, Dorset, UK), in accordance with manufacturer's instruction. Briefly, medium was removed from 25cm² flask with between 70 – 90% confluence and 1ml of TRI Reagent added. The cell lysate was collected and then transferred into an eppendorf before adding 100 µl of 1 Bromo-3-chloro-propane (Sigma-Aldrich, Dorset, UK). The solution was then centrifuged in a refrigerated centrifuge (Fisher Scientific UK, Fig.2.2.) at 4°C and 12,000rpm for 15 minutes. Separation of the solution is achieved into a top RNA rich aqueous phase, a middle DNA containing interphase and a lower, protein containing organic phase.

The top aqueous phase was removed and transferred to an eppendorf

containing 500 μ l of isopropanol (Fisher Scientific UK). This solution was thoroughly mixed and then centrifuged at 4 °C and 12,000rpm for 10 minutes resulting in precipitation of the RNA as a white pellet at the bottom of the eppendorf.

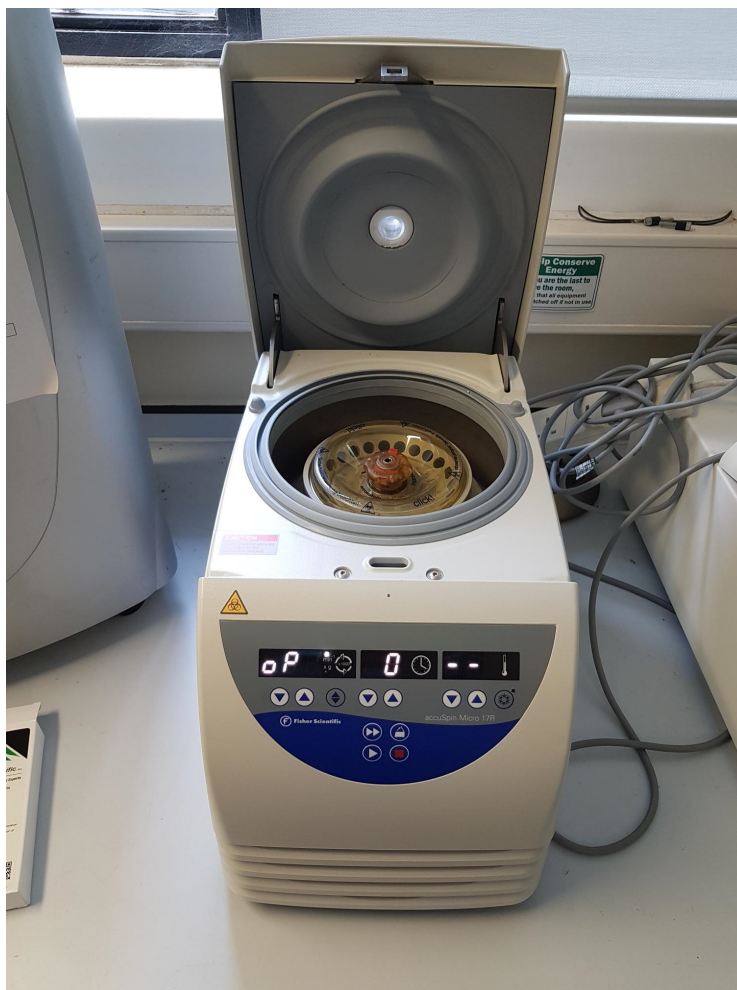


Fig.2.2. Refrigerated Centrifuge, Fisher Scientific accuSpin Micro 17R

The supernatant was discarded, and the pellet, which mainly contained total RNA, was washed with 75% ethanol (ethanol with Diethylpyrocarbonate [DEPC] water 3:1) and vortexed for around 5 seconds before centrifuging at 4°C and 7500rpm for 5 minutes. The supernatant was removed and the RNA pellet was air dried in an oven (Techne, Hybridiser HB-1D, Wolf laboratories, York, UK) for approximately 5 minutes, taking care to not dry the pellet completely.

The pellet was then dissolved with DEPC water. Depending on the pellet's size, the volume of DEPC water used was between 20 to 50 μl . DEPC is used to inhibit the action of any RNases that may be present.

RNA was quantified using a Nanophotometer (Geneflow, Litchfield, UK; Fig.2.3), configured to detect and quantify RNA ($\mu\text{g}/\mu\text{l}$) through comparison to a DEPC blank. RNA samples were then standardized to 0.5 μg of RNA per sample before undergoing reverse transcription.



Fig. 2.3. *Nanophotometer (Geneflow, Litchfield, UK)*

A GoScript™ Reverse Transcription kit (Promega) was used for reverse transcription of extracted RNA of which a fixed amount of 0.5 µg RNA was combined with 1 µl of Oligo dT primer and PCR water up to a final volume of 5 µl. RNA with primer was then incubated at 70°C for 5 minutes and then placed on ice for 5 minutes. Following this 15 µl of RT mix (composing 5X reaction buffer, MgCl₂, dNTPs, recombinant RNasin ribonuclease inhibitor and GoScript reverse transcriptase) was added, assembling a 20 µl reaction, and subjected to the following protocol in a thermocycler (SimpliAmp, Fisher Scientific, Leicestershire, UK Fig 2.4.): 25°C for 5 minutes; 42°C for 60 minutes; 70°C for 15 minutes; 4°C hold. Following reverse transcription, acquired cDNA was diluted 1:4 using PCR water and stored at -20°C.



Fig.2.4. *SimpliAmp™ thermocycler (Fisher Scientific, Leicestershire, UK)*

2.4. Polymerase Chain Reaction (PCR)

PCR was performed to amplify desired gene region sequences using specific primers (Table 2.3.) and GoTaq Green Master Mix (Promega, Madison, USA) subjecting it to an adequate number of cycles in a thermocycler (Table 2.4.), (Fig.2.4).

The primers were designed either using Beacon Designer software or using Primer-BLAST and were synthesised by Sigma (Sigma-Aldrich, Dorset, UK). Following amplification, products were separated according to size using electrophoresis (performed with setting 95V for an appropriate time depending on product size) on 0.8% - 2.0% agarose gel stained with SYBR Safe Gel Stain (Fisher Scientific, Leicestershire, UK), 8-15µl of sample per well. A PCR Ranger 100bp ladder (Geneflow, Litchfield, UK) was added to allow confirmation of product size and a negative control, where cDNA was replaced with PCR water in the reaction, was also included to highlight potential contamination. Visualisation was achieved using a U:Genius3 gel doc system (Syngene, Cambridge, UK) Fig. 2.5.

Table 2.3. Primers used in study with quoted sequence. Z sequence ACTGAACCTGACCGTACA.

Primer name	Sequence (5'-3')	Product size (bp)
GAPDHF8	GGCTGCTTTTAACTCTGGTA	475bp
GAPDHR8	GACTGTGGTCATGAGTCCTT	
GAPDH F1	AAGGTCATCCATGACAACCTT	87bp
GAPDHZR1	<u>ACTGAACCTGACCGTACA</u> GCCATCCACAGTCTTCTG	
DAP3F8	TGCCTGATGGTAAGGAAA	528bp
DAP3R8	AGTGGTTCTTCCCCAAAG	
DAP3 F1	AAAGCACTGAAAAAGGGAGT	107bp
DAP3 Zr1	<u>ACTGAACCTGACCGTACA</u> CCTCTTTAGCTCTTTCAGCA	
CRYABF8	TGGACTCTCAGAGATGCG	216bp
CRYABR8	GAAGTAATGGTGAGAGGGTC	
PaxilF22	CTGACGAAAGAGAAGCCTAA	Variant specific Transcript variant 531bp
PaxilR22	CTTTTCACAGTAGGGCTGTC	
HSP90AF1	GTAACTGGTACCAAGAAAAGG	739bp
HSP90AR1	TAGGTTACCTGTGTCTGTC	
HSP90AZR1	<u>ACTGAACCTGACCGTACA</u> AGATCCTTGTAGAGGTGTTG	<u>173bp vs F1</u>
HSP90BF1	GAGTATCTCAATTTTATCCGTGGTG	653bp
HSP90BR1	CAAGGTGAAGACACAAGTCTA	
HSP90BZR1	<u>ACTGAACCTGACCGTACA</u> CAGAGAAGAGCTCAAGGCACT	<u>139bp vs F1</u>
TF7	TAATACGACTCACTATAGGG	Plasmid/insert specific
RBTOF	CTGATGAGTCCGTGAGGACGAA	
RBBMR	TTCGTCCTCACGGACTCATCAG	
PDPL F8	GAATCATCGTTGTGGTTATG	101bp
PDPL Zr	<u>ACTGAACCTGACCGTACA</u> CTTTTCATTTGCCTATCACAT	

Table 2.4. *PCR conditions for thermocycler*

	30-35 cycles					
temperature	94 °C	94 °C	55 °C	72 °C	72 °C	4 °C
time	5min	30s	30s	40s	10min	∞



Fig. 2.5. *U:Genius3 gel doc system (Syngene, Cambridge, UK)*

2.5. RT-qPCR

RT-qPCR was performed using Precision 2X qPCR Mastermix (Primer Design, UK) and Uniprobe – universal primer, with forward and reverse primers (containing Z sequence, underlined in table 2.3) of selected molecules (Table 2.3) designed for target gene amplification. Uniprobe is a universal probe/primer, based on the Molecular Beacon technology and is tagged with a FAM fluorophore, for detection of amplicons. The probe worked with the specific primer with a complementary Z-sequence, to amplify a FAM tagged specific PCR product.

Primers were diluted to 10 μ M concentration and reverse primers, containing the Z-sequence, were further diluted to 1 μ M concentration. The reaction was set up in 96 well microamp fast optical qPCR plates (Fisher Scientific, Leicestershire, UK).

Samples were run simultaneously alongside standards of known copy numbers (ranging from 10¹ to 10⁸ copies of PDPL) prepared in duplicate.

Specificity of used primers was validated using a positive control known to express the molecule of interest and a negative control, where instead of cDNA, PCR water was used.

PCR amplification was performed using an Applied Biosystems® Step One Plus Real- Time PCR Thermocycler (Fig.2.6.). The instrument was programmed to detect FAM tagged amplicons at the annealing stage. Quantitative PCR data were analysed and normalized to GAPDH (housekeeping gene) expression within the samples.

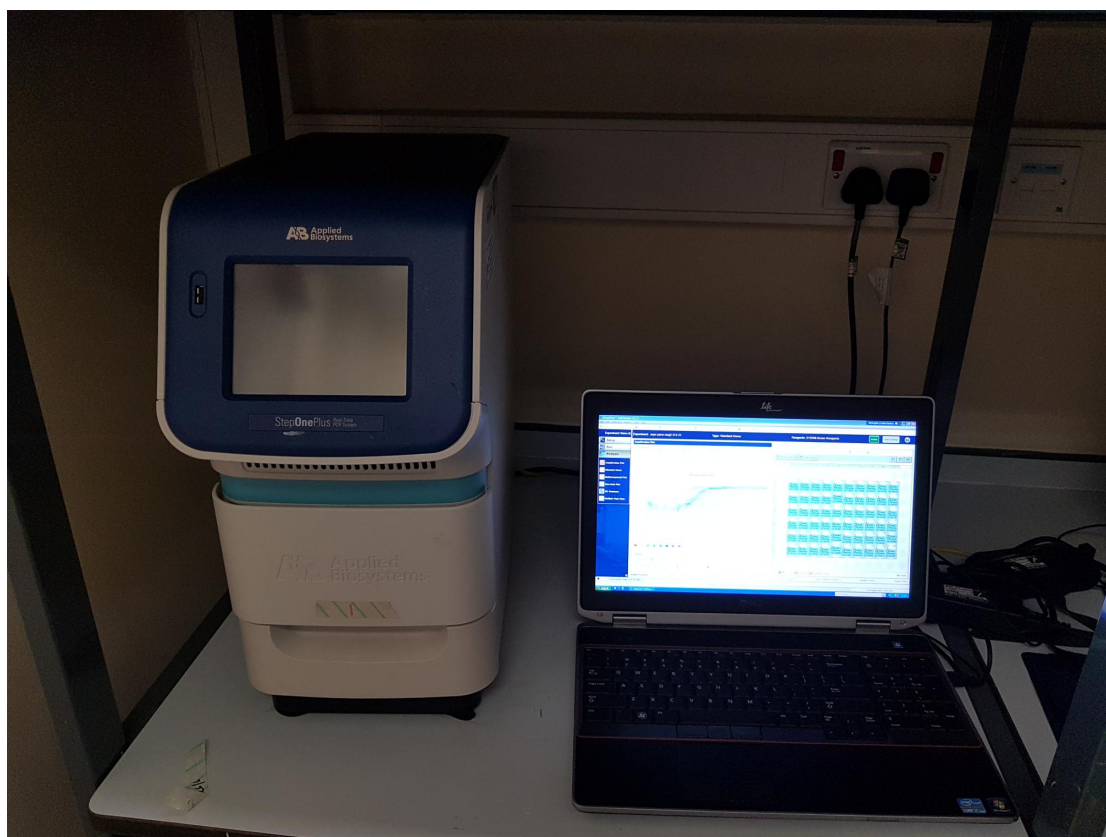


Fig.2.6. *Applied Biosystems® Step One Plus Real- Time PCR Thermocycler*

2.6. Protein extraction and protein quantification

For protein extraction cells were cultured in a T75 flask until 70 – 90% confluent. A sterile scrapper was used do detach cells which were then transferred to a universal container and centrifuged at 1600 rpm for 5 minutes in cold PBS. The supernatant was discarded and the acquired cell pellet was then resuspended in 100-300 µl of cell lysis buffer (dependent on size of pellet) and transferred to a 1.5 ml eppendorf. The eppendorfs were loaded onto a Labinco rotating wheel (Wolf laboratories, York, UK, Fig.2.7.) set at 25 rpm for an hour at 4°C. The eppendorfs were then centrifuged at 15,000 rpm for 15 minutes. The supernatant containing the desired protein was then transferred to a new eppendorf and stored at -20°C or quantified immediately.



Fig.2.7. *Labincos rotating wheel (Wolf laboratories, York, UK)*

Quantification of protein in samples was performed in order to standardize the amount of protein used in Western blotting. Protein quantification was carried out according to Bio-Rad DC Protein Assay kit using a micro-plate assay protocol (Bio-Rad Laboratories, Hemel-Hempstead, UK). Bovine serum albumin (BSA) was used as a standard. In a 96 well plate a graduated standard (50mg/ml serially diluted to 0.02mg/ml) was generated. Subsequently, 5 μ l of standard or protein samples were added in duplicate or triplicate to clean wells. Bio-rad DC Reagent A supplemented with Reagent S (1ml:20 μ l) was added to each well (standard wells and sample wells) and finally 200 μ l Bio-rad DC Reagent B added to each well. The plate was then left for 10 – 30 minutes

to allow the colorimetric reaction to occur.

Once developed, the plate was read in ELx800 plate reading spectrophotometer (Bio-Tek, Wolf laboratories, York, UK) with a wavelength setting of 620 nm. Readings were transferred on a spreadsheet, then a curve was generated from the standards, which was used to calculate the protein concentration of the samples being analyzed.

A uniform concentration of protein solution was prepared (depending on the lowest concentration sample). The protein samples were added to equal volume of 2X Laemmli buffer (Sigma-Aldrich, Dorset, UK), boiled at 100°C for 10 minutes in an oil heater and stored at -20°C.

2.6.1. Breast tissue cohort

A number of standardised proteins from paired normal and breast cancer tissue samples were available from the cohort described in Wazir et al 2012 and these were utilized for Kinexus protein array assay in our study.

Tissue samples studied in this cohort were originally collected from 1990 to 1994, 127 cancerous breast tissues and associated 33 non-cancerous tissues. The original samples were collected under ethical approvals issued by Bro Taf Health Authority (ethics approval numbers 01/4303 and 01/4046).

All the patients were treated according to local guidelines. Breast-conserving surgery was followed by radiotherapy. Oestrogen receptor (ER) positive patients received adjuvant endocrine treatment in the form of Tamoxifen. ER negative, high-grade cancers, and node-positive cases were treated with adjuvant therapy. No neo-adjuvant treatment was used. Collected anonymous clinicopathological data was collated into a database.

Sample collection followed institutional guidelines and ethical approval and informed consent were adhered to. A tumour sample and an associated non-cancerous tissue from within 2cm from the tumour area was taken, without affecting tumour margins assessment.

2.7. Kinexus and paired tissue samples

The antibody microarray used in our study was Kinextm Antibody Microarray-880 (KAM-880) (Kinexus Bioinformatics Corporation, BC, Canada) which track the differential binding of dye- or biotin- labelled proteins in lysates prepared from cells and tissues (168). This yields useful insights into differences in protein expression, covalent modifications such as phosphorylation, and protein-protein interactions and define antibody reagents.

KAM permits simultaneous probing of hundreds of target proteins and phosphorylation sites. KAM-880 utilizes an antibody microarray chip, which features 877 pan- and phosphosite-specific antibodies, which have been selected from more than 6000 different commercial antibodies to identify immunological reagents to track important signal transduction proteins. This assay was available at the of the study and as this field is constantly evolving, the currently offered microarray chip is KAM-1325 with about 627 unique proteins tracked.

To explore potential DAP-3 interacting partners paired normal and cancerous breast tissues (as described in section 2.6) were immunoprecipitated with a DAP-3 antibody (as mentioned in section 2.8) before being used on the Kinexus KAM-880 platform.

Patients chosen from this cohort were:

Patient ID 114, Grade 3 Invasive ductal carcinoma, Stage 2

Patient ID 135, Grade 3, Invasive ductal carcinoma, Stage 2

On completion of the instrument evaluation, the data of each protein probe were compared between normal (annotated as control) and tumour (annotated as treated) for the levels of fluorescence signal, the difference between two comparing pairs. This would allow interrogation of the degrade of a given protein interacted with DAP-3 and the difference between the two tissue types.

The candidate priority targets that interacted with DAP-3 were subject to analysis of their role in signalling pathways. This was done by way of Reactome (www.Reactome.org), an online tool for pathway exploration.

2.8. Sodium dodecyl sulphate-polyacrylamide gel electrophoresis (SDS-PAGE) and western blotting

SDS-PAGE was performed on 8%-12% resolving gels (depending on the protein being studied) and 5% stacking gels (according to modified Harlow and Lane formula) within which wells are made to contain the protein samples.

The resolving gel was prepared as described in table 2.5 and pipetted into a cassette, held upright with adequate space remaining for subsequent addition of the stacking gel. Following setting of the resolving gel the stacking gel was prepared (Table 2.5.) and overlaid on the resolving gel with a plastic comb added to allow formation of wells as stacking gel set.

Once the gels had set, the cassette was placed in an electrophoresis tank (Fig.2.8.), which was filled with running buffer (Tris-Glycine-SDS Buffer; Sigma-Aldrich, Dorset, UK). The combs to form the wells were removed, followed by loading of the samples. The first well was loaded with a molecular weight reference marker (Broad Range Marker sc- 2361;

Insight Biotechnologies, Middlesex, UK). OmniPAGE VS10 vertical electrophoresis system (OminPAGE, Wolf Laboratories, York, UK) was used (at 120V, 150 mA and 50W, 105mins) until sufficient separation was visualized by observing the molecular weight markers progression down the gel.



Fig. 2.8. *OmniPAGE VS10 vertical electrophoresis system (OminPAGE, Wolf Laboratories, York, UK)*

The cassette was then removed from the electrophoresis tank and the gel removed with the stacking gel being discarded. The resolving gel was placed in a SD10 SemiDry Maxi System blotting unit (Wolf Laboratories, York, UK) (Fig.2.9.) in a sandwich composition consisting of [anode, 3X filter paper, PVDF membrane, gel, 3X filter paper, cathode] for electroblotting (15V, 500mA, 50W, 50mins – depending on sizes of molecules transferred) to transfer protein samples onto the Immobilon-P PVDF Membrane (Merck Millipore Ltd / Sigma_Aldrich, Dorset, UK). Filter papers were pre-soaked in transfer buffer (Tris-Glycine buffer;

Sigma-Aldrich, Dorset, UK), and the PVDF membrane was initially activated briefly in methanol (Fisher Scientific, UK) before washing and soaking in transfer buffer.

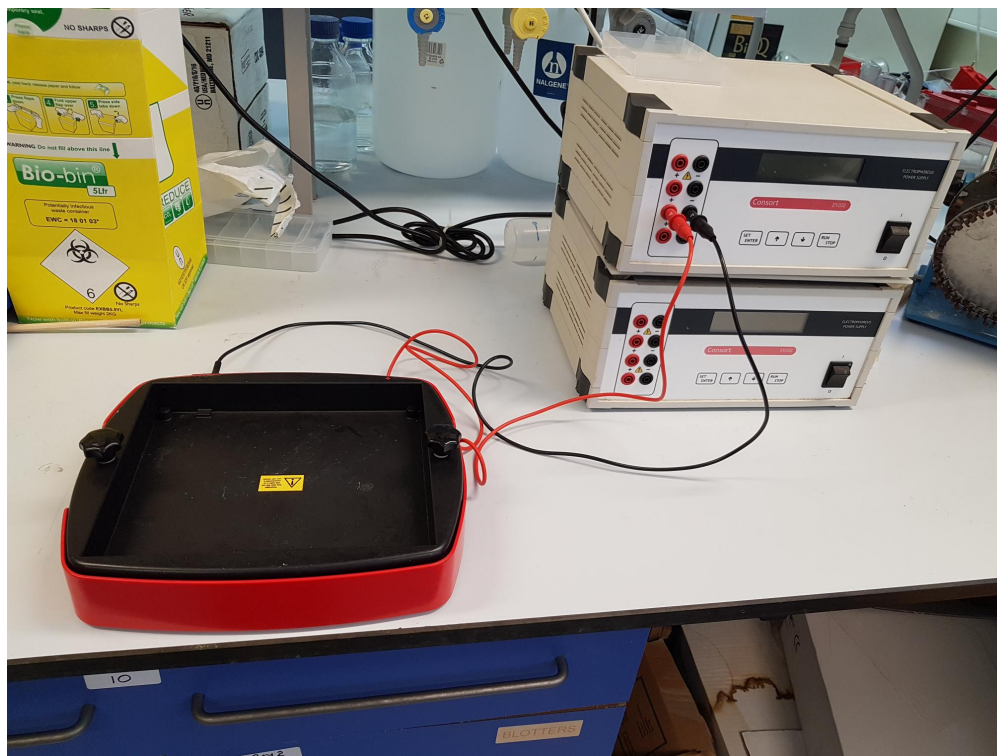


Fig.2.9. SD10 SemiDry Maxi System blotting unit (Wolf Laboratories, York, UK)

Antibody binding to the membrane was achieved on a Snap-id protein probing system (Merck Millipore Ltd / Sigma_Aldrich, Dorset, UK) (Fig.2.10.). Antibodies used for detecting specific proteins are listed in Table 2.6. and were used in higher than usual concentrations in accordance with the Snap-id recommended protocol. Initially, the membranes were washed with blocking buffer. The Snap-id instrument was initiated to suction the buffer through the membrane. The membrane was then incubated in the primary antibody for 10 minutes. The membranes were then three times washed under constant suction with washing buffer.

The membrane was then incubated in the secondary antibody (Anti-Mouse IgG produced in rabbit) for 10 minutes, then suctioned away and

as previously washed 3 times with washing buffer.

Subsequently, the membrane was developed using a EZ-ECL detection kit (Geneflow, Litchfield, UK), through addition of reagents and incubation for 30 sec – 5 mins in the dark.

Visualisation was achieved on G:BOX Chemi XRQ protein detection system (Syngene, Cambridge, UK) (Fig.2.11.).



Fig.2.10. Snap-id protein probing system (Merck Millipore Ltd / Sigma_Aldrich, Dorset, UK)



Fig.2.11. *G:BOX Chemi XRQ protein detection system (Syngene, Cambridge, UK)*

Table 2.5. Modified Harlow and Lane formula used to prepare Resolving and Stacking gels for western blotting

	5% stacking gel (5mls) for 2 gels	8% Resolving gel (15mls) for 2 gels	10% Resolving gel (15mls) for 2 gels	12% Resolving gel (15mls) for 2 gels
Distilled H2O	3.4 ml	6.9 ml	5.9 ml	4.9 ml
30% acrylamide mix	0.83 ml	4.0 ml	5.0 ml	6.0 ml
1.5 M Tris (pH8.8)	1.0 M Tris (pH 6.8) 0.63 ml	3.8 ml	3.8 ml	3.8 ml
10% Sodium dodecyl sulphate (SDS)	0.05 ml	0.15 ml	0.15 ml	0.15 ml
10% ammonium persulphate (APS)	0.05 ml	0.15 ml	0.15 ml	0.15 ml
TEMED	0.01ml	0.009 ml	0.006 ml	0.006 ml

Table 2.6. Primary Antibodies used for probing

Antibody name	Supplier, code	species	dillution
DAP-3	BD 610051	mouse	1:150
HSP90	SC 4772	mouse	1:100
GAPDH	SC 374182	mouse	1:300

2.9. Co-immunoprecipitation

DAP-3 antibody (50 µl, 1/150 dilution) was added to standardised protein in Eppendorf tube (100 µl) and placed for 24hrs onto a Labinc rotating wheel (Wolf laboratories, York, UK) set at 25 rpm at 4°C (Fig.2.7). Following this 20 µl Protein AG with agarose beads (Insight Biotechnologies, Middlesex, UK) was added to the eppendorf and loaded onto the rotating wheel for 60 mins at 25 rpm at 4°C. Subsequently the samples were centrifuged at 7500 rpm for 5 mins, supernatant discarded and the pellet washed with lysis buffer - this was repeated twice and following this, pellets were resuspended in 1X Laemmli buffer and boiled at 100°C for 5mins, then stored at -20°C. Non-precipitated proteins were also prepared in Laemmli buffer and boiled to allow detection of GAPDH and other molecules of interest in non-precipitated samples.

2.10. Reamplification of DAP-3 knock-down plasmids

DAP-3 knockdown plasmids had been prepared as part of previous study in our laboratory as reported by Jia et al. (17). This was tested and reported to be a highly effective and specific tool to knockdown DAP-3 from cancer cells.

This anti-DAP-3 ribozyme transgene was initially developed by discovering a suitable target site by the hammerhead ribozyme based on the secondary structure of human DAP-3 mRNA (Fig 2.12). As previously described (17), a touch down PCR was employed to generate the ribozyme, before being cloned into a mammalian vector. The amplified ribozymes were cloned into the pEF6/V5-His TOPO TA plasmid vector (Invitrogen, Paisley, UK) (Figure 2.13). The vector carried selection markers, allowing selection with antibiotics in both mammalian cells (blastidicin) and prokaryotic *E.coli* cells (ampicillin).

From a limited stock available in the host laboratory, we reamplified the plasmids for our stock in the current study.

Cloning of the ribozyme transgene plasmids was accomplished by using the OneShot TOP10 chemically competent *E. coli* and associated protocol. 1 µl of the cloning product (dsDNA) was added to 25 µl of One Shot TOP10 Chemically Competent *E. coli* and incubated for 30 minutes on ice. This was then suddenly placed in a water bath of 42°C for 30 seconds ('heat shock') and subsequently placed on ice. 250 µl of SOC medium was added and the samples were shaken horizontally at 200rpm for 1 hour at 37°C on a horizontal orbital shaker (Bibby Stuart Scientific, UK). Following this the samples were added directly to universal containers containing 100µg/ml ampicillin supplemented LB broth (one tube per sample) and incubated overnight.

Plasmid extraction was performed using the Sigma GenElute Plasmid MiniPrep Kit and protocol (Sigma-Aldrich, Dorset, UK). Universal containers containing samples were centrifuged for 5 minutes at 3000 rpm and supernatant discarded. Subsequently, re-suspension solution, containing RNase, was added to and used to resuspend the pellet before transferring to a 1.5ml eppendorf and lysing by adding 200 µl of lysis buffer and mixing through gentle inversion for no longer than 4 minutes. Following this 350 µl of Neutralization/binding solution was added and then centrifuged at 12,000 rpm for 10 minutes.

A GenElute MiniPrep Binding column was inserted into each collection tube and 500 µl of Column preparation solution added to each Miniprep column. This was centrifuged at 12,000 rpm for 1 minute and the flow through liquid was discarded. The clear cell lysate was then added to the column and centrifuged at 12,000 rpm for 1 minute and again the flow through liquid was discarded.

700 µl of wash solution (containing ethanol) was added and centrifuged at 12,000 rpm for 1 minute with the flow through liquid being discarded. This process was repeated twice.

The Miniprep column was transferred to a fresh collection tube. Plasmid DNA was eluted as a result of adding 50 µl of elution solution and spinning the column at 12,000 rpm for 1 minute and then further adding 20µl of elution solution and again centrifuging 12,000 rpm for 1 minute. We have used these samples to check plasmid orientation using a combination of plasmid specific (T7F) and ribozyme transgene specific (RbToPF and RbBMR) primers. This product was then stored at -20°C.

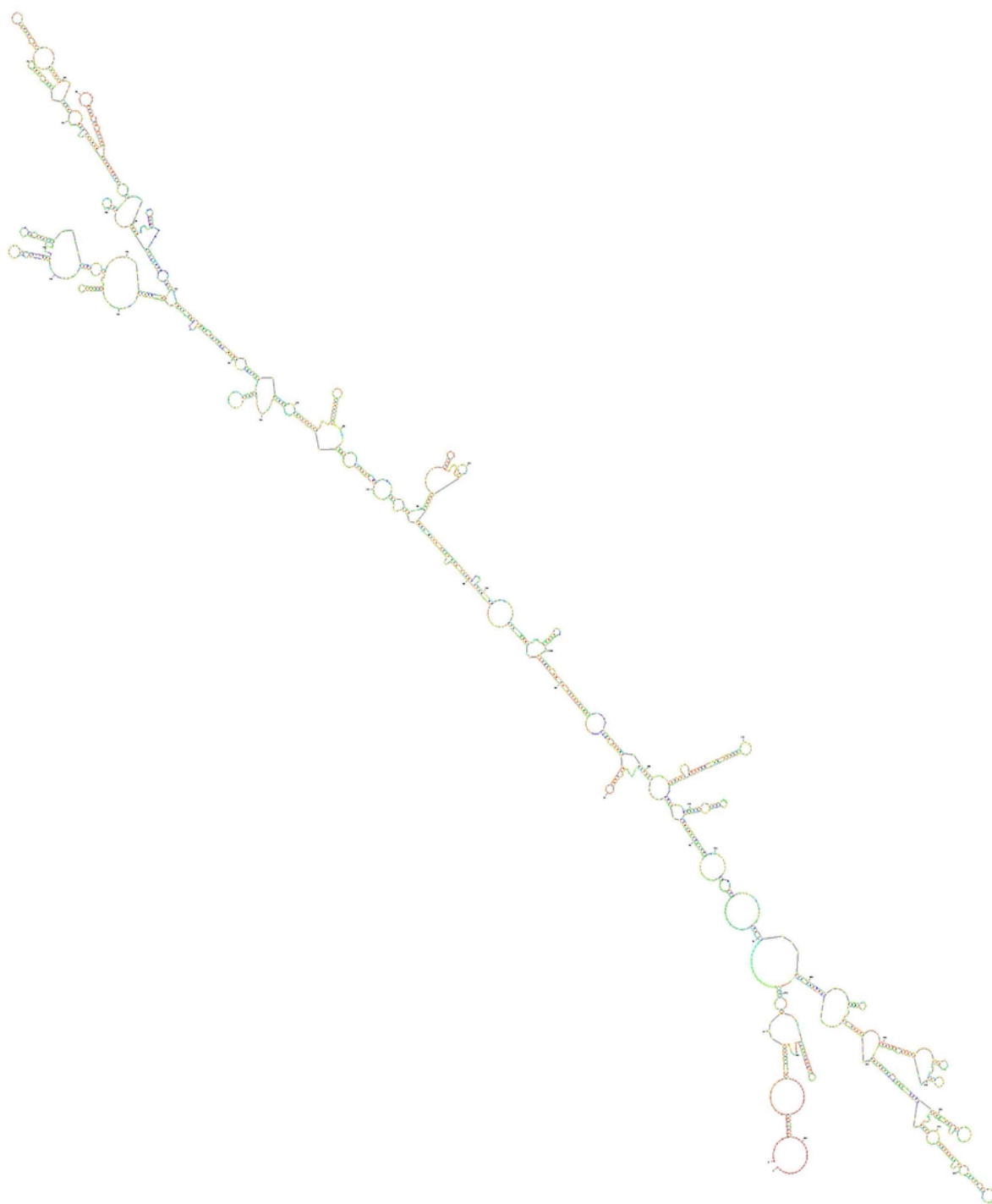


Figure 2.12. Secondary structure of human DAP-3 mRNA, generated using the Zucker RNA programme (Provided by CCMRC host laboratory).

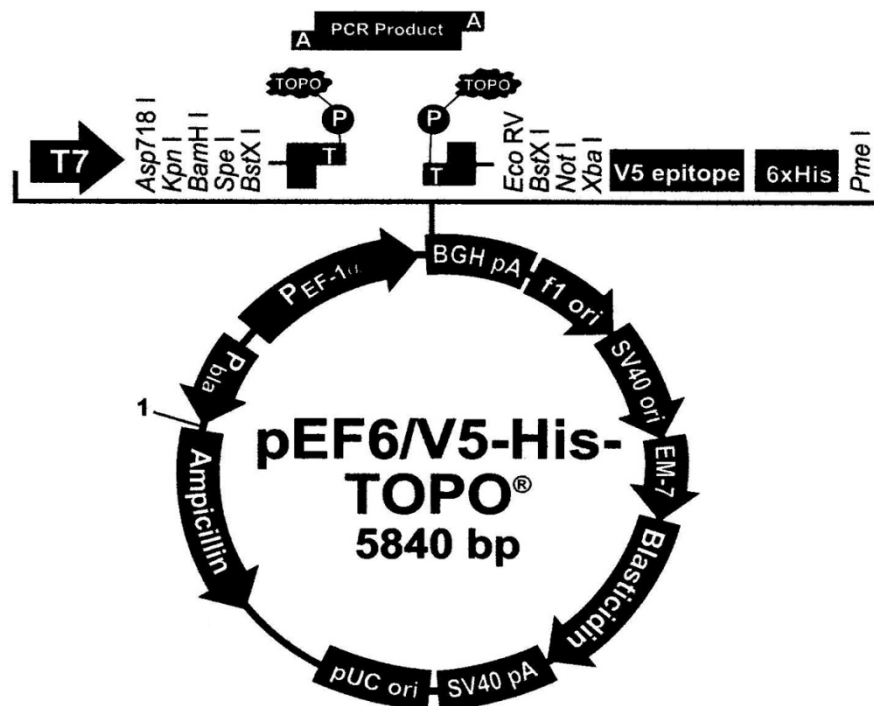


Figure 2.13. pEF6 Vector used in constructing the anti-DAP-3 ribozyme transgene (<https://www.thermofisher.com>).

2.11. Transfection of anti-DAP-3 ribozyme transgene into breast cancer cell lines

Wild type MCF-7 and MDA-MB-231 cells were detached from tissue cultures flasks, transferred to universal containers and centrifuged at 1600rpm for 6 minutes. Supernatant was discarded and remaining pellets resuspended in 2 ml of growth medium. Cells were counted using a haemocytometer and a suspension of 1,000,000 cells in 800 μ l generated for each cell line. To each aliquot of the cell suspension, 3-5 μ g of purified plasmid solution was added consisting of either a closed control pEF6 plasmid or a pEF6 plasmid containing a DAP-3 specific ribozyme transgene. The mixture was prepared in an electroporation cuvette (Geneflow, Litchfield, UK), which was then slotted into an electroporator (Gene Pulser Xcell, Bio-Rad, Hemel-Hempstead, UK). The cells were then subjected to an electrical pulse of 290V and 1000 μ F for MCF-7 and 310V and 1500 μ F for MDA-MB-231.

Following electroporation, the cells were transferred to tissue culture flasks containing pre-warmed growth medium and incubated.

After 1-2 days of incubation, growth medium was changed to selection growth medium containing 5 μ g/ml of blasticidin S. This triggers the selection process lasting 5-7 days. Over this period selection medium was replaced every 2 – 3 days, depending on the levels of cell death, with fresh selection medium. Following this period resistant populations of cells could be observed under the microscope and the selection medium was replaced with maintenance medium containing 0.5 μ g/ml of blasticidin S which was subsequently used in for maintaining the growth of the transfected cell line.

2.12. Functional assays

2.12.1. Growth assay

This assay was used to determine growth of the selected cell line (modified methodology from Bonnekoh, Wevers et al. 1989)

Three identical 96 well plates were seeded with 6 replicates per cell line (3000 cells in 200 µl growth medium per well) and incubated. Plates were either incubated for over-night (reference plate), 3 days or 5 days. Following appropriate incubation, the medium was aspirated from all wells and 200µl of 4% formalin (Fisher Scientific, UK) added for 10 minutes before removal and addition of 200 µl of 0.5% crystal violet (Sigma-Aldrich, Dorset, UK) for 5 minutes. The crystal violet was then washed off and the plates allowed to dry before adding 200 µl of 10% Acetic acid (Sigma-Aldrich, Dorset, UK) was pipetted to each well, mixed to dissolve the cell stain and then read in an ELx800 plate reading spectrophotometer (Bio-Tek, Wolf laboratories, York, UK) with a wavelength setting of 540 nm.

Spectrophotometer readings were then processed with percentage change from the reference plate calculated at 3 and 5 day periods.

2.12.2. Adhesion assay

Adhesion assays were used to assess the ability of cells to adhere to an artificial basement membrane which was simulated by Matrigel (Corning, Flintshire, UK).

Matrigel is mixture of proteins secreted by Engelbreth-Holm-Swarm (EHS) mouse sarcoma cells and is found to adequately simulate a natural basement membrane for purposes of studying tumour cell interactions.

This assay was performed in a 96 well plate with 6 replicates per cell line. The bottom of each well was coated with Matrigel (5 μ g/100 μ l using Serum Free DMEM) and dried in oven for 2 hours before rehydrating the matrigel layer with serum-free DMEM for 30 minutes. This medium was subsequently aspirated before seeding 40,000 cells in 200 μ l DMEM into each well.

Following incubation for 45 minutes the medium in wells was discarded, non-adherent cells removed through washing with PBS and 200 μ l 10% Formalin pipetted into each well. After 10 minutes, the formalin was removed and 200 μ l of 0.5% crystal violet was added to each well following which after 5 minutes liquid content of wells was carefully washed off and wells were let to dry.

Adherent cells were consequently assessed under a microscope at 20x objective magnification with pictures of 3 representative fields per well taken (Fig.2.14.) and Image J program (US National Institutes of Health, Bethesda, Maryland, USA) was used to count cells.



Fig.2.14. *Olympus CKX31 microscope*

2.12.3. Invasion assay

Invasion assays were used to assess the ability of studied cells to invade through a basement membrane which was simulated by 8.0 μm pore Falcon well inserts pre-coated in Matrigel (50 $\mu\text{g}/100\ \mu\text{l}$ using Serum Free DMEM). 24 well Greiner plates, housing inserts were used, with 3 replicates per sample (Fig.2.15).

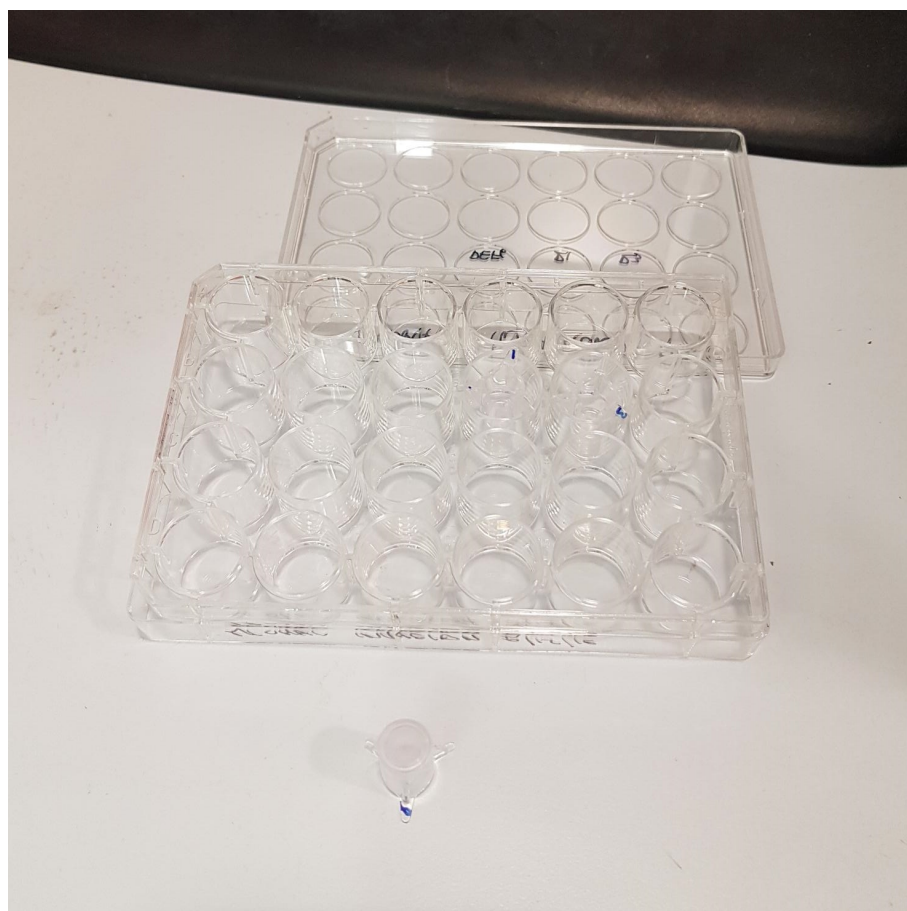


Fig.2.15. 24 well Greiner plate with an 8.0 μ m pore Falcon well insert

Once dried, Matrigel was rehydrated with serum free DMEM over 30 mins and medium was discarded. 1 ml of DMEM was pipetted into the 24 wells followed by carefully placing insert into wells. Subsequently 40,000 cells in 200 μ l of DMEM were seeded into each insert and incubated for 3 days.

After incubation, medium was removed, and inserts were removed from wells and 200 μ l of 4% Formalin placed in the wells. The inside of the inserts were cleaned with a cotton swab to remove matrigel and remaining non-invasive cells and the undersides of the inserts were fixed in 4% formalin by placing the inserts back to the formalin containing wells for 10 minutes before staining with 0.5% crystal violet, washing and leaving to dry.

Cells that had successfully invaded the simulated basement membrane and progressed to the underside of the insert were then assessed under a microscope using 20X objective magnification with pictures of 3 representative fields per well taken and Image J program (US National Institutes of Health, Bethesda, Maryland, USA) was used to count cells.

2.12.4. Scratch wounding assay

Cell migration was examined using scratch wounding assay. 24 well Greiner plates were used, with 3 replicates per cell line. 400,000 cells in 1ml DMEM were seeded and cultured until a confluent monolayer was formed. A scratch was made through each monolayer with a sterile pipette tip, the monolayer was washed gently in PBS and allowed to recover for 10 minutes in the incubator before pictures taken under microscope with 20X objective magnification at this start point of the experimental procedure. Subsequently further pictures taken at 1, 2, 3, and 4 hours from initial scratch in a defined consistent location along the scratch. The width of the scratch was measured by 3 separate readings, per scratch, with Image J program (US National Institutes of Health, Bethesda, Maryland, USA) and these were then processed to calculate the length that the scratch fronts had migrated from the initial image.

2.13. Small molecule inhibitors

HSP90 small molecule inhibitor (Benzisoxazole Hsp90 inhibitor; purchased from Santa Cruz Biotechnologies Inc., Santa Cruz, California, USA) was used to treat MCF-7 and MDA-MB-231 cells either in concentration gradient or time gradient (Table 2.7.). Benzisoxazole (SC-223790, Chemical ID CAS 1012788-65-6) is known to bind to the N-terminal domain of

the HSP90 protein and blocking the docking of the HSP90 protein partners. The IC₅₀ for Benzisoxazole is 30nM on multiple cell types. In our complex cell models, in which DAP-3 expression was knocked down, Benzisoxazole was used to suppress the activity of HSP90.

Table 2.7. *HSP90 small molecule inhibitor Concentration gradient and Time gradient*

Concentration gradient (nM)	0	3	15	30	150	300
Time gradient (hrs)	0	0.5	1	2	4	24

Cells were prepared in a 6 well plate. For the concentration gradient experiments increasing concentrations of the HSP90 small molecule inhibitor were used (0,3,15,30,150 and 300 nM). These were incubated for 4 hours. For the time gradient experiments cells were treated with 30nM concentration of the HSP90 small molecule inhibitor for 0, 0.5, 1, 2, 4, 24 hour periods. Following appropriate incubation, cells were subject to RNA extraction as outlined in section 2.3.

This protocol was used to determine the expression of DAP-3 in HSP90 small molecule inhibitor treated WT cell lines and also in functional studies in DAP-3 KD cell lines.

2.14. Statistical analysis

Statistical analyses were carried out using SigmaPlot 11.0 software (Systat Software, Inc., San Jose, California, USA). Statistical methods conducted were t-test, Mann Whitney, ANOVA. Survival analysis was carried using SPSS26. Methods used in each dataset are given in the respective chapters. Experimental procedures

were undertaken a minimum of three independent times and statistical significance was taken as $p < 0.05$.

CHAPTER 3

Screening and establishment of DAP-3 modified breast cancer cell lines

3.1. Introduction

DAP-3 expression varies across the spectrum of different cancers in humans. It is also varied in terms of lower/higher expression levels being associated with prognosis. 5-year survival analysis in liver, head and neck, renal and pancreatic cancer show higher expression levels and are associated with decreased survival. In liver and renal cancer higher expression of DAP-3 is considered a negative prognostic indicator (143). In contrary, lower expression of DAP-3 appear to have positive effects on survival in urothelial and cervical cancer, although reaching significance only in cervical cancer group (143). DAP-3 protein expression appears to be detected in almost all tissues at variable levels. DAP-3 mRNA distribution does not seem to be tissue or cell type specific and appears to be present in all tissues (144)

In a study completed in our laboratories previously, the expression of DAP-3 mRNA in breast cancer was demonstrated to decrease with increasing Nottingham Prognostic Index (NPI2 vs. 3, $p=0.036$), TNM stage (TNM1 vs. 3, $p=0.07$), and tumour grade (grade 1 vs. 3, $p=0.08$). Lower DAP-3 expression levels were significantly associated with local recurrence ($p=0.013$), distant metastasis ($p=0.0057$) and mortality ($p=0.019$) (152) and explored the functional impact of DAP-3 in breast cancer cells (153). The cell cultures utilised in the above study were MDA-MB-231 and MCF-7 breast cancer cell lines. We have opted to use the same breast cancer cell lines in our experiments (as described in Methods section 2.1.) and our work with functional assays followed on from this study (153). These cell lines are commonly used as an *in vitro* model of breast cancer and represent 2 different variants. MDA-MB-231 is a triple negative breast cancer representing a more aggressive disease. MCF-7 is commonly opted for when a less aggressive breast cancer cell line is sought as it is

oestrogen and progesterone receptor positive and modelling an early-stage disease.

In this chapter we aimed to investigate the levels of DAP-3 expression across a number of breast cell lines and generated new breast cancer cell models to further explore the relationship between DAP-3 and breast cancer in the subsequent chapters of the thesis.

3.2. Methods

3.2.1. Cells and Cell culture

Eight breast cancer cell lines and 1 benign breast cell line of human origin (as described in Chapter 2.1.) were used for DAP-3 PCR screen.

Wild type MCF-7 and MDA-MB-231 cells were grown in DMEM medium. Transfected cells were cultured in DMEM medium supplemented with blasticidin S (5µg/ml) for selection post transfection and subsequently for maintenance in a lower concentration (0.5µg/ml) of blasticidin S following the selective period (as detailed in Chapter 2.1.).

3.2.2. RNA extraction, quantification and cDNA synthesis

The TRI Reagent protocol was followed for cell RNA extraction. RNA was precipitated from a top RNA phase following separation of cell lysate which was obtained when TRI reagent was applied to desired cells. The precipitated RNA in a pellet was washed with DEPC water and ethanol solution. The pellet was consequently dissolved

in DEPC water, RNA was quantified using a Nanophotometer and standardized.

GoScript™ Reverse Transcription kit was used for reverse transcription of obtained RNA. Together with OligodT primer this was incubated, following which RT mix was added and further incubation was undertaken and cDNA acquired. Details of this process are described in Chapter 2.2.

3.2.3. Polymerase Chain Reaction (PCR)

PCR was performed to amplify desired gene region sequences utilising specific primers listed in Table 2.3. Following amplification, electrophoresis was used for separation according to size. Visualisation was achieved using a U:Genius3 gel doc system (Syngene, Cambridge, UK). Full details of this method were described in Chapter 2.3.

3.2.4. Protein extraction and quantification

The cells from confluent flasks were detached, centrifuged and consequently lysed by applying lysis buffer. The acquired protein was then stored at -20°C.

To standardise the amount of the obtained protein quantification was carried out according to Bio-Rad DC Protein Assay kit used in a Micro-plate Assay Protocol.

A graduated standard was created utilising Bovine serum albumin in 96 well plate with subsequent addition of protein samples. Further reagents were added according to the protocol and once developed the plate was read in

ELx800 plate reading spectrophotometer. From the readings a curve from the standards was generated and used to calculate concentration of the protein samples analysed. Depending on the lowest sample concentration a uniform protein concentration was prepared with Laemmli buffer addition, boiled and stored at -20°C. Details of this method were described in Chapter 2.5.

3.2.5. SDS-polyacrylamide gel electrophoresis (SDS-PAGE) and Western blotting

SDS-PAGE was performed on 8%-12% resolving gels and 5% stacking gels. Protein samples were separated and transferred onto PVDF membrane utilizing electrophoresis systems. Antibodies for detecting specific proteins (as listed in Table 2.6.) were used and then visualization was achieved. Full details of this method are listed in Chapter 2.7.

3.2.6. Reamplification of plasmid, plasmid extraction and confirmation of ribozyme insert orientation

DAP-3 knockdown plasmids (prepared as part of a previous study outlined in by Jia et al. (169)) were reamplified in OneShot TOP10 chemically competent *E. coli* and associated protocol. Following this, plasmid extraction was undertaken using the Sigma GenElute Plasmid MiniPrep Kit and protocol. Correct orientation of the ribozyme transgene inserts in the plasmid was confirmed using a combination of plasmid specific and ribozyme transgene specific primers (as described in Chapter 2.9.).

3.2.7. Transfection of pEF6/V5-HIS TOPO TA vector containing DAP-3 ribozyme into breast cancer cell lines

A closed control pEF6 plasmid or a pEF6 plasmid containing a DAP-3 specific ribozyme transgene were

transfected, using electroporation method, into wild type MCF-7 and MDA-MB-231 cells. This was followed by selection in Blasticidin S (5µg/ml) containing medium. Full details of this method are described in Methods section 2.11.

3.2.8. RT-qPCR

Primers of selected molecules designed for target gene amplification were used for RT-qPCR. Positive control was utilised to validate specificity of used primers. PCR amplification was performed and qPCR data were analysed and normalized to GAPDH. Full details of this method were described in Methods section 2.4.

3.3. Results

3.3.1. PCR screening of DAP-3/GAPDH expression in 9 Breast cell lines

Conventional PCR was used to screen DAP-3 expression and the housekeeping GAPDH gene in 8 breast cancer cell lines and 1 benign breast tissue cell line (Fig 3.1.). DAP-3 expression was observed in the majority of breast cancer cell lines. This has further demonstrated a decreased expression in MDA-MB-361 and a mild decrease in BT-483 and MDA-MB-231.

Previous studies in our laboratories had used MDA-MB-231 and MCF-7 as model systems to explore DAP-3 in breast cancer (153). The aims of the current research were to explore mechanistic implications of DAP-3 in breast cancer. Therefore, we chose these previous model lines for the purposes of our current studies.

These 2 cell lines are well fitting representatives of breast cancer dynamics as MDA-MB-231 represents a more aggressive variant

being a triple negative breast cancer and MCF-7 represents a model of early-stage breast cancer with oestrogen and progesterone receptor positivity.

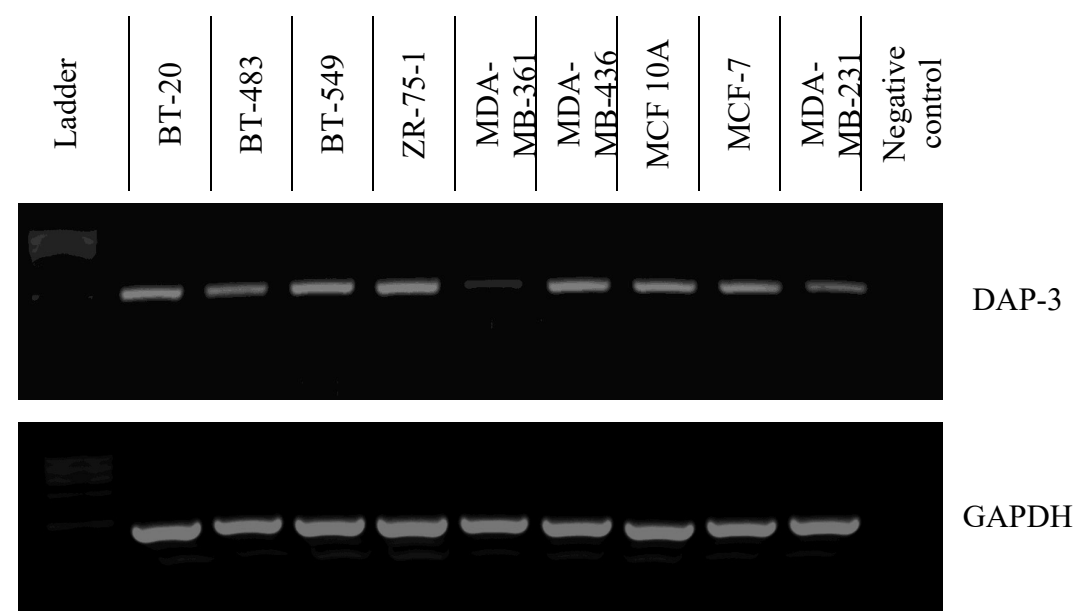


Fig.3.1. Expression analysis of DAP-3 and GAPDH in 9 cell lines using conventional PCR. Decreased expression in MDA-MB-361 and a mild decrease in BT-483 and MDA-MB-231. GAPDH is utilised as a house-keeping control. Representative data shown.

3.3.2. Western blot screening of DAP-3/GAPDH expression in chosen MCF-7 and MDA-231 cell lines

Western blot screening of DAP-3 and GAPDH protein expression was performed in chosen cell lines (MCF-7 and MDA-MB-231) (Fig.3.2.). Both MCF-7 and MDA-MB-231 were shown to express DAP-3 protein at the expected size.

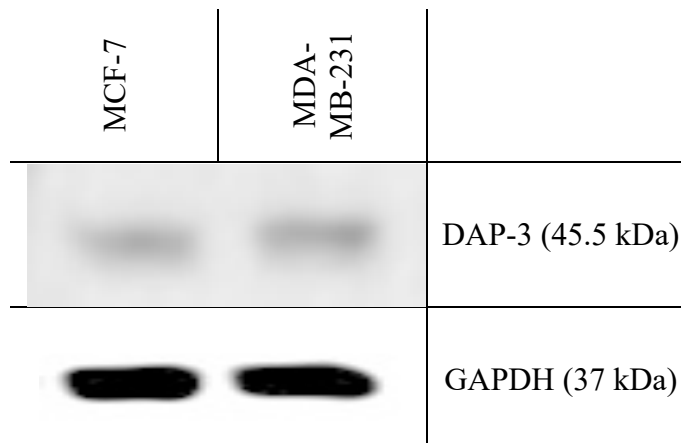


Fig.3.2. Western blot analysis of DAP-3/GAPDH protein expression in MCF-7 and MDA-MB-231 breast cancer cell lines. Representative data shown, GAPDH expression presented as housekeeping gene.

3.3.3. Reamplification of DAP-3 ribozyme plasmids, plasmid purification and orientation checking

Plasmids containing DAP-3 ribozyme transgenes had previously been generated and utilised in the host department (153, 169). DAP-3 ribozyme plasmids available for targeting DAP-3 are outlined in Table 3.1. For the use in the current study, re-amplification of these plasmids and subsequent confirmation of correct orientation of the insert was undertaken to generate stocks.

Table 3.1. List of DAP-3 ribozyme plasmids available for re-amplification. (Ribosome 1-3, Bacterial colonies 2,5,6,7,8,11)

DAP-3 Rib 3 (Col 6)
DAP-3 Rib 3 (Col 2)
DAP-3 Rib 3 (Col 8)
DAP-3 Rib 3 (Col 11)
DAP-3 Rib 1 (Col 5)
DAP-3 Rib 2 (Col 8)
DAP-3 Rib 1 (Col 7)

Following re-amplification and plasmid extraction, their presence was verified and their size confirmed between 5-6kDa (in accordance with the 5840bp size of the plasmid) against a PCR High Ranger ladder (GeneFlow, Litchfield, UK) through gel electrophoresis of plasmid samples (Fig.3.3.). Following this, orientation checking was performed through PCR using T7F, RbTopF, RbBMR primers. Two separate reactions were tested on the reamplified plasmids. Products in the first primer combination, TF7 vs RbTopF, represented incorrect orientation of the insert whereas products in the second, TF7 vs RbBMR, represented the correct orientation of the insert. All re-amplified plasmids showed positive expression in the correct orientation reaction, with no expression noted in the incorrect orientation reaction, which confirmed correct insert orientation of all amplified plasmids (Fig 3.4.).

DAP-3 Rib 1 (Col 5), DAP-3 Rib 2 (Col 8), DAP-3 Rib 3 (Col 2) ribozyme plasmids were selected for use for the knock-down of DAP-3 in MCF-7 and MDA-MB-231 cell lines.

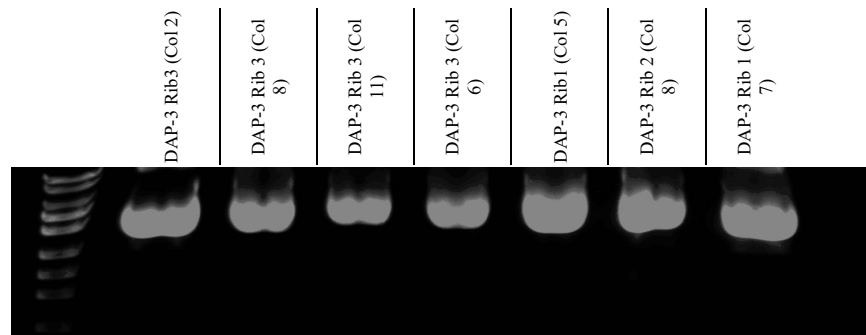


Fig.3.3. PCR Verification of plasmid presence and size confirming size between 5-6kDa after amplification and size separation using gel electrophoresis.

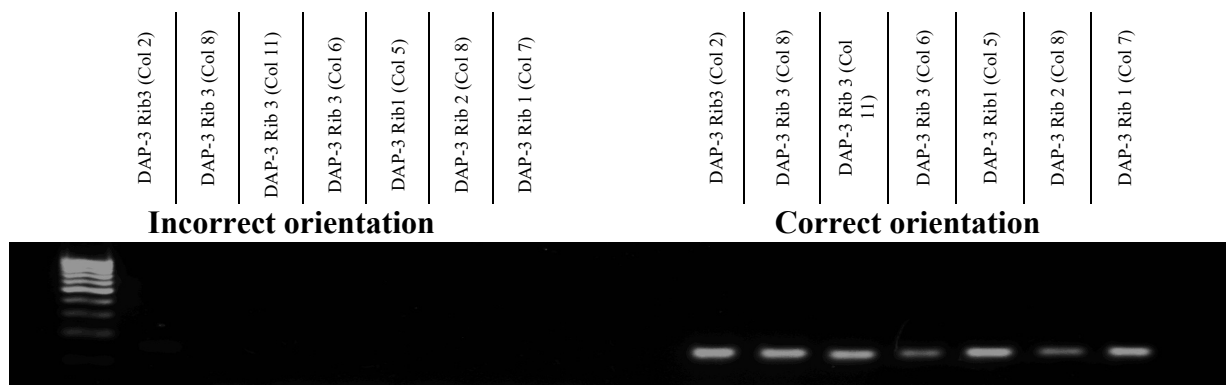


Fig.3.4. PCR Orientation check of all amplified plasmids. Primer combination TF7 vs RbTopF represented incorrect orientation (Left) and TF7 vs RbBMR represented the correct orientation (Right).

3.3.4. Quantitative PCR confirmation of DAP-3 knockdown in MCF-7 and MDA-231 cell line models (qPCR)

DAP-3 expression was knocked down in MCF-7 and MDA-MB-231 breast cancer cell lines using ribozyme transgene technology and verified at the transcript level using quantitative polymerase chain reaction (qPCR).

MCF-7 and MDA-MB-231 cell lines were transfected with either pEF6 control plasmid or plasmids containing DAP-3 ribozyme transgene 1, 2 or 3. Following selection and quantification of transcript expression ribozyme transgene 1 and transgene 3 showed most effective and statistically significant knockdown of DAP-3 in MCF-7 and MDA-MB-231 respectively, with both demonstrating a significant reduction in comparison to the respective pEF6 control cell lines (both $p < 0.05$) (Fig 3.5.).

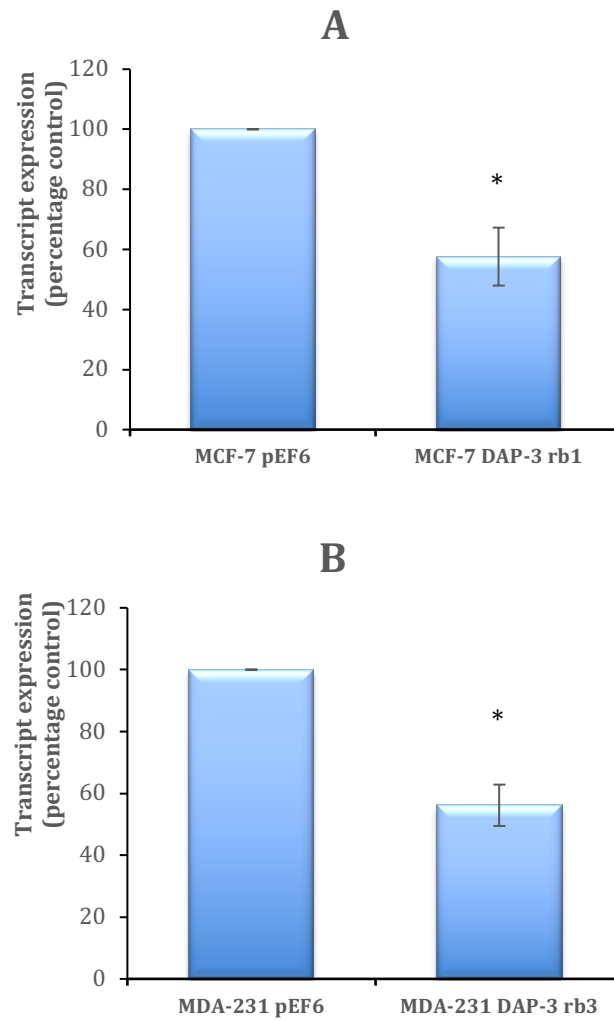


Fig.3.5. Expression of DAP-3 in MCF-7 (A) and MDA-MB-231 (B) DAP-3 KD cell lines and pEF6 controls using qPCR. Confirmation of DAP-3 transcript knockdown in (A) MCF-7 and (B) MDA-MB-231 cell lines following transfection with DAP-3 ribozyme transgenes in comparison to the relative plasmid control line. Data shown represents mean percentage pEF6 control from of a minimum of 3 samples. * represents $p < 0.05$. Error bars represent SEM.

3.4. Discussion

A variety of 9 cell lines has been selected for screening of DAP-3. They represent a combination of various breast cancer types as well as 1 benign breast tissue - fibrocystic change. All were confirmed to express DAP-3 in our experiment, although there was some variability detected. This would be in keeping with findings in The Human Protein Atlas describing variability in DAP-3 expression in various tissues. Variability in DAP-3 expression in breast cancer though does not appear to have impact on prognosis where 5-year survival in low vs high expression demonstrate very similar outcomes (143, 144). Han *et al.* in their study utilised RNA-seq dataset from the Cancer Genome Atlas (TCGA) to analyse the expression of DAP-3 across a selection of human cancers and their paired non-tumour tissues. There appears to be variability in the expression levels of DAP-3 comparing the various non-tumour tissues and they demonstrate that, compared to tumour samples, there is significant upregulation of DAP-3 expression in 17 out of the 22 cancer types including breast cancer (150, 170). The observed differences could be due to the nature of the experiment (i.e., qPCR detection vs RNA-seq), cohort size and or composition but further work is required to further evaluate this.

The combination of cell lines chosen (MCF-7 and MDA-MB-231), represents model scenarios simulating early and late-stage breast cancer. This combination has been also utilised in a previous study in our laboratories (153) and we have aimed to replicate this to further explore the downstream effectors of DAP-3 in additional experiments.

We have established knock down variants of MCF-7 and MDA-MB-231 cell lines using ribosome transgene technology. This technology was used to be able to better correlate our results with Wazir *et al.* study and since it remains an effective approach. Knock down in both cell lines in our experiments was confirmed by qPCR verification and reached significance. The generation of such models will facilitate further

experiments to explore potential interactions, mechanistic actions of DAP-3 in breast cancer and functional effects of such mechanisms in the later sections of this thesis.

Chapter 4

Potential interactions and mechanistic actions of DAP-3 in breast cancer

4.1. Introduction

As discussed in Chapter-1, DAP-3 has shown a number of links to human cancers and has been implicated in a range of activities, both as potential predictive factors for outcomes, influencing cellular functional assays and potentially influencing cancer cell resistance to chemotherapeutic agents. These aspects are discussed in greater detail in later chapters of this thesis. Collectively, therefore, DAP-3 appears to be an interesting and important molecule though currently research is limited. Importantly, research into the mechanisms through which DAP-3 exerts its functions in relation to cancer remain to be fully elucidated. A previous study by Wazir et al. (153) explored the transcriptional impact of DAP-3 suppression on caspase-8, caspase-9, DELE, IPS1, p21 and cyclin D1, identifying a significant or borderline significant decrease in caspase-9 and IPS1 expression following knockdown of DAP-3 in MCF-7 but not MDA-MB-231 cell lines. Establishing the effector pathways linked to DAP-3's role in cancer will provide additional vital information in therapeutic and biomarker design. DAP-3 has been identified as a protein predominantly located intramitochondrially, although in smaller quantities it has been found in cell cytoplasm. The interactions between DAP-3 and other proteins, including signalling proteins remain unknown. The central purpose of this chapter was to comprehensively explore proteins that interacted with DAP-3 in breast cancer cells, by way of a protein antibody array. The study went on to determine the promising pathways associated with DAP-3 in breast cancer cells. Such pathways of interest are explored further in the later chapters.

4.2. Materials and Methods

4.2.1. Cells and Cell Cultures

Eight human breast cancer cell lines and 1 benign breast cell line (as described in Chapter 2.1.) were used for PCR screening.

MCF-7 and MDA-MB-231 were routinely cultivated in maintenance DMEM medium, supplemented with FCS. Where transfections were taken place as indicated in Chapter-2 and stated later in the chapter, DMEM medium containing blasticidin S was used for selection (5µg/ml) post transfection and for maintenance (0.5µg/ml), following the selective period and for routine culture (as described in Chapter 2.1.).

4.2.2. RNA extraction, quantification and cDNA synthesis

For cell RNA extraction the TRI Reagent protocol was adhered to. Precipitated RNA was obtained after TRI reagent was applied to desired cells. RNA was dissolved in DEPC water and subsequently quantified and standardized.

GoScript™ Reverse Transcription kit was used for reverse transcription of obtained RNA and cDNA was acquired. Details of this process were described in Chapter 2.2.

4.2.3. Protein extraction and quantification

As stated in Chapter-2, the cells were lysed by applying lysis buffer. The acquired protein was then stored at -20 °C. Quantification was performed according to Bio-Rad DC Protein Assay kit used in a micro-plate Assay Protocol to standardise the amount of the acquired protein. A graduated bovine serum albumin standard with protein samples was pipetted to 96 well plate with addition of reagents according to the protocol. Once developed, the plate was read by spectrophotometer creating a curve from generated readings and used to calculate concentration of the protein samples. A uniform protein concentration was prepared with Laemmli buffer addition, boiled and stored at - 20°C. Details of this method were described in Chapter 2.5.

4.2.4. Co-Immunoprecipitation

DAP-3 antibody (Table 2.6.) was added to standardised protein and placed for 24hrs onto a Labinco rotating wheel (Wolf laboratories, York, UK) set at 25 rpm at 4°C (Fig.2.7). Following this 20 µl Protein AG with agarose beads (Insight Biotechnologies, Middlesex, UK) was added to the eppendorf and loaded onto the rotating wheel for 60 mins at 25 rpm at 4°C. Subsequently the samples were centrifuged at 7500 rpm for 5 mins, supernatant discarded and the pellet washed with lysis buffer - this was repeated twice and following this, pellets were resuspended in 1X Laemmli buffer and boiled at 100°C for 5mins, then stored at -20°C. Non-precipitated proteins were also prepared in Laemmli buffer and boiled to allow detection of GAPDH and other molecules of interest in non-precipitated samples.

4.2.5. Kinexus antibody microarray

Kinextm Antibody Microarray-880 (KAM-880) (Kinexus Bioinformatics Corporation, BC, Canada) was the antibody microarray (as described in Section 2.6) (168), with chip featuring 877 pan- and phosphosite-specific antibodies (518 pan-specific antibodies for protein expression and 359 phospho- site-specific antibodies for phosphorylation) that we utilised for our study to track differential binding of DAP-3 in protein lysates from paired normal and cancerous breast tissues (as described in section 2.5). These tissue lysates were immunoprecipitated with a DAP-3 antibody (as mentioned in section 2.8) before being sent to Kinexus Bioinformatics Corporation for testing on a KAM-880.

The following information/data was generated from the platform test:

Globally Normalized Signal Intensity – This is the reading from the instrument and is background corrected intensity values and further globally normalized. The Globally Normalized Signal Intensity is calculated by summing the intensities of all the net signal median values for a sample (supplied by Kinexus).

.%CFC - The percent change of the treated sample in Normalized Intensity from the specified control. The algorithm of calculation is:

$$\text{CFC} = (\text{Globally Normalized Treated} - \text{Globally Normalized Control}) / \text{Globally Normalized Control} * 100$$

Z Scores - Z score transformation corrects data internally within a single sample.

Z Score Difference - The difference between the observed protein Z scores in samples in comparison.

Z Ratios - Divide the Z Score Differences by the SD of all the differences for the comparison.

4.2.6. Polymerase Chain Reaction

For the purpose of screening molecules of interest in chosen cell lines, desired gene region sequences were amplified using specific primers (listed in Table 2.3.) with GoTaq Green Master Mix then placed in the thermocycler, programmed as indicated in Table 2.4. Following amplification and product separation by electrophoresis, visualisation was obtained using a U:Genius3 gel doc system. Full details of this process are described in Section 2.3.

4.2.7. Pathway mapping by Reactome

From the top DAP-3 reactive proteins discovered from Kinexus platform, the potential signalling pathways involving these proteins were explored using the Reactome package (<https://reactome.org>).

4.2.8. SDS-polyacrylamide gel electrophoresis (SDS-PAGE) and Western blotting

8%-12% resolving gels and 5% stacking gels were chosen for SDS-PAGE. Separated protein samples were transferred onto PVDF membrane by a semi-dry blotting system. To detect specific proteins, antibodies listed in Table 2.6. were used and subsequent visualization performed. Details of this method are described in Chapter 2.7.

4.3. Results

4.3.1. Kinexus protein microarray - Identification of potential DAP-3 interacting partners

To explore and highlight potential interacting partners and their significance in breast cancer a kinexus protein micro-array was undertaken using protein previously generated from 2 independent sets of paired normal and breast cancer tissues. DAP-3 precipitation within these samples was conducted before samples were sent to Kinexus Bioinformatics to perform the micro-array on a KAM-880 array. Proteins co-precipitated with the DAP-3 antibody were applied to the Kinexus platform. (Figure 4.1).

Experimental reports were returned and explored to highlight potential partners of interest. Table 4.1 – 4.4 displays the top and bottom 25 differentially DAP-3 precipitated proteins between normal and cancer tissue identified in the 2 paired samples (4.1/4.2

and 4.3/4.4 representing respective pairs), based on their percentage change from control (%CFC). Based on these results together with the importance, the intimate link and previous interests of the host laboratory HSP90, were chosen for further investigation and verification.

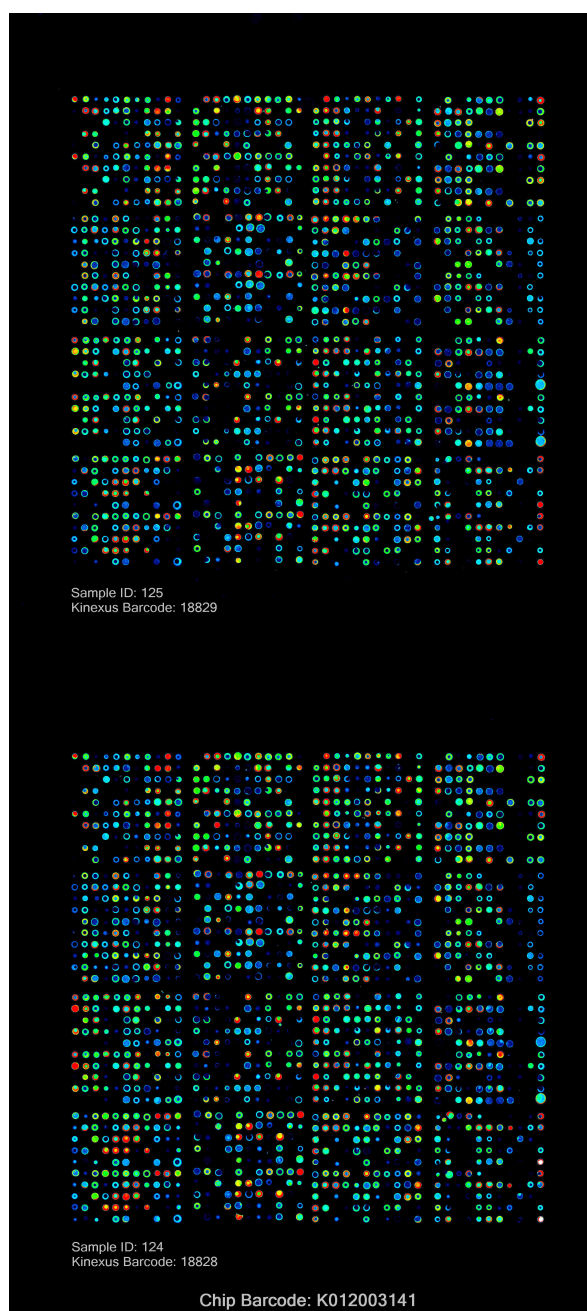


Figure 4.1. Sample protein array images obtained from the Kinexus platform when the DAP-3 protein precipitates were applied. ID124 and ID125 from normal breast and breast cancer tissues of the same patients.

Table 4.1. Bottom 25 differentially DAP-3 precipitated proteins between normal and cancer tissues. Data summarised from Kinexus report and is based on scaling according to percentage change from control (%CFC).

Target Protein Name	Phospho Site (Human)/Pan specific	Full Target Protein Name	Normal tissues	Tumour tissue	%CFC (T vs N)
Cdc25B	Pan-specific	Cell division cycle 25B phosphatase	6362	1701	-73
RIPK	Pan-specific	Receptor-interacting protein-serine kinase 1	3692	988	-73
Crystallin aB	Pan-specific	Crystallin alpha B (heat-shock 20 kDa like-protein)	7417	2175	-71
Vimentin	S33	Vimentin	267	81	-69
Bcl2	Pan-specific	B-cell lymphoma protein 2 alpha	342	115	-66
JAK1	Y1022	Janus protein-tyrosine kinase 1	263	90	-66
CDC42	Pan-specific	Cell division control protein 42 homolog	1151	406	-65
Dab1	Y198	Disabled homolog 1	1133	429	-62
Hsp90a	Pan-specific	Heat shock 90 kDa protein alpha	2610	998	-62
TrkB	Y705	BDNF/NT3/4/5 receptor- tyrosine kinase	363	146	-60
STAT1	Y701	Signal transducer and activator of transcription 1 alpha	1140	459	-60
RIP2/RICK	Pan-specific	Receptor-interacting serine/threonine-protein kinase 2 (RIPK2)	725	294	-59
STAT1	S727	Signal transducer and activator of transcription 1 alpha	966	392	-59
Jun	Y170	Jun proto-oncogene-encoded AP1 transcription factor	262	107	-59
Paxillin 1	Y118	Paxillin 1	1324	539	-59
CDK2	Pan-specific	Cyclin-dependent protein-serine kinase 2	2012	820	-59
Rac1/cdc42	S71	Ras-related C3 botulinum toxin substrate 1	534	219	-59
Hsp60	Pan-specific	Heat shock 60 kDa protein 1 (chaperonin, CPN60)	1507	623	-58
Smad2/3	Pan-specific	SMA- and mothers against decapentaplegic homolog 2/3	741	313	-58
NFKB p65	S529	NF-kappa-B p65 nuclear transcription factor	417	176	-57
BRCA1	S1423	Breast cancer type 1 susceptibility protein	1470	635	-57
Paxillin 1	Y31	Paxillin 1	2984	1293	-56
PSD-95	Pan-specific	Disks large homolog 4	732	321	-56
IRS1	S312	Insulin receptor substrate 1	294	129	-56
STAT3	Y704	Signal transducer and activator of transcription 3	4340	1919	-56

Table 4.2. Top 25 differentially DAP-3 precipitated proteins between normal and cancer tissues. Data summarised from Kinexus report and is based on scaling according to percentage change from control (%CFC).

Target Protein Name	Phospho Site (Human)/Pan specific	Full Target Protein Name	Normal tissues	Tumour tissue	%CFC (T vs N)
HDAC4	Pan-specific	Histone deacetylase 4	119	249	111
ErbB4	Pan-specific	Receptor tyrosine-protein kinase erbB-4	13740	27629	102
Caveolin 2	S36	Caveolin 2	1413	2804	100
Cyclin B1	Pan-specific	Cyclin B1	3395	6732	99
Src	Pan-specific	Src proto-oncogene-encoded protein-tyrosine kinase	999	1954	97
p18 INK4c	Pan-specific	p18 INK4c cyclin-dependent kinase inhibitor	5860	10652	83
Cyclin B1	S147	Cyclin B1	291	524	81
BRCA1	S1497	Breast cancer type 1 susceptibility protein	780	1397	80
Progesterone Receptor	S294	Progesterone receptor	206	362	76
Rb	Pan-specific	Retinoblastoma-associated protein 1	531	894	69
p73	Pan-specific	Tumor suppressor protein p73	15014	25197	69
LIMK1	Pan-specific	LIM domain kinase 1	353	589	68
FAS	Pan-specific	Tumor necrosis factor superfamily member 6 (Apo1, CD95)	5595	9288	67
Mcl1	Pan-specific	Myeloid cell leukemia differentiation protein 1	3509	5798	66
JAK2	Y1007+Y1008	Janus protein-tyrosine kinase 2	77	127	65
PKCt	Pan-specific	Protein-serine kinase C theta	505	823	64
p38a MAPK	Pan-specific	Mitogen-activated protein-serine kinase p38 alpha	4522	7373	64
Hsp90b	Pan-specific	Heat shock 90 kDa protein beta	1412	2254	61
Cdc2 p34	Pan-specific	Cyclin-dependent protein-serine kinase 1	2961	4598	56
FAK	Y576+Y577	Focal adhesion protein-tyrosine kinase	656	1018	56
Raf1	Pan-specific	Raf1 proto-oncogene-encoded protein-serine kinase	1859	2858	55
ERK3	Pan-specific	Extracellular regulated protein-serine kinase 3	4242	6495	54
JAK3	Pan-specific	Janus protein-tyrosine kinase 3	9061	13753	53
ANXA2	Y238	Annexin A2	7762	11697	52
ERK5	Pan-specific	Extracellular regulated protein-serine kinase 5 (Big MAP kinase 1 (BMK1))	2945	4433	51

Table 4.3. Bottom 25 differentially DAP-3 precipitated proteins between normal and cancer tissues. Data summarised from Kinexus report and is based on scaling according to percentage change from control (%CFC).

Target Protein Name	Phospho Site (Human)/Pan specific	Full Target Protein Name	Normal tissues	Tumour tissue	%CFC (T vs N)
Striatin	Pan-specific	Striatin	22969	7918	-65
Src	Y418	Src proto-oncogene-encoded protein-tyrosine kinase	805	342	-57
PKR1	T446	Double-stranded RNA-dependent protein-serine kinase	200	107	-47
PKA Cb	S338	cAMP-dependent protein-serine kinase catalytic subunit beta	2720	1564	-42
ANXA2	Y238	Annexin A2	12174	8009	-34
PKCm (PKD)	S738/S742	Protein-serine kinase C mu (Protein kinase D)	279	190	-32
PI3-Kinase	Pan-specific	Phosphatidylinositol 3-kinase regulatory subunit alpha	775	545	-30
PKCm (PKD)	S916	Protein-serine kinase C mu (Protein kinase D)	3111	2213	-29
MEK2 mouse	T394	MAPK/ERK protein-serine kinase 2 (MKK2) (mouse)	18946	13479	-29
Akt1 (PKBa)	S473	RAC-alpha serine/threonine-protein kinase	592	424	-28
IKKa	T23	Inhibitor of NF-kappa-B protein-serine kinase alpha (CHUK)	183	133	-27
MKK4	Pan-specific	MAPK/ERK protein-serine kinase 4 (MKK4)	19451	14258	-27
Synapsin 1	Pan-specific	Synapsin 1 isoform Ia	745	550	-26
Jun	Pan-specific	Jun proto-oncogene-encoded AP1 transcription factor	495	367	-26
RIP2/RICK	Pan-specific	Receptor-interacting serine/threonine-protein kinase 2 (RIPK2)	717	536	-25
Arrestin b	Pan-specific	Arrestin beta 1	759	567	-25
ZAP70	Pan-specific	Zeta-chain (TCR) associated protein-tyrosine kinase, 70 kDa	673	503	-25
FasL	Pan-specific	Tumor necrosis factor ligand, member 6	704	527	-25
Cdc25C	Pan-specific	Cell division cycle 25C phosphatase	7412	5592	-24
MAPKAPK2	T222	Mitogen-activated protein kinase-activated protein kinase 2	1567	1198	-23
STAT1	S727	Signal transducer and activator of transcription 1 alpha	431	331	-23
MKK3	S189	MAPK/ERK protein-serine kinase 3 beta isoform (MKK3 beta)	108	83	-23
Tau	S400	Microtubule-associated protein tau	612	474	-22
CDK6	Y13	Cyclin-dependent protein-serine kinase 6	261	202	-22
RSK1/2/3	T573	Ribosomal S6 protein-serine kinase 1/2/3	82	64	-22

Table 4.4. Top 25 differentially DAP-3 precipitated proteins between normal and cancer tissues. Data summarised from Kinexus report and is based on scaling according to percentage change from control (%CFC).

Target Protein Name	Phospho Site (Human)/Pan specific	Full Target Protein Name	Normal tissues	Tumour tissue	%CFC (T vs N)
LIMK1	Pan-specific	LIM domain kinase 1	1219	2135	76
RSK1/2	S380/S386	Ribosomal S6 protein-serine kinase 1/2	505	883	75
ERK1/2	Y204+Y187	Extracellular regulated protein-serine kinase 1 (p44 MAP kinase) + Extracellular regulated protein-serine kinase 2 (p42 MAP kinase)	497	785	58
Cyclin B1	S147	Cyclin B1	855	1346	58
ERK5	T218+Y220	Extracellular regulated protein-serine kinase 5 (Big MAP kinase 1 (BMK1))	1088	1666	54
4G10	pTyr	Phosphotyrosine (Clone 4G10)	5019	7622	52
Hsc70	Pan-specific	Heat shock 70 kDa protein 8	2280	3389	49
Hsp90b	Pan-specific	Heat shock 90 kDa protein beta	4242	6240	47
CDK11A	T583	Cell division cycle 2-like 2 protein kinase	11125	15984	44
CDK2	Pan-specific	Cyclin-dependent protein-serine kinase 2	2967	4251	44
ERK5	Pan-specific	Extracellular regulated protein-serine kinase 5 (Big MAP kinase 1 (BMK1))	4178	5950	43
ERK1	Pan-specific	Extracellular regulated protein-serine kinase 1 (p44 MAP kinase)	11318	15975	41
PTEN	S380/T382/T383	Phosphatidylinositol-3,4,5-trisphosphate 3-phosphatase and protein phosphatase and tensin homolog deleted on chromosome 10	166	233	41
4E-BP1	S65	Eukaryotic translation initiation factor 4E binding protein 1 (PHAS1)	195	268	38
ERK3	Pan-specific	Extracellular regulated protein-serine kinase 3	7033	9634	37
RSK1	T348	Ribosomal S6 protein-serine kinase 1	382	524	37
COX2	Pan-specific	Cyclo-oxygenase 2 (prostaglandin G/H synthase 2 precursor)	534	726	36
ERK1	Pan-specific	Extracellular regulated protein-serine kinase 1 (p44 MAP kinase)	19677	26362	34
PKG1b-NT	Pan-specific	cGMP-dependent protein kinase 1, beta isozyme	5008	6672	34
PKCb2	T641	Protein-serine kinase C beta 2	681	907	33
ALK	Y1507	Anaplastic lymphoma kinase	7944	10576	33
Src	Pan-specific	Src proto-oncogene-encoded protein-tyrosine kinase	817	1079	32
B-Raf	Pan-specific	RafB proto-oncogene-encoded protein-serine kinase	21474	28300	32
ASK1	S966	Apoptosis signal regulating protein-serine kinase 1	140	184	32
PLCg2	Y753	1-phosphatidylinositol-4,5-bisphosphate phosphodiesterase gamma-2	174	228	31

4.3.2. DAP-3 Pathway analysis

Mathematical models were used to calculate the mostly likely targets. This was based on the default % CFC, calculated as the percentage of signals in tumour over normal and the Z-score (Z-ratio) (Chapter-2). This resulted in a final priority list from all the tests (Table 4.5). From the top shortlisted priority proteins that interacted with DAP-3, we predicted the pathways that these proteins are mostly likely involved in. This was done by the Reactome online tool (www.reactome.org). Figure-4.2 has shown the genome wide view of these key DAP-3 interactive proteins and their involvement in cell signalling. Signalling exploration has generated the top signalling pathways that are most likely to be involved by DAP-3 and its most interactive proteins (Table 4.6).

Most notable pathways include ERBB pathways (ERBB4/HER4, ERBB2/HER2), MAPK and AKT, BRAF pathways (Table 4.6). ERBB4/HER2 and ERBB2/HER2 pathways are particularly interesting as they are well established pathways contributing to the development and progression of breast cancer. Figures 4.3/4.5/4.9/4.11/4.12/4.14 exhibited a number of the top pathways and the key components in the respective pathways in this context, including the top two, the ERBB4/HER4 pathway and the ERBB2/HER2 regulating cell motility pathway. Figures 4.4 and 4.6 respectively showed the changes of the key components in the ERBB4/HER4 and ERBB2/HER2 pathway from the Kinexus array. Additionally, we also noted subtle yet interesting changes of the key components in the ER-alpha pathway, a pathway that has clear role in breast cancer (Figure 4.7 and Figure 4.8). This finding lead to studies in Chapter-4 to examine the relationship between DAP-3 and HER2, HER4 in a clinical context. Additionally, changes in the components of the RAF, Sema3A PAK dependent axon repulsion and

ERK pathways in the kinexus arrays are indicated in Figure 4.10, 4.13 and 4.15 respectively.

Of the single DAP-3 interactive proteins, HSP90 have very high occurrence and play important part in over half of these pathways. This includes HSP90a in ERBB4/HER4, the long-term potentiation pathway, IL4 signalling pathway, IL13 signalling pathway and HSP90b in ERBB2/HER2 pathway, PI3K/AKT, PP2A pathways, Post NMDA receptor activation Pathway, IL4 signalling pathway, IL13 signalling pathway. Figure 4.16 demonstrates the degree of differences between normal and tumour tissues of the proteins signalling events that are associated with HSP90 in our Kinexus dataset.

From the platform analysis, we have identified several other key pathways that are linked to DAP-3 with changes from normal and tumour tissues and also relevant to the studies to be carried out in the next phase. They include the SRC pathway (Figure 4.18 and 4.18), Paxillin participated pathway (Figure 4.19 and 4.20). The changes of the key components in these pathways are presented in these figures. The current study is unable to fully explore the full impact of these pathways but hopes to provide references for future studies.

These findings from the platform screening collectively indicated the key role for DAP-3 and its interactive protein in ERBB4/HER4, ERBB2/HER2 and pointing a key role for HSP90 family in the action of DAP-3. This finding led to the exploration of HSP90 in our cell model systems in order to examine the role played by HSP90 and potential mechanistic interactions with DAP-3 in the biological behaviours in breast cancer cells.

Table 4.5. *Identified targets of interest and priority leads from Kinexus analysis*

Target Protein Name	Full Target Protein Name	Normal	Tumour	%CFC (Tumour vs normal)	Z-ratio	Best Leads
ErbB4	Receptor tyrosine-protein kinase erbB-4	13740	27629	102	1.81	Priority
Caveolin 2	Caveolin 2	1413	2804	100	1.96	Priority
Cyclin B1	Cyclin B1	3395	6732	99	1.89	Priority
Src	Src proto-oncogene-encoded protein-tyrosine kinase	999	1954	97	1.95	Priority
p18 INK4c	p18 INK4c cyclin-dependent kinase inhibitor	5860	10652	83	1.62	Priority
LIMK1	LIM domain kinase 1	1219	2135	76	4.06	Priority
p73	Tumor suppressor protein p73	15014	25197	69	1.34	Priority
Mcl1	Myeloid cell leukemia differentiation protein 1	3509	5798	66	1.41	Priority
p38a MAPK	Mitogen-activated protein-serine kinase p38 alpha	4522	7373	64	1.36	Priority
Hsp90b	Heat shock 90 kDa protein beta	1412	2254	61	1.40	Priority
Cdc2 p34	Cyclin-dependent protein-serine kinase 1	2961	4598	56	1.27	Priority
Raf1	Raf1 proto-oncogene-encoded protein-serine kinase	1859	2858	55	1.28	Priority
ERK5	Extracellular regulated protein-serine kinase 5 (Big MAP kinase 1 (BMK1))	1088	1666	54	3.13	Priority
JAK3	Janus protein-tyrosine kinase 3	9061	13753	53	1.12	Priority
ANXA2	Annexin A2	7762	11697	52	1.11	Priority
FRS2	Fibroblast growth factor receptor substrate 2	4263	2046	-52	-1.78	Priority
eIF4G	Eukaryotic translation initiation factor 4 gamma 1	8988	4229	-53	-1.89	Priority
NFKB p65	NF-kappa-B p65 nuclear transcription factor	1997	939	-53	-1.77	Priority
Tau	Microtubule-associated protein tau	1669	779	-53	-1.77	Priority
STAT3	Signal transducer and activator of transcription 3	4340	1919	-56	-1.99	Priority
Paxillin 1	Paxillin 1	2984	1293	-56	-2.01	Priority
CDK2	Cyclin-dependent protein-serine kinase 2	2012	820	-59	-2.13	Priority
Hsp90a	Heat shock 90 kDa protein alpha	2610	998	-62	-2.32	Priority
Striatin	Striatin	22969	7918	-65	-7.57	Priority
Crystallin aB	Crystallin alpha B (heat-shock 20 kDa like-protein)	7417	2175	-71	-3.08	Priority
RIPK	Receptor-interacting protein-serine kinase 1	3692	988	-73	-3.26	Priority
Cdc25B	Cell division cycle 25B phosphatase	6362	1701	-73	-3.31	Priority

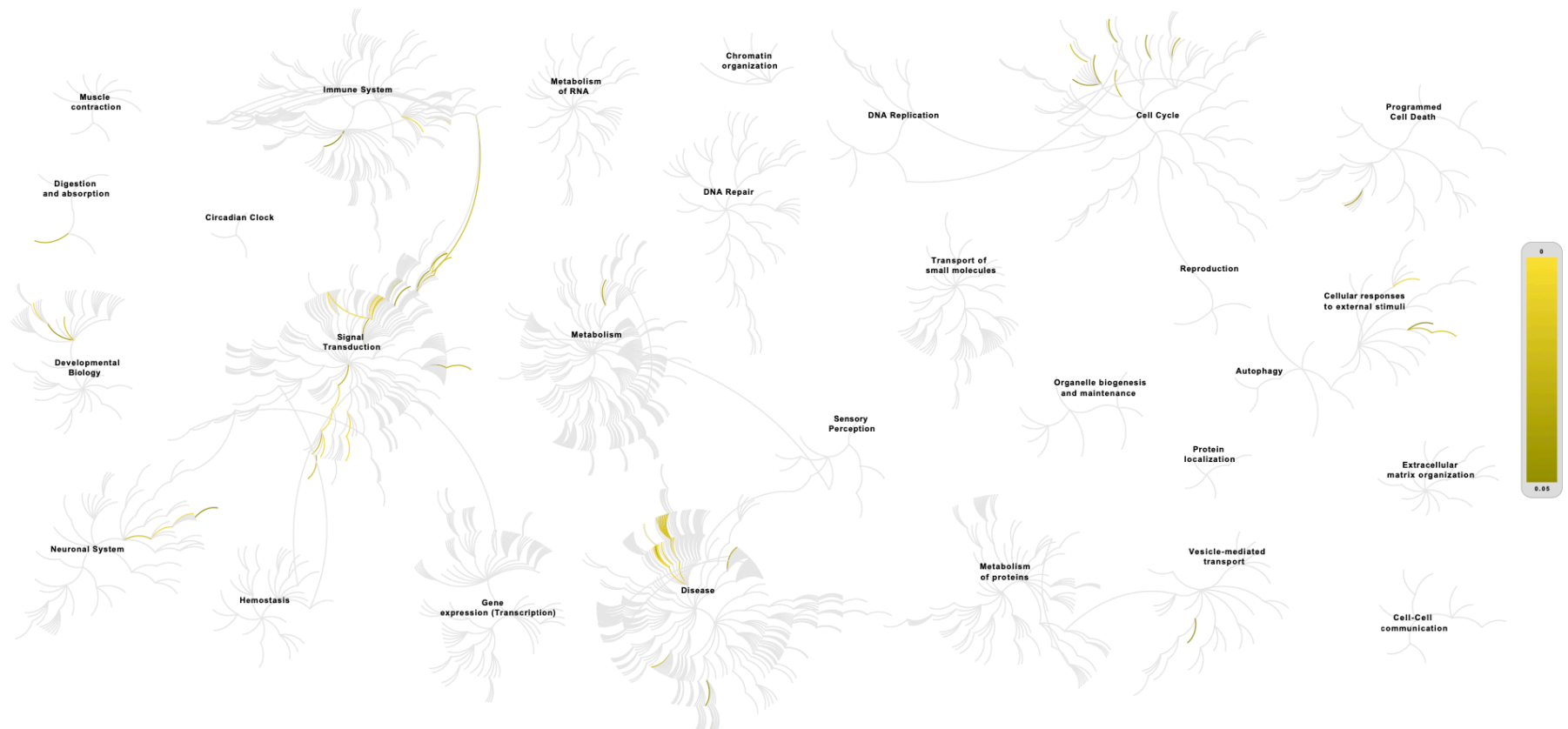


Figure 4.2. Genome-wide view of the key processes in which the DAP-3 interactive protein signalling (darker lines) are likely to be involved. Generated from www.reactome.org

Table 4.6. The top twenty five pathways that are most relevant to DAP-3 and its reactive proteins.

Pathway name	Entities				Reactions	
	found	ratio	p-value	FDR*	found	ratio
Downregulation of ERBB4 signaling	6 / 91	0.004	3.84e-04	0.062	5 / 5	3.72e-04
ERBB2 Regulates Cell Motility	3 / 38	0.002	4.02e-04	0.062	2 / 2	1.49e-04
MAPK1/MAPK3 signaling	12 / 607	0.028	4.14e-04	0.062	46 / 82	0.006
RAF/MAP kinase cascade	11 / 509	0.024	6.04e-04	0.062	40 / 75	0.006
Signaling by high-kinase activity BRAF mutants	3 / 44	0.002	6.15e-04	0.062	4 / 6	4.47e-04
Sema3A PAK dependent Axon repulsion	4 / 45	0.002	6.56e-04	0.062	4 / 6	4.47e-04
Signalling to ERKs	4 / 107	0.005	7.01e-04	0.062	11 / 32	0.002
ERBB2 Activates PTK6 Signaling	4 / 47	0.002	7.43e-04	0.062	2 / 2	1.49e-04
Long-term potentiation	6 / 109	0.005	7.51e-04	0.062	1 / 7	5.21e-04
PI5P, PP2A and IER3 Regulate PI3K/AKT Signaling	9 / 295	0.014	8.16e-04	0.062	5 / 7	5.21e-04
Signaling by RAF1 mutants	3 / 49	0.002	8.38e-04	0.062	7 / 7	5.21e-04
MAP2K and MAPK activation	3 / 49	0.002	8.38e-04	0.062	11 / 12	8.94e-04
Post NMDA receptor activation events	10 / 308	0.014	0.001	0.062	4 / 39	0.003
Interleukin-21 signaling	2 / 13	6.01e-04	0.001	0.062	4 / 5	3.72e-04
GRB2 events in ERBB2 signaling	3 / 54	0.002	0.001	0.062	2 / 4	2.98e-04
Negative regulation of the PI3K/AKT network	9 / 324	0.015	0.001	0.062	5 / 10	7.45e-04
ERKs are inactivated	2 / 15	6.93e-04	0.001	0.062	2 / 2	1.49e-04
Signaling by ERBB2 TMD/JMD mutants	5 / 132	0.006	0.002	0.062	9 / 13	9.68e-04
Senescence-Associated Secretory Phenotype (SASP)	4 / 137	0.006	0.002	0.069	5 / 22	0.002
Interleukin-4 and Interleukin-13 signaling	7 / 351	0.016	0.002	0.077	26 / 47	0.004
Signaling downstream of RAS mutants	3 / 70	0.003	0.002	0.079	7 / 7	5.21e-04
Paradoxical activation of RAF signaling by kinase inactive BRAF	3 / 70	0.003	0.002	0.079	6 / 7	5.21e-04
Signaling by moderate kinase activity BRAF mutants	3 / 70	0.003	0.002	0.079	6 / 7	5.21e-04
Signaling by RAS mutants	3 / 70	0.003	0.002	0.079	7 / 9	6.70e-04
Signaling by BRAF and RAF fusions	3 / 73	0.003	0.003	0.086	5 / 5	3.72e-04

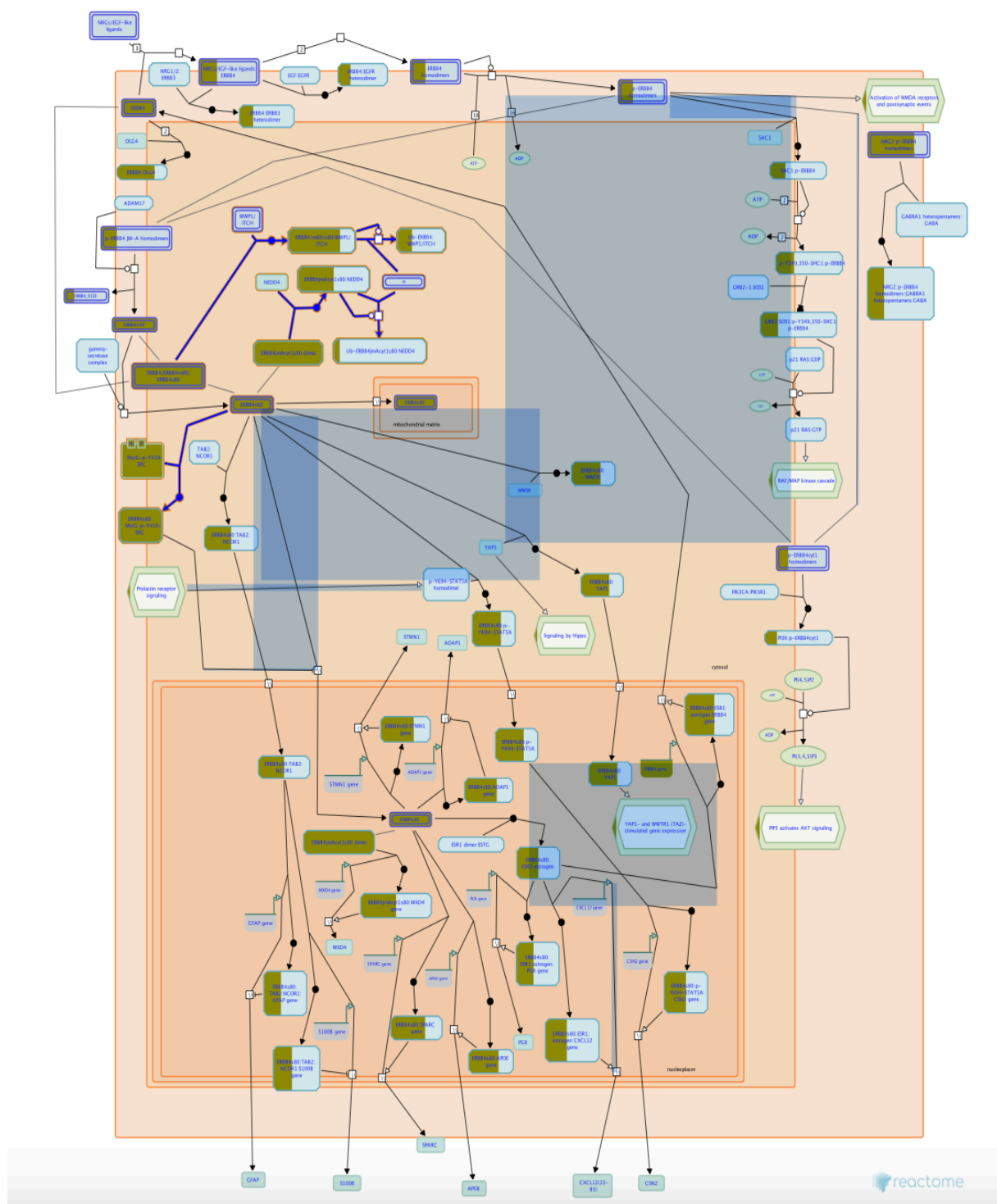


Figure 4.3. ERBB4/HER4 pathway, the top DAP-3 related pathways in breast cancer. (www.reactome.org)

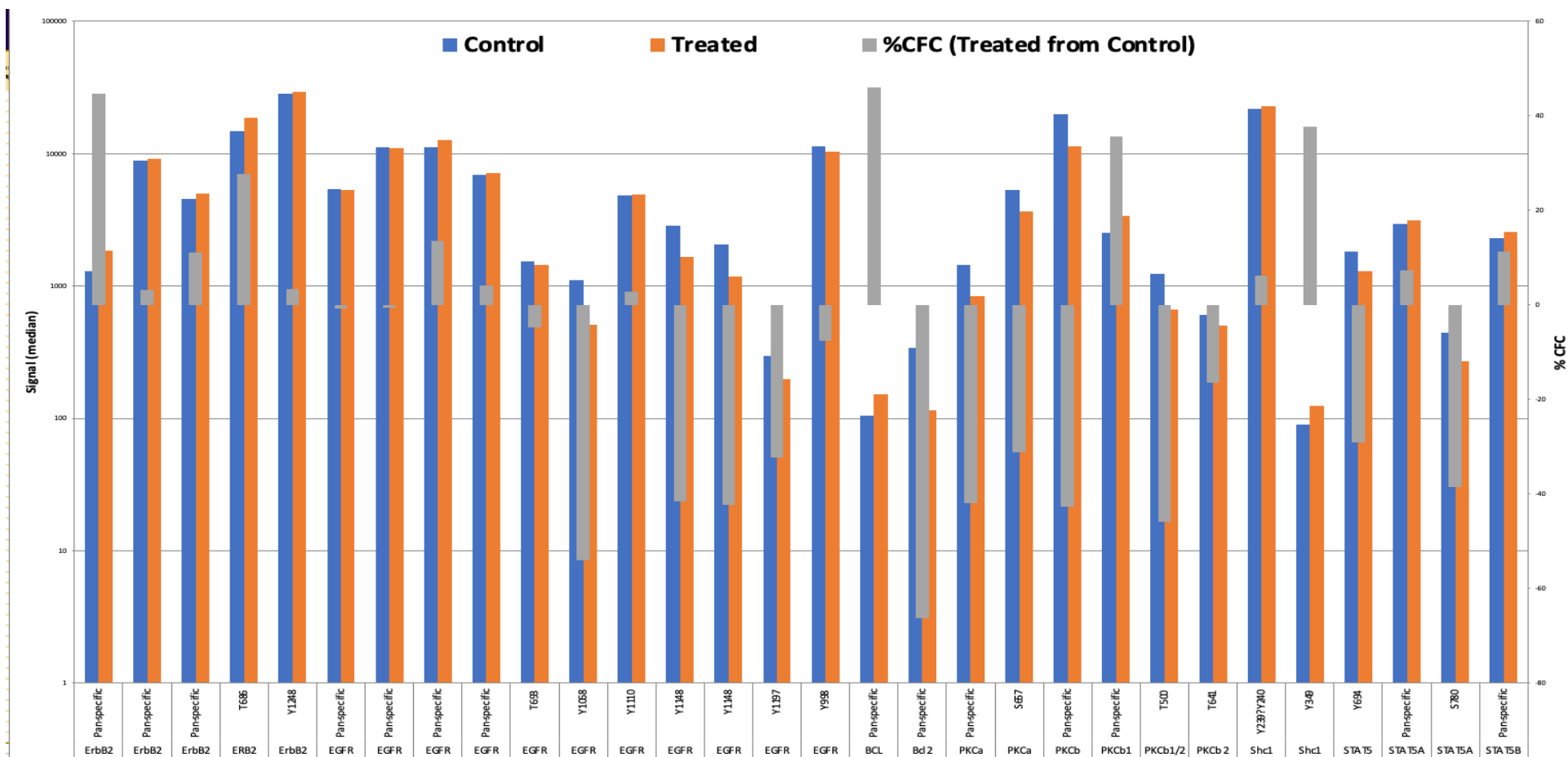


Figure 4.4. The changes of DAP-3 interactive proteins that are forming the ERBB4 pathway, as shown by the Kinexus protein array. Control: annotated for Normal tissues; Treated: annotated for tumour tissues. Grey bars: % CFC tumour versus normal tissue.

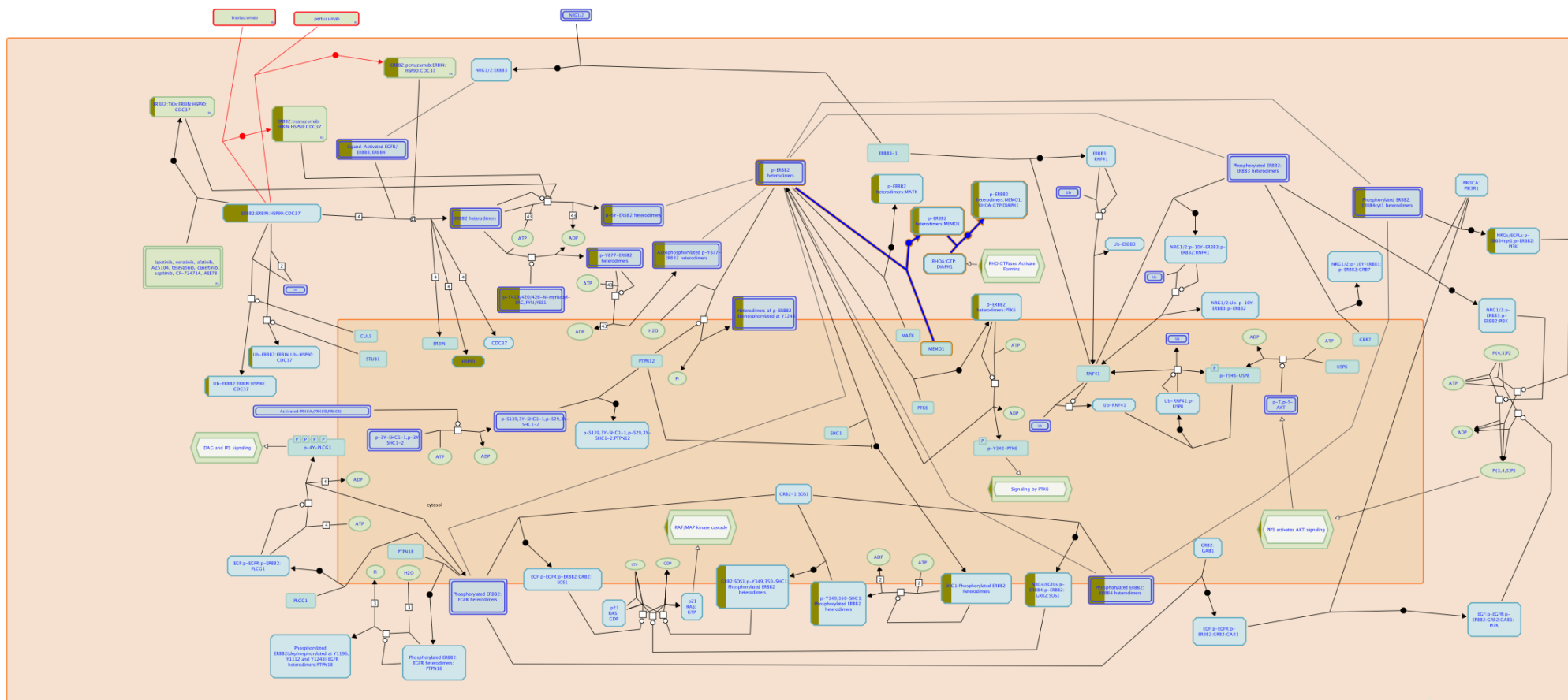


Figure 4.5. *ERBB2/HER2 motility regulating pathway*

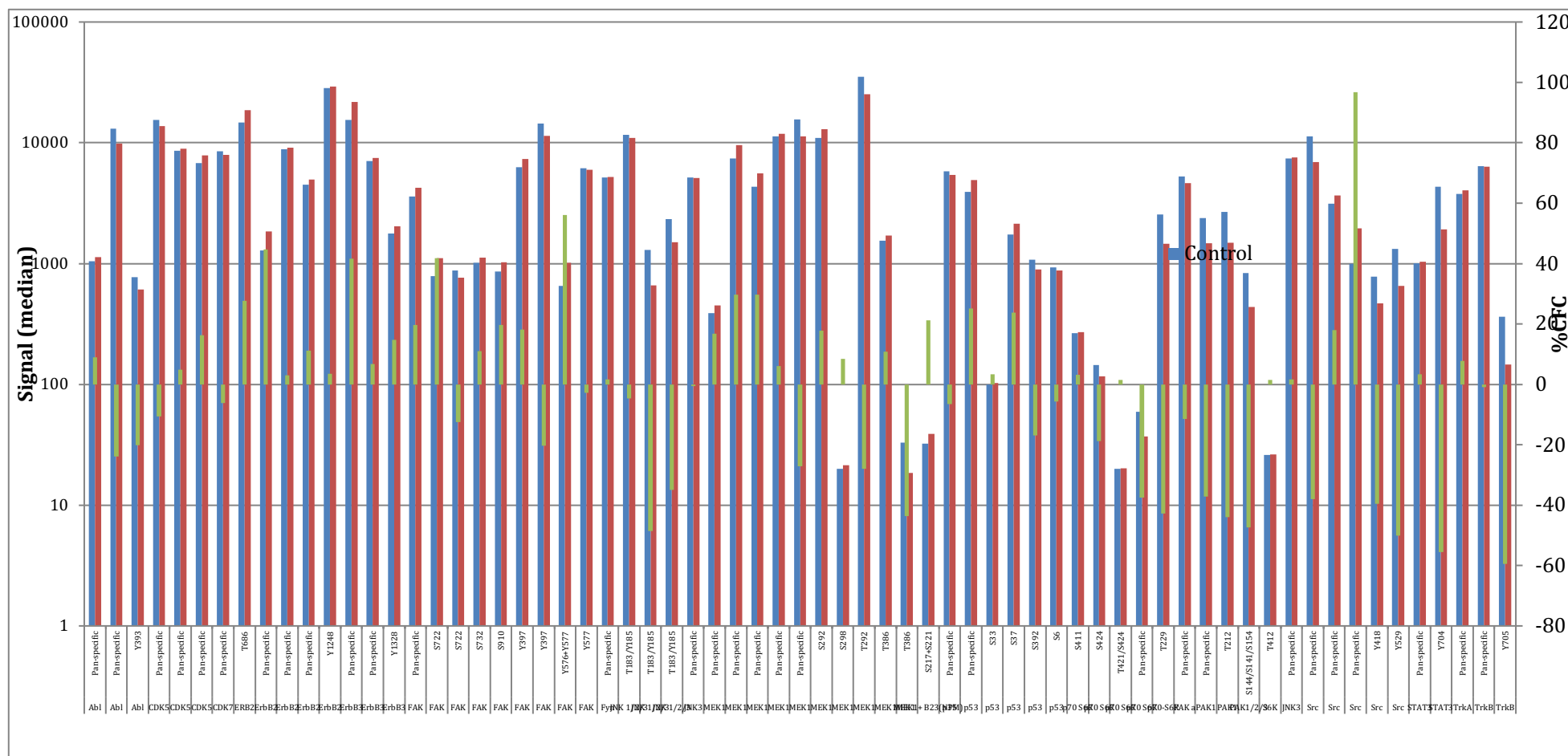


Figure 4.6. The changes of DAP-3 interactive proteins that are forming the ERBB2 pathway, as shown by the Kinexus protein array. Control: annotated for Normal tissues; Treated: annotated for tumour tissues. Green bars: % CFC tumour versus normal tissue.

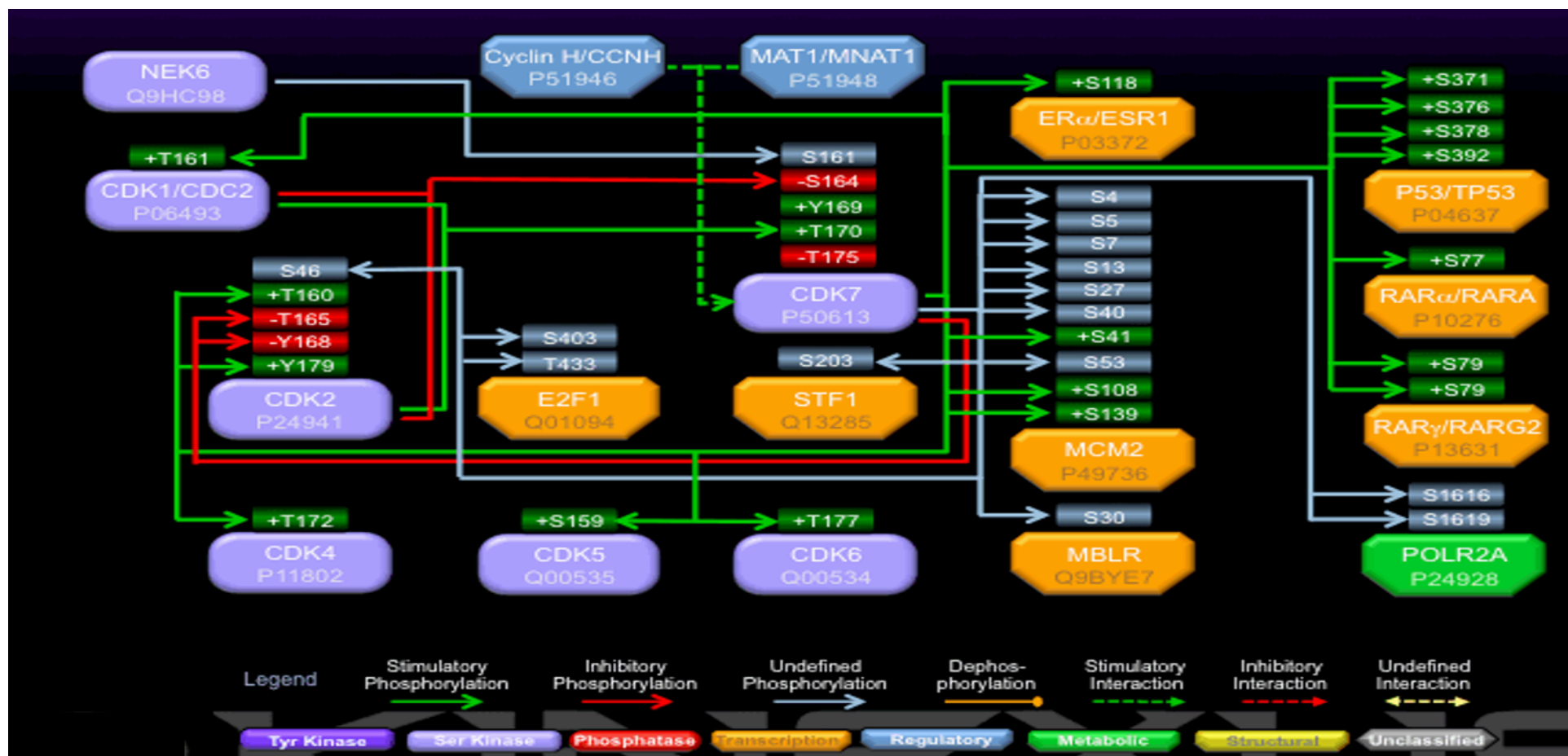


Figure 4.7. ER- α signalling pathway and the available protein components in the Kinexus (Kinexus Connection Map P50613).

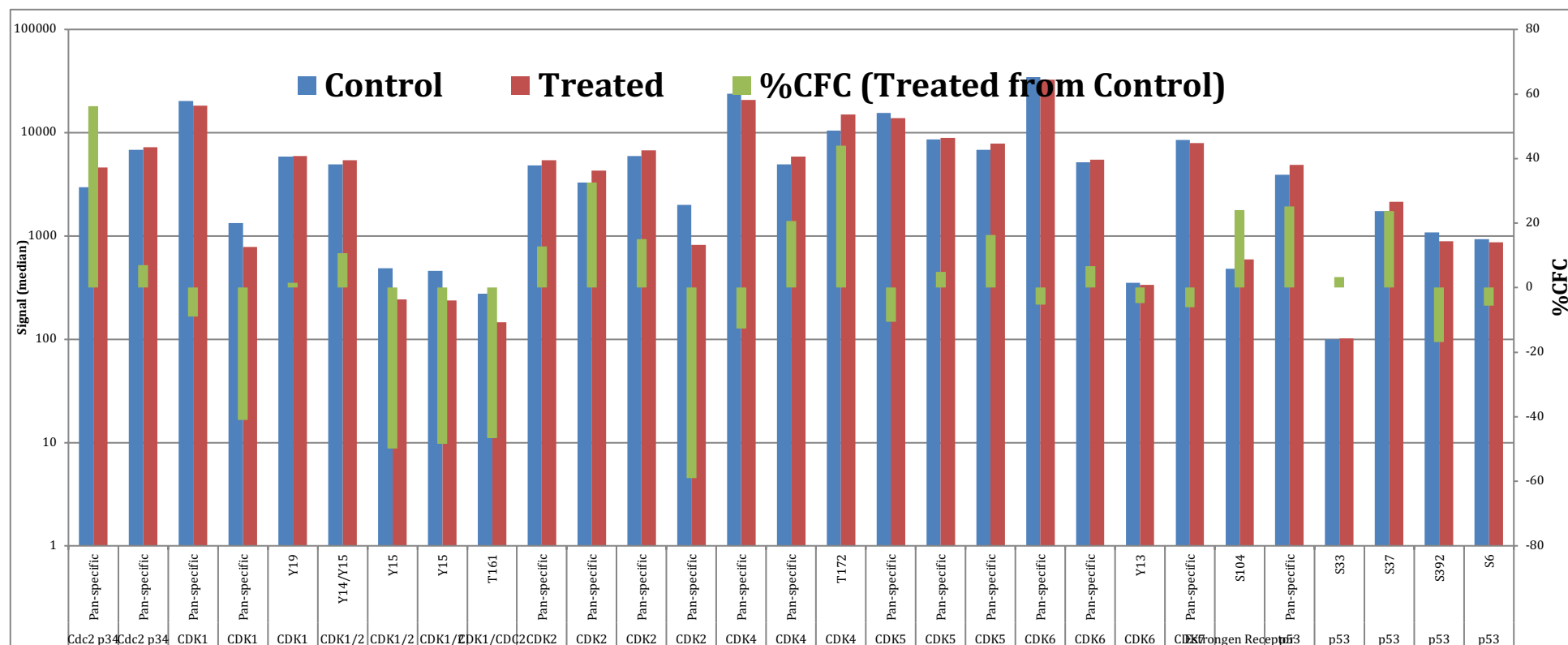


Figure 4.8. ER-alpha signalling pathway proteins and kinases that interacted with DAP-3 from the Kinexus protein array. Control: annotated for Normal tissues; Treated: annotated for tumour tissues. Green bars: % CFC tumour versus normal tissue.

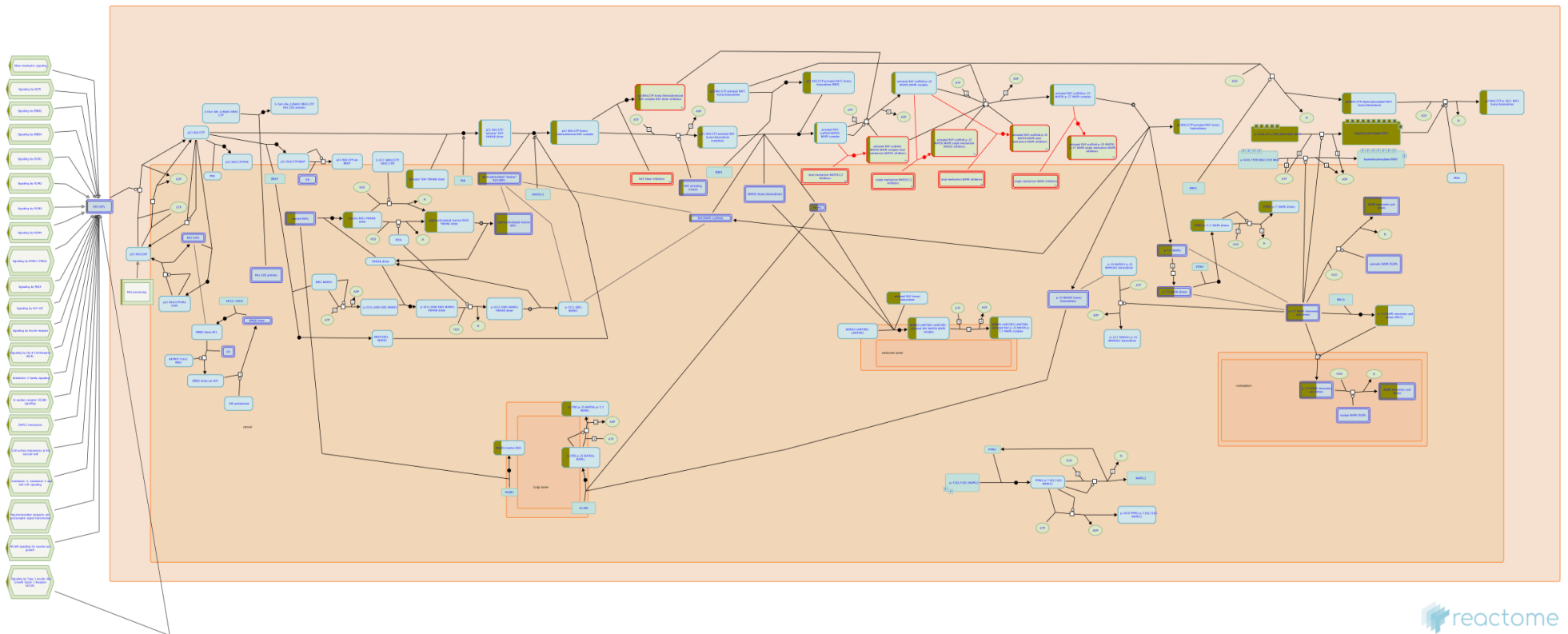


Figure 4.9. The RAF-RAS-MEK-ERK pathway

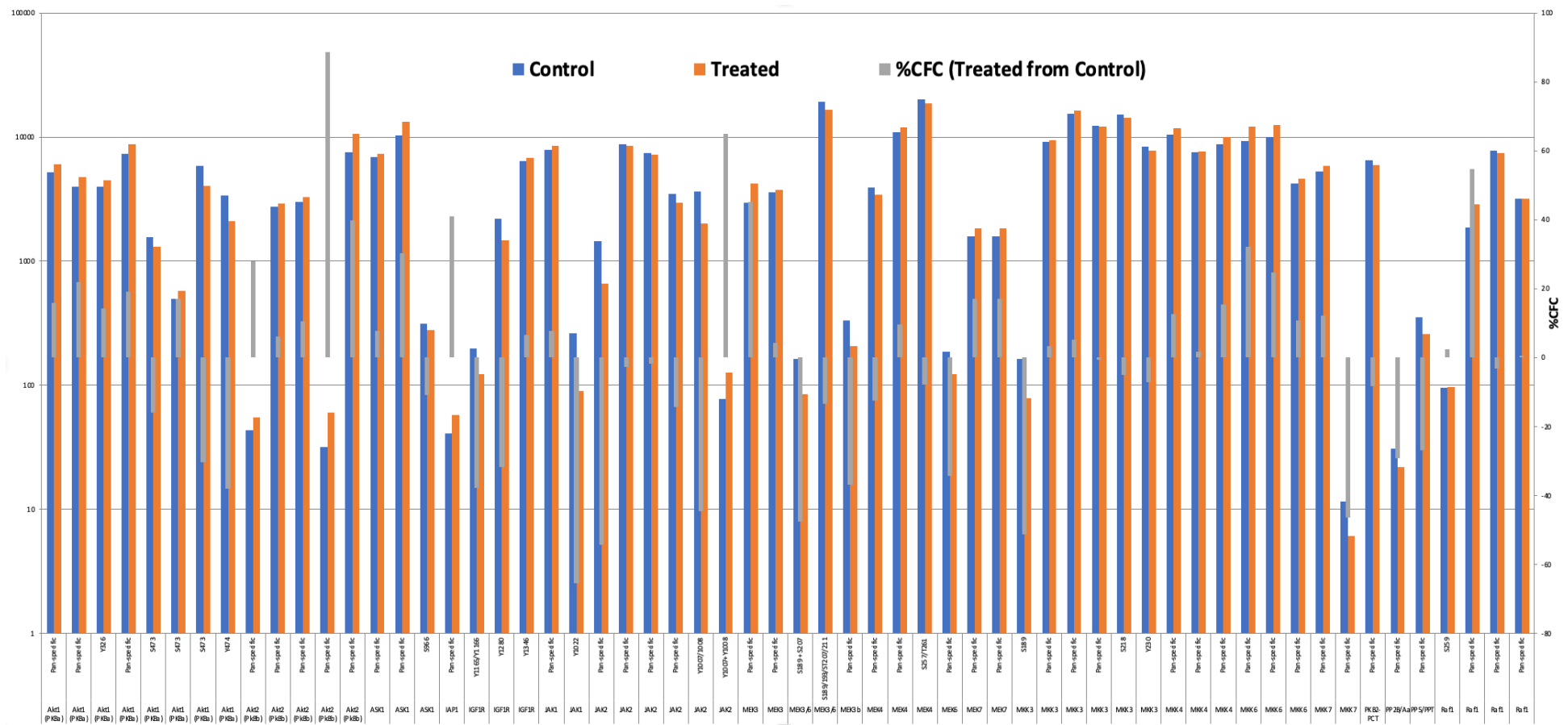


Figure 4.10. RAF signalling pathway proteins and kinases (Kinexus pathway Q99683) that interacted with DAP-3 from the Kinexus protein array. Control: annotated for Normal tissues; Treated: annotated for tumour tissues. Grey bars: % CFC tumour versus normal tissue.

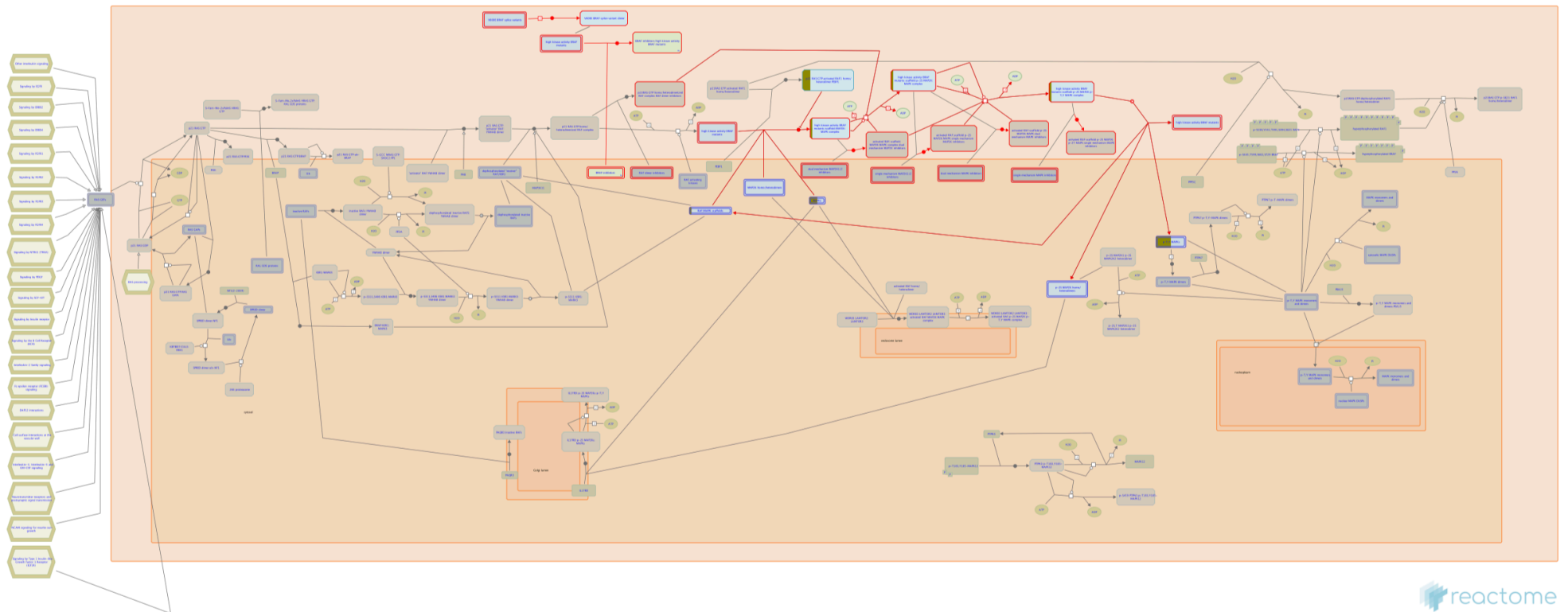


Figure 4.11. The signalling pathway by high kinase activity BRAF mutants.

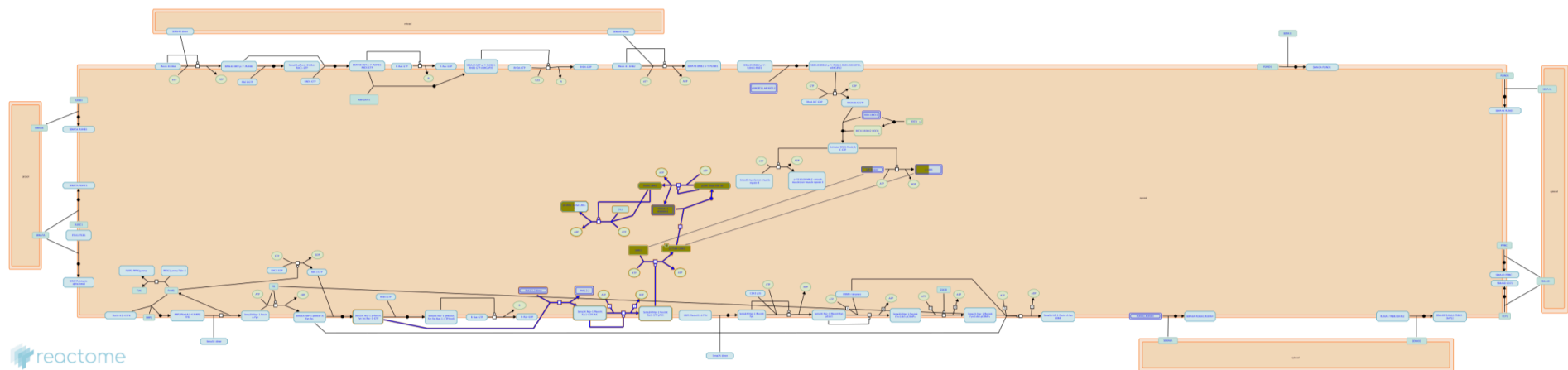


Figure 4.12. *Sema3A PAK dependent Axon repulsion pathway.*

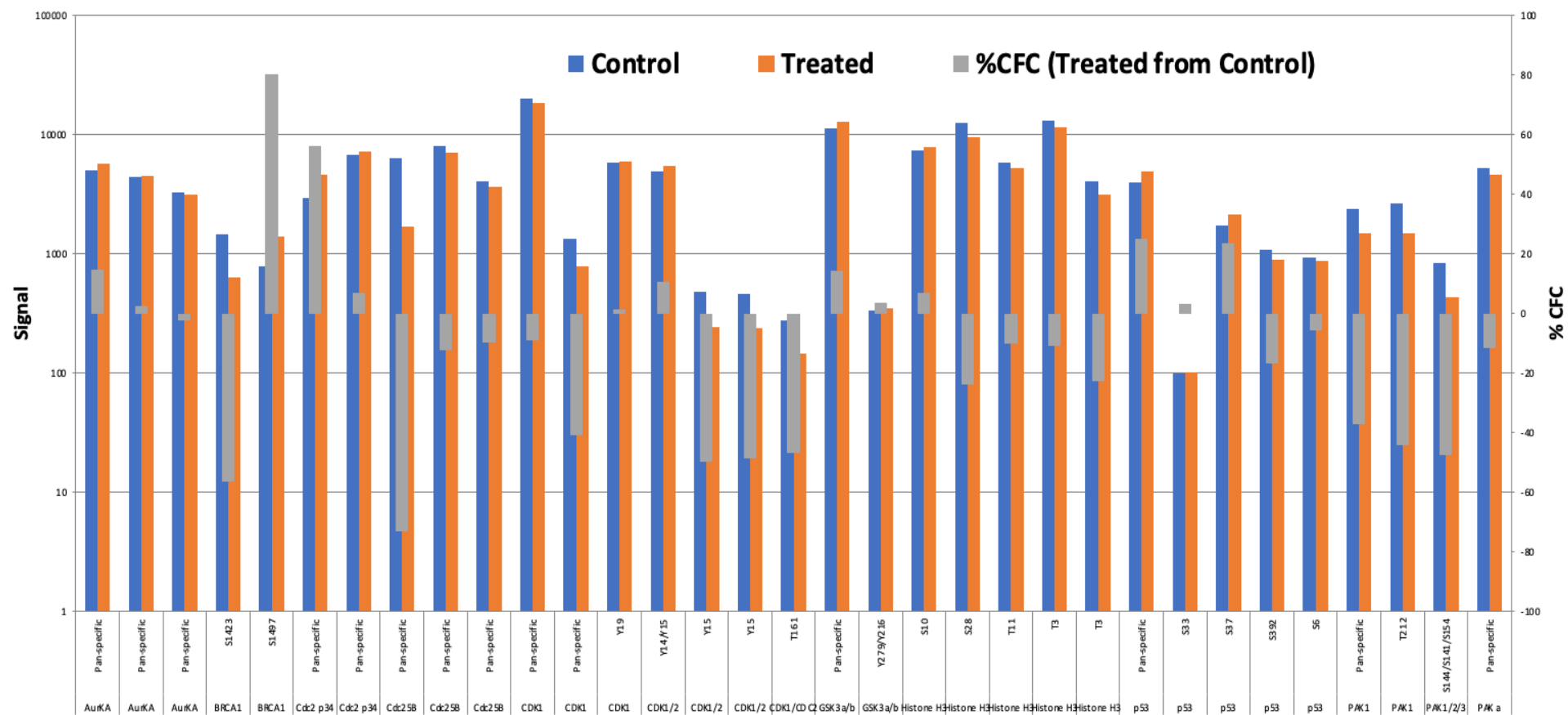


Figure 4.13. Changes in the key protein interacted with DAP-3 in the Sema3A PAK dependent Axon repulsion pathway (Kinexus pathway (014965)).

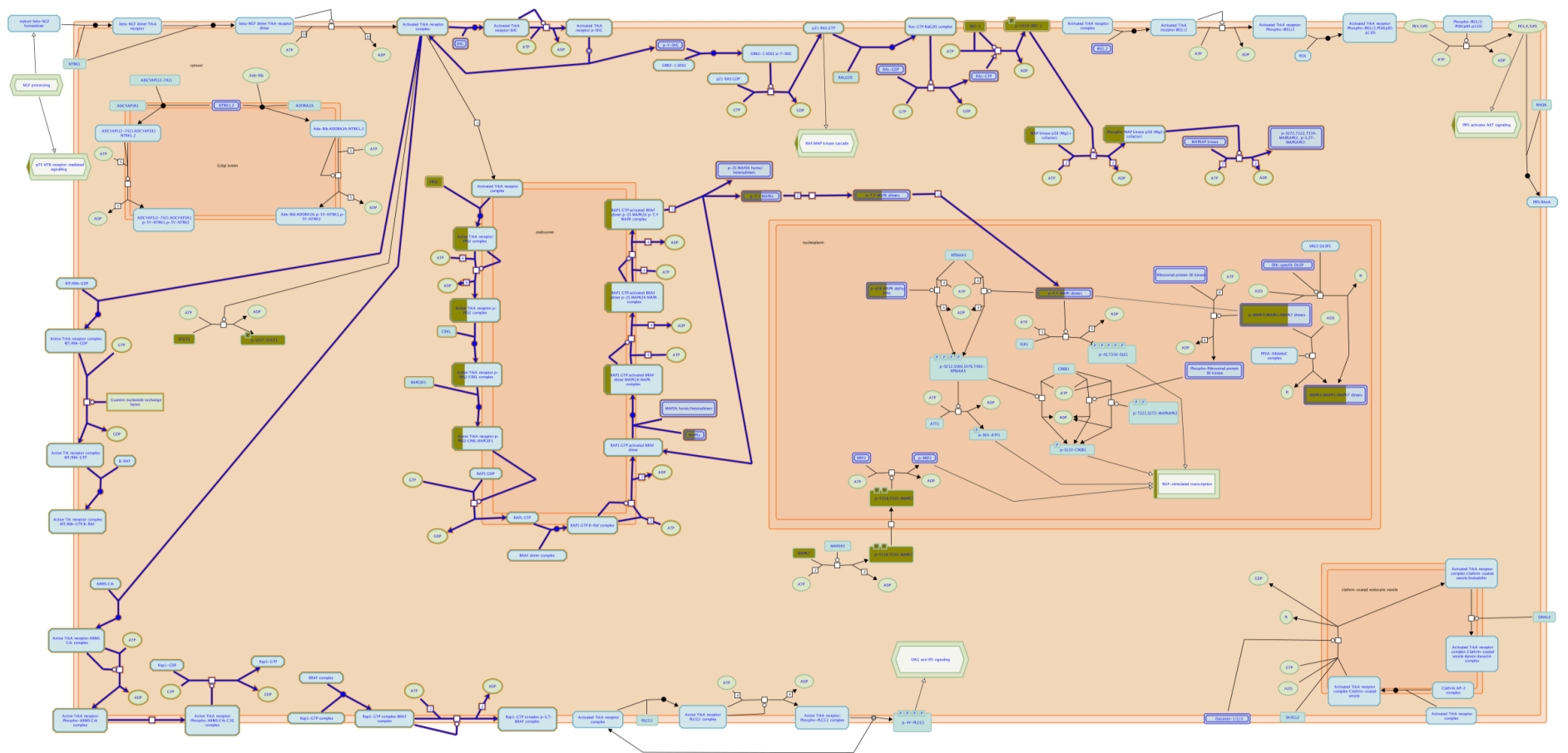


Figure 4.14. The ERK pathway.

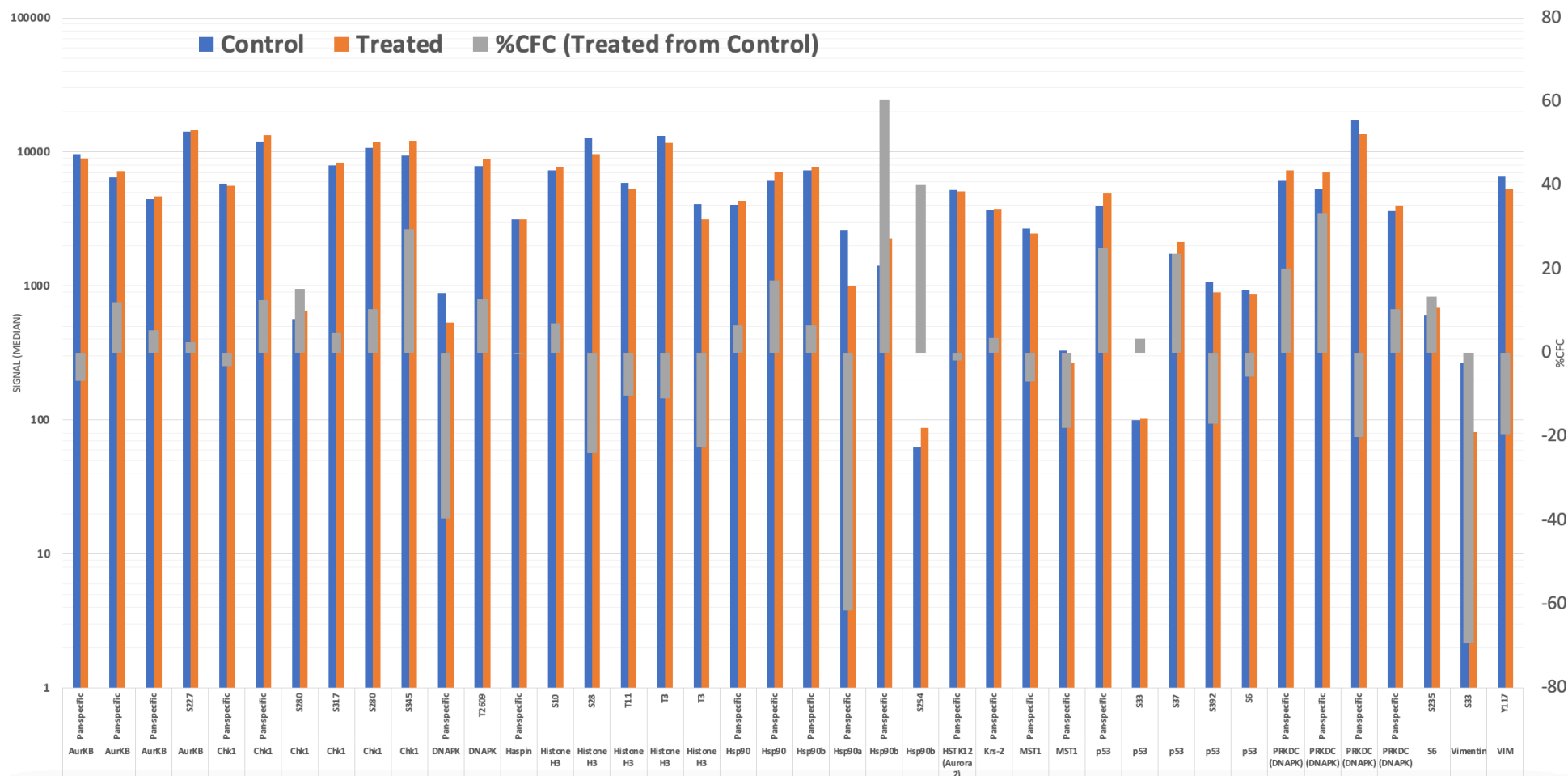


Figure 4.16. Differential expression of DAP-3 interactive protein, HSP90 and related kinases between normal and tumour tissues, from the Kinexus analyses. Control: annotated for Normal tissues; Treated: annotated for tumour tissues. Grey bars: % CFC tumour versus normal tissue.

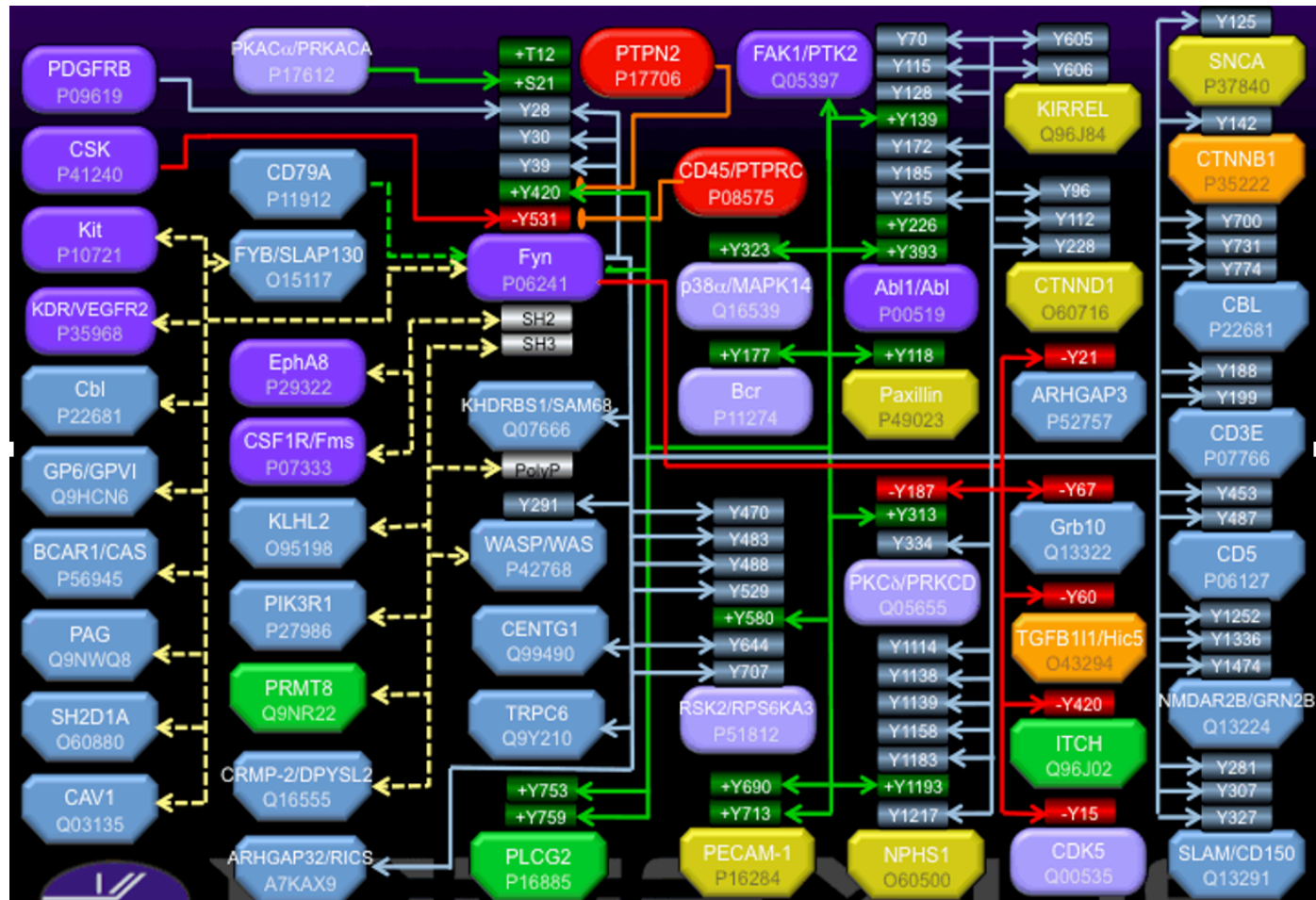


Figure 4.17. The paxillin participating pathway (Kinexus pathway P06241)

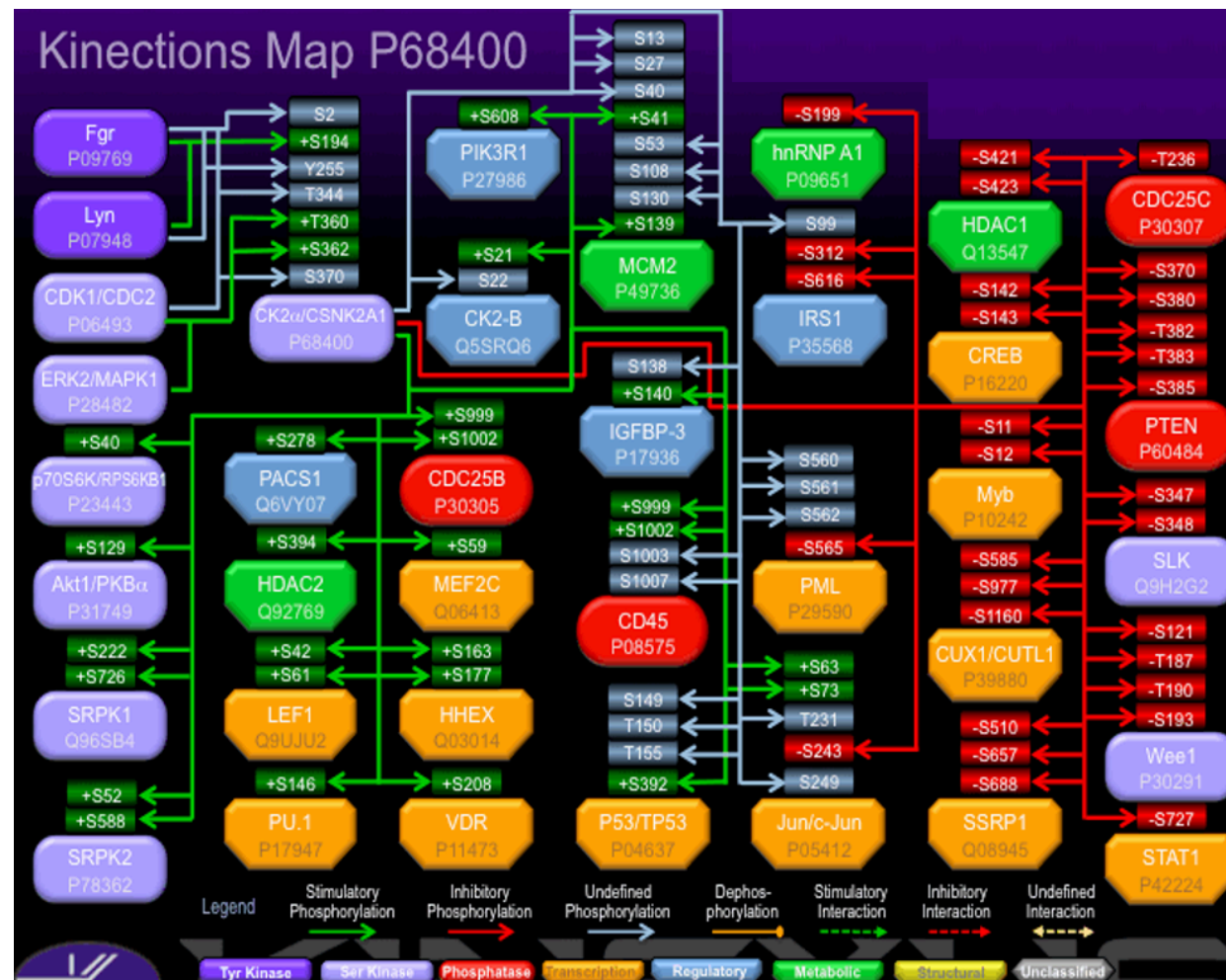


Figure 4.19. Key components of the SRC pathway in the Kinexus platform (Kinexus pathway P68400)

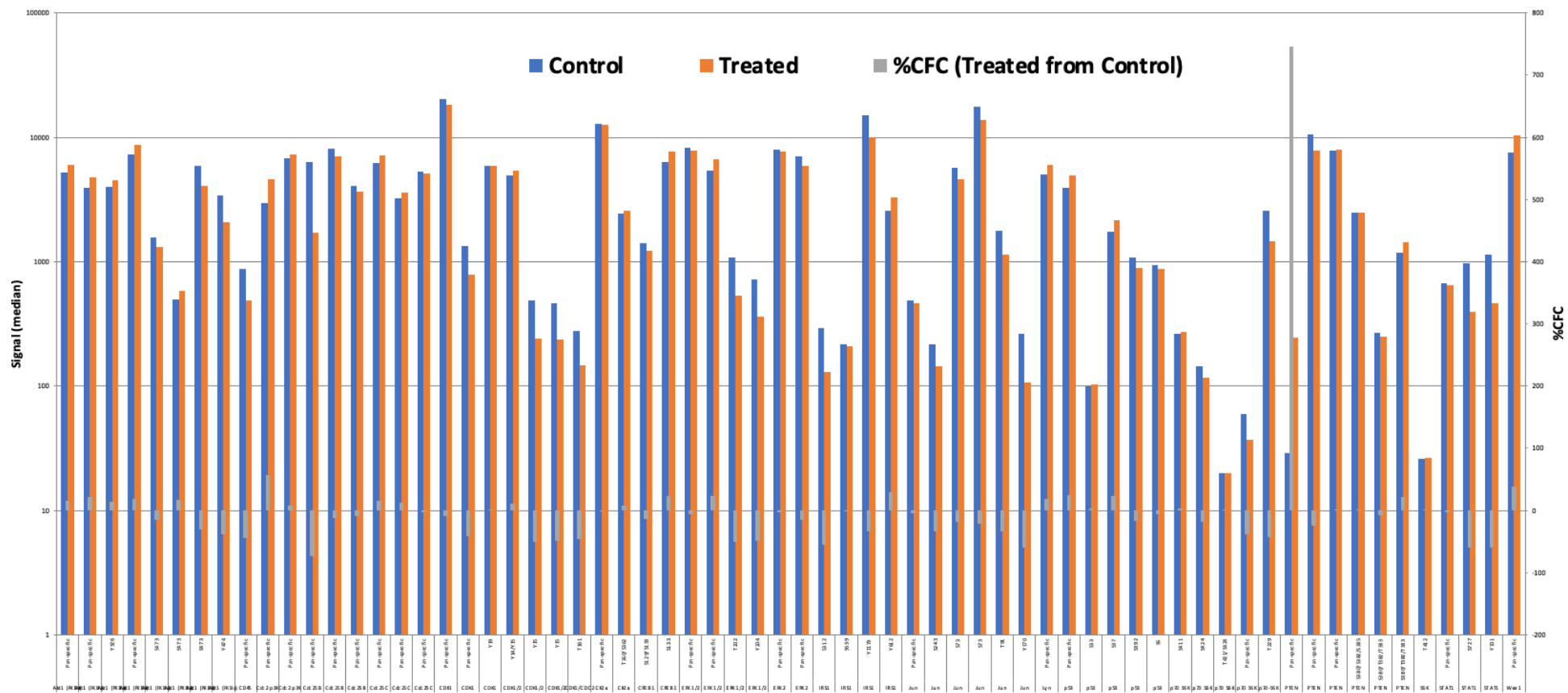


Figure 4.20. Changes of the key components of the SRC pathway that are interactive with DAP-3 in the Kinexus platform (Kinexus pathway P68400), from normal tissue to breast cancer tissues.

4.3.3. Expression of Heat shock protein 90 in breast cancer cells lines

Protein microarray analysis, following DAP-3 immunoprecipitation of breast cancer samples highlighted an interaction between DAP-3 and a number of molecules. Given its implication and importance in a number of the identified signalling pathways and clinical relevance, we chose to focus on the HSP90 molecule for in-depth analysis in the current study. We performed screening of HSP90 expression using conventional PCR and western blotting across the previously selected 9 cell lines (as described in Chapter 2.1.).

4.3.3.1. PCR screen for expression of HSP90 gene transcript

We performed a PCR screen of the selected molecules in the cohort of 8 breast cancer cell lines and 1 benign breast tissue cell line (Fig 4.21.) This has demonstrated a similar expression pattern between DAP-3 and HSP90a where decreased expression was present in BT-483, MDA-MB-361. Expression of HSP90b appeared uniform throughout all cell lines.

4.3.3.2. Expression of HSP90 proteins as detected by Western Blot

Similarly to the above, we also screened the protein expression of HSP90 in two of the cells that used in the subsequent experiments, namely MCF-7 and MDA-MB-231 As shown in Figure 4.22, HSP90 protein is strongly expressed in breast cancer cells.

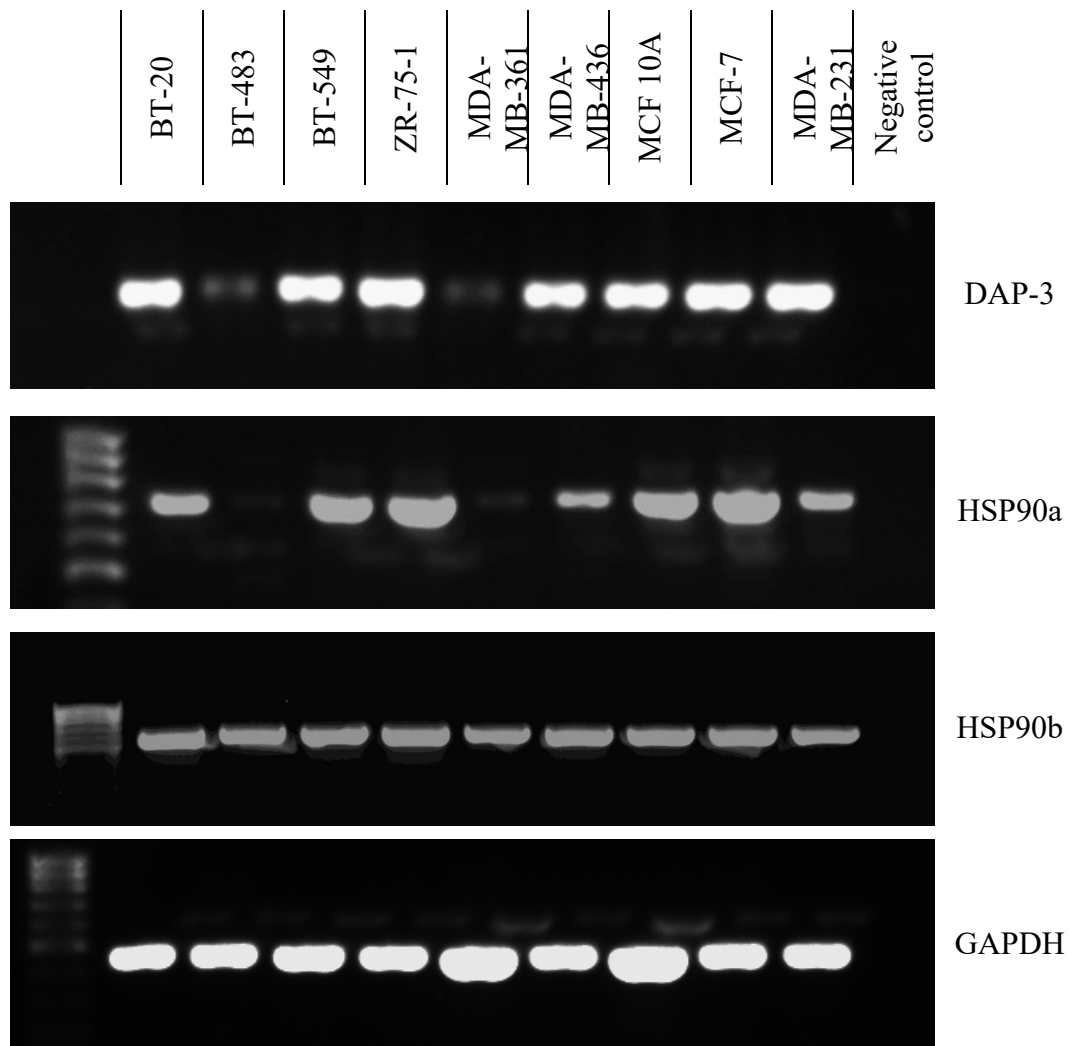


Fig. 4.21. Expression of DAP-3, HSP90 and GAPDH in 9 cell lines using conventional PCR. Representative images shown.

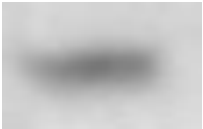
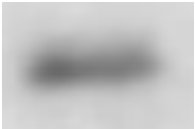



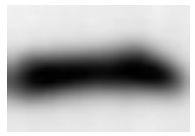
MCF-7	MDA-MB-231	
		DAP-3(45.5 kDa)
		HSP90(90 kDa)
		GAPDH(37 kDa)

Fig.4.22. Western blot screen of HSP90 candidate molecules in MCF-7 and MDA-MB-231 cell lines. Representative bands chosen to demonstrate expression of DAP-3, HSP90 and GAPDH in WT MCF-7 and MD-MB-231 cell lines. Images cropped for conciseness and composite preparation. Comparative bands for molecules of interest were taken from same images for comparison. DAP-3 and HSP90 expression confirmed in MCF-7 and MDA-MB-231,

4.4. Discussion

The study presented in this chapter aimed to explore which proteins interacted with DAP-3 in breast cancer and which of the proteins are differentially linked to DAP-3 in normal and tumour mammary tissues. Here, the study adopted a traditional method, namely immunoprecipitation, by which we used anti-DAP-3 antibody to pull out those interacting with DAP-3 from the tissues and then subject these samples to a protein platform to identify the key interacting proteins and also compared the difference between normal and tumour tissues. This protein platform KAM-880, which was available at the time of the study featuring 877 pan- and phosphosite-specific antibodies that were selected from over 6000 different commercial antibodies. Currently available platform is KAM-1325 (with approximately 627 proteins tracked) showing an obvious advancement of technology with expansion in the number of tested antibodies (168). Hence now, utilising the newest platform, we may have had identified more protein interactions and protein pathways.

The nature of the protein platform is that it recognises rather large number of proteins and kinases, as indeed shown in our study, in that a large number of proteins were found to be higher in tumour than normal, whereas others showing opposite (168). Using mathematical models to compared the degree of the difference, we obtained a list of proteins that are regarded as the priority targets of DAP-3 as shown in Table 4.5. Again, these are made of proteins either high in tumour or lower in tumour, compared with normal tissues. With this critical list, pathways significantly associated with this list of DAP-3 interactive proteins were constitutes. Very interestingly, amongst all the pathways identified were ERBB4 and ERBB2 pathways, the two classical pathways well known for their role in breast cancer. These two pathways hence became the centre of analysis for the relationship between clinical and outcome of the patients, patients' response to treatment in the context of DAP-3 expression in Chapter-6. Other interesting pathways including the ERK

pathway, BRAF, IL4/IL14 pathways are of strong interest and importance and hopefully will be explored in the context of DAP-3 in future studies.

As seen in the results of the priority protein targets for DAP-3 and HSP90 (both HSP90a and HSP90b) had a high-profile presence in half of the pathways discovered. These two heat shock proteins were also highly different in their association with DAP-3, namely heightened interaction in tumour tissues compared with normal tissues. Whilst the role of HSP90 in cancer and in breast cancer has already been discussed in the introduction, this finding does indeed suggest that HSP90 is a key partner protein of DAP-3 and that our results have shown that both are highly expressed in breast cancer. This has formed a base in the next chapter to explore how the DAP-3 and HSP90 interaction may impact on breast cancer cells.

We are though aware of the limitations of the *in vitro* models and the fact that DAP-3 is mainly intramitochondrial protein and HSP90 has more ubiquitous presence. Due to this it might be suggested that their interaction might be limited and facilitated with cell and mitochondrial lysis in or experiments. As suggested in final discussion chapter, validating this relationship *in vivo* models would be the ideal next step in future studies.

Chapter 5

Relationship between DAP-3 and HSP90 in breast cancer

5.1. Introduction

DAP-3 is a relatively novel protein, which is involved in programmed cell death and is believed to have proapoptotic and antioncogenic effects. It has been suggested that it is essential to embryonic development and it plays a key role in regulating mitochondrial function and its role in cell death (171, 172).

In breast cancer a strong inverse correlation between DAP-3 and tumour grade, Nottingham Prognostic Index, clinical stage, and clinical outcome has been identified. Furthermore, Kaplan-Meier analysis has shown better survival in the high transcription group, with this trend approaching significance (152).

Our laboratories have previously demonstrated that DAP-3 expression is linked to the progression of a number of human cancers including breast cancer and gastric cancer where higher expression is associated with patient prognosis (152, 154).

In a previous *in vitro* study conducted in our laboratories, the functional effects of DAP-3 knockdown on breast cancer cell lines were investigated. DAP-3 knockdown sub-lines of MCF-7 and MDA-MB-231 demonstrated significantly increased adhesion and decreased growth. Furthermore, invasion and migration were significantly increased in the MDA-MB-231^{DAP-3kd} cells vs. the controls. Taken together this led the authors to suggest DAP-3 silencing plays a part in breast carcinogenesis by increasing cell adhesion, migration and invasion (153).

Han *et al.* report that DAP-3 was found to be overexpressed across 17 cancer types. Knockdown of DAP-3 significantly decreased the malignant

properties of oesophageal squamous cell carcinoma (ESCC) and hepatocellular carcinoma (HCC), and this tumour-suppressing phenotype could be markedly rescued by recovering DAP-3 expression in cancer cells supporting that DAP-3 is a strong oncogene in cancer (150).

In gastric tumours higher DAP-3 expression was related to better prognosis. Increased cell migration and enhanced resistance to chemotherapy, through inhibition of apoptosis, was induced by DAP-3 expression knockdown (154) and the β -catenin/LGR5 axis has been shown to be involved in this pathway (173).

DAP-3 knockdown has also been demonstrated to lead to defects in mitochondria-encoded protein synthesis. Autophagy is shown to be inhibited by DAP-3 depletion, which results in sensitization of cells to intrinsic death stimuli (171).

The early-stage work of the present study (Chapter 3 and Chapter 4) has discovered that a member of the heat shock protein family, HSP90 was amongst the most notable protein which coprecipitated with DAP-3 in breast cancer and also demonstrated a marked difference between normal and tumour tissues. HSP90 and its 4 isoforms (HSP90a and HSP90b found in cytosol, GRP94 in endoplasmic reticulum and Trap1 in mitochondria) is thought to be the most abundant member of the Heat Shock Protein family and is a ubiquitously expressed ATP dependent chaperone protein that interacts with a great number of other proteins called clients (158). In normal cells, HSP90 is a vital regulator of the cell cycle, proliferation, signal transduction and transcriptional regulation. Under stress conditions, HSP90 induction is markedly upregulated to promote the misfolding and overexpression of client proteins (159). Positive expression of HSP90 and pyruvate kinase M2 (PKM2) in hepatocellular carcinoma was correlated with poor clinicopathological features and shown to be a strong predictive factor of poor prognosis of HCC patients (164).

Overexpression of oestrogen receptors is observed in most of breast cancer patients and they are also a class of clients of HSP90. These steroid receptors are HSP90 dependent clients that activate their target genes after binding to HSP90 (174).

As HSP90 is a potential significant target in cancer, HSP90 inhibitors have attracted a great amount of research attention with many currently in ongoing clinical trials (159), some of which have now reached Phase 2 and 3 clinical trials investigating effects of inhibition in non-small cell lung cancer, prostate cancer, gastrointestinal stromal tumours, melanoma, multiple myeloma and pancreatic cancer (175-180). HSP90 inhibitors have also been investigated in the breast cancer setting in HER2 positive disease (181, 182), suggesting synergistic action with Trastuzumab, overcoming Trastuzumab resistance.

Following our initial observations identifying an association and potential interaction between DAP-3 and HSP90, the aim of the current chapter is to explore the regulatory and functional implications of this association in breast cancer cell lines.

5.2. Methods

5.2.1. Cell lines

MCF-7 and MDA-MB-231 cell lines were selected as described previously and below. Both WT and DAP-3 knockdown variants described in earlier sections were utilised (152, 153).

5.2.1.1. MCF-7

This cell line represents a human breast adenocarcinoma derived from a 69-year-old Caucasian female metastatic pleural effusion. It is ER and PR positive and represents a model of early-stage disease.

5.2.1.2. MD-MB-231

This cell line represents a human breast adenocarcinoma derived from 51- year-old Caucasian female metastatic pleural effusion. It is ER/PR negative, HER2 negative, E-Cadherin negative and is commonly used to model late-stage breast cancer.

5.2.2. RT-qPCR

RT-qPCR (as described in Methods section 2.4.) was performed with primers of selected molecules designed for target gene amplification (Table 2.3). Specificity of used primers was validated using a positive control.

PCR amplification was performed and qPCR data were analysed and normalized to GAPDH.

5.2.3. Functional Assays

Functional assays provide model environments designed to assess specific cell functions and behaviours in an *in vitro* setting. These specific cell functions i.e. growth, adhesion, invasion and migration are important attributes of cancer progression.

5.2.3.1. Growth assay

This assay was used to determine growth of the selected cell line.

Cells were seeded and incubated in 96 well plates with specific concentrations of HSP90 inhibitor.

Plates were either incubated for over-night (reference plate), 3 days or 5 days. Following appropriate incubation cells were fixed with 4% formalin, stained with 0.5% crystal violet and, following extraction of the stain with 10% acetic acid, spectrophotometer readings were acquired before being processed with percentage change from the reference plate. Full details of this method were described in Methods chapter 2.12.1.

5.2.3.2. Adhesion assay

The adhesion assay was used to assess the ability of cells to adhere to an artificial base membrane, simulated by Matrigel.

Cells were seeded and incubated in Matrigel covered 96 well plates (5µg/well) with added specific concentration of HSP90 inhibitor. Following 45 minutes incubation, cells fixed with 4% formalin and stained with 0.5% crystal violet before being counted under the microscope. Full details of this method were described in Methods chapter 2.12.2.

5.2.3.3. Invasion assay

Invasion assay was used to assess the ability of studied cells to invade through basement membrane simulated by 8.0 µm pore Falcon well inserts pre-coated in Matrigel (50µg/well).

Cells were seeded into inserts and incubated in 24 well plates for 3 days with HSP90 inhibitor added in specific concentrations. Cells that invaded through the base of inserts with Matrigel coating were fixed in 4% formalin, stained with 0.5% crystal violet and counted under the microscope. Full details of this method were described in Methods chapter 2.12.3.

5.2.3.4. Scratch assay

Cell migration was examined using a scratch assay. 24 well plates were seeded and incubated till confluent. A scratch was made through each monolayer of cells using a plastic pipette tip. Measurement of the width of the scratch at specified time intervals was made, determining migration abilities of the studied cell line through rate of wound closure. Full details of this method were described in Methods chapter 2.12.4.

5.2.4. HSP90 Inhibitor

HSP90 small molecule inhibitor was used to treat either WT cells, to assess subsequent expression of DAP-3, or to treat DAP-3 KD and control variants of MCF-7 and MDA-MB-231 cell lines to assess potential combined effects on cell function.

The impact of the HSP90 inhibitor was tested in both concentration and time gradient capacities. Full details of this technique were described in Methods chapter 2.13.

5.2.5. Statistical analysis

Statistical analysis was undertaken using SigmaPlot and Graphpad statistical software packages as outlined in section 2.14. of the methods chapter. Comparisons were drawn using either two-sample, two tailed t-tests / Mann Whitney tests or One Way Analysis of Variance (ANOVA) / Kruskal Wallis tests based on data parameters and number of groups analysed.

5.3. Results

5.3.1. Expression analysis of HSP90 a/b in DAP-3 KD MDA-MB-231 and MCF-7 cells

The potential relationship between DAP-3 and HSP90 was explored in the DAP-3 knockdown MCF-7 and MDA-MB-231 cells (Fig 5.1) to establish if suppression of DAP-3 had implications on HSP90 transcript expression. qPCR highlighted a significant decrease of HSP90a transcript expression in MCF-7 DAP-3 KD cells (Fig 5.1A; $p=0.05$) and a similar trend was seen for HSP90b expression, though this was not found to be statistically significant (Fig 5.1B; $p=0.089$). A significant decrease in HSP90b expression was seen in MDA-MB-231 expression following DAP-3 knockdown (Fig 5.1D; $p=0.013$) and a similar trend was seen for HSP90a expression, though this was not quite significant (Fig 5.1C; $p=0.06$).

5.3.2. Expression profile of DAP-3 following HSP90 inhibition

Following the observation that DAP-3 suppression could influence HSP90 expression, we also explored the impact of HSP90 inhibition on DAP-3 expression in wild type MCF-7 and MDA-MB-231 cells.

The impact of HSP90 inhibition was assessed over a time course, where MCF-7 and MDA-MB-231 cells were treated with 30nM (IC₅₀ value of the inhibitor) over a broad time gradient (0, 0.5, 1, 2, 4, 24 hrs). Following treatment, DAP-3 expression in the cells was examined using qPCR (Fig 5.2). Few differences were seen in DAP-3 expression in either cell line following HSP90 inhibition at any of the tested timepoints and this was confirmed as non-significant both for MCF-7 (Fig 5.2A; $p=0.943$) and MDA-MB-231 (Fig 5.2B; $p=0.173$).

We further explored the impact of HSP90 inhibitor over a concentration gradient (0,3,15,30,150,300 nM) with MCF-7 and MDA-MB-231 cells exposed to such concentrations over a 4-hour period (Fig 5.3). Similar to the observations of the time course assessment, no significant changes in DAP-3 transcript expression were observed in either MCF-7 (Fig 5.3A; $p=0.121$) or MDA-MB-231 (Fig 5.3B; $p=0.781$).

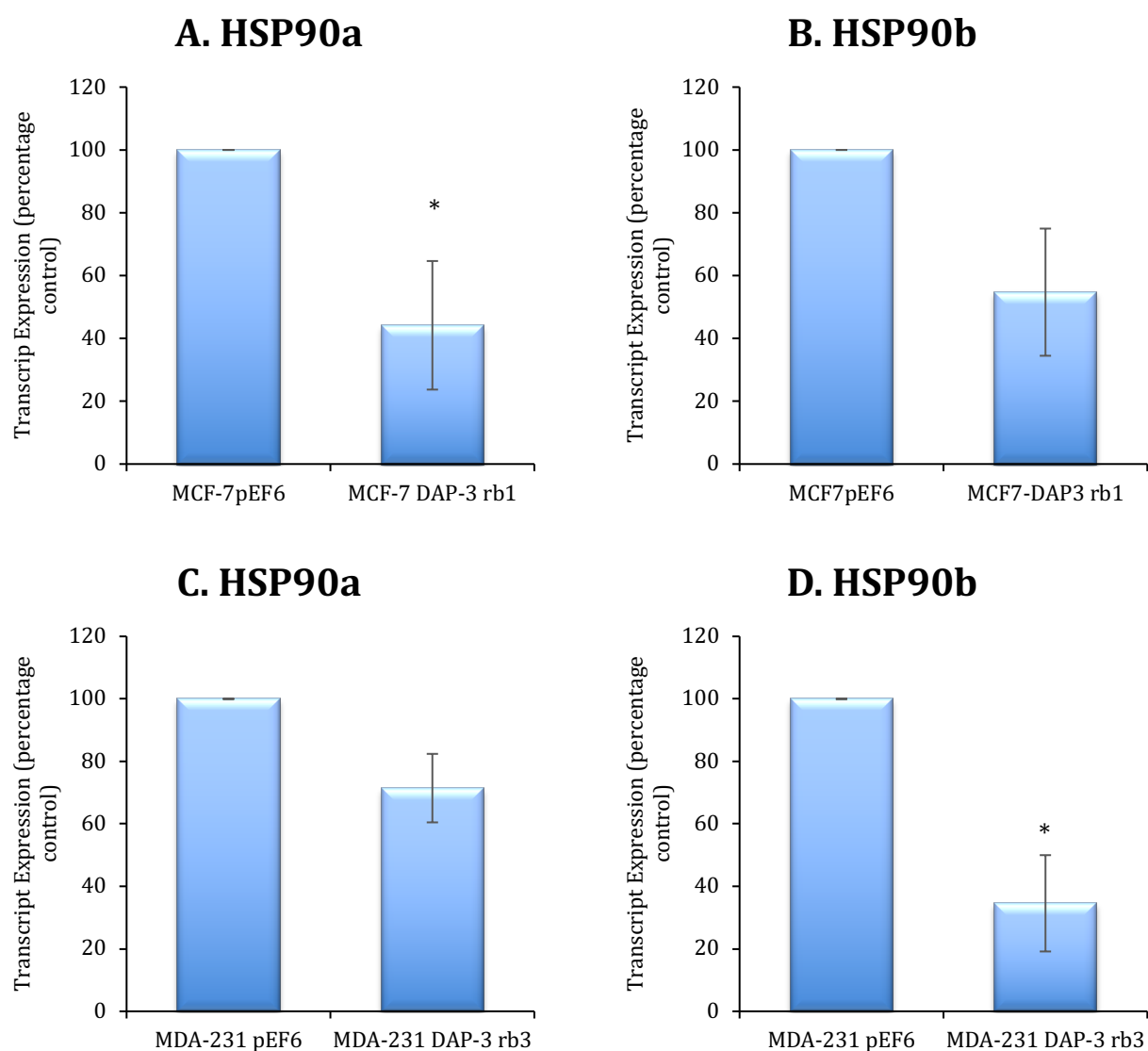


Fig.5.1. The expression profile of HSP90a/b at mRNA level in DAP-3 KD cell lines. (A) Significant decrease of HSP90a expression was observed in MCF-7 DAP-3 KD cells, and (B) a similar trend was seen for HSP90b expression. (C) Reduced levels of HSP90a were apparent in MDA-MB-231 DAP-3 knockdown cells and a significant decrease in HSP90b expression was seen in MDA-MB-231 cells following DAP-3 suppression (D). Data shown represents mean percentage increase of a minimum of 3 samples. * represents $p < 0.05$. Error bars represent SEM.

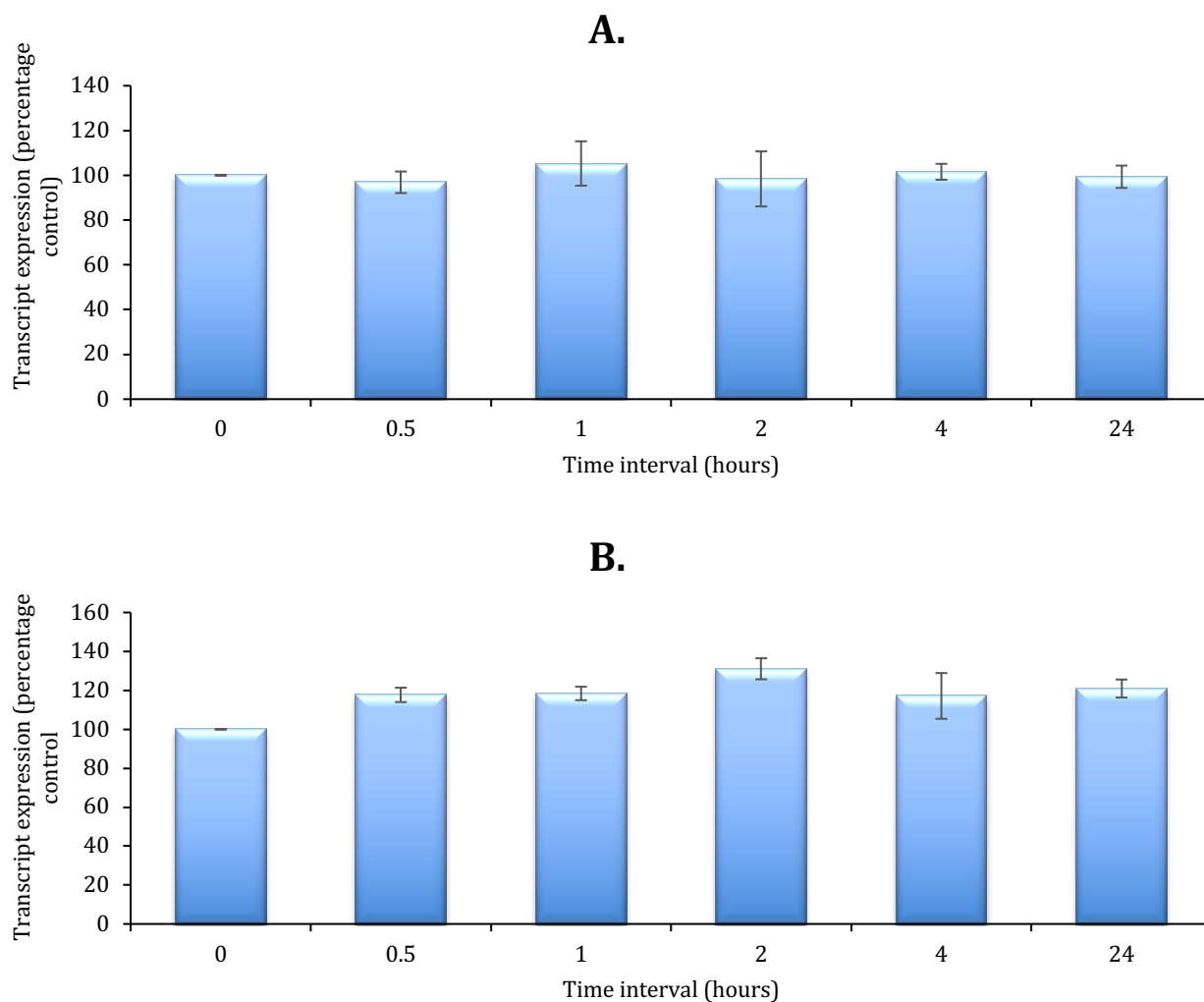


Fig. 5.2. Impact of HSP90 inhibition on DAP-3 expression over time. Wild type MCF-7 (**A**) and MDA-MB-231 (**B**) cells treated with 30 nM concentration of HSP90 inhibitor over indicated time periods. DAP-3 expression was assessed using qPCR. Data shown represents mean percentage untreated control. Error bars represent SEM.

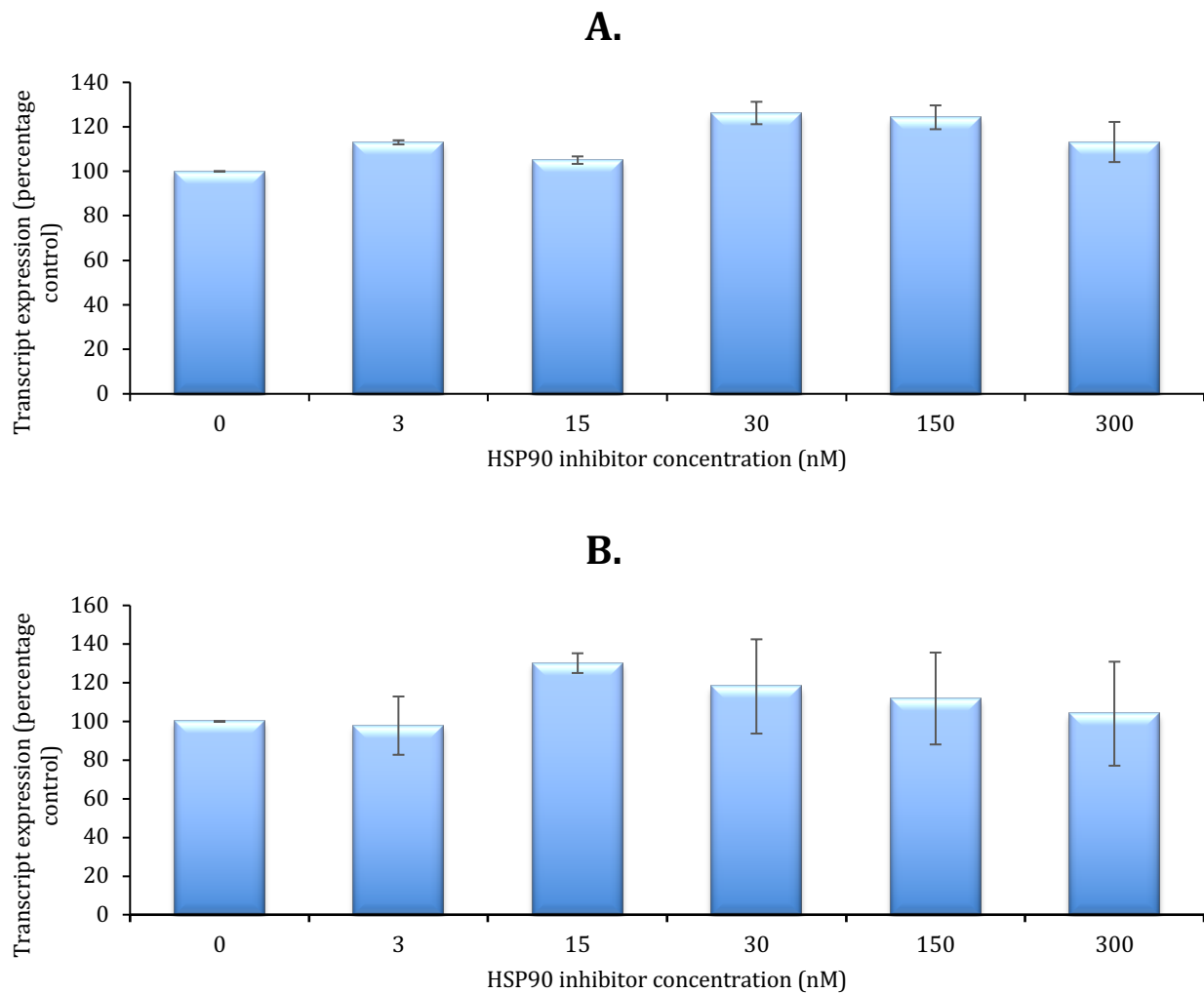


Fig. 5.3. Impact of increasing concentration of HSP90 inhibitor on DAP-3 expression. Wild type MCF-7 (**A**) and MDA-MB-231 (**B**) cells treated with a concentration gradient of HSP90 inhibitor over a 4-hour period. DAP-3 expression was assessed using qPCR. Data shown represents mean percentage untreated control. Error bars represent SEM.

5.3.3. Functional implications of the DAP-3 - HSP90 relationship

To gain a better understanding of the potential relationship between DAP-3 and HSP90 and its functional implication on breast cancer cells, we undertook a range of functional analysis to explore combined or differential effects in DAP-3 knockdown and control cells.

5.3.3.1. Growth Assay

The impact of DAP-3 suppression in combination with HSP90 inhibition on cell growth rates was explored using *in vitro* growth assays.

5.3.3.1.1. MCF-7

Growth assays were undertaken using both control pEF6 and DAP-3 suppressed MCF-7 cells in conjunction with a range of HSP90 inhibitor concentrations with an assessment of 3 day growth. Comparisons between untreated pEF6 and DAP-3 KD variant did not show any significant difference (Fig. 5.4.A).

The pEF6 cell variant was then treated with HSP90 inhibitor, over a range of concentrations, to explore its potential effects on cell growth. No significant change in growth rate was demonstrated across all concentration gradients (Fig. 5.4.B).

Further exploring the potential differential effects of HSP90 inhibition in DAP-3 knockdown cells, we also assessed the impact of a range of concentrations of the HSP90 inhibitor on MCF-7 DAP-3 KD cell variant. No significant differences were observed in this group (Fig. 5.4.C).

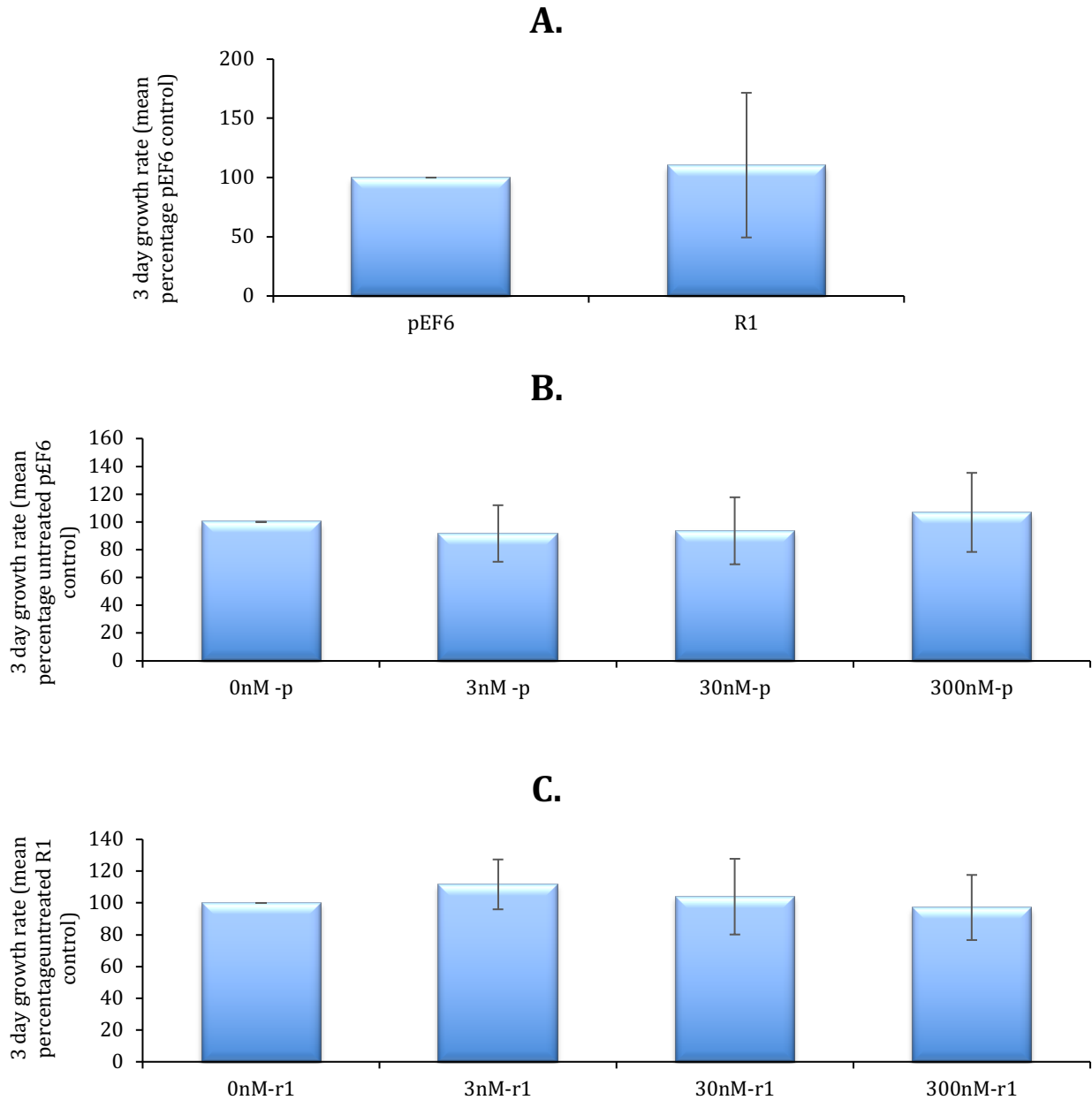


Fig. 5.4. Impact of DAP-3 suppression and HSP90 inhibition on MCF-7 cell growth.

A) Impact of DAP-3 Knockdown via ribozyme 1 on MCF-7 growth. Data shown represents mean percentage control 3-day growth rate. (B) Impact of HSP90 inhibition over a concentration gradient on control pEF6 cellular growth. Data shown represents mean untreated pEF6 percentage control. (C) Impact of HSP90 inhibition on MCF-7 ribozyme1 knockdown on cellular growth. Data shown represents mean untreated ribozyme 1 percentage control. Error bars represent SEM.

5.3.3.1.2. MDA-MB-231

Similarly, as for the MCF-7 cell line, growth assays were used to assess MDA-MB-231 cell growth utilising both control and DAP-3 suppressed MDA-MB-231 cells in conjunction with the HSP90 small molecule inhibitor over a range of concentrations over a 3-day incubation. No significant difference was demonstrated between untreated pEF6 and DAP-3 KD variant (Fig. 5.5.A).

Potential effects on cell growth were then explored by treatment of pEF6 cell variant with a HSP90 inhibitor over a range of concentrations. No obvious change was demonstrated in the 3nM treatment group. A general increase in growth rate was observed after adding 30nM and 300nM concentration of HSP90 inhibitor created a more prominent growth rate increase at the day 3 endpoint, but this did not reach significance (Fig. 5.5.B).

Possible differential impact of HSP90 inhibition in cells with suppressed DAP-3 expression were also explored. We assessed the impact of a range of concentrations of the HSP90 inhibitor on MDA-MB-231 RIB3 cell variants. Similar trends were observed as in the pEF6 lines, there were mild nonsignificant increases observed across all the concentration gradients with the 30nM concentration being the more pronounced (Fig. 5.5.C).

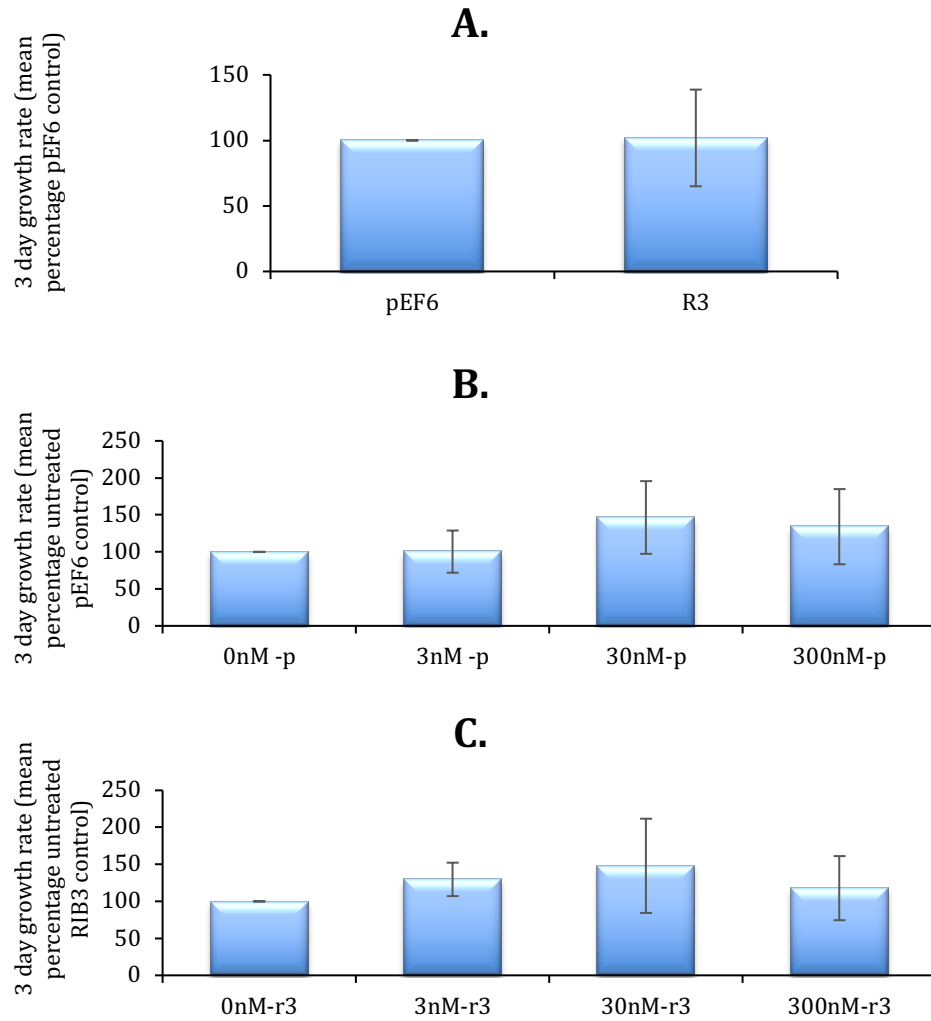


Fig. 5.5. Impact of DAP-3 suppression and HSP90 inhibition on MDA-MB-231 cell growth. (A) Impact of DAP-3 Knockdown via ribozyme 3 on MDA-MB-231 growth. Data shown represents mean percentage control 3-day growth rate. (B) Impact of HSP90 inhibition over a concentration gradient on control pEF6 cellular growth. Data shown represents mean relevant untreated pEF6 percentage control (C) Impact of HSP90 inhibition on MDA-MB-231 ribozyme3 knockdown cellular growth. Data shown represents mean untreated ribozyme 3 percentage control. Error bars represent SEM.

5.3.3.2. Adhesion Assay

The impact of DAP-3 suppression and HSP90 inhibition on cell matrix-adhesion was investigated using a Matrigel cell adhesion assay.

5.3.3.2.1. MCF-7

Matrigel adhesion assays were undertaken using both DAP-3 suppressed MCF-7 cells and HSP90 inhibitor treatment over a range of HSP90 inhibitor concentrations. Comparisons between untreated cells demonstrated a general but non-significant increase in MCF-7 adhesion following DAP-3 suppression (Fig 5.6.A).

This was further analysed in conjunction with the HSP90 inhibitor to explore the capacity of HSP90 inhibition on MCF-7 cell matrix adhesion through treatment of the control pEF6 MCF-7 cells with 3, 30 or 300nM HSP90 inhibitor. Matrix adhesion was calculated as a percentage of untreated pEF6 adhesion rate. Addition of the HSP90 inhibitor appeared to enhance matrix adhesion of the pEF6 cell lines, with significant differences being observed within this group ($p=0.009$). Post hoc analysis subsequently highlighted significant elevations in both the 3nM and 30nM concentration ($p<0.01$ and $p<0.05$ respectively vs. untreated pEF6 control) with a less apparent and non-significant effect observed following 300nM (Fig 5.6.B).

To explore potential differential effects of HSP90 inhibition in DAP-3 suppressed cells, we also explored the impact of a range of concentrations of the HSP90 inhibitor on MCF-7 cells containing DAP-3 ribozyme 1 (Fig 5.6.C). Adhesion was calculated as a percentage of the relative untreated DAP-3 ribozyme 1 controls and displayed similar trends to the pEF6 lines, namely a general increase in adhesion rates compared to

untreated cells with more prominent effects observed at 3nM and 30nM and reduced or no effect of 300nM, though such trends were not found to be statistically significant.

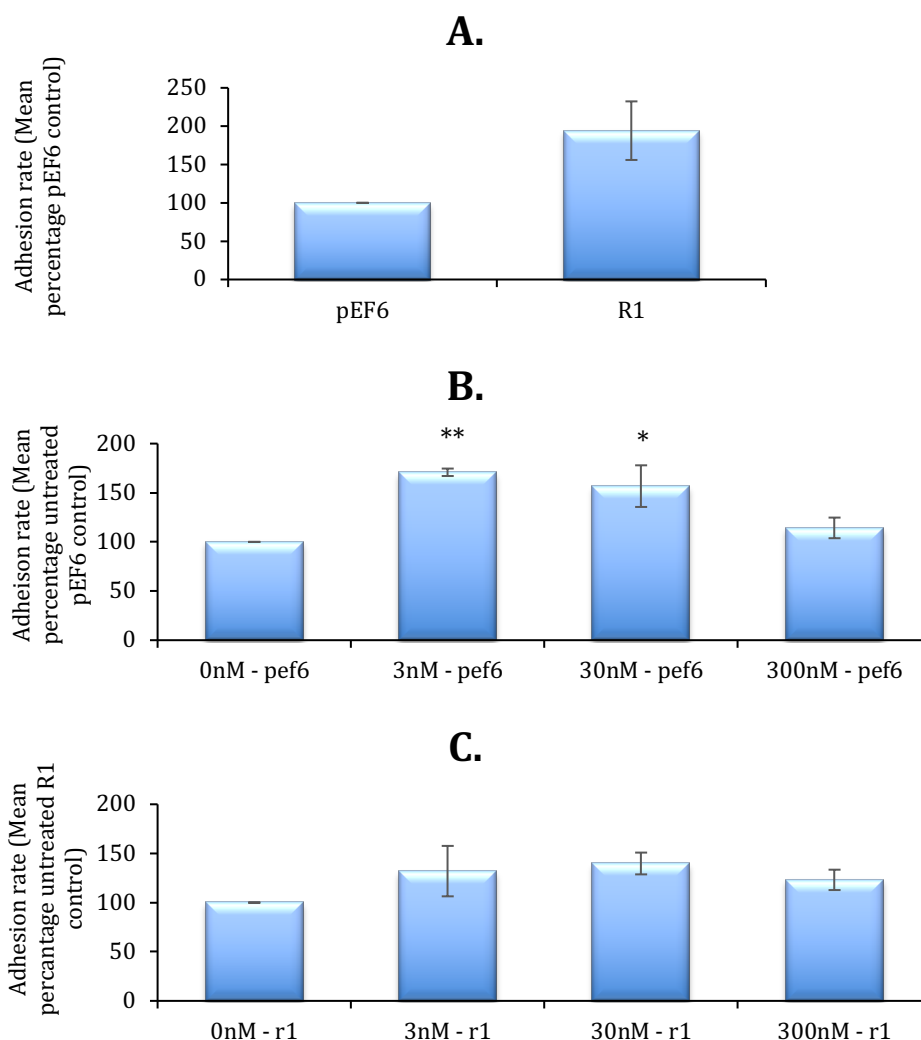


Fig.5.6. Impact of DAP-3 suppression and HSP90 inhibition on MCF-7 cell matrix adhesion. (A) Impact of DAP-3 Knockdown via ribozyme 1 on MCF-7 adhesion to Matrigel. Data shown represents mean pEF6 percentage control data. (B) Impact of HSP90 inhibition on control pEF6 cellular adhesion to Matrigel. Data shown represents mean untreated pEF6 percentage control. (C) Impact of HSP90 inhibition on MCF-7 ribozyme1 knockdown on cellular adhesion to Matrigel. Data shown represents mean untreated ribozyme 1 percentage control. Error bars represent SEM. ** represents $p < 0.01$ and * represents $p < 0.05$.

5.3.3.2.2. MDA-MB-231

As in MCF-7, Matrigel adhesion assays were undertaken using both DAP-3 suppressed MDA-MB-231 cells and HSP90 treatment over a range of HSP90 inhibitor concentrations.

Comparisons between all untreated cells demonstrated no significant difference in MDA-MB-231 adhesion following DAP-3 suppression (Fig 5.7.A).

This was further analysed in conjunction with the HSP90 inhibitor, through treatment of the control pEF6 MDA-MB-231 cells with a concentration gradient of HSP90 inhibitor. The addition of the HSP90 inhibitor seemed to augment adhesion at the lower 3nM and 30nM concentration with no obvious reaction observed following 300nM treatment (Fig 5.7.B).

Potential differential impact of inhibiting HSP90 in MDA-MB-231 DAP-3 suppressed cells was explored via application of range of concentrations of HSP90 inhibitor (Fig 5.7.C). In this group we observed a gradual decrease in adhesion of cells to Matrigel with increasing concentrations of HSP90 inhibitor demonstrated with 30nM and 300nM and the differences reached significance ($p=0.018$) within this group, though subsequent, post hoc analysis did not identify significant differences in any group compared to the untreated control, with only close to significant ($p=0.08$ adjusted p values) being obtained for the highest concentration.

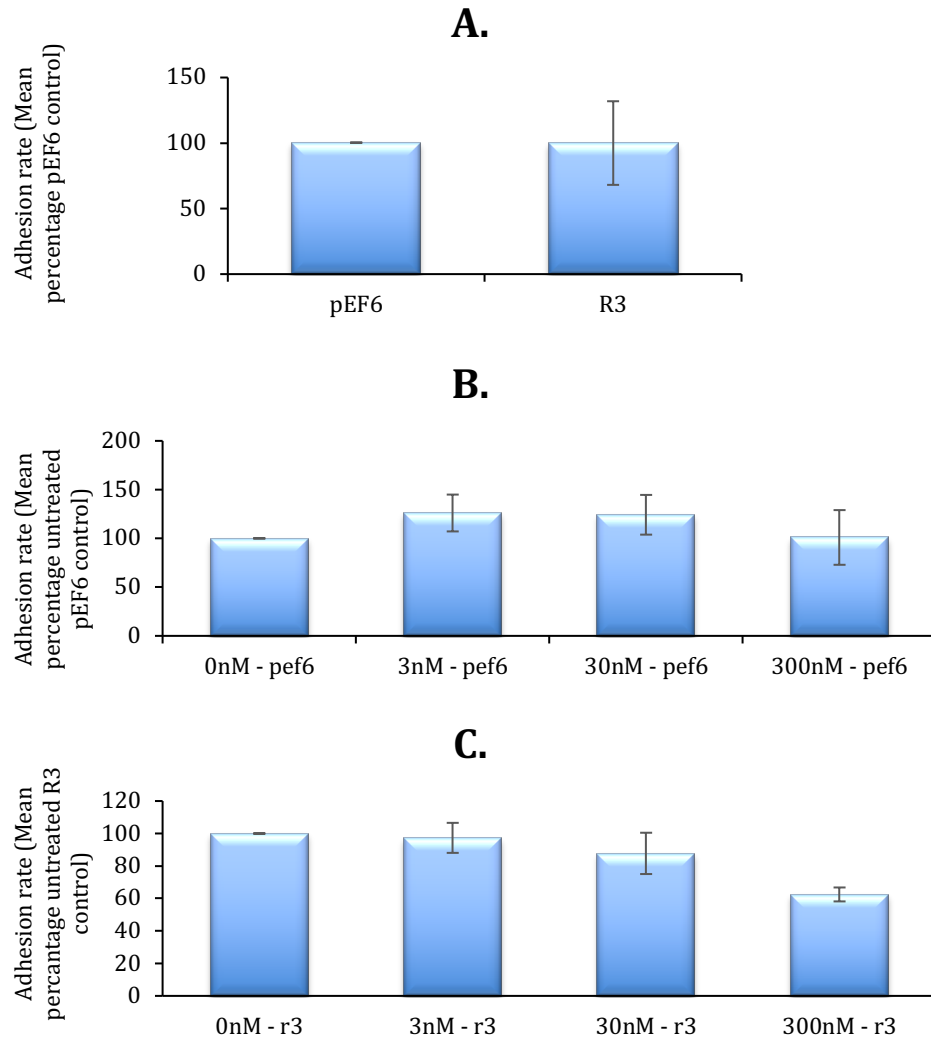


Fig.5.7 Impact of DAP-3 suppression and HSP90 inhibition on MDA-MB-231 cell matrix adhesion (A) Impact of DAP-3 Knockdown via ribozyme 3 on MDA-MB-231 adhesion to Matrigel. Data shown represents mean pEF6 percentage control data. (B) Impact of HSP90 inhibition on control pEF6 cellular adhesion to Matrigel. Data shown represents mean percentage untreated pEF6 control. (C) Impact of HSP90 inhibition on MDA-MB-231 ribozyme 3 knockdown on cellular adhesion to Matrigel. Data shown represents mean percentage untreated ribozyme 3 (R3) control. Error bars represent SEM.

5.3.3.3. Invasion Assay

Invasion assays were used to assess the ability of studied cells to invade through a simulated Matrigel basement membrane. The potential interaction and influence of DAP-3 and HSP90 was assessed using this functional assay. Cells that invaded through the porous base of a Falcon insert coated with layer of Matrigel were counted. Endpoint analysis was calculated based on the cell count after 3 days relative to controls (pEF6/untreated).

5.3.3.3.1. MCF-7

Matrigel invasion assays were conducted using MCF-7 DAP-3 KD cells and treatment with a concentration gradient of HSP90 inhibitor.

DAP-3 knockdown has demonstrated very mild nonsignificant increases in invasion compared to pEF6 controls (Fig 5.8.A). We further analysed this in combination with the HSP90 inhibitor treatment to determine the potential effects of HSP90 inhibition on MCF-7 cell matrix invasion by treatment of the control pEF6 MCF-7 cells with 3, 30 or 300nM HSP90 inhibitor. Invasion was calculated as a percentage of untreated pEF6 invasion rate. HSP90 inhibition seemed to augment matrix invasion at the higher 30nM and 300nM concentration with a less obvious impact observed following 3nM, although changes did not reach significance in this group (Fig 5.8.B).

We further explored the impact of HSP90 inhibition on MCF-7 cells with knocked down DAP-3 expression (Fig 5.8.C). Invasion was calculated as a percentage of the relative untreated DAP-3 RIB1 controls displaying similar

trends as the pEF6 lines, namely a general increase in invasion rates compared to untreated cells. This was more notable at 3nM and 30nM concentration and less pronounced at 300nM with close to significant changes identified within this group ($p=0.062$).

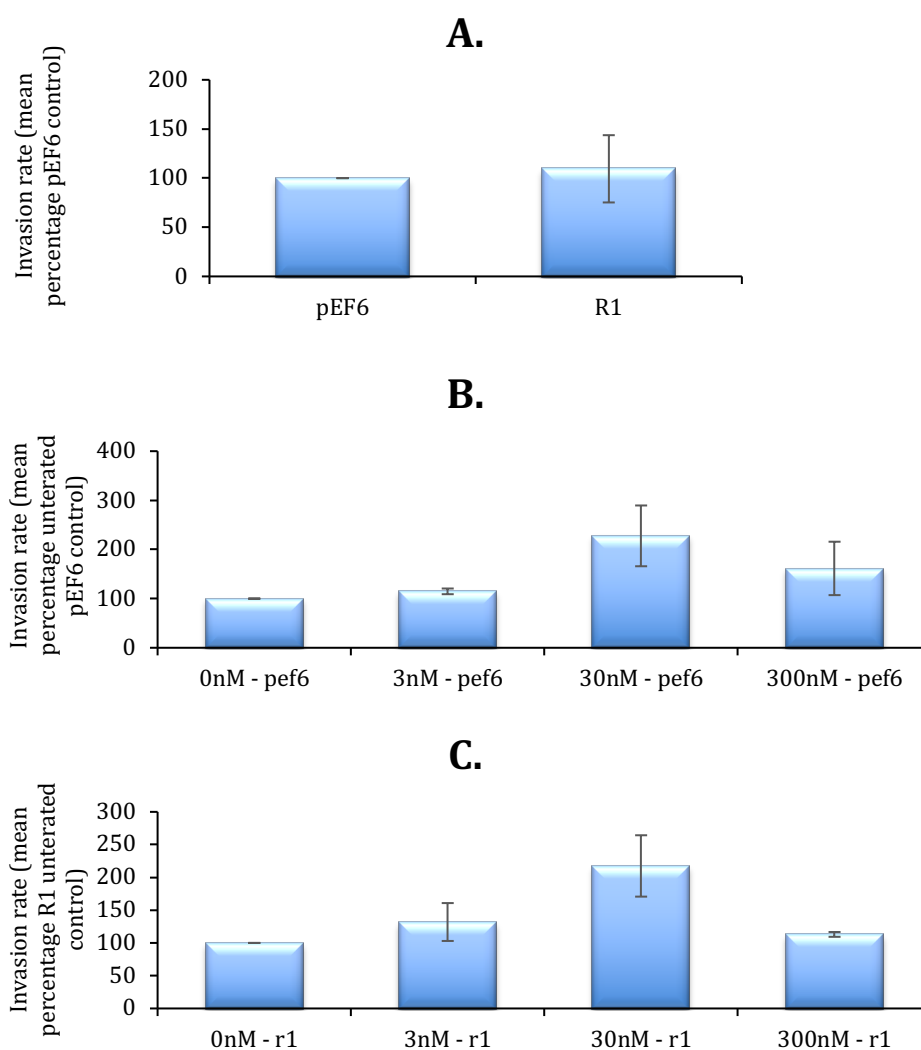


Fig. 5.8. Impact of DAP-3 suppression and HSP90 inhibition on MCF-7 cell invasion. (A) Effect of DAP-3 knockdown (RIB1) on MCF-7 invasion. Data shown represents mean pEF6 percentage control data. (B) Impact of HSP90 inhibition on control pEF6 cellular invasion. Data shown represents mean percentage untreated pEF6 control. (C) Impact of HSP90 inhibition on MCF-7 DAP-3 KD (RIB1) on cell invasion. Data shown represents mean percentage untreated RIB1 control. Error bars represent SEM.

5.3.3.3.2. MDA-MB-231

MDA-MB-231 DAP-3 KD cells were used to explore cell invasion along with treatment with a concentration gradient of HSP90 inhibitor.

In this cell line, knockdown of DAP-3 appeared to enhance invasion compared to pEF6 control, albeit non-significantly. (Fig 5.9.A).

Further analysis to explore the effects of HSP90 inhibition on invasion with the application of a concentration gradient on pEF6 cell variant was performed. Invasion was calculated as a percentage of untreated pEF6 invasion rate. The inhibition of HSP90 appeared to generally amplify invasion at the higher 30nM and 300nM concentration and this was less apparent at 3nM. Although the changes have not reached significance in this group (Fig 5.9.B).

MDA-MB-231 DAP-3 KD cells were subsequently assessed for the effect of HSP90 inhibition across a concentration gradient of HSP90 inhibitor in conjunction with DAP-3 knockdown (Fig 5.9.C). Invasion was calculated as a percentage of the relative untreated DAP-3 RIB3 controls manifesting an increase in invasion rates compared to untreated cells observed at 3nM and 30nM concentration and with no changes at 300nM. Changes within this group did not reach significance.

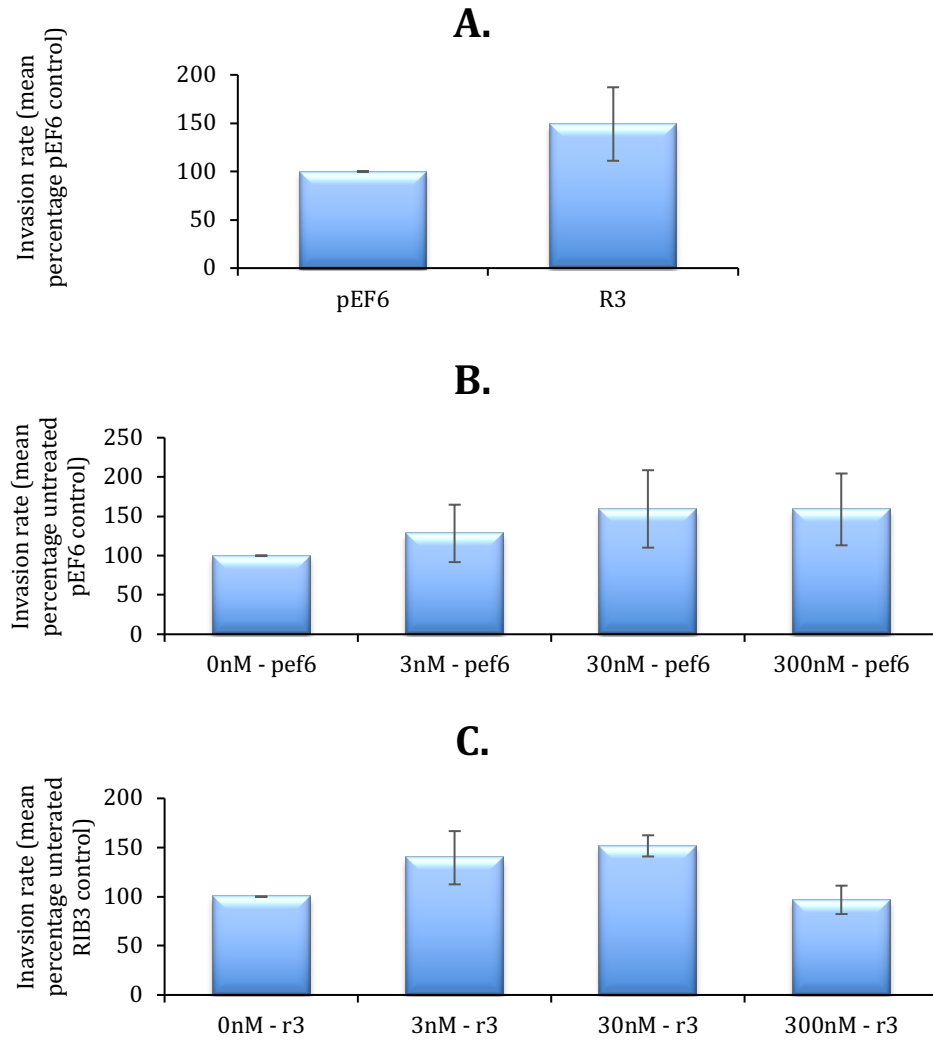


Fig. 5.9. Impact of DAP-3 suppression and HSP90 inhibition on MDA-MB-231 cell invasion (A) Effect of DAP-3 knockdown (RIB3) on MDA-MB-231 invasion. Data shown represents mean pEF6 percentage control data. (B) Impact of HSP90 inhibition on control pEF6 cellular invasion. Data shown represents mean percentage untreated pEF6 control. (C) Impact of HSP90 inhibition on MDA-MB-231 DAP-3 KD (RIB3) on cell invasion. Data shown represents mean percentage untreated RIB3 control. Error bars represent SEM.

5.3.3.4. Scratch migration assay

The impact of DAP-3 and HSP90 and possible interactions was undertaken using a scratch / wounding migration assay. Confluent monolayers were scratched/wounded and migration tracked over a range of timepoints. Endpoint analysis was calculated based on the wound width after 4 hours relative to the 0-hour wound width with decreased wound width indicative of migration.

5.3.3.4.1. MCF-7

Migration in MCF-7 cells was firstly compared in untreated MCF-7 DAP-3 KD RIB1 variant and pEF6 controls at the experimental 4-hour endpoint. Such analysis did not highlight any significant change in rates of migration following DAP-3 knockdown (Fig.5.10. A).

Migration was further assessed in MCF-7 pEF6 subgroup of cells treated with a concentration gradient (0, 3, 30, 300 nM) of HSP90 inhibitor and measured at the 4-hour endpoint to explore the isolated effect of HSP90 on cell migration. This has again not shown any significant difference in pEF6 cell migration at any of the concentrations tested, suggesting minimal impact of HSP90 on MCF-7 cell migration rates (Fig.5.10. B).

We have further explored the combined effect of DAP-3 KD together with a concentration gradient of HSP90 inhibitor in MCF-7 cells. The MCF-7 DAP-3 KD (RIB1) cell variant did not show any significant difference in migration across all HSP90 inhibitor concentration gradient treatments (Fig. 5.10 C).

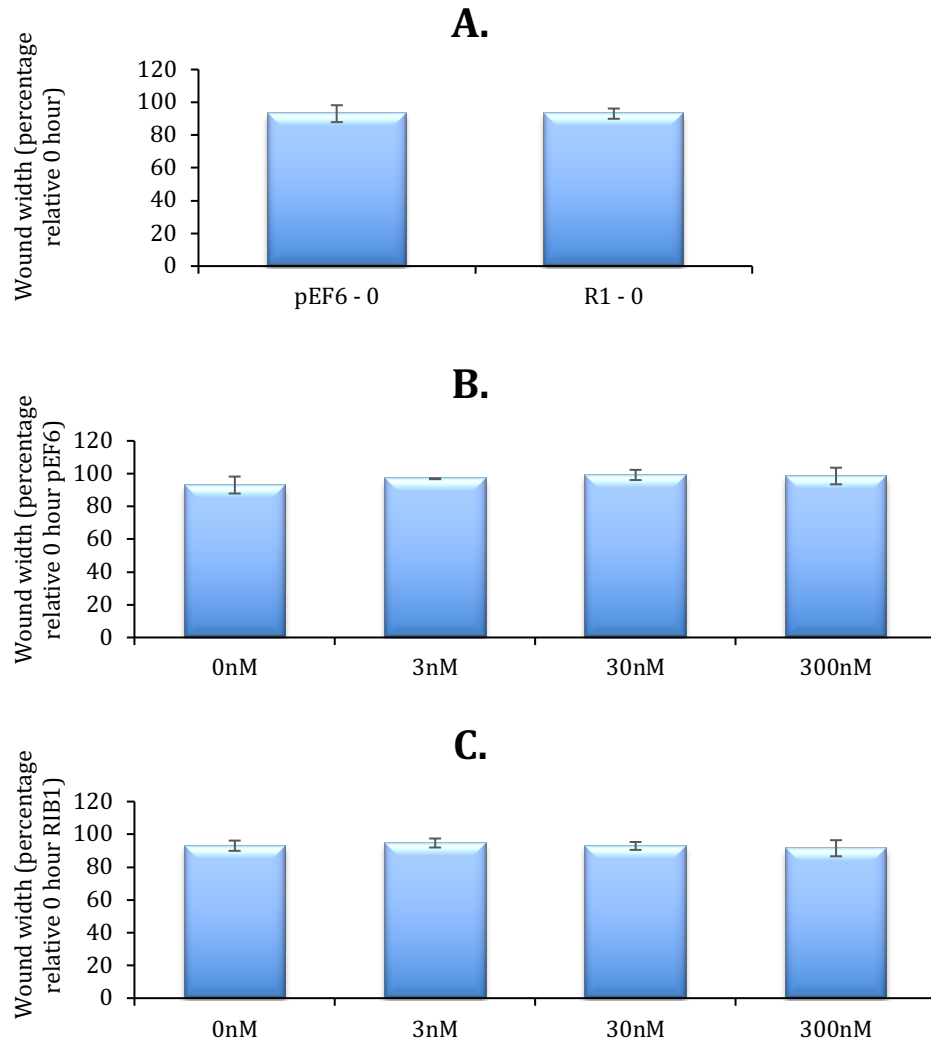


Fig. 5.10. Impact of DAP-3 suppression and HSP90 inhibition on MCF-7 cell migration rates. (A) Effect of DAP-3 knockdown (RIB1) on MCF-7 cell migration. Data shown represents mean percentage change in wound width, after 4 hours, based on relative 0-hour width. (B) Impact of HSP90 inhibition over a concentration gradient on control pEF6 cellular migration. Data shown represents mean percentage change in wound width, after 4 hours, based on relative 0-hour width. (C) Impact of HSP90 inhibition over a concentration gradient on MCF-7 DAP-3 KD (RIB1) on cell migration. Data shown represents mean percentage change in wound width, after 4 hours, based on relative 0-hour width. Error bars represent SEM.

5.3.3.4.2. MDA-MB-231

Migration in MDA-MB-231 cells was initially assessed in relation to impact of DAP-3 knockdown over the 4-hour period. Such analysis did not highlight any significant changes in migration between pEF6 control and DAP-3 RIB3 suppressed cells although reduction in migration has been observed in DAP-3 KD variant. (Fig. 5.11. A)

Migration was further assessed in MDA-MB-231 pEF6 cells treated with a concentration gradient (0, 3, 30, 300 nM) of HSP90 inhibitor and assessed at the 4-hour endpoint to explore the isolated effect of HSP90 on MDA-MB-231 migration. This has not demonstrated any significant impact of HSP90 inhibition on MDA-MB-231 control pEF6 cell migration (Fig. 5.11. B)

The combined effect of DAP-3 knockdown together with a concentration gradient of HSP90 inhibitor in MDA-MB-231 cells was subsequently explored. This again did not show any significant differences across the applied concentration gradient of HSP90 inhibitor on migration of the DAP-3 KD variant MDA-MB-231 cells (RIB3), although there appears to be a general increase in migration observed across the concentration gradients (Fig. 5.11. C).

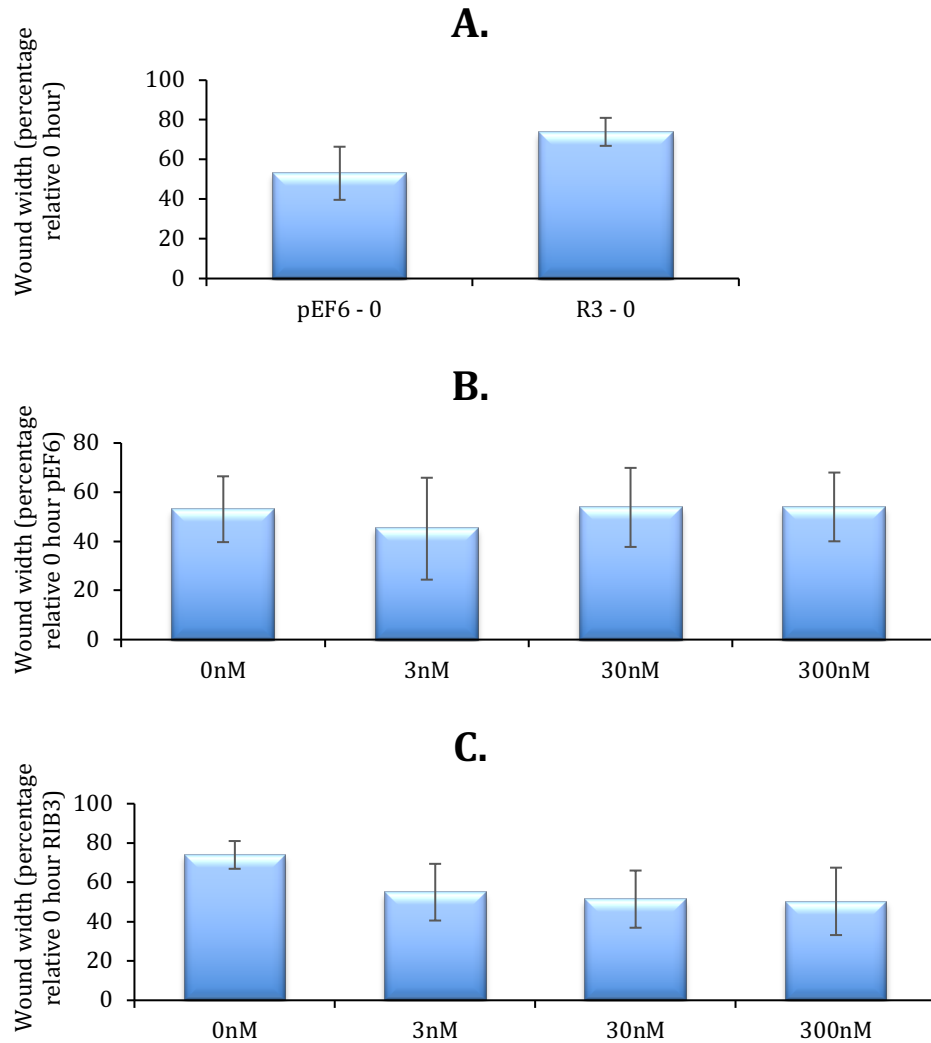


Fig. 5.11. Impact of DAP-3 suppression and HSP90 inhibition on MDA-MB-231 cell migration rates. (A) Effect of DAP-3 knockdown (RIB3) on MDA-MB-231 cell migration. Data shown represents mean percentage change in wound width, after 4 hours, based on relative 0-hour width. (B) Impact of HSP90 inhibition over a concentration gradient on control pEF6 cellular migration. Data shown represents mean percentage change in wound width, after 4 hours, based on relative 0-hour width. (C) Impact of HSP90 inhibition over a concentration gradient on MDA-MB-231 DAP-3 KD (RIB3) on cell migration. Data shown represents mean percentage change in wound width, after 4 hours, based on relative 0-hour width. Error bars represent SEM.

5.4. Discussion

The link between DAP-3 and HSP90 in human breast cancer has not been described before and DAP-3 has not been identified as a client protein to HSP90 (158). As far as we are aware the only mention in the literature is by Hulkko *et al.* where, in yeast models, they indicate a weak interaction between DAP-3 and HSP90 (183).

To further explore the potential relationship between HSP90 and DAP-3 we explored the impact of DAP-3 knockdown on HSP90 expression. qPCR results highlighted a significant decrease of HSP90a expression in MCF-7 DAP-3 KD cells and a similar trend was seen for HSP90b expression. A significant decrease in HSP90b expression was also seen in MDA-MB-231 expression following DAP-3 knockdown and a similar trend was seen for HSP90a expression.

Furthermore, we explored the impact of inhibiting HSP90 using a small molecule inhibitor (Benzisoxazole) on the expression of DAP-3 in wildtype MCF-7 and MDA-MB-231 cells. Interestingly, MCF-7 and MDA-MB-231 wild type cells treated with HSP90 inhibitor did not demonstrate any significant differences in DAP-3 expression levels over a range of time points or concentration gradients in the conducted experiments. These results indicate that DAP-3 influences HSP90 expression but there does not seem to be a reverse effect, as HSP90 inhibition had no significant effect on DAP-3 expression which may suggest that HSP90 could be a downstream transcriptionally regulated effector of DAP-3.

DAP-3, as a mitochondrial ribosomal protein, is essential for the *de novo* mitochondrial-encoded protein synthesis and its interactions have been well described in literature. Knockdown of DAP-3 has shown to decrease cellular ATP production, cause protein synthesis defects and mitochondrial dissipation. Xiao *et al.* 2015 suggest that knockdown of

DAP-3 regulates the phosphorylation of dynamin-related protein 1 (Drp1) and promotes mitochondrial fission and facilitates cell death (171).

DAP-3, kept inactive as a phosphoprotein by the action of protein kinase B (AKT/PKB), once activated interacts with FAS Associated Death Domain (FADD) and participates in the formation of Death inducing signalling complex (DISC) (146). Death ligand signal enhancer (DELE), whose knockdown in HeLa cells was found to inhibit apoptosis, has also been described to bind with DAP-3 (147). DAP-3 was also described as one of the binding partners of hNOA1, the human homologue of AtNOA1 (*Arabidopsis thaliana* nitric oxide-associated protein 1) which appears to play a role in mitochondrial respiration and apoptosis (184). Although there does not to be any reports of known downstream effectors transcriptionally regulated by DAP-3 as we describe in our study.

The functional effects of DAP-3 expression knockdown in gastric cancer promoted cell migration and enhanced resistance to chemotherapy by inhibiting apoptosis (173). In breast cancer DAP-3 knock down has been observed to cause increase in cell adhesion, migration and invasion (153). This compares favourably to our results where we observed non-significant increase in adhesion and invasion. Although we observed decreased migration following DAP-3 knockdown. These results could potentially be explained by the use of different methodology used to explore breast cancer migration (Electric cell-substrate impedance sensing (ECIS) vs scratch/migration assay) or potentially cancer type specific differences between breast and gastric cell lines.

HSP90 inhibition appears remarkably appealing as it has the capacity to simultaneously disrupt multiple cancer pathways by acting on a single target. HSP90 is essential for the stability and function of a wide spectrum of oncogenic proteins that among others directly contribute to distinctive features resulting from genetic and epigenetic alterations of key regulatory proteins – these have been described as Hallmarks of

cancer (185). They include 1. sustaining proliferative signalling, 2. evading growth suppressors, 3. resisting cell death, 4. enabling replicative immortality, 5. inducing angiogenesis, 6. activating invasion and metastasis, 7. deregulated cellular energetics, 8. avoiding immune destruction, 9. tumour-promoting inflammation, and 10. genome instability and mutation.

The effects of HSP90 inhibition that we have observed in breast cancer cell lines showed non-significant increase in growth and invasion, while increases in adhesion has reached significance. No obvious changes were observed in cell migration following HSP90 inhibitor treatment. Oh *et al.* 2017, evaluated effects of HSP90 inhibition on MDA-MB-231 cells and reported decrease in both migration and growth (186). Further authors describe decrease in invasion, migration and proliferation in MDA-MB-231 cell lines following HSP90 inhibitor treatment (187-189).

This appears to be in contrast to our results although they have used much higher concentrations, longer exposure to HSP90 inhibitor and a different HSP90 inhibitor. This could explain the discrepancy in our results as the effects could be dose and exposure-time dependent. There are 17 HSP90 inhibitors that were evaluated for the treatment of cancer. Majority of these work through inhibition of the N-terminal ATP-ase . Into this group are included Geldanamycin (which is the first described HSP90 inhibitor), Radicicol and Gantespib. Further mechanisms of action involve disruption of the co-chaperone interactions into which group belong Coumermycin A, Novobiocin and Chlorobiocin. Other mechanism of action is inhibition of the C-terminus of HSP90 into which group belong Celastrol, Gedunin, Antimycin A and Curcumin (190).

Within our experiments, the most obvious combined effect of HSP90 inhibition and DAP-3 KD seems to be inhibition of adhesion and also general increase of invasion which would be in keeping within our experiments' observed isolated DAP-3 KD and HSP90 inhibitor effects.

This could suggest that HSP90 inhibition potentially further enhances the effects of DAP-3 knockdown on adhesion and invasion and warrants further investigation as this has not been previously described in literature.

Taken together, our results indicate that DAP-3 may play an important role in modulating the expression of HSP90 and also interact with this molecule and give more insight into potential DAP-3 downstream effectors. Such data may reveal a potential lead for new targeted therapies.

Chapter 6

Clinical Implications of DAP-3 and HSP90 in breast cancer progression and chemo resistance

6.1. Introduction

HSP90, as a ubiquitous chaperone protein, is involved in many biochemical pathways. Further proteins called co-chaperones fine-regulate these chaperone processes. There have also been described post translational changes to HSP90 to further regulate its function (191). As described in Chapter 1, HSP90 inhibitors have been evaluated as potential therapeutic agents in treatment for various types of cancer with number of clinical trials under way.

Chemotherapy in breast cancer plays an important part of treatment especially in the triple negative variant.

Paclitaxel and docetaxel are potent chemotherapy drugs that have found their clinical use from 1990s (192). Since then, both have been evaluated in a number of clinical trials either as monotherapy or combination therapy in various subgroups of breast cancer. Anthracyclines as well have been broadly used with significant patient benefits (99, 193-199).

Resistance to these cytotoxic drugs remains a big challenge and there has been a significant drive to try to overcome this (200). Selection of patients based on the presence of specific biomarkers has been a path that has been evaluated in clinical trials and combination therapy being favoured over monotherapy in many cases. Paclitaxel with an inhibitor of apoptosis agent in patients with identified gene expression signature showed promising results (201). The LOTUS trial investigated the benefits of an PI3K/AKT inhibitor when added to paclitaxel treatment demonstrating longer progression free survival in patient with triple negative breast cancer (202).

Expression of one of our molecules of interest, DAP-3 was also evaluated in the context of chemotherapy resistance in patients with gastric cancer.

Jia et al. have demonstrated that DAP-3 knockdown enhanced resistance to chemotherapy in gastric cancer (154).

As presented in previous chapters, our exploration of potential signalling and interactive events associated with DAP-3, by way of immunoprecipitation and protein kinase array, has demonstrated that the HSP90 proteins, both HSP90a and HSP90b, are amongst the most prominent proteins partners thus identified.

The study presented in this chapter, was based on the early findings and aimed to establish a relationship between DAP-3 and HSP90 in relation to therapy response in both in clinical settings and at a cellular level. The study assessed the expression levels of HSP90 in relation to clinical factors and clinical outcomes of the patients. We also intended to reveal any links of HSP90 combined with DAP-3 to OS and DFS. As chemotherapy resistance is a significant limiting factor in breast cancer treatments, we aimed also to concentrate on assessing the potential relevance of expression levels of DAP-3 and HSP90 in different chemotherapy response groups, by taking advantages of both our cell models and also available chemoresistance information of existing public database.

6.2. Materials and Methods

6.2.1. Cell lines and cell cultures

MCF-7 and MDA-MB-231 cell lines were selected as described previously. Both vector control and DAP-3 knockdown variants described in earlier sections were utilised. MCF-7, being an ER and PR positive variant, represents a model of early-stage disease. MDA-MB-231 is a triple negative variant representing a late-stage disease model.

Both cell lines were grown in maintenance DMEM medium. DMEM medium supplemented with blasticidin S (5µg/ml) was used for selection post transfection. A medium with lower concentration of blasticidin S (0.5µg/ml) was used for maintenance and routine culture (as detailed in Chapter 2.1.).

6.2.2. RNA extraction, quantification and cDNA synthesis

For cell RNA extraction the TRI Reagent protocol was followed. RNA was precipitated in a form of a pellet which was repeatedly washed with DEPC water and ethanol solution. The pellet was subsequently dissolved in DEPC water and a Nanophotometer was used to quantify the acquired RNA.

GoScript™ Reverse Transcription kit was used for reverse transcription of obtained RNA to obtain cDNA (Details of this process were described in Chapter 2.2.).

6.2.3. RT-qPCR

RT-qPCR was performed with primers of chosen molecules tailored for target gene amplification. Positive control was used to validate specificity of used primers. Following PCR amplification, qPCR data were normalized to GAPDH and analysed (as described in detail in Methods section 2.4.).

6.2.4. Clinical cohort

Standardised proteins and genetic material from paired normal and breast cancer tissue samples were available from a cohort described in a previous study from our laboratories (152). Tissue samples studied in this cohort were collected from 1990 to 1994. 127 cancerous breast tissues and associated 33 non-

cancerous tissues were collected under ethical approvals issued by Bro Taf Health Authority (ethics approval numbers 01/4303 and 01/4046).

Patients were treated according to local guidelines with breast-conserving surgery and followed by radiotherapy. Oestrogen receptor (ER) positive patients received adjuvant Tamoxifen. ER negative, high-grade cancers, and node-positive cases were treated with adjuvant therapy. No neo-adjuvant treatment was used (full details are listed in section 2.7.).

Transcript levels of HSP90 from breast cancer specimens were compared to the associated non-cancerous tissue followed by correlation of 10-year follow-up period of gathered clinicopathological data.

6.2.5. HSP90, DAP-3 and sensitivity to chemotherapy in patients with breast cancer.

Here, we used a comprehensive public database as reported by Fekete and Gyorffy (2019) (www.rocplot.org) (203), in that the database combined multiple public available databases with, in total, 3014 patients with breast cancer and with therapeutic options recorded. The database took the approach of ROC (receiver operating characteristic curve) which allows classification of patients' sensitivity to a therapy. Here, the AUC (Area Under the Curve) values and the statistical value for sensitivity to treatment were recorded. Additionally, the levels of the respective gene expression of the gene of interest were also displayed together with their statistical power (by Mann-Whitney U test).

6.2.6. Chemotherapy agents and Chemotherapy resistance assessment in cell models

Paclitaxel and Docetaxel chemotherapeutic agents were used in this study. Pure compounds of Paclitaxel and Docetaxel were purchased from Sigma-Aldrich for the present study. Paclitaxel and Docetaxel are commonly used agents with a number of publications utilising such compounds over a range of concentrations (204). For our studies, based on these literature and previous work within our group we utilised 50nM as our test concentration as this concentration has demonstrated cytotoxic effects in both cell lines, with concentrations above 50nM paclitaxel reported to have little further effect in an early report (205). Concentrations of 50nM were applied to MCF-7 and MDA-MB-231 cell lines either with or without a HSP90 inhibitor (section 2.12.) alongside untreated controls in a growth assay.

6.2.7. Growth assay

A growth assay was used to determine growth of the selected cell line and impact of the tested chosen treatments (HSP90 inhibitor and or Chemotherapy agents).

Cells were seeded and incubated in 96 well plates with specific concentrations of HSP90 inhibitor and or Chemotherapy agents. Plates were incubated for 3 days. Following incubation, cells were fixed with 4% formalin, stained with 0.5% crystal violet and, following extraction of the stain with 10% acetic acid, spectrophotometer readings were acquired before being processed with percentage change from the reference plate. (Details of this process were described in Methods chapter 2.11.1.)

6.2.8. HSP90 inhibitor

HSP90 small molecule inhibitor (Benzisoxazole Hsp90 inhibitor, purchased from Santa Cruz Biotechnologies Inc., Santa Cruz,

California, USA) was used here as a chemical tool to block the activity of HSP90. Benzisoxazole (SC-223790, Chemical ID CAS 1012788-65-6) is known to bind to the N-terminal domain of the HSP90 protein and blocking the docking of the HSP90 protein partners. The IC50 for Benzisoxazole is 30nM on multiple cell types. In our complex cell models, in which DAP-3 expression was knocked down as presented in early chapters, Benzisoxazole was used to suppress the activity of HSP90. Here, the HSP90 small molecule inhibitor was used to treat either pEF6 control variants of MCF-7 and MDA-MB-231 cells or DAP-3 KD variant with or without added chemotherapeutic agents Paclitaxel and Docetaxel.

6.2.9. Statistical analysis

SigmaPlot and Graphpad statistical software packages were utilised for statistical analysis (outlined in section 2.13.). Comparisons were drawn using either two-sample, two tailed t-tests / Mann Whitney tests or One Way Analysis of Variance (ANOVA) / Kruskal Wallis tests based on number of groups analysed and data parameters. Correlations were carried out using the Spearman ranked correlation test.

6.3. Results

6.3.1. Clinical cohort analysis (HSP90A & HSP90B)

Expression of HSP90A and HSP90B gene transcripts in our breast cancer cohort as stated earlier was explored. The levels in different groups were presented, together with the relationship to incidence of local recurrence and metastasis.

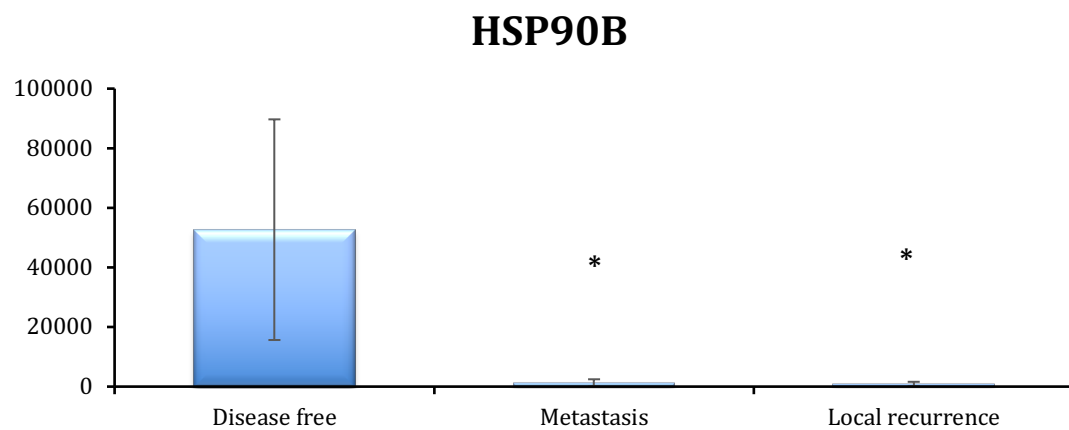
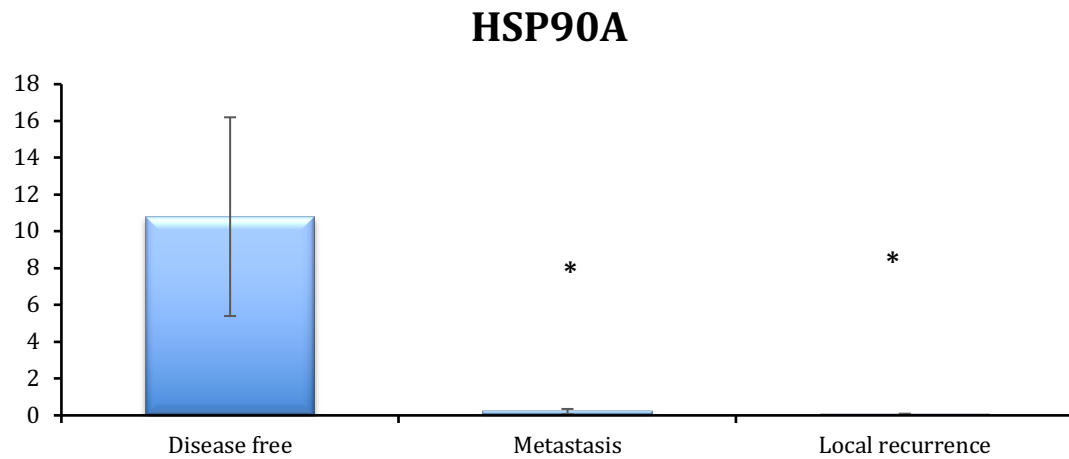
Table 6.1. has shown the levels of expression of both HSP90A and HSP90B in the breast cohort. HSP90A and HSP90B appears to show a

different pattern of expression. Tumour tissues had lower levels of HSP90A although the difference is not statistically significant ($p=0.10$). There does not appear to be a significant link between HSP90A with tumour grade, NPI (Nottingham Prognostic Index) and tumour staging. However, tumours from patients who development distant metastases and with local recurrence had significantly different levels of HSP90A than tumours from those who remained disease free ($p=0.05$ and $p=0.048$, respectively). The other noteworthy finding was that HSP90A levels in ER-beta positive tumours were significantly lower than the negative ones ($p=0.007$). The same was not seen with ER. HSP90B transcription levels were significantly higher in ER positive tumours than ER negative ones ($p=0.0097$), however no significant difference was observed in ER variant.

Low expression of HSP90A and HSP90B in breast cancer tissue was linked to local recurrence and metastasis and is presented graphically in Fig.6.1.

Table 6.1. Expression of HSP90A and HSP90B transcripts in the Cardiff breast cancer cohort.

			HSP90A		HSP90B	
		(n)	Transcript levels	p value	Transcript levels	p value
Tissue type	Normal	33	2.28±1.09		800246±667139	
	Tumour	127	8.73±3.77	0.10	85815±51543	0.30
NPI	<3.4	68	10.54±6.91		18872±10094	
	3.4-5.4	38	7.42±3.94	0.70	102934±83682	0.33
	>5.4	16	2.76±1.43	0.27	318889±317940	0.36
Grade	1	24	5.26±4.8		157798±156548	
	2	43	17.5±11.4	0.33	14147±6316	0.37
	3	7	10.02±6.45	0.56	682004±681340	0.48
TNM staging	1	2	0.744±0.744		68251±68251	
	2	40	6.38±3.59	0.13	16656±13670	0.59
	3	7	10.02±6.45	0.20	682004±681340	0.40
	4	4	0.179±0.095	0.59	58.7±58.3	0.50
Outcome	Live & Well	90	10.81±5.36		52664±37026	
	With met.	7	0.209±0.136	0.05	1255±1203	0.17
	With local recurr.	5	0.0528±0.038	0.048	853±759	0.17
	Died of BrCa	16	7.51±5.17	0.66	349235±317072	0.37
	All BrCa incidence	28	4.24±2.92	0.28	194503±176708	0.44
	(-)	75	6.21±2.47		4454±1680	
ER	(+)	38	4.17±2.55	0.57	105392±81146	0.0096
ERβ	(-)	91	6.84±2.29		46890±35406	
	(+)	24	0.432±0.272	0.007	9037±6221	0.30



	RNA normalised relative transcript expression		
	Disease free	Metastasis	Local recurrence
HSP90A			
Mean	10.8	0.209	0.0528
SEM	5.4	0.14	0.038
p vs. DF		0.05	0.048
HSP90B			
Mean	52664	1255	853
SEM	37026	1203	759
p vs. DF		0.17	0.17

Fig. 6.1. HSP90A (top) and HSP90B (bottom) expression with regards to Disease free survival, Metastasis, and Local recurrence. Mean data shown, error bars represent SEM. * represents $p < 0.05$.

6.3.2. HSP90 survival analysis (OS & DFS for HSP90A, HSP90B, HSP90A & DAP-3 combined and HSP90B & DAP-3 combined)

Survival analysis was performed on our clinical cohort alongside available clinico-pathological parameters and follow up data. Overall survival and disease-free survival were assessed with regards to HSP90A or HSP90B alone and also in combination with DAP-3.

6.3.2.1. OS and DFS for HSP90A

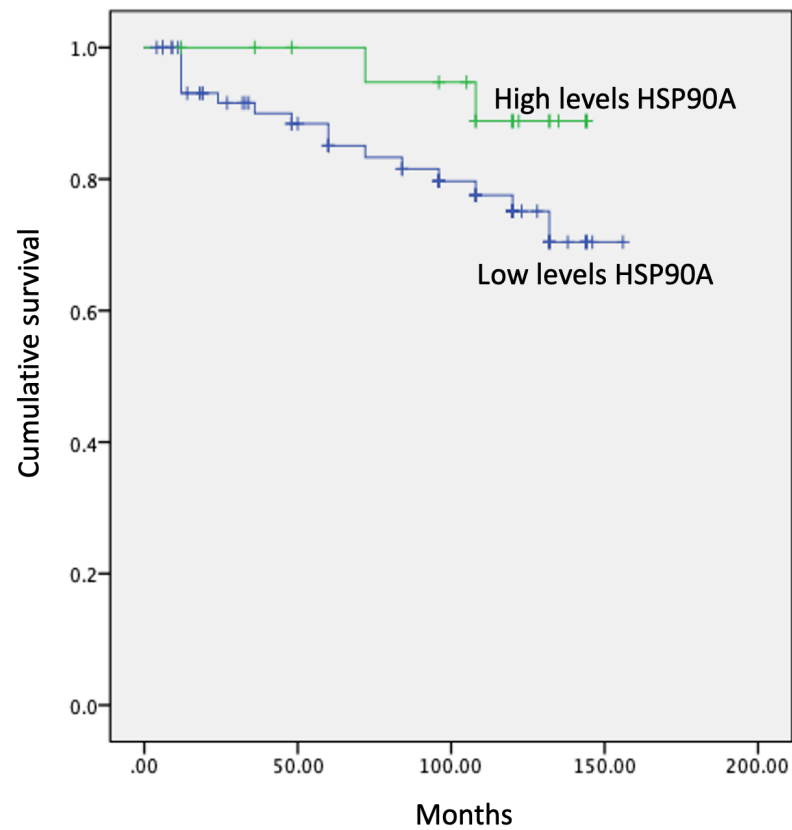
We first assessed the value of HSP90A on the overall survival and disease-free survival of the patients. As shown in Figures 6.2 and 6.3, patients with high levels of HSP90A and HSP90B in breast tumours had a longer overall and disease-free survival. However, they were not significant, with a possibility that the sample size was limited.

6.3.2.2. OS and DFS HSP90B

We similarly analysed the relationship between HSP90B and both overall survival (Figure 6.4) and disease-free survival (Figure.6.5.).

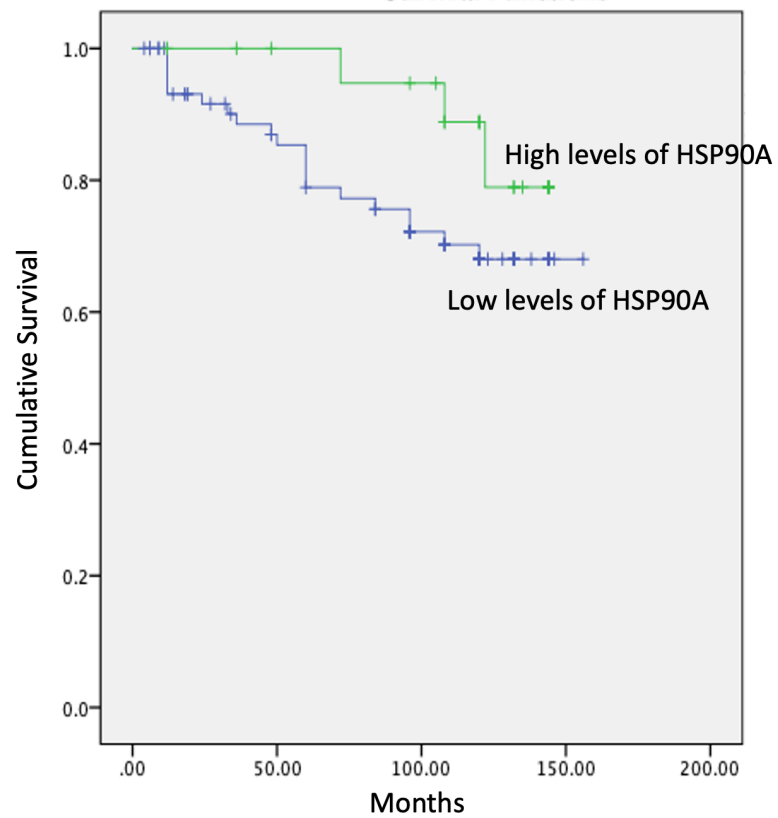
Similar to HSP90A, there was a weak but non-significant difference between HSP90B and the overall survival in that high levels of HSP90B had longer survival (Figure 6.4). However, high levels of HSP90B are significantly associated with a longer disease-free survival of the patients (Figure 6.5).

Tables 6.2. and 6.3. demonstrated the Cox regression model (Table 6.2.) and multivariate analyses (Table 6.3.) against both OS and RFS.



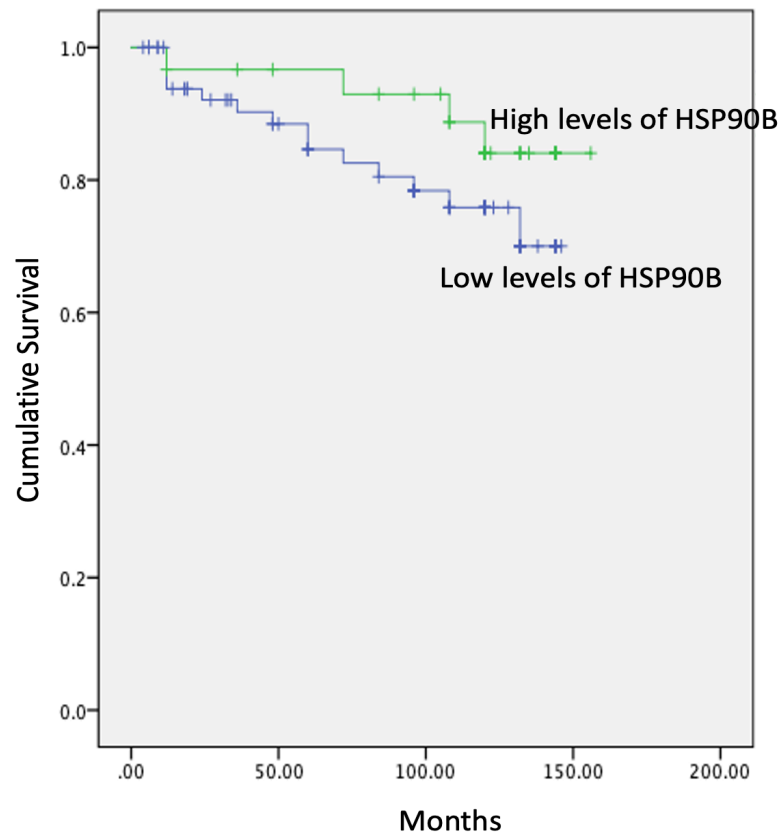
Overall Comparisons			
	Chi-Square	df	Sig.
Log Rank (Mantel-Cox)	2.319	1	.128
Breslow (Generalized Wilcoxon)	2.561	1	.110
Tarone-Ware	2.451	1	.117
Test of equality of survival distributions for the different levels of VAR00014.			

Fig.6.2. Kaplan-Meier analysis of overall survival. Patients were stratified by the expression level of HSP90A.



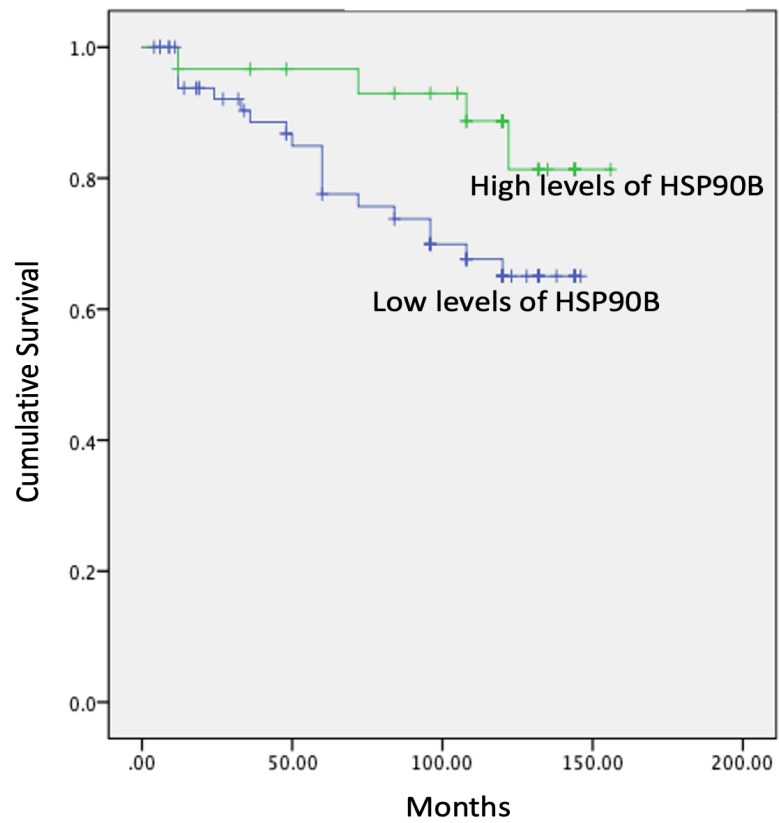
Overall Comparisons			
	Chi-Square	df	Sig.
Log Rank (Mantel-Cox)	2.282	1	.131
Breslow (Generalized Wilcoxon)	3.529	1	.060
Tarone-Ware	3.011	1	.083
Test of equality of survival distributions for the different levels of VAR00014.			

Fig.6.3. Kaplan-Meier analysis of disease-free survival. Patients were stratified by the expression level of HSP90A.



Overall Comparisons			
	Chi-Square	df	Sig.
Log Rank (Mantel-Cox)	1.675	1	.196
Breslow (Generalized Wilcoxon)	1.847	1	.174
Tarone-Ware	1.777	1	.183
Test of equality of survival distributions for the different levels of VAR00021.			

Fig.6.4. Kaplan-Meier analysis of overall survival. Patients were stratified by the expression level of HSP90B



Overall Comparisons			
	Chi-Square	df	Sig.
Log Rank (Mantel-Cox)	3.747	1	.053
Breslow (Generalized Wilcoxon)	4.418	1	.036
Tarone-Ware	4.235	1	.040
Test of equality of survival distributions for the different levels of VAR00021.			

Fig.6.5. Kaplan-Meier analysis of disease-free survival.
Patients were stratified by the expression level of HSP90B

Table 6.2. Cox regression analysis of HSP90A and HSP90B against the survival of the patients

	OS		RFS	
	p value	Exp(B)	p value	Exp(B)
HSP90A	0.318	0.369	0.941	1.09
HSP90B	0.9	0.909	0.259	0.341

Table 6.3. Multivariate analysis against OS and DFS for both HSP90A and HSP90B

	OS		DFS	
Factors	F value	p value	F value	p value
NPI	2.014	0.1	3.375	0.039
Grade	0.381	0.822	0.245	0.783
TNM staging	2.08	0.09	1.455	0.239
Nodal status	2.754	0.033	4.058	0.021
ER status	2.632	0.04	4.199	0.018
ER β status	0.959	0.434	0.11	0.896
HSP90A	1.788	0.139	3.294	0.042
HSP90B	1.1	0.362	2.496	0.088

6.3.2.3. Correlations between DAP-3 and HSP90 in breast cancer

Following observations in earlier chapters highlighting a highly interesting interaction between DAP-3 and HSP90, we also analysed how the two molecules may be correlated in the breast cancer cohort. Here, we correlated the two complexes in our breast cancer cohort and also in the TCGA public database (170)(both from gene microarray and from RNAseq) (Table 6.4).

Overall, HSP90A and HSP90B are well correlated from both the TCGA and Cardiff cohort. The two TCGA platform datasets showed that both are significantly correlated although the correlation coefficients are at relatively low range. The Cardiff cohort has shown a highly marked correlation between the two HSP90 members, both in tumours and also when tumour and normal are combined (all the tissues tested).

However, when the correlation between DAP-3 and HSP90 are examined, there are discrepancies. Firstly, both TCGA datasets showed a similar significant correlation between DAP-3, HSP90A and HSP90B. In the Cardiff breast cancer cohort, DAP-3 was found significantly correlated with HSP90A in tumour tissues. The same correlation was not seen between DAP-3 and HSP90B in tumour tissues.

Within the Cardiff cohort, we also undertook separately analysis of the correlations in normal tissues and the entire cohort. As shown in Table 6.4., there was no significant correlations between any of the three molecules, with a possible reason that the sample size was small (n=33). However, when the entire

cohort of normal and tumour tissues combined, DAP-3 was significantly correlated with both HSP90A and HSP90B.

Table 6.4. Correlations between DAP-3 and HSP90s. Data from the Cardiff cohort, from the TCGA cohorts of gene microarray and RNAseq studies.

TCGA (gene array)	Tumour		HSP90A	HSP90B
Tumour^a	DAP-3 vs	r	0.1712	0.2329
		p	<0.001	<0.001
	HSP90A	r		0.1427
		p		<0.001
TCGA^b (RNAseq) Tumour	DAP-3 vs	r	0.1367	0.1353
		p	<0.001	<0.001
	HSP90A	r		0.2883
		p		<0.0001
Cardiff^c Tumour	DAP-3 vs	r	.289**	0.141
		p	0.005	0.182
	HSP90A	r		.656**
		p	.	<0.00001
Cardiff^d Normal	DAP-3 vs	r	-0.071	-0.024
		p	0.766	0.922
	HSP90A	r		-0.027
		p		0.909
Cardiff^e Normal+Tumour	DAP-3 vs	r	.303**	.208*
		p	0.001	0.026
	HSP90A	r		.675**
		p		<0.000001

* by Spearman ranked correlation

r: correlation coefficient

^a n=4929

^b n=1090

^c n=127

^d n=33

^e n=160

6.3.2.4. OS and DSF for DAP-3 and HSP90A/HSP90B combined

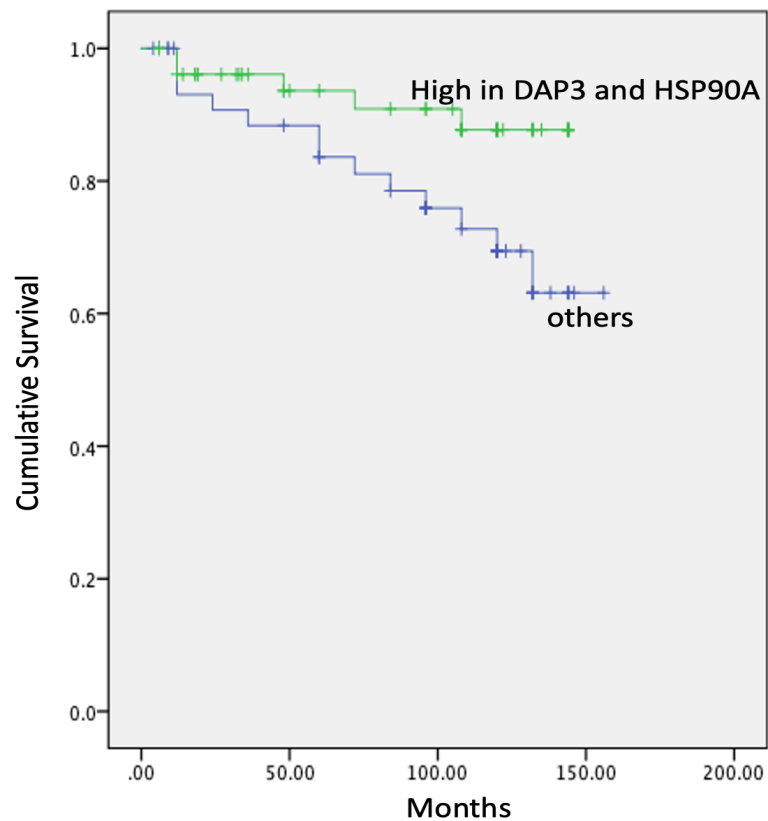
From the survival analysis of single molecules against patient's overall survival, it is clear that neither HSP90A nor HSP90B had a marked impact on assessing the survival of the patients. In light of the potential interaction between DAP-3 and HSP90 proteins, the significant correlations between these molecules in the breast cancer cohort (both TCGA and our Cardiff cohort), it was possible that when these molecules were combined in their pattern of expression, there may be a stronger impact and higher value than analysed individually.

Here, we separately combined DAP-3 with HSP90A, DAP-3 with HSP90B, DAP-3 with HSP90A and HSP90B and reanalysed the relationship with patients' survival.

6.3.2.4.1. OS and DSF for DAP-3 and HSP90A combined

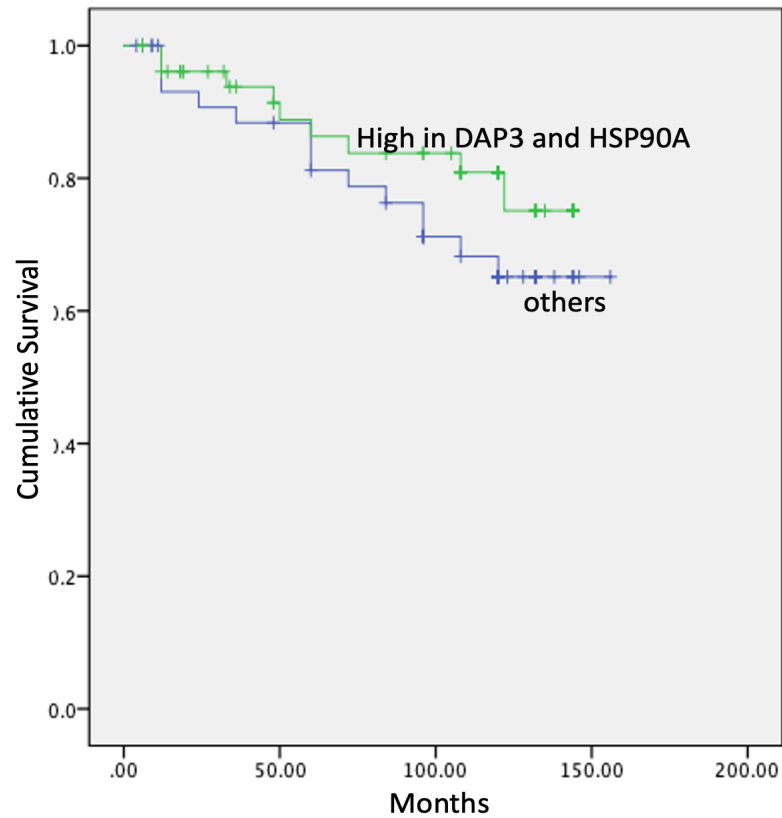
Overall Survival was found to be significantly improved in the group with combined higher expression of DAP-3 and HSP90A (Fig.6.6.).

However, the combined expression of DAP-3 and HSP90A, did not seem to have any significant impact on disease free survival (Fig.6.7.).



Overall Comparisons			
	Chi-Square	df	Sig.
Log Rank (Mantel-Cox)	4.409	1	.036
Breslow (Generalized Wilcoxon)	3.491	1	.062
Tarone-Ware	3.932	1	.047
Test of equality of survival distributions for the different levels of DAP-3HSP90AAllHighsAre2.			

Fig.6.6. Overall survival for combined DAP-3 and HSP90A. Patients were divided into those having high levels of one or both DAP-3 and HSP90A, or those with either with both low in DAP-3 and HSP90A (designated as others).



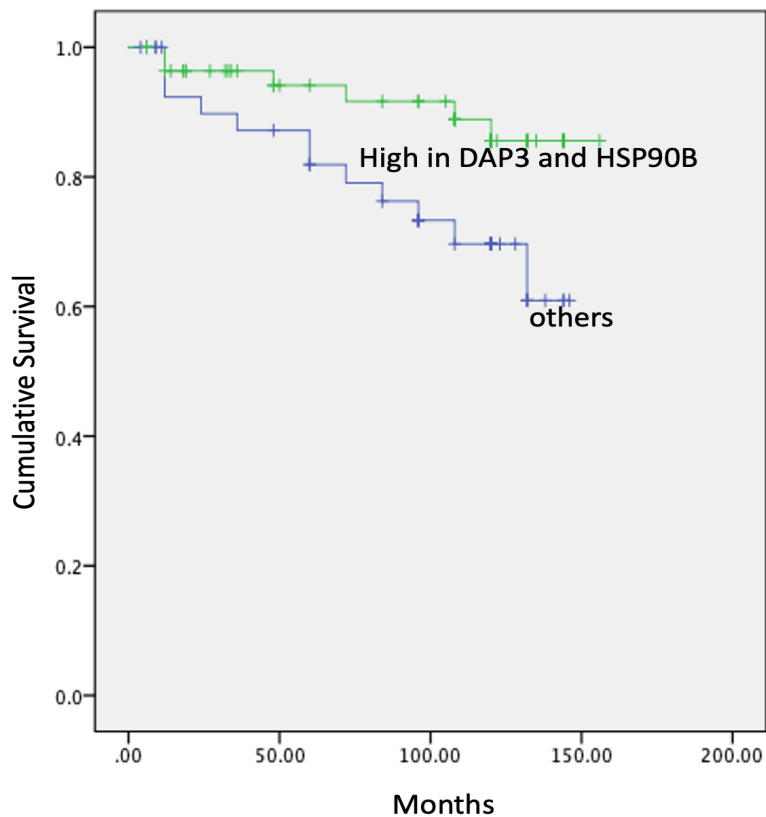
Overall Comparisons			
	Chi-Square	df	Sig.
Log Rank (Mantel-Cox)	1.482	1	.223
Breslow (Generalized Wilcoxon)	1.562	1	.211
Tarone-Ware	1.577	1	.209
Test of equality of survival distributions for the different levels of DAP-3HSP90AAllHighsAre2.			

Fig.6.7. Disease free survival for combined DAP-3 and HSP90A. Patients were divided into those having high levels of one or both DAP-3 and HSP90A, or those with either with both low in DAP-3 and HSP90A (designated as others).

6.3.2.4.2. OS and DFS for DAP-3 and HSP90B combined

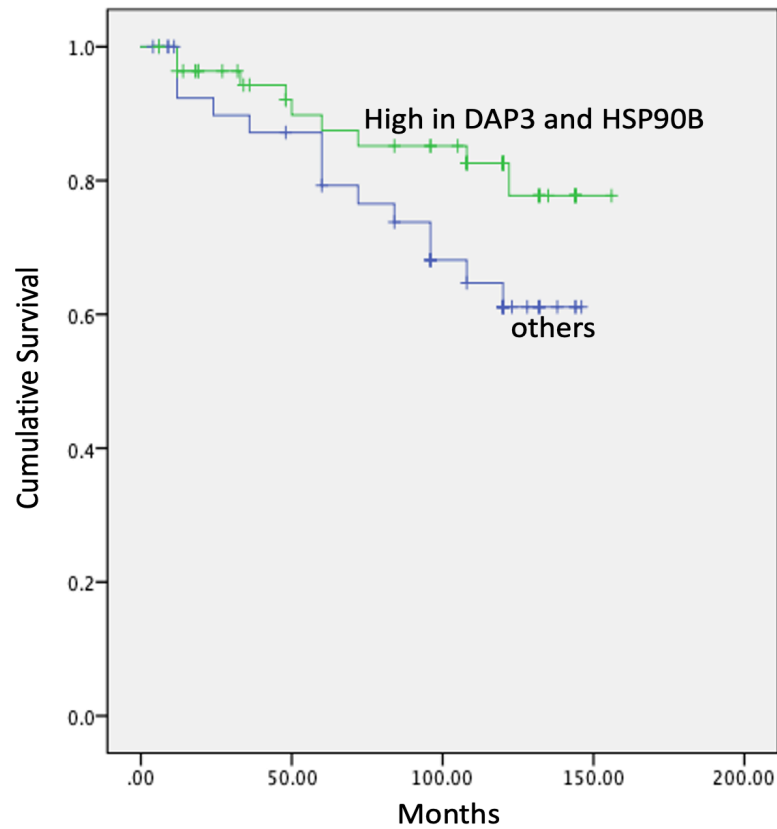
Similarly, the combined expression of DAP-3 and HSP90B was useful in indicating patient overall survival, with those patients having high expression of one or both molecules showing significantly better survival than those with low expression for both molecules (Fig.6.8.).

However, once again, the combined expression of DAP-3 and HSP90B didn't not significantly impact disease free survival rates (Fig.6.9.).



Overall Comparisons			
	Chi-Square	df	Sig.
Log Rank (Mantel-Cox)	4.709	1	.030
Breslow (Generalized Wilcoxon)	4.234	1	.040
Tarone-Ware	4.478	1	.034
Test of equality of survival distributions for the different levels of DAP-3HSP90BAllHighsAre2.			

Fig.6.8. Overall survival for combined DAP-3 and HSP90B. Patients were divided into those having high levels of one or both DAP-3 and HSP90B, or those with either with both low in DAP-3 and HSP90B (designated as others).



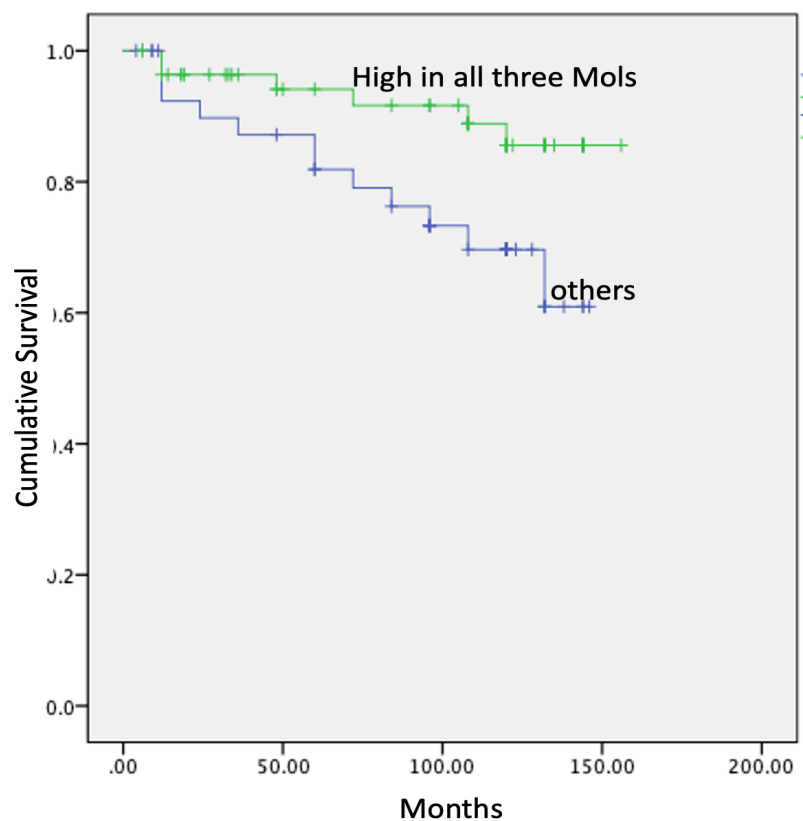
Overall Comparisons			
	Chi-Square	df	Sig.
Log Rank (Mantel-Cox)	3.269	1	.071
Breslow (Generalized Wilcoxon)	3.198	1	.074
Tarone-Ware	3.315	1	.069
Test of equality of survival distributions for the different levels of DAP-3HSP90BAIIHighsAre2.			

Fig.6.9. Disease free survival for combined DAP-3 and HSP90B. Patients were divided into those having high levels of one or both DAP-3 and HSP90B, or those with either with both low in DAP-3 and HSP90B (designated as others).

6.3.2.4.3. Survival analysis with the expression patterns of DAP-3, HSP90A and HSP90B combined

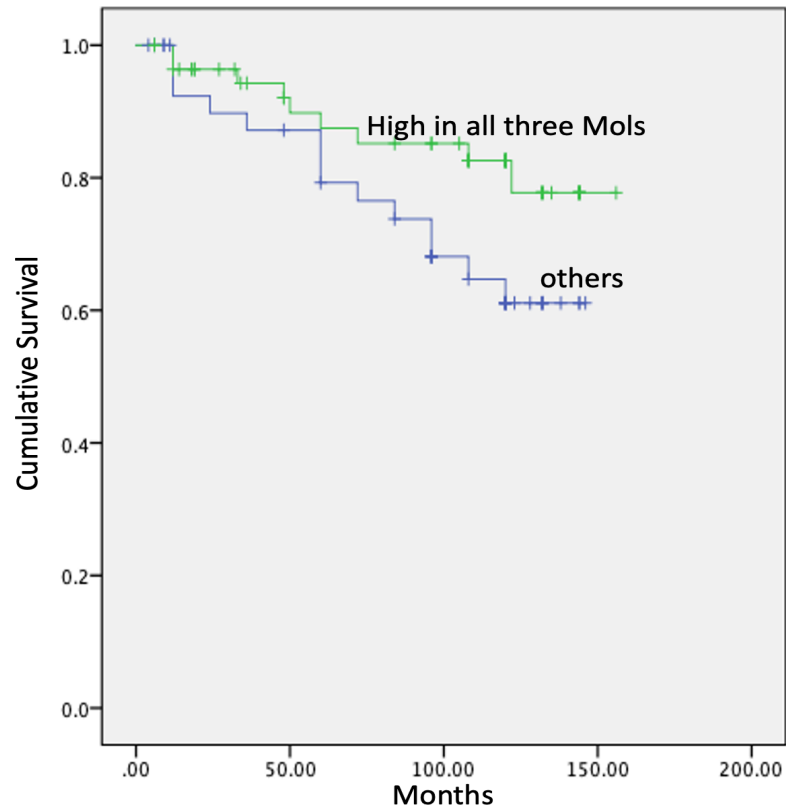
From the last two sections, it is clear that when DAP-3 and HSP90 expression profiles are combined, there was an improvement on the value in predicting the survival of the patients. Following on from these observations, we attempted to combined the patterns of all three related molecules and conducted Kaplan Meier survival analysis.

Combined expression of DAP-3 and HSP90A and HSP90B significantly impacted overall survival rates, with patients who had high levels of any individual or all molecules displaying longer overall survival compared to those who had low levels of all three molecules (Fig.6.10.). However, the combined expression of DAP-3, HSP90A and HSP90B did not seem to impact disease free survival rates compared to patients with low expression for all three molecules (Fig.6.11.). This combination yielded the same results as the DAP-3/HSP90B combination suggesting that the DAP-3/HSP90A fall into this group and that the combination of three cover well the groups.



Overall Comparisons			
	Chi-Square	df	Sig.
Log Rank (Mantel-Cox)	4.709	1	.030
Breslow (Generalized Wilcoxon)	4.234	1	.040
Tarone-Ware	4.478	1	.034
Test of equality of survival distributions for the different levels of AllHighsAre3.			

Fig. 6.10. Overall survival for combined DAP-3, HSP90A and HSP90B. Patients were divided into those having high levels of one or more of three molecules, namely DAP-3, HSP90A and HSP90B, or those with low levels for all (designated as others).



Overall Comparisons			
	Chi-Square	df	Sig.
Log Rank (Mantel-Cox)	3.269	1	.071
Breslow (Generalized Wilcoxon)	3.198	1	.074
Tarone-Ware	3.315	1	.069
Test of equality of survival distributions for the different levels of AllHighsAre3.			

Fig.6.11. Disease free survival for combined DAP-3, HSP90A and HSP90B. Patients were divided into those having high levels of one or more of three molecules, namely DAP-3, HSP90A and HSP90B, or those with lows for all (designated as others).

6.3.2.4.4. Multivariate survival analysis for the combined expression pattern of DAP-3, HSP90A and HSP90B

With the combination analysis, the patterns of DAP-3, HSP90A and HSP90B have enhanced value in predicting the survival of the patients. Multivariate analysis was carried out as shown in Table 6.5. Overall, this analysis has partially improved the statistical power compared with a single molecule. However, it remains just outside of statistical significance.

Table 6.5. multivariate analysis of DAP-3, HSP90A and HSP90B expression profile combinations

Factors	OS		RFS	
	F	Sig.	F	Sig.
NPI	2.014	0.1	3.375	0.039
Grade	0.381	0.822	0.245	0.783
TNM staging	2.08	0.09	1.455	0.239
Nodal status	2.754	0.033	4.058	0.021
ER status	2.632	0.04	4.199	0.018
ER β status	0.959	0.434	0.11	0.896
DAP-3HSP90A	2.558	0.044	2.303	0.106
DAP-3/HSP90AB	2.126	0.084	2.594	0.08
DAP-3/HSP90A/HSP90B	2.208	0.075	2.735	0.07

6.3.3. Implications in therapy resistance using online datasets – (DAP-3/HSP90A/HSP90B relationship to responsiveness to chemo therapy)

In light of the recent report that DAP-3 may be associated with drug resistance in certain cancers, i.e. gastric cancer (154, 173), we attempted to further evaluate if the connection exists between the expression level of DAP-3, HSP90A and HSP90B, and patient's response to drug therapies.

Online dataset (Fekete and Gyorffy 2019) (203) was analysed and used to determine implications of chemotherapy (taxane and anthracycline chemotherapy treatment) on selected breast cancer subgroups (ER+, ER-, HER2+, HER2-, Triple negative) examining the expression of DAP-3, HSP90A and HSP90B in chemotherapy treatment 'responders' and 'non-responders'. Five-year interval follow up data with recurrence free survival was evaluated as part of the online dataset.

6.3.3.1. DAP-3 expression

6.3.3.1.1. Oestrogen receptor positive breast cancer

DAP-3 gene expression was observed at a significantly higher level in ER+ breast cancer group that responded well to taxane and also to anthracycline chemotherapy (Fig.6.12.A. and B.).

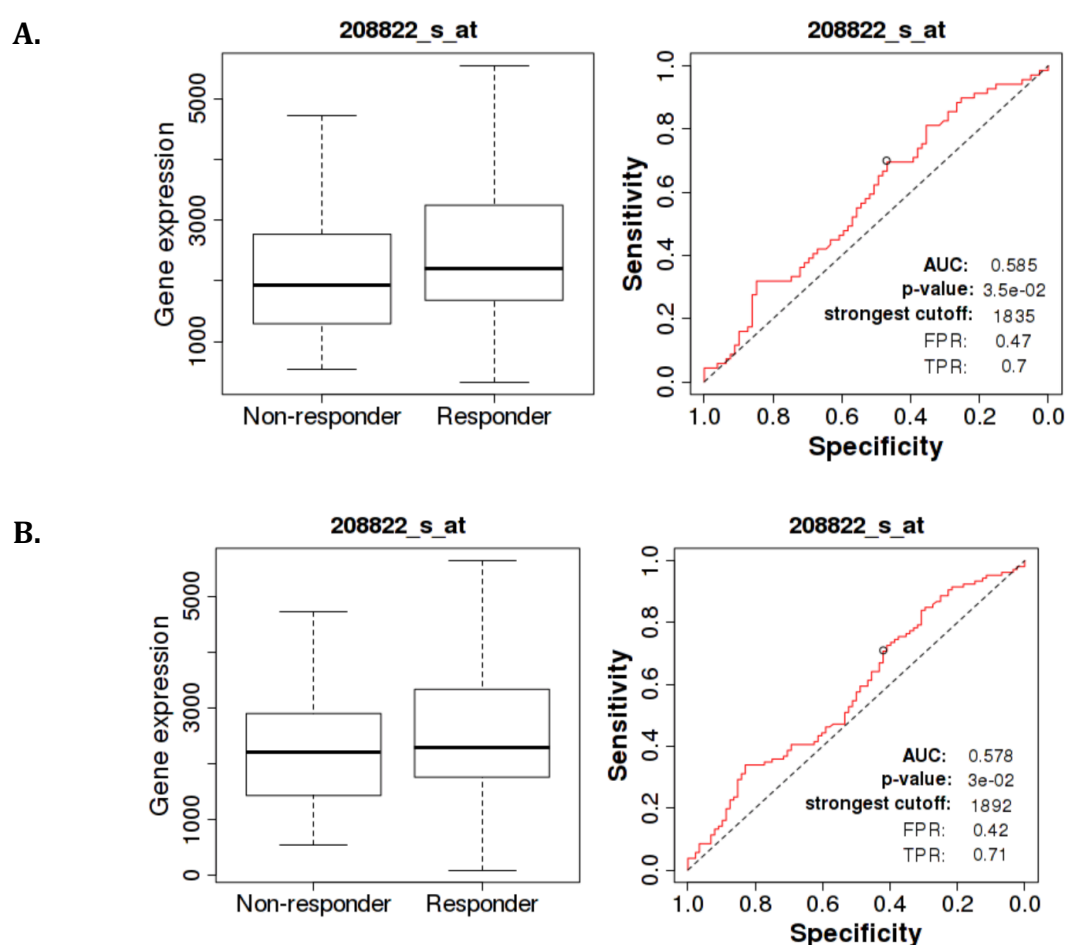


Fig. 6.12. Expression of DAP-3 in ER+ breast cancer treated with (A.) taxane chemotherapy and (B.) anthracycline chemotherapy assessed in responders and non-responders.

6.3.3.1.2. Oestrogen receptor negative breast cancer

DAP-3 gene expression in ER- breast cancer group treated with taxane chemotherapy showed no significant difference between responders and non-responders although in the responders group of anthracycline chemotherapy we observed increased levels of DAP-3 expression (Fig.6.13.A and B).

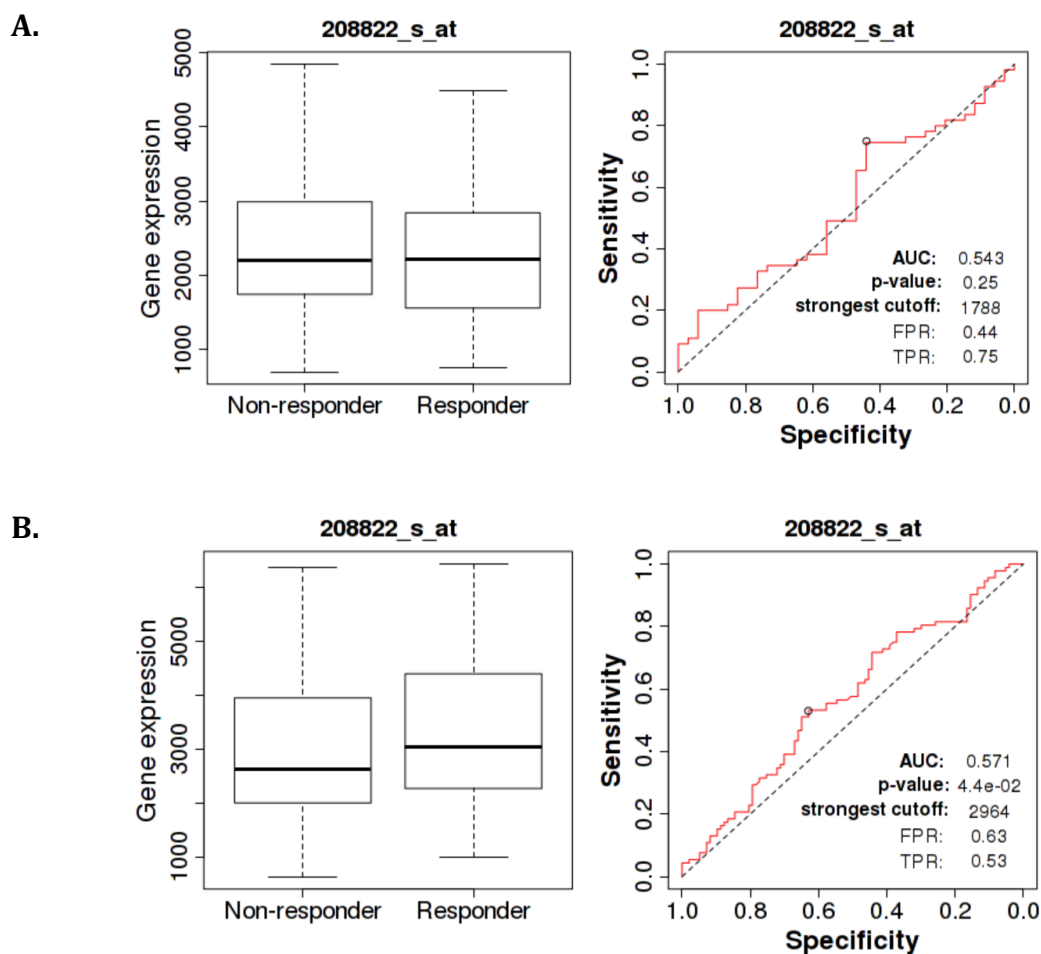


Fig. 6.13. Expression of DAP-3 in ER- breast cancer treated with (A.) taxane chemotherapy and (B.) anthracycline chemotherapy assessed in responders and non-responders.

6.3.3.1.3. HER2 positive breast cancer

The expression of DAP-3 in HER2+ breast cancer subtype treated with either taxane or anthracycline chemotherapy was of no significant difference between responders and non-responders (Fig.6.14.A. and B.).

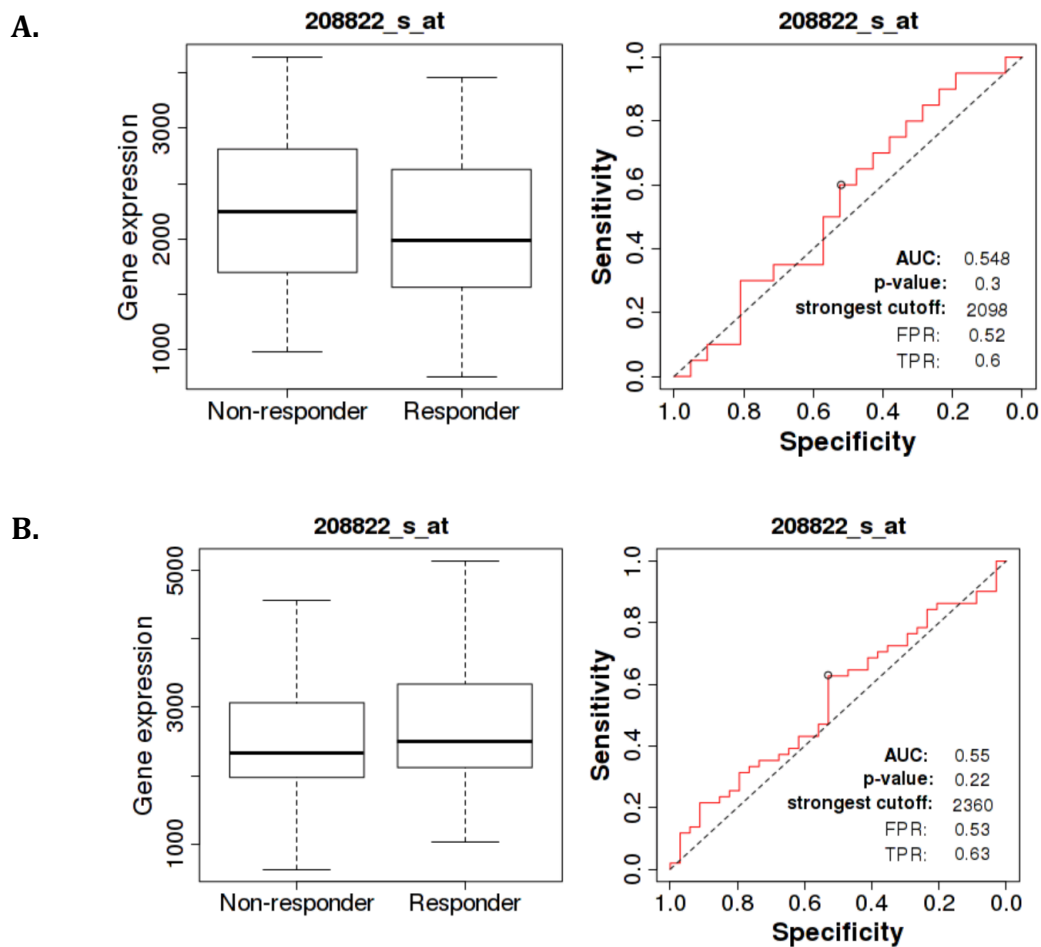


Fig. 6.14. Expression of DAP-3 in HER2+ breast cancer treated with (A.) taxane chemotherapy and (B.) anthracycline chemotherapy assessed in responders and non-responders.

6.3.3.1.4. HER2 negative breast cancer

The expression of DAP-3 in HER2 negative breast cancer variant treated with taxane chemotherapy did not show any significant difference between responders and non-responders although there was a higher level of DAP-3 expression recorded in anthracycline chemotherapy responders group (Fig.6.15.A. and B.).

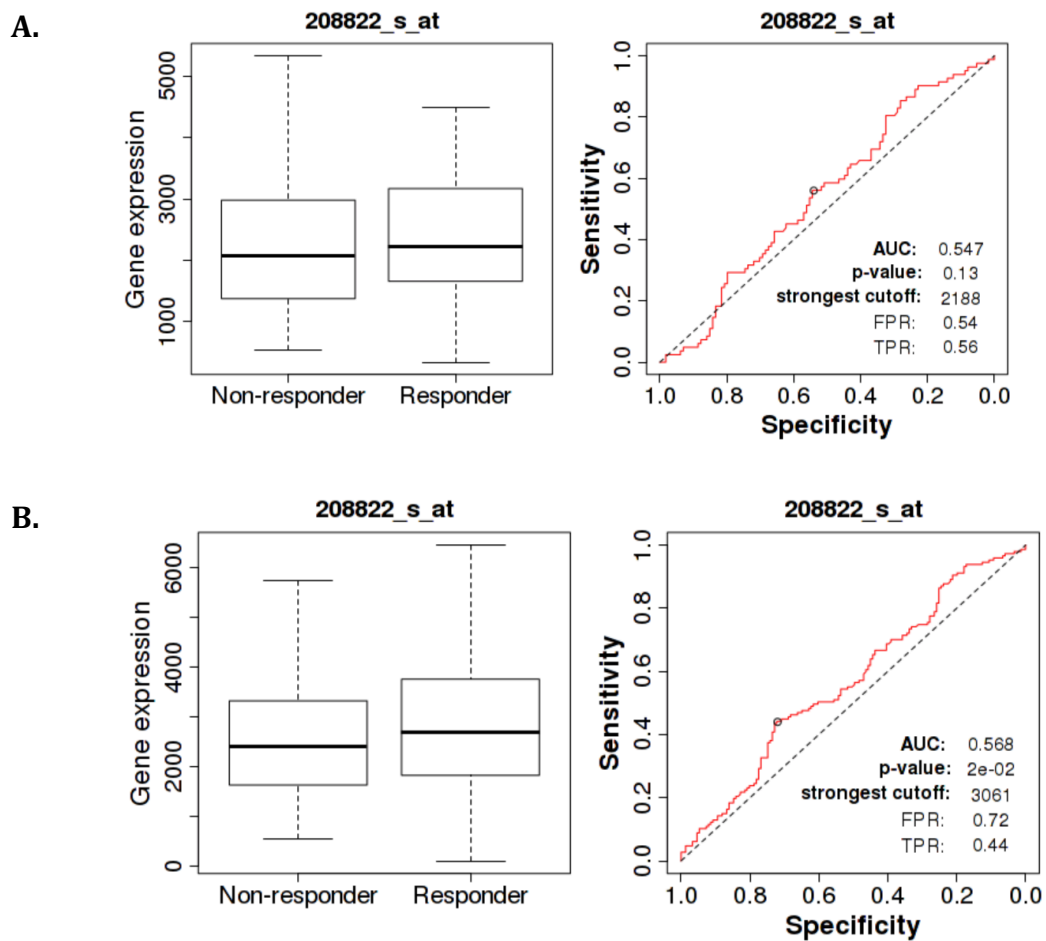


Fig. 6.15. Expression of DAP-3 in HER2- breast cancer treated with (A.) taxane chemotherapy and (B.) anthracycline chemotherapy assessed in responders and non-responders.

6.3.3.1.5. Triple negative breast cancer (ER-, PR-, HER2-)

Response to taxane or anthracycline chemotherapy treatment in the triple negative breast cancer subgroup does not appear to be associated with any significant difference in expression of DAP-3 gene (Fig.6.16. A. and B.).

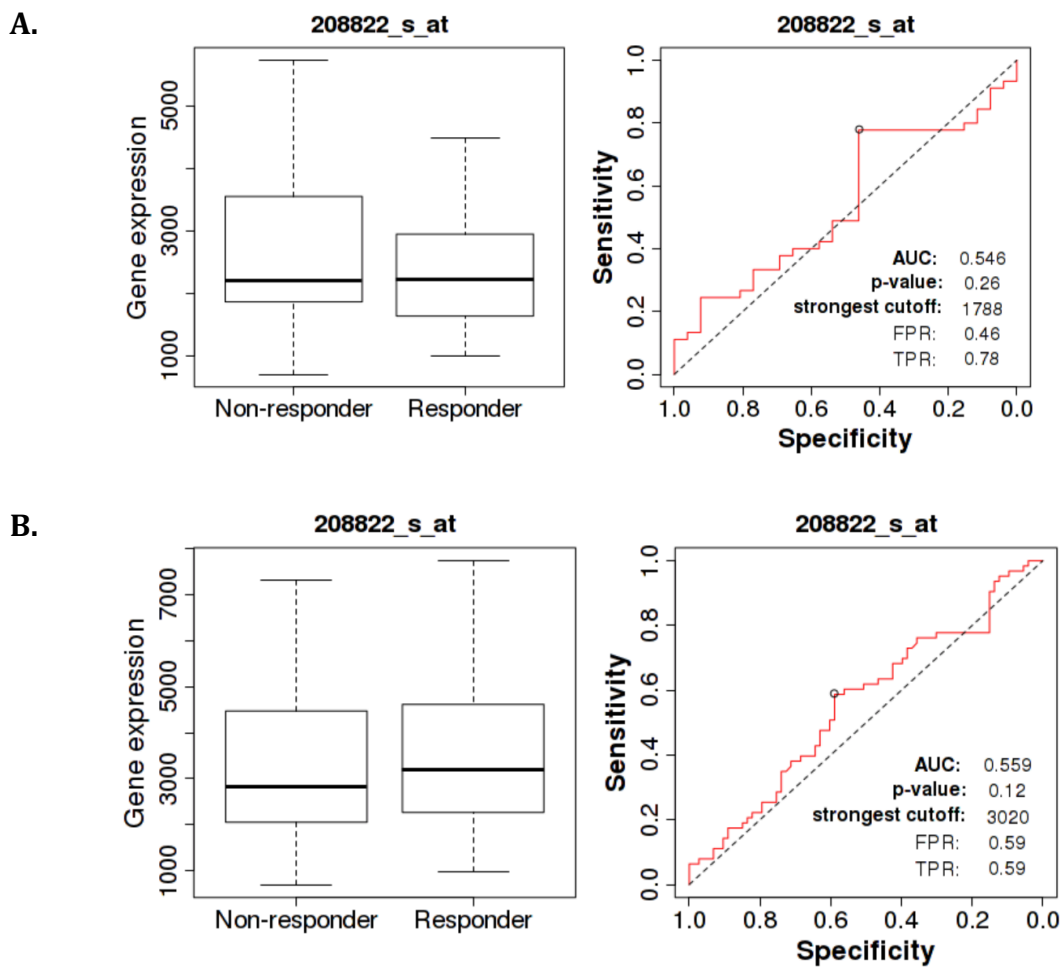


Fig. 6.16. DAP-3 expression in triple negative breast cancer treated with (A.) taxane chemotherapy and (B.) anthracycline chemotherapy assessed in responders and non-responders.

6.3.3.2. HSP90A expression

6.3.3.2.1. Oestrogen receptor positive breast cancer

In ER+ breast cancer, the expression of HSP90A does not appear to be different with regards to taxane chemotherapy treatment response although there was a trend observed in the anthracycline treatment group where good response was seen with higher expression of HSP90A. This has though not reached significance (Fig.6.17.A. and B.).

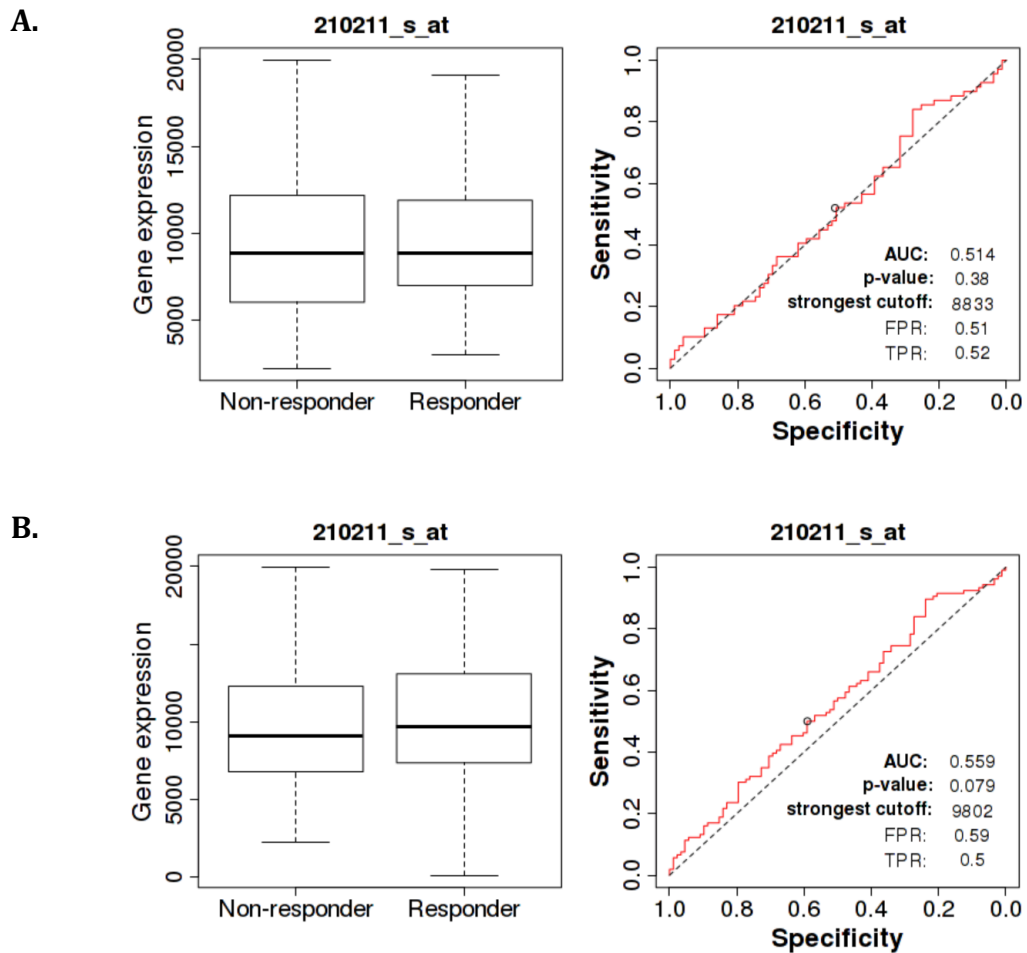


Fig. 6.17. Expression of HSP90A gene in responders and non-responders to taxane (A.) and anthracycline (B.) treatment in ER + breast cancer.

6.3.3.2.2. Oestrogen receptor negative breast cancer

Expression of HSP90A did not significantly differ with respect to response to taxane chemotherapy in the ER- subgroup of Breast cancer although there was significant increase in expression observed with good response to anthracycline treatment (Fig.6.18.A. and B.).

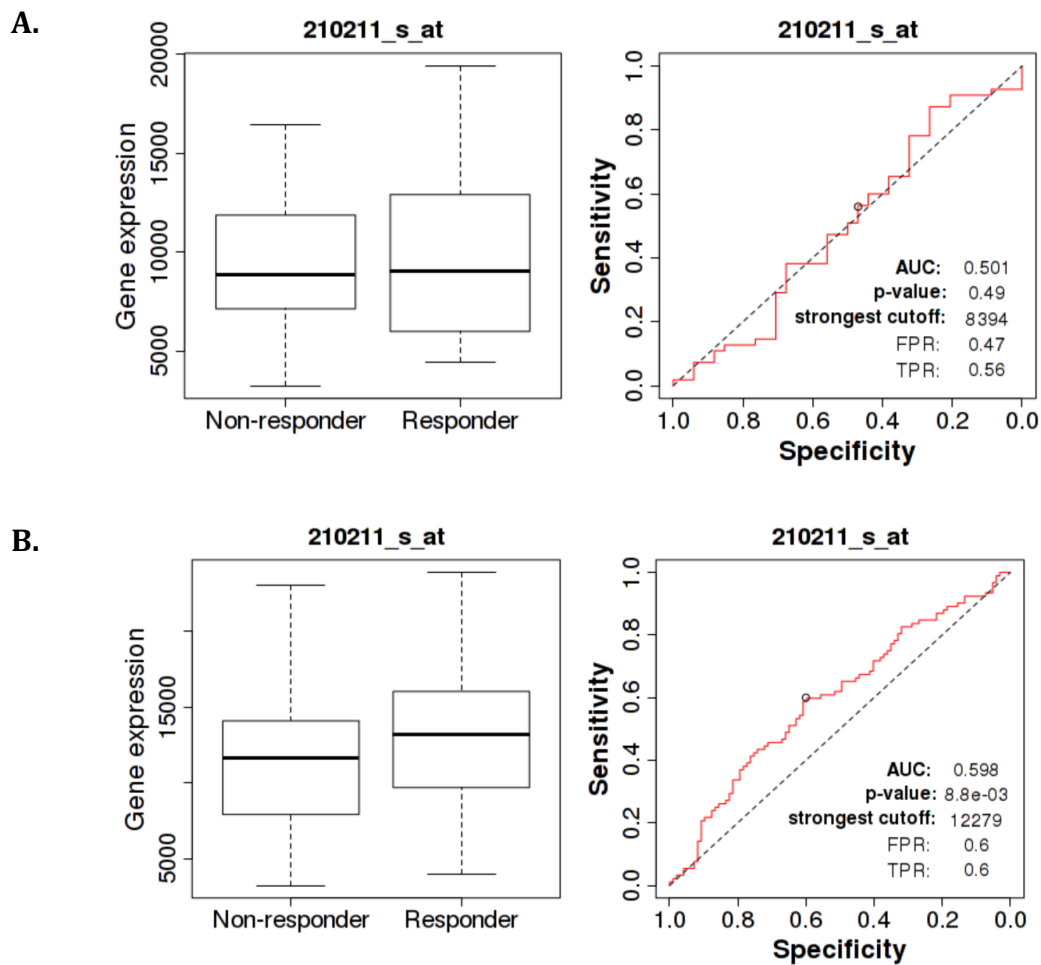


Fig. 6.18. Expression of HSP90A gene in responders and non-responders to taxane (A.) and anthracycline (B.) treatment in ER - breast cancer.

6.3.3.2.3. HER2 positive breast cancer

Expression of HSP90A did not significantly change with respect to response to taxane or anthracycline chemotherapy in the HER2 positive subgroup of breast cancer (Fig.6.19.A and B.).

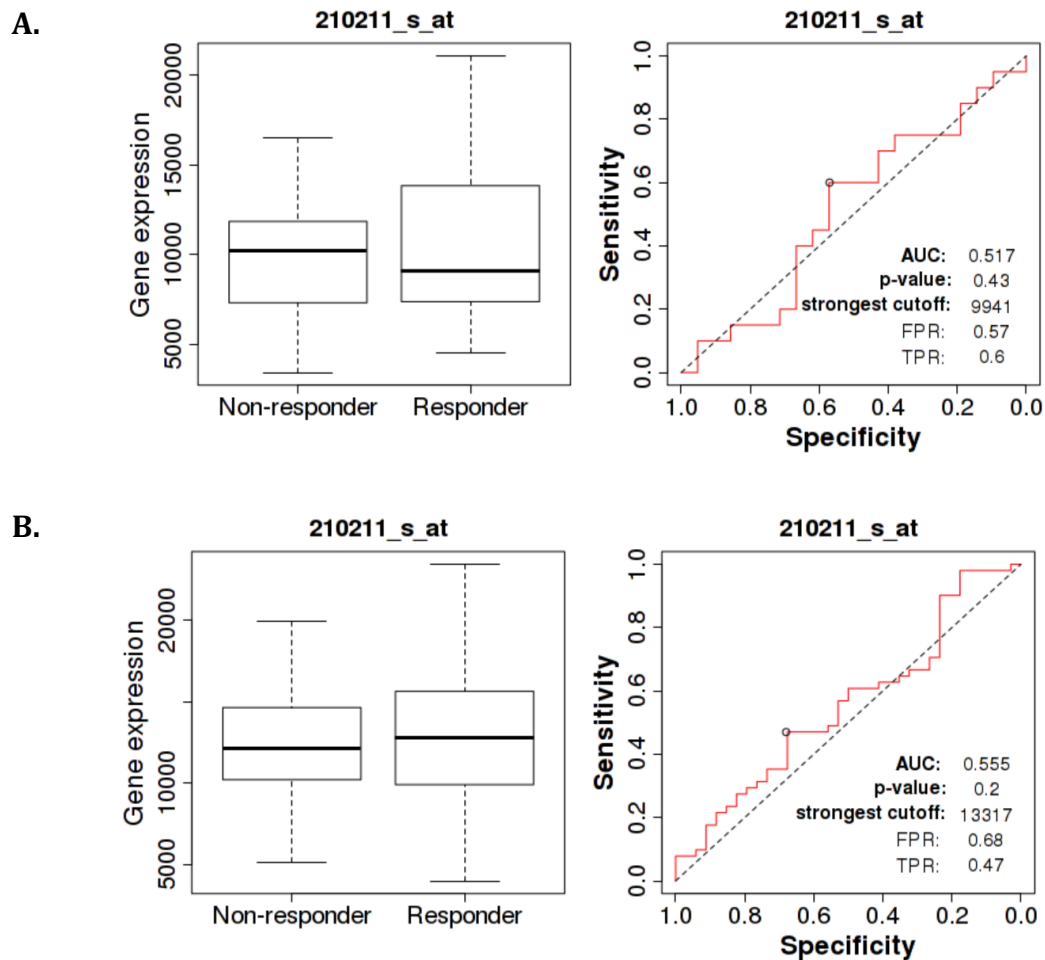


Fig. 6.19. Expression of HSP90A gene in responders and non-responders to taxane (A.) and anthracycline (B.) treatment in HER2 + breast cancer.

6.3.3.2.4. HER2 negative breast cancer

HSP90A expression was not significantly altered with respect to response to taxane chemotherapy in the HER2 negative variant of Breast cancer although there was a trend towards higher HSP90A expression in anthracycline responders group, not reaching significance though (Fig.6.20.A. and B.).

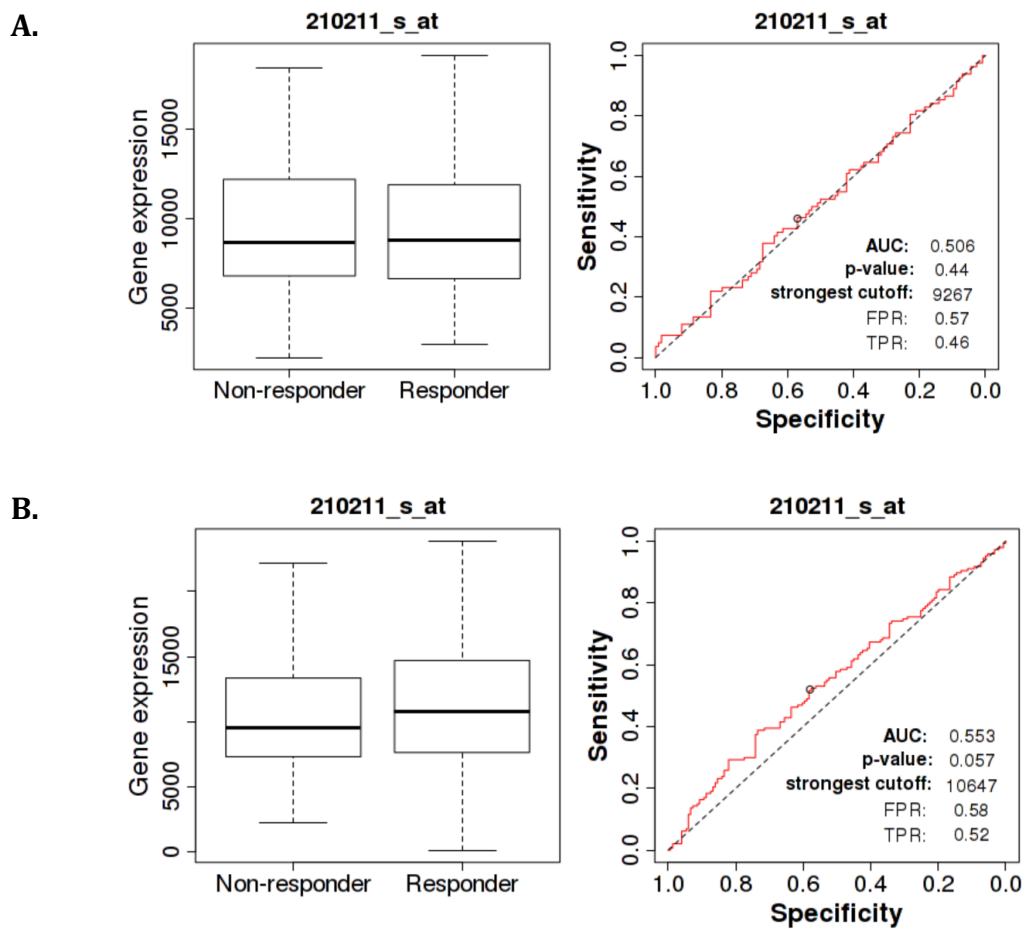


Fig. 6.20. Expression of HSP90A gene in responders and non-responders to taxane (A.) and anthracycline (B.) treatment in HER2 - breast cancer.

6.3.3.2.4.1. Triple negative breast cancer (ER-, PR-, HER2-)

Within the taxane chemotherapy treatment group in triple negative breast cancer, there was no significant difference in HSP90A expression. However in the anthracycline treatment group, there has been a significantly increased expression of HSP90A in the responders category (Fig.6.21.A. and B.)

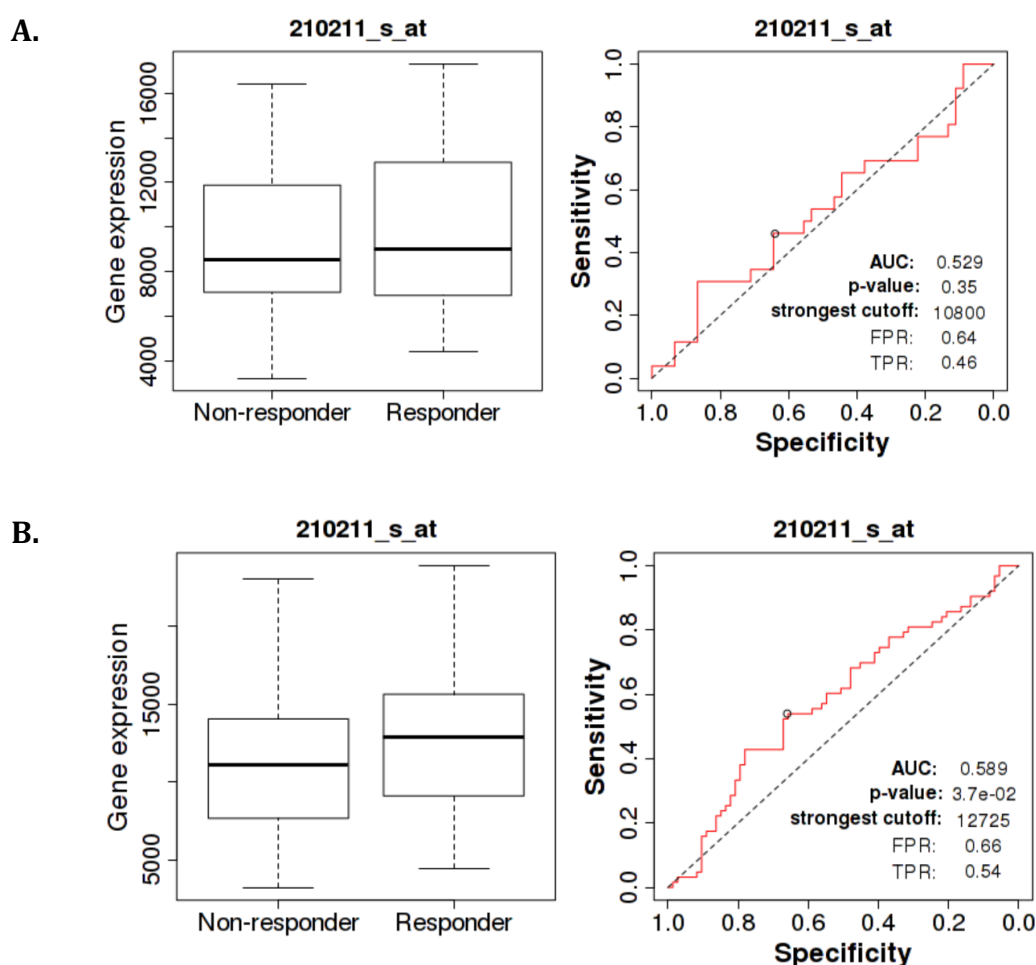


Fig. 6.21. Expression of HSP90A gene in responders and non-responders to taxane (A.) and anthracycline (B.) treatment in triple negative breast cancer.

6.3.3.3. HSP90B expression

6.3.3.3.1. Oestrogen receptor positive breast cancer

Breast cancer with positive ER status that has shown good response to taxane chemotherapy was associated with increased levels of HSP90B expression, while in the anthracycline group there was no significant difference HSP90B expression observed (Fig.6.22.A. and B.)

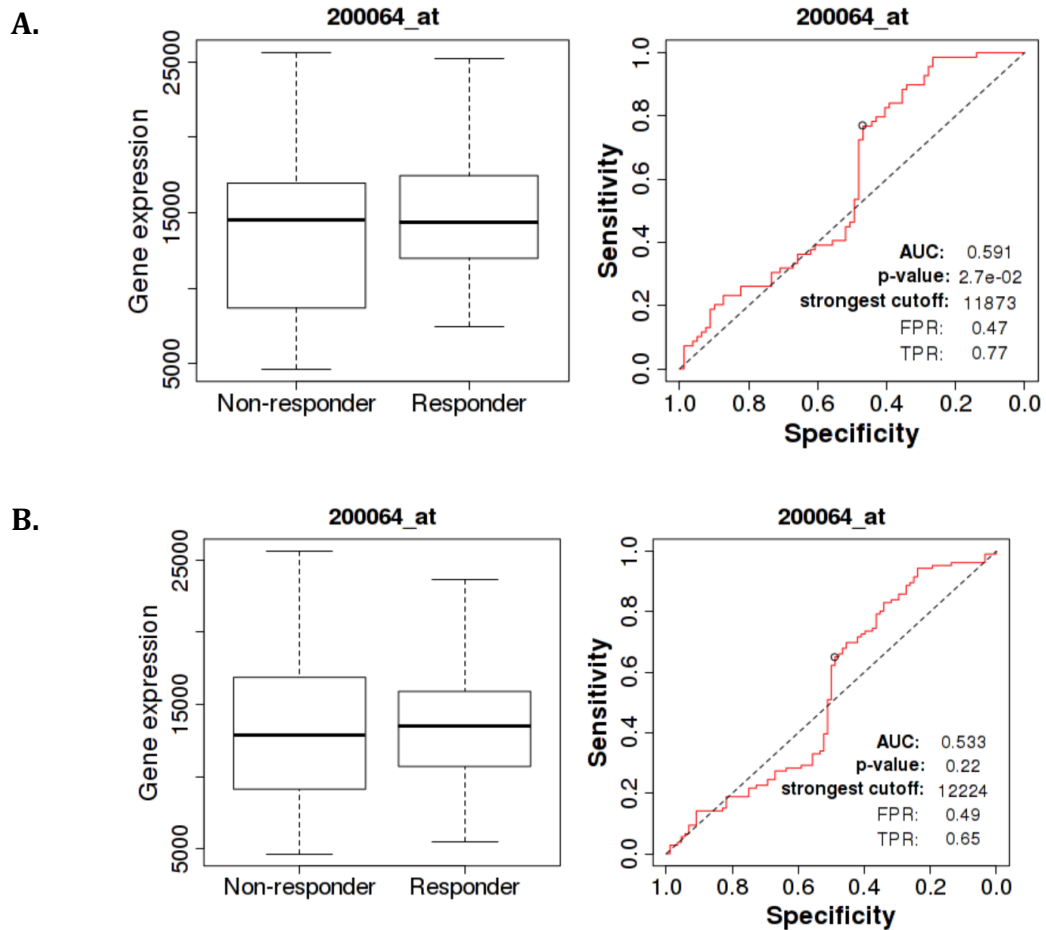


Fig. 6.22. HSP90B expression in responders and non-responders to taxane (A.) and anthracycline (B.) treatment in ER+ breast cancer.

6.3.3.3.2. Oestrogen receptor negative breast cancer

No significant change in HSP90B expression was detected within taxane or anthracycline chemotherapy treatment response groups of ER-breast cancer (Fig.6.23.A. and B.).

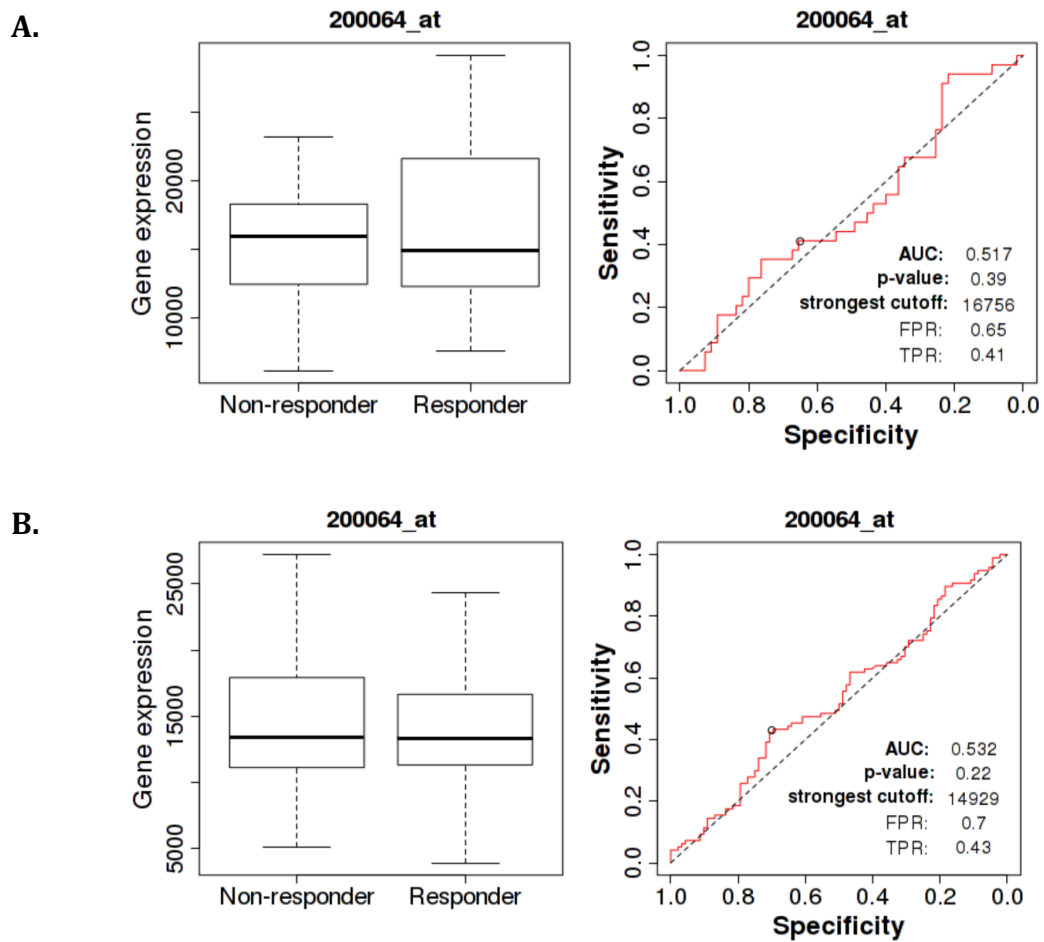


Fig. 6.23. HSP90B expression in responders and non-responders to taxane (A.) and anthracycline (B.) treatment in ER- breast cancer.

6.3.3.3. HER2 positive breast cancer

No difference in the expression of HSP90B was observed in neither taxane or anthracycline treatment response groups in HER2 positive breast cancer (Fig.6.24.A. and B.).

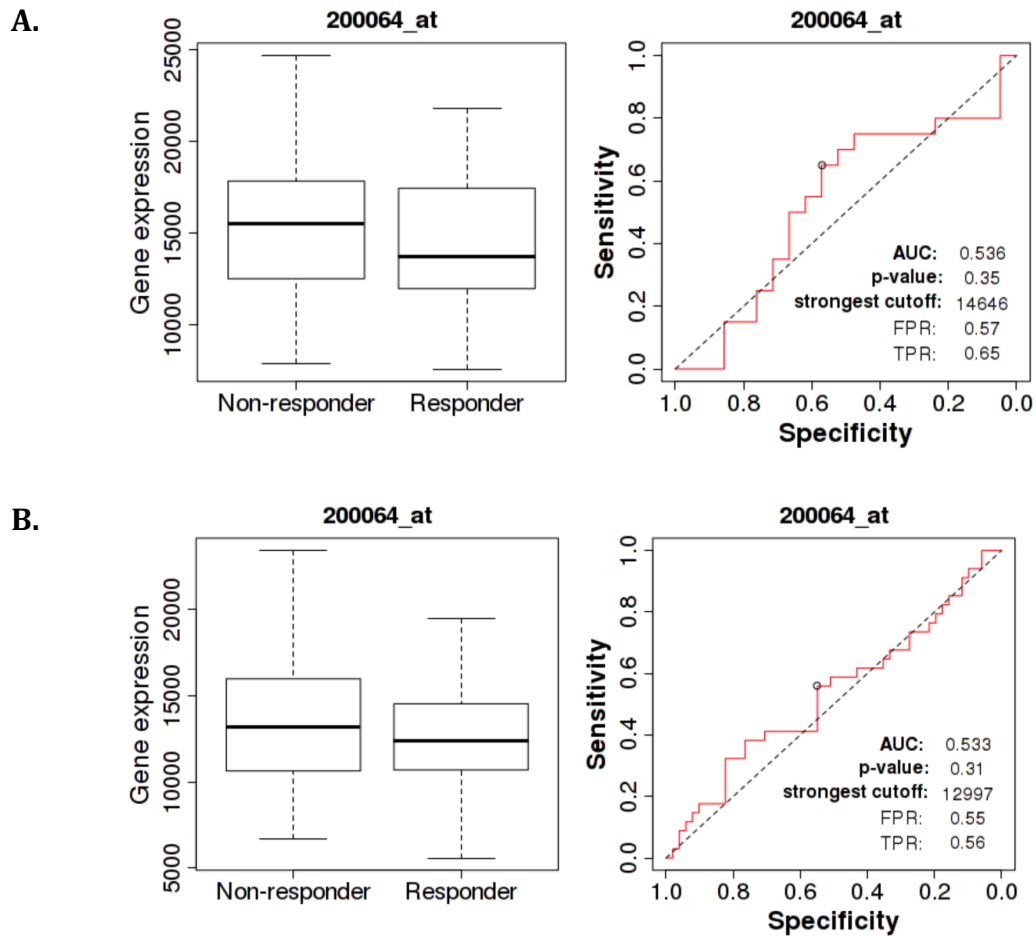


Fig. 6.24. HSP90B expression in responders and non-responders to taxane (A.) and anthracycline (B.) treatment in HER2+ breast cancer.

6.3.3.3.4. HER2 negative breast cancer

Breast cancer with negative HER2 receptor status that has manifested good response to taxane chemotherapy has demonstrated significantly raised expression levels of HSP90B, while in the anthracycline chemotherapy group there were no differences in HSP90B expression observed (Fig.6.25.A. and B.).

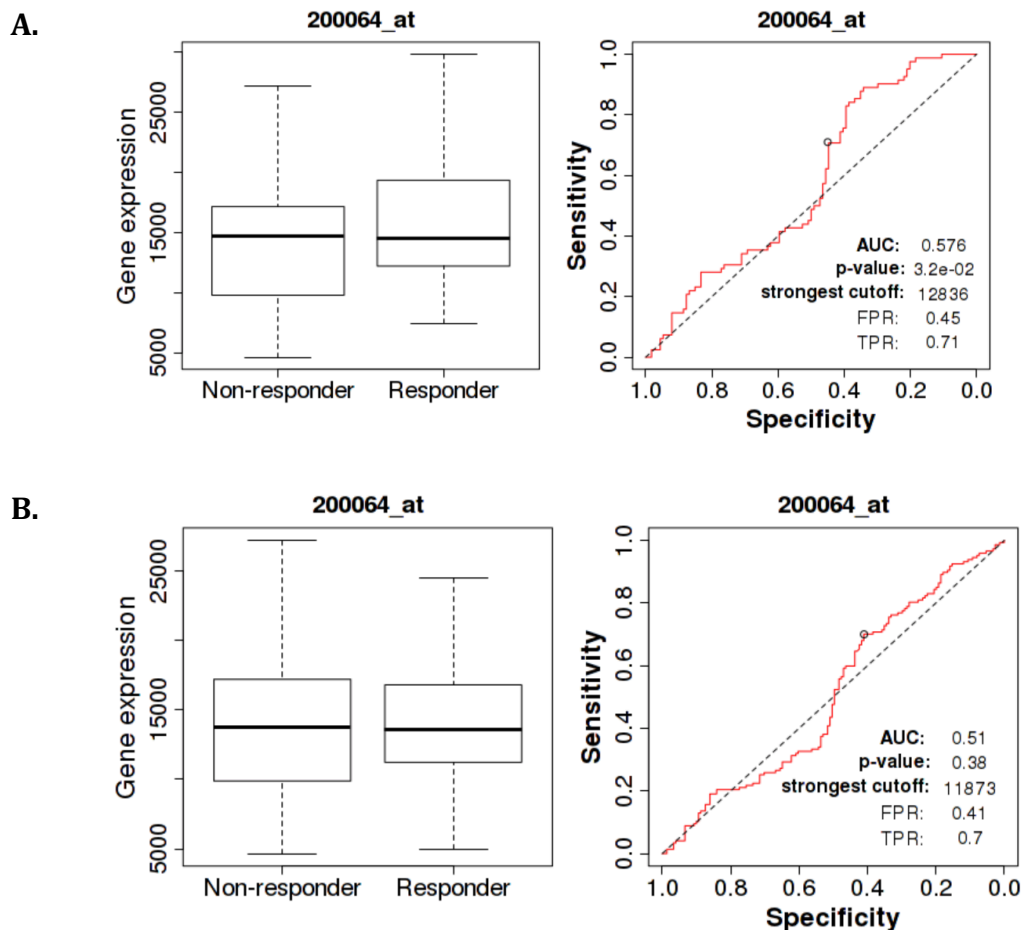


Fig. 6.25. HSP90B expression in responders and non-responders to taxane (A.) and anthracycline (B.) treatment in HER2 negative breast cancer.

6.3.3.3.5. Triple negative breast cancer (ER-, PR-, HER2-)

There were no obvious differences in HSP90B expression levels recorded in triple negative breast cancers treated with taxane anthracycline chemotherapy response groups (Fig.6.26.A. and B.)

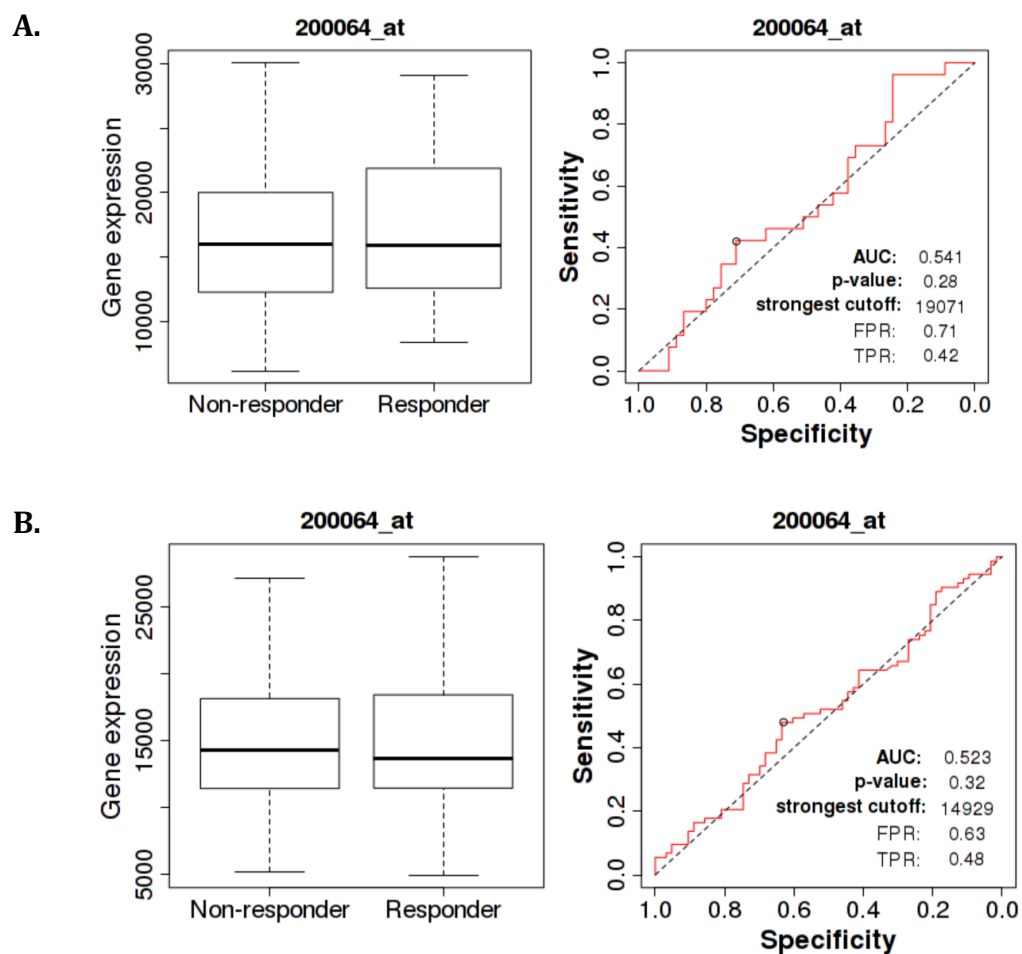


Fig. 6.26. HSP90B expression in responders and non-responders to taxane (A.) and anthracycline (B.) treatment in triple negative breast cancer.

6.3.4. Impact on chemoresistance

In order to supplement the clinical observations between DAP-3 and HSP90, together with their potential collective roles we explored the effects of 2 chemotherapeutic agents (Paclitaxel and Docetaxel) with or without HSP90 inhibitor treatment on DAP-3 KD MCF-7 and MDA-MB-231 cell lines in comparison to pEF6 controls.

6.3.4.1. MCF-7

6.3.4.1.1. Paclitaxel

Growth assay were used to assess response of MCF-7 pEF6 control cells to HSP90 inhibitor (30nM) with and without paclitaxel treatment (50nM). ANOVA analysis within the group demonstrated significant differences. Post-hoc (Holm-Sidak) analysis revealed significant differences between untreated pEF6 vs. paclitaxel treated pEF6 groups ($p < 0.001$); untreated pEF6 vs. combined HSP90 inhibitor and paclitaxel treated pEF6 groups ($p < 0.001$); HSP90 inhibitor treated vs. paclitaxel treated pEF6 groups ($p < 0.001$); HSP90 inhibitor treated vs. combined paclitaxel and HSP90 inhibitor treated pEF6 groups ($p < 0.001$). No significant difference was observed between either untreated pEF6 vs. HSP90 inhibitor treated pEF6 groups or paclitaxel treated vs combined HSP90 inhibitor and paclitaxel treated pEF6 groups. Collectively, this suggests that the main cytotoxic impact is derived from the action of the paclitaxel chemotherapeutic agent and HSP90 inhibitor has little additional impact in MCF-7 pEF6 cells. (Fig. 6.27.)

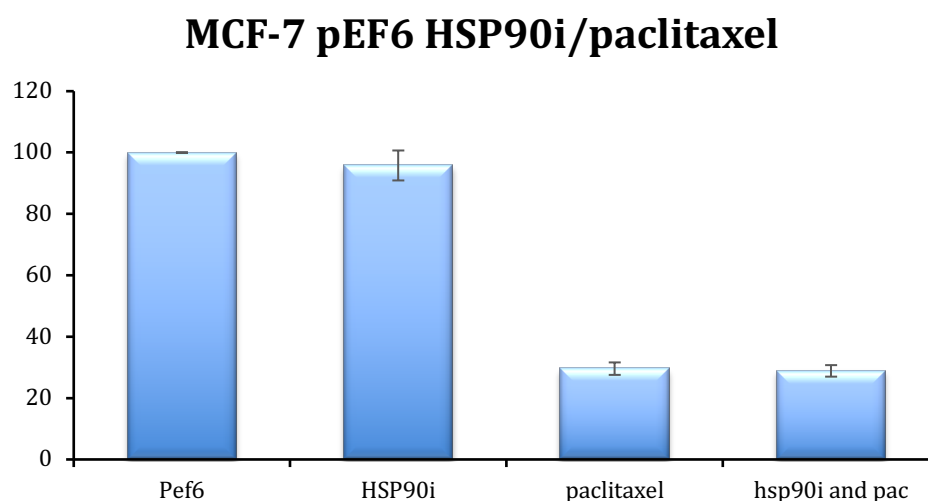


Fig. 6.27. Growth assay of MCF-7 pEF6 control cell lines and the response to treatment with HSP90 inhibitor (30nM), Paclitaxel (50nM) and combination of both. Data shown represents mean percentage untreated pEF6 control cells (n=3), error bars represent SEM.

Following on from this, a similar approach was undertaken to investigate if DAP-3 knockdown brought about a differential response to HSP90 inhibition and paclitaxel treatment.

ANOVA analysis indicated significant differences within the group. Post-hoc (Holm-Sidak) analysis revealed significant differences between untreated DAP-3 KD vs. paclitaxel treated DAP-3 KD groups ($p < 0.001$); untreated DAP-3 KD vs. combined HSP90 inhibitor and paclitaxel treated DAP-3 KD groups ($p < 0.001$); HSP90 inhibitor treated DAP-3 KD vs. paclitaxel treated DAP-3 KD groups ($p < 0.001$); HSP90 inhibitor treated DAP-3 KD vs. combined paclitaxel and HSP90 inhibitor treated DAP-3 KD groups ($p < 0.001$). No significant difference was observed between either untreated DAP-3 KD vs. HSP90 inhibitor treated DAP-3 KD

groups or paclitaxel treated DAP-3 KD vs combined HSP90 inhibitor and paclitaxel treated DAP-3 KD groups (Fig. 6.28.). Again, these observations implied the predominant cytotoxic effect was derived through paclitaxel treatment and HSP90 inhibitor has little additional impact in MCF-7 DAP-3 KD cells. This early result indicates that in MCF-7 cells, DAP-3 and/or HSP90 may not play a significant role in paclitaxel response.

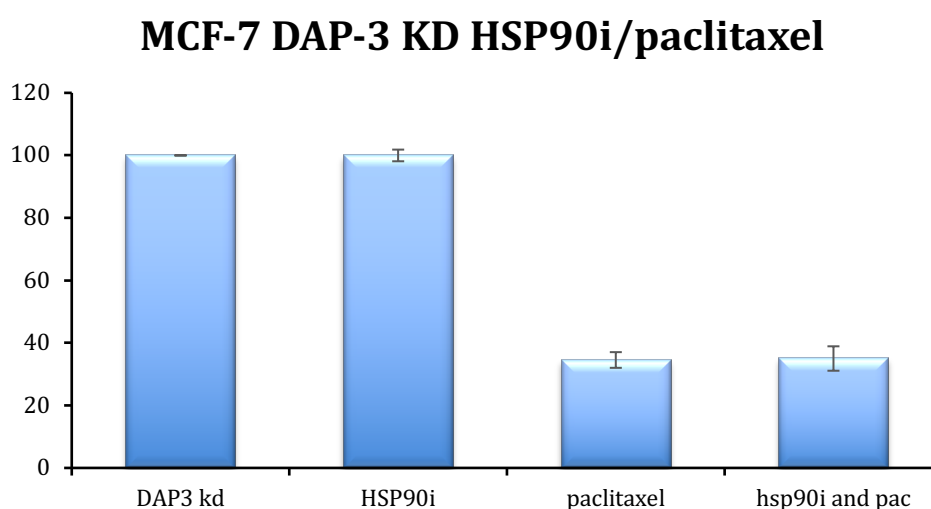


Fig. 6.28. Growth assay of MCF-7 DAP-3 KD cell lines and the response to treatment with HSP90 inhibitor (30nM), Paclitaxel (50nM) and combination of both. Data shown represents mean percentage untreated DAP-3 KD cells ($n=3$), error bars represent SEM.

6.3.4.1.2. Docetaxel

Growth assays were used to assess response of MCF-7 pEF6 control cells to HSP90 inhibitor (30nM) with and without docetaxel treatment (50nM) (Fig. 6.29.). ANOVA analysis within the group demonstrated significant differences. Post-hoc (Holm-Sidak) analysis revealed significant differences between untreated pEF6 vs. docetaxel treated pEF6 groups ($p<0.001$); untreated pEF6

vs. combined HSP90 inhibitor and docetaxel treated pEF6 groups ($p<0.001$); HSP90 inhibitor treated vs. docetaxel treated pEF6 groups ($p<0.001$); HSP90 inhibitor treated vs. combined docetaxel and HSP90 inhibitor treated pEF6 groups ($p<0.001$). No significant difference was observed between either untreated pEF6 vs. HSP90 inhibitor treated pEF6 groups or docetaxel treated vs combined HSP90 inhibitor and docetaxel treated pEF6 groups as with the paclitaxel treatments, our observations here suggests that the main cytotoxic impact is derived from the action of the docetaxel chemotherapeutic agent and HSP90 inhibitor has little additional impact in MCF-7 pEF6 cells.

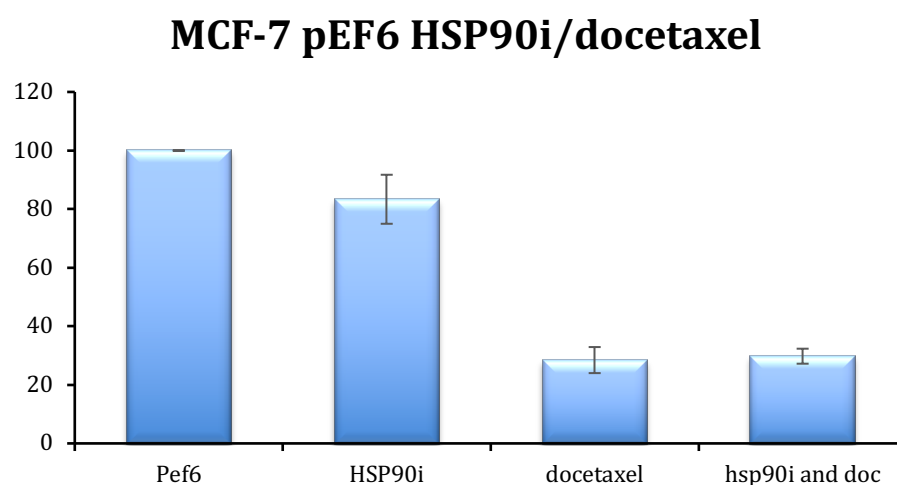


Fig. 6.29. Growth assay of MCF-7 pEF6 cell lines and the response to treatment with HSP90 inhibitor (30nM), Docetaxel (50nM) and combination of both. Data shown represents mean percentage untreated pEF6 cells ($n=3$), error bars represent SEM.

Similarly, we investigated the impact of such treatments following DAP-3 knockdown in MCF-7 cells (Fig. 6.30.). ANOVA analysis within the group demonstrated significant differences. Post-hoc (Holm-Sidak) analysis revealed significant differences between untreated DAP-3 KD vs. docetaxel treated DAP-3 KD groups ($p < 0.001$); untreated DAP-3 KD vs. combined HSP90 inhibitor and docetaxel treated DAP-3 KD groups ($p < 0.001$); HSP90 inhibitor treated vs. docetaxel treated DAP-3 KD groups ($p < 0.001$); HSP90 inhibitor treated vs. combined docetaxel and HSP90 inhibitor treated DAP-3 KD groups ($p < 0.001$). No significant difference was observed between either untreated DAP-3 KD vs. HSP90 inhibitor treated DAP-3 KD groups or docetaxel treated vs combined HSP90 inhibitor and docetaxel treated DAP-3 KD groups.

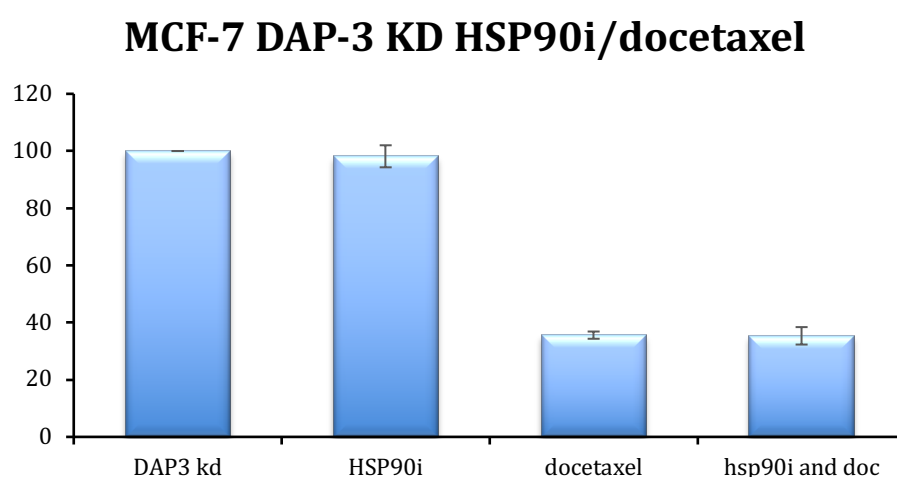


Fig. 6.30. Growth assay of MCF-7 DAP-3 KD cell lines and the response to treatment with HSP90 inhibitor (30nM), Docetaxel (50nM) and combination of both. Data shown represents mean percentage untreated pEF6 cells ($n=3$), error bars represent SEM

6.3.4.2. MDA-MB-231

Similar to the MCF-7 model, the impact of DAP-3 knockdown, HSP90 inhibition and either paclitaxel or docetaxel were explored in relation to the MDA-MB-231 breast cancer cell line.

6.3.4.2.1. Paclitaxel

Observations within the MDA-MB-231 group in regard to paclitaxel response in addition to HSP90 inhibition and DAP-3 knockdown were in keeping with the MCF-7 cell line.

Within the pEF6 cell lines ANOVA analysis demonstrated significant differences, with post-hoc (Holm-Sidak) analysis revealing significant differences between untreated pEF6 vs. paclitaxel treated pEF6 groups ($p < 0.001$); untreated pEF6 vs. combined HSP90 inhibitor and paclitaxel treated pEF6 groups ($p < 0.001$); HSP90 inhibitor treated vs. paclitaxel treated pEF6 groups ($p < 0.001$); HSP90 inhibitor treated vs. combined paclitaxel and HSP90 inhibitor treated pEF6 groups ($p < 0.001$). No significant difference was observed between either untreated pEF6 vs. HSP90 inhibitor treated pEF6 groups or paclitaxel treated vs combined HSP90 inhibitor and paclitaxel treated pEF6 groups (Fig. 6.31).

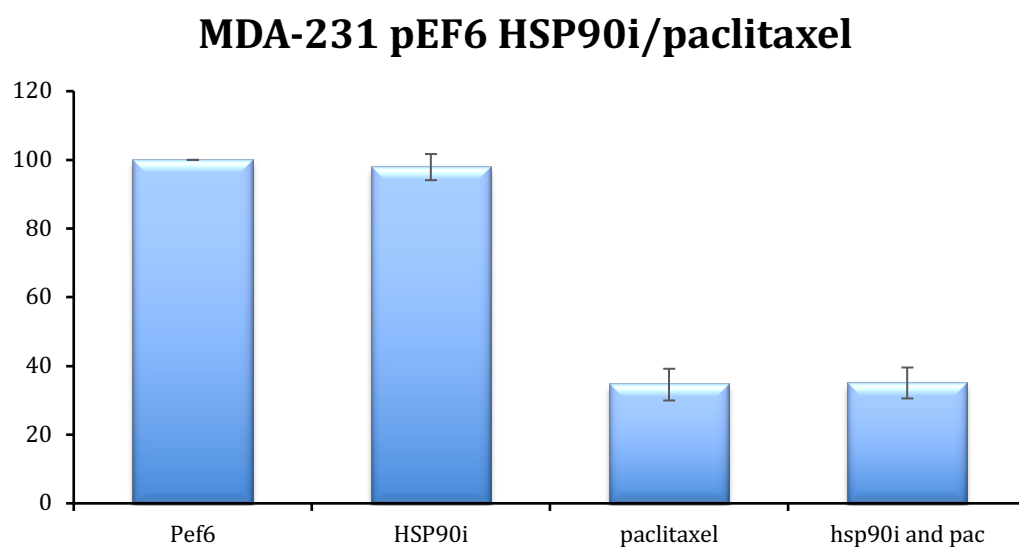


Fig.6.31. Growth assay of MDA-MB-231 pEF6 cell lines and the response to treatment with HSP90 inhibitor (30nM), Paclitaxel (50nM) and combination of both. Data shown represents mean percentage untreated pEF6 cells (n=3), error bars represent SEM

The impact of such treatments on MDA-MB-231 DAP-3 KD cell lines was largely in keeping with those in the control pEF6. ANOVA analysis indicated significant differences within the group. Post-hoc (Holm-Sidak) analysis revealed significant differences between untreated DAP-3 KD MDA-MB-231 cells vs. paclitaxel treated DAP-3 KD groups ($p < 0.001$); untreated DAP-3 KD vs. combined HSP90 inhibitor and paclitaxel treated DAP-3 KD groups ($p < 0.001$); HSP90 inhibitor treated DAP-3 KD vs. paclitaxel treated DAP-3 KD groups ($p < 0.001$); HSP90 inhibitor treated DAP-3 KD vs. combined paclitaxel and HSP90 inhibitor treated DAP-3 KD groups ($p < 0.001$). No significant difference was observed between either untreated DAP-3 KD vs. HSP90 inhibitor treated DAP-3 KD groups or paclitaxel treated DAP-3 KD vs combined HSP90 inhibitor and paclitaxel treated DAP-3 KD groups (Fig. 6.32.).

No differential impact of HSP90 inhibition, paclitaxel or a combination of both were seen between pEF6 control and DAP-3 KD cells.

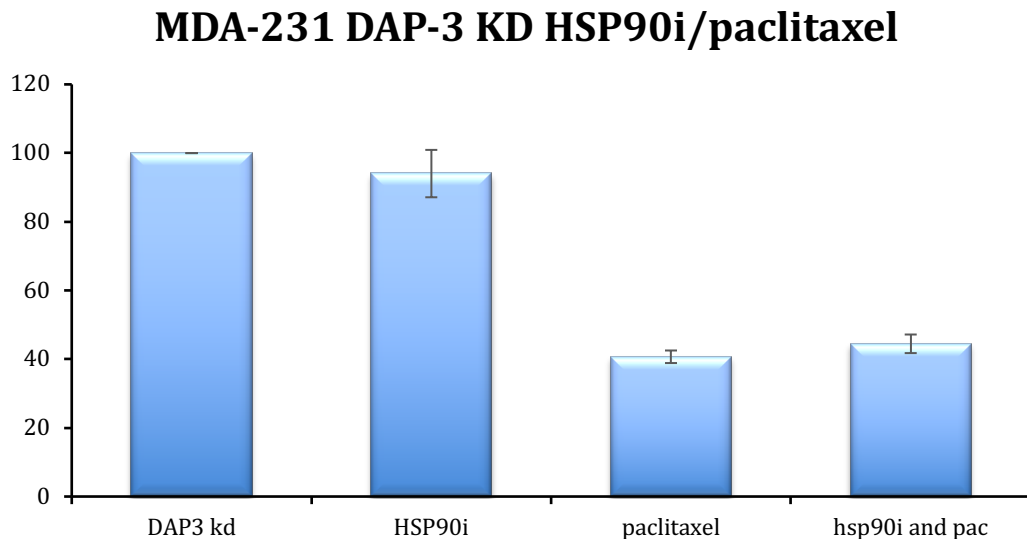


Fig. 6.32. Growth assay of MDA-MB-231 DAP-3 KD cell lines and the response to treatment with HSP90 inhibitor (30nM), Paclitaxel (50nM) and combination of both. Data shown represents mean percentage untreated pEF6 cells (n=3), error bars represent SEM

6.3.4.2.2. Docetaxel

Again, observations within the MDA-MB-231 group in regard to docetaxel response in addition to HSP90 inhibition and DAP-3 knockdown were similar to those observed in the MCF-7 cell models.

Within the pEF6 cell variant a significant difference was observed following ANOVA analysis. Significant differences were observed through post hoc (Holm-Sidak) analysis between untreated pEF6 MDA_MB-231 groups vs. docetaxel treated pEF6 groups ($p < 0.001$); untreated pEF6 vs. combined HSP90 inhibitor and docetaxel treated pEF6 groups ($p < 0.001$); HSP90 inhibitor treated vs. docetaxel treated pEF6 groups ($p < 0.001$); HSP90 inhibitor treated

vs. combined docetaxel and HSP90 inhibitor treated pEF6 groups ($p < 0.001$). Post hoc analysis revealed no significant difference between either untreated pEF6 vs. HSP90 inhibitor treated pEF6 groups or docetaxel treated vs combined HSP90 inhibitor and docetaxel treated pEF6 groups (Fig. 6.33).

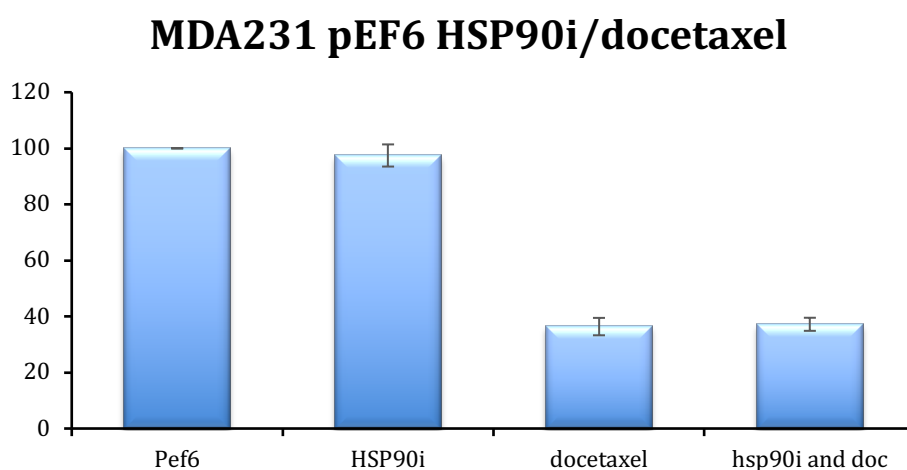


Fig.6.33. Growth assay of MDA-MB-231 pEF6 cell lines and the response to treatment with HSP90 inhibitor (30nM), Docetaxel (50nM) and combination of both. Data shown represents mean percentage untreated pEF6 cells ($n=3$), error bars represent SEM

Similar observations were seen in the MDA-MB-231 DAP-3 KD cell group regarding responses to HSP90 inhibition and docetaxel response. ANOVA analysis within the DAP-3 KD group highlighted significant differences with post-hoc (Holm-Sidak) analysis revealing significant differences between untreated DAP-3 KD MDA-MB-231 vs. docetaxel treated DAP-3 KD groups ($p < 0.001$); untreated DAP-3 KD vs. combined HSP90 inhibitor and docetaxel treated DAP-3 KD groups ($p < 0.001$); HSP90 inhibitor treated vs. docetaxel treated DAP-3 KD groups ($p < 0.001$); HSP90 inhibitor treated vs. combined docetaxel and HSP90 inhibitor treated DAP-3 KD groups ($p < 0.001$). There was

no significant difference observed between either untreated DAP-3 KD vs. HSP90 inhibitor treated DAP-3 KD groups or docetaxel treated vs combined HSP90 inhibitor and docetaxel treated DAP-3 KD groups (Fig. 6.34.).

Similar to the paclitaxel investigations, suppression of DAP-3 or inhibition of HSP90 in MDA-MB-231 cells did not appear to have a clear impact on the response to docetaxel.

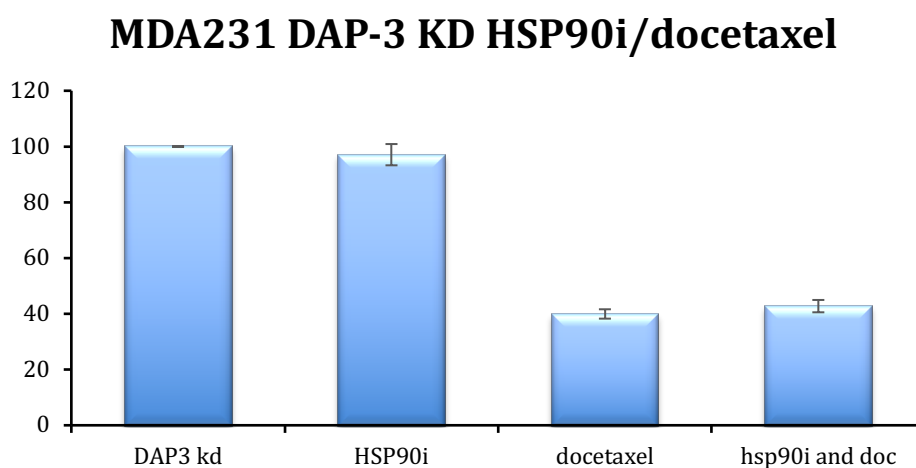


Fig.6.34. Growth assay of MDA-MB-231 DAP-3 KD cell lines and the response to treatment with HSP90 inhibitor (30nM), Docetaxel (50nM) and combination of both. Data shown represents mean percentage untreated pEF6 cells (n=3), error bars represent SEM

6.4. Discussion

In our study, we explored within our cohort the association between expression levels of HSP90A and HSP90B and clinical outcomes. We have demonstrated that low expression levels of these 2 molecules were associated with local recurrence and metastasis.

For comparison the results that we sourced from an online database suggest that OS is significantly improved with increased HSP90B expression, but we have not demonstrated this with HSP90A.

We have further explored the association between HSP90 and DAP-3 and assessed this relationship with regards to OS and DFS. A combined higher expression of DAP-3 and HSP90A and also DAP-3 and HSP90B was linked to significantly improved OS.

Previous work from our laboratories (Wazir et al. 2012) reported that high expression levels of DAP-3 in breast cancer were associated with improved OS (152). Similar outcomes were reported also in gastric cancer (154).

In view of these results, it does appear, that higher expression levels of both HSP90 and DAP-3 would be associated with better survival. Although, there appears to be variability with regards to clinical outcomes and expression levels of HSP90 in published literature. Dimas et al. 2018 in their meta-analysis report that higher expression is associated with worse OS and marginally worse DFS (206). Literature on DAP-3 and breast cancer clinical outcomes is rather sparse and mainly comes from our group as described above.

Expression levels of DAP-3, HSP90A and HSP90B in relation to response to either taxane or anthracycline chemotherapy utilising data from

online datasets has not revealed any clear patterns. Although certain breast cancer subgroups in the 'responder' category of these 2 chemotherapy treatments were demonstrating significantly higher expression levels of DAP-3/HSP90A/HSP90B (Fig.6.35.). The expression of our target molecules in all the selected breast cancer subgroups in the context of chemotherapy treatment and their response to it appears heterogenous. In order to find any obvious patterns more chemotherapeutic agents would need to be evaluated and also with the utilisation of other available online datasets.

Paclitaxel treatment	ER+	ER-	HER2+	HER2-	Triple negative
DAP-3	*				
HSP90A					
HSP90B	*			*	

Anthracycline treatment	ER+	ER-	HER2+	HER2-	Triple negative
DAP-3	*	*		*	
HSP90A		*			*
HSP90B					

Fig. 6.35. * indicates significantly increased expression of relevant molecule in a certain receptor variant of breast cancer treated by taxane/anthracycline chemotherapy.

Jia et al. 2014, also indicated that DAP-3 is a potential marker of response to neoadjuvant chemotherapy, where DAP-3 knockdown enhanced resistance to chemotherapy. FOLFOX regimen (oxiplatin, folinic acid and 5-FU) has been used in this study for treatment of gastric cancer (154). In our study, we looked to further explore the potential links between DAP-3, its relationship with HSP90 and the impact on breast cancer therapy response. Unfortunately, due to the associated restrictions and disruption caused by the emerging COVID-19 pandemic this aspect was limited and hence only initial observations were able to be conducted. In this regard, our study focused on responsiveness to minimal numbers of treatment concentrations, as outlined in the methods section of this chapter, investigating the response in relation to 50nM concentration of chemotherapeutic agents and 30nM concentration of HSP90 inhibitor. Such concentrations were based on our previous work, the literature and ic_{50} values. Ideally, such responses would be calculated over a range of concentrations to compare response rates over this range to investigate if DAP-3 knockdown cells responsive rates (ic_{50} etc.) differ to those in control cells. Hence, there are limitations to our current work which offers an initial observation but requires more in-depth analysis. As such, our initial data did not indicate any differential impact of DAP-3 knockdown, either alone or in combination with HSP90 inhibition in response to 50nM paclitaxel or docetaxel, with the cytotoxic effects appearing to be predominantly in response to the chemotherapeutic agent. However, as indicated above, this requires further clarification as it may be that differential responses could be observed at lower concentrations of the agents.

Chapter 7

General Discussion

This study was a continuation and further expansion of work done at our laboratories (152, 153). In order to replicate the KD studies we have decided for the same choice of cell lines (MCF-7 and MDA-MB-231) and used same methodology only with small discrepancies.

These cell lines represent model scenarios simulating early and late-stage breast cancer. We have aimed to replicate this to further explore the downstream effectors of DAP-3 in additional experiments.

DAP-3 knock down variants of MCF-7 and MDA-MB-231 cell lines were established using ribosome transgene technology to better correlate our results with Wazir et al. study and since it remains an effective approach.

Following this we have investigated potential interacting partners of DAP-3 in breast cancer and which of the proteins are differentially linked to DAP-3 in normal and tumour mammary tissues utilising immunoprecipitation. We used anti-DAP-3 antibody to pull out those interacting with DAP-3 and processed these in protein array (Kinexus) - a platform to determine the main interacting proteins and also evaluated the difference between normal and tumour tissues.

This protein platform supplied us a list of proteins that are regarded as the priority targets of DAP-3 either high in tumour or lower in tumour, in comparison with normal tissues. With this list, pathways significantly associated with this list of DAP-3 interactive proteins were constituted. Among identifies pathways were ERBB4 and ERBB2 pathways which are well known for their role in breast cancer.

Other interesting pathways including the ERK pathway which was also described in the context of HSP90 in the introduction section, BRAF and IL4/IL13.

DAP-3 and HSP90 (both HSP90a and HSP90b) had a high-profile presence in half of the pathways revealed. These two heat shock proteins were also highly different in their association with DAP-3, namely heightened interaction in tumour tissues compared with normal tissues. This suggests that HSP90 is a key partner protein of DAP-3 and that our results have shown that both are highly expressed in breast cancer.

This is a newly described interaction in human breast cancer. As far as we are aware, the only previous note in the literature indicate weak interaction between DAP-3 and HSP90 (183).

We went on to further characterise this new interaction and explored the impact of DAP-3 knockdown on HSP90 expression. We have demonstrated a significant decrease of HSP90a expression in MCF-7 DAP-3 KD cells with a similar trend in HSP90b expression. Similarly, A significant decrease in HSP90b expression was also seen in MDA-MB-231 expression following DAP-3 knockdown and a similar trend was seen for HSP90a expression.

To describe this relationship close we set to investigate if the inhibition of HSP90 has any effect on DAP-3 expression in wildtype MCF-7 and MDA-MB-231 cells. Interestingly, this pathway wasn't affected and there does not seem to be a reverse effect. This may suggest that HSP90 could be a downstream transcriptionally regulated effector of DAP-3.

Knockdown of DAP-3 has shown to decrease cellular ATP production, cause protein synthesis defects and mitochondrial dissipation. Xiao *et al.* 2015 suggest that knockdown of DAP-3 regulates the phosphorylation of dynamin-related protein 1 (Drp1) and promotes mitochondrial fission and facilitates cell death (171).

As described in Chapter 1, DAP-3 is kept inactive as a phosphoprotein by the action of protein kinase B (AKT/PKB). It interacts with FAS Associated Death Domain (FADD) once activated and takes part in the formation of Death inducing signalling complex (DISC) (146). Death ligand signal enhancer (DELE), also described as ligand of DAP-3, found to inhibit apoptosis when knocked down (147). Although with regards to known downstream effectors transcriptionally regulated by DAP-3, there does not to be any reports of these.

In gastric cancer the effects of DAP-3 expression knockdown on cell functions promoted cell migration and increased resistance to chemotherapy by inhibiting apoptosis (173) while in breast cancer DAP-3 knock down has been witnessed to cause increase in cell adhesion, migration and invasion (153).

Our experiments yielded similar results we observed non-significant increase in adhesion and invasion. The only differing result was decreased migration following DAP-3 KD, although this could be explained by the use of different methodology used to explore breast cancer migration (Electric cell-substrate impedance sensing (ECIS) vs scratch/migration assay) or also cancer type specific differences between breast and gastric cell lines.

HSP90 inhibition has the capacity to simultaneously disrupt multiple cancer pathways by acting on a single target hence appears very appealing. HSP90 is essential for the stability and function of a wide spectrum of oncogenic proteins that among others directly contribute to distinctive features resulting from genetic and epigenetic alterations of key regulatory proteins – these have been described as Hallmarks of cancer (185).

In our study, the HSP90 inhibition effects that we have recorded in breast cancer cell lines were non-significant increase in growth and invasion, while increases in adhesion has reached significance. Cell migration was not affected. Oh *et al.* 2017, evaluated effects of HSP90 inhibition on MDA-MB-231 cells and reported decrease in both migration and growth (186). Further studies report decrease in invasion, migration and proliferation in MDA-MB-231 cell lines following HSP90 inhibitor treatment (187-189).

We could explain these contrasting results with the fact that they have used much higher concentrations, longer exposure to HSP90 inhibitor and a different HSP90 inhibitor molecule hence these effects could be dose and exposure-time dependent.

Inhibition of adhesion appeared to be most obvious result along with general increase of invasion of the combined effect of DAP-3 KD and HSP90 inhibition which are aligned with our results of isolated DAP-3 KD and HSP90 inhibitor effects. We feel that this warrants further investigation as this has not been previously described in literature.

Our results indicate that DAP-3 may play an important role in modulating the expression of HSP90 and also interact with this molecule and give more insight into potential DAP-3 downstream effectors. Such data may reveal a potential lead for new targeted therapies.

Within our cohort, we explored the link between expression levels of HSP90A and HSP90B and clinical outcomes. Low expression levels of these 2 molecules were associated with local recurrence and metastasis. When comparing our results to that we sourced from an online database it is suggested that OS is significantly improved with increased HSP90B expression, but not with HSP90A.

Further exploring the association between HSP90 and DAP-3 and their relationship with regards to OS and DFS showed a combined higher

expression of DAP-3 and HSP90A and also DAP-3 and HSP90B was linked to significantly improved OS.

Wazir et al. reported that high expression levels of DAP-3 in breast cancer were associated with improved OS (152) and similar outcomes were reported also in gastric cancer (154).

In view of these results, it does appear, that higher expression levels of both HSP90 and DAP-3 would be associated with better survival. Although, there appears to be variability with regards to clinical outcomes and expression levels of HSP90 in published literature. Dimas et al. 2018 in their meta-analysis report that higher expression is associated with worse OS and marginally worse DFS (206). Literature on DAP-3 and breast cancer clinical outcomes is rather sparse and mainly comes from our group as described above.

Results of our assessment of expression levels DAP-3, HSP90A and HSP90B with regards to response to chemotherapy agents (taxane and anthracycline chemotherapeutics) have not revealed any clear patterns. (Fig.6.35.). Although Jia et al. 2014, suggest that DAP-3 is a potential marker of response to neoadjuvant chemotherapy, where DAP-3 knockdown enhanced resistance to chemotherapy, albeit they have used a different chemotherapy regimen (FOLFOX oxiplatin, folinic acid and 5-FU) and it was for treatment of gastric cancer (154).

Unfortunately, the COVID-19 pandemic with its restrictions has hindered our further intentions to look further and explore the potential links between DAP-3, its relationship with HSP90 and the impact on breast cancer therapy response. This has hence been limited and only initial observations conducted.

In this part of the study with the above-mentioned restrictions in place we focused on responsiveness to just a limited numbers of chemotherapy treatment concentrations (as detailed in Methods section 6.2.). These concentrations were chosen based on our previous work, concentrations described in other studies and ic50 values.

There are limitations to our current work which offers an initial observation (as a range of concentrations has not been used due to restrictions). Analysis of our initial data did not highlight any differential impact of DAP-3 knockdown, either alone or in combination with HSP90 inhibition in response to 50nM paclitaxel or docetaxel. However, as indicated above, this requires further clarification as it may be that differential responses could be observed at lower concentrations of the agents.

Our observations in this study may lead to a conclusion that the newly described association of DAP-3 and HSP90 given further research might lead to revealing of potential targeted therapies in breast cancer.

Limitation of the present study and future research leads

My studies span a most difficult period of COVID19 pandemic with a substantial portion coincided with the national lockdown. There are some aspects of the study that I wish to be able to pursue but unable due to the lockdown and also the time frame of my study. Furthermore, the study has raised some fascinating leads for future research.

1. *In vivo* model. Two important research findings stemmed from the present study would be ideally validated using in vivo tumour models.

- a. DAP-3 and HSP90 relationship to tumour growth. The cell lines created in the present study would be ideally tested

using a suitable tumour model in order to evaluate the impact on tumour growth;

- b. DAP-3 and HSP90 and chemosensitivity. From the limited *in vitro* results and overwhelming information from the public dataset, it is clear there is a strong relationship between DAP-3/HSP90 and cell and patients' response to chemotherapies. An ideal step would be to apply the cell models established here in a suitable *in vivo* tumour model and to evaluate the response to specific drugs and the regime of treatment.
2. Responsive targets downstream of DAP-3/HSP90 in particular those which responded to treatment. It would be highly informative for prospective clinical studies to discover if a responsive target profile exists in the DAP-3/HSP90 model in relation to their response to treatment. The findings from the study have indicated that the pattern of DAP-3 and HSP90 in breast cancer cells and clinical breast tumour has important bearing to both clinical outcome and also patients' response to treatment. It would be plausible to explore if the differential combination of DAP-3 and HSP90 in breast cancer (cells) is linked to a gene or protein pattern that are responsible for the important clinical link. Identification such pattern is valuable not only for the assessment of patient's clinical course and outcome, but also aid in the choice of drug treatments.
3. Other pathways significantly linked to DAP-3.

As presented in Chapter-4, the present study has discovered multiple pathways that are linked to DAP-3, including for example the HER2 pathway, the crystallin alpha B pathway, the paxillin pathway and indeed a few other pathways that are connected with the HER family protein kinases. Limited by time frame of the research programme and indeed by the lockdown, the present study had to focus on one of

the most interesting pathways to me, namely HSP90. These other pathways would make important part of the DAP-3 network and warrant further investigations.

Perhaps the most interesting pathways for the future is the HER2 (ERBB2) and HER4 (ERBB4) pathways, given their significance in the development and progression of clinical cancer and the development of treatment options in targeting these receptor kinases. The prominence of these two pathways in the most regulated pathways by DAP-3 discovered in the present study (i.e. Table 4.4.) further project the importance for future investigation and is likely to be a highly fertile area of scientific and clinical cancer research.

REFERENCES:

1. JH B. The Edwin Smith Surgical Papyrus. The University of Chicago Oriental Institute Publications. 1930;1,2.
2. Ades F, Tryfonidis K, Zardavas D. The past and future of breast cancer treatment-from the papyrus to individualised treatment approaches. *Ecancermedicalscience*. 2017;11:746-.
3. Lakhtakia R. A Brief History of Breast Cancer: Part I: Surgical domination reinvented. *Sultan Qaboos Univ Med J*. 2014;14(2):e166-e9.
4. Papavramidou N, Papavramidis T, Demetriou T. Ancient Greek and Greco-Roman methods in modern surgical treatment of cancer. *Ann Surg Oncol*. 2010;17(3):665-7.
5. Sudhakar A. History of Cancer, Ancient and Modern Treatment Methods. *J Cancer Sci Ther*. 2009;1(2):1-4.
6. Gulczyński J, Izycka-Swieszewska E, Grzybiak M. Short history of the autopsy. Part I. From prehistory to the middle of the 16th century. *Pol J Pathol*. 2009;60(3):109-14.
7. The title page of the 1556 edition of Avicenna's *The Canon of Medicine* (Al-Qanun fi al-Tibb). *Encyclopædia Britannica*.
8. Halsted WS. I. The Results of Operations for the Cure of Cancer of the Breast Performed at the Johns Hopkins Hospital from June, 1889, to January, 1894. *Ann Surg*. 1894;20(5):497-555.
9. Fisher B. United States trials of conservative surgery. *World J Surg*. 1977;1(3):327-30.
10. Patey DH. A review of 146 cases of carcinoma of the breast operated on between 1930 and 1943. *Br J Cancer*. 1967;21(2):260-9.

11. Madden JL, Kandalaft S, Bourque RA. Modified radical mastectomy. *Ann Surg.* 1972;175(5):624-34.
12. Veronesi U, Saccozzi R, Del Vecchio M, Banfi A, Clemente C, De Lena M, et al. Comparing radical mastectomy with quadrantectomy, axillary dissection, and radiotherapy in patients with small cancers of the breast. *N Engl J Med.* 1981;305(1):6-11.
13. Fisher B, Jeong JH, Anderson S, Bryant J, Fisher ER, Wolmark N. Twenty-five-year follow-up of a randomized trial comparing radical mastectomy, total mastectomy, and total mastectomy followed by irradiation. *N Engl J Med.* 2002;347(8):567-75.
14. Veronesi U, Volterrani F, Luini A, Saccozzi R, Del Vecchio M, Zucali R, et al. Quadrantectomy versus lumpectomy for small size breast cancer. *Eur J Cancer.* 1990;26(6):671-3.
15. Veronesi U, Luini A, Del Vecchio M, Greco M, Galimberti V, Merson M, et al. Radiotherapy after breast-preserving surgery in women with localized cancer of the breast. *N Engl J Med.* 1993;328(22):1587-91.
16. Veronesi U, Cascinelli N, Mariani L, Greco M, Saccozzi R, Luini A, et al. Twenty-year follow-up of a randomized study comparing breast-conserving surgery with radical mastectomy for early breast cancer. *N Engl J Med.* 2002;347(16):1227-32.
17. NIH consensus conference. Treatment of early-stage breast cancer. *Jama.* 1991;265(3):391-5.
18. Mandelblatt JS, Edge SB, Meropol NJ, Senie R, Tsangaris T, Grey L, et al. Sequelae of axillary lymph node dissection in older women with stage 1 and 2 breast carcinoma. *Cancer.* 2002;95(12):2445-54.
19. Morton DL, Wen DR, Wong JH, Economou JS, Cagle LA, Storm FK, et al. Technical details of intraoperative lymphatic mapping for early stage melanoma. *Arch Surg.* 1992;127(4):392-9.

20. Alex JC, Krag DN. Gamma-probe guided localization of lymph nodes. *Surg Oncol.* 1993;2(3):137-43.
21. Veronesi U, Viale G, Paganelli G, Zurrada S, Luini A, Galimberti V, et al. Sentinel lymph node biopsy in breast cancer: ten-year results of a randomized controlled study. *Ann Surg.* 2010;251(4):595-600.
22. Veronesi U, Paganelli G, Viale G, Luini A, Zurrada S, Galimberti V, et al. A randomized comparison of sentinel-node biopsy with routine axillary dissection in breast cancer. *N Engl J Med.* 2003;349(6):546-53.
23. National Guideline A. National Institute for Health and Care Excellence: Clinical Guidelines. Early and locally advanced breast cancer: diagnosis and management. London: National Institute for Health and Care Excellence (UK) Copyright © NICE 2018.; 2018.
24. Wilhelm Conrad Röntgen – Facts. NobelPrize.org. Nobel Media AB 2021. Thu. 18 Mar 2021.
<<https://www.nobelprize.org/prizes/physics/1901/rontgen/facts/>>.
25. Rayter Z. JM. History of Breast Cancer Therapy, Medical Therapy of Breast Cancer. Cambridge University Press. 2003.
26. Fisher B, Anderson S, Bryant J, Margolese RG, Deutsch M, Fisher ER, et al. Twenty-year follow-up of a randomized trial comparing total mastectomy, lumpectomy, and lumpectomy plus irradiation for the treatment of invasive breast cancer. *N Engl J Med.* 2002;347(16):1233-41.
27. Clarke M, Collins R, Darby S, Davies C, Elphinstone P, Evans V, et al. Effects of radiotherapy and of differences in the extent of surgery for early breast cancer on local recurrence and 15-year survival: an overview of the randomised trials. *Lancet.* 2005;366(9503):2087-106.
28. Whelan TJ, Pignol JP, Levine MN, Julian JA, MacKenzie R, Parpia S, et al. Long-term results of hypofractionated radiation therapy for breast cancer. *N Engl J Med.* 2010;362(6):513-20.

29. Lievens Y. Hypofractionated breast radiotherapy: financial and economic consequences. *Breast*. 2010;19(3):192-7.
30. Murray Brunt A, Haviland JS, Wheatley DA, Sydenham MA, Alhasso A, Bloomfield DJ, et al. Hypofractionated breast radiotherapy for 1 week versus 3 weeks (FAST-Forward): 5-year efficacy and late normal tissue effects results from a multicentre, non-inferiority, randomised, phase 3 trial. *Lancet*. 2020;395(10237):1613-26.
31. Vicini FA, Cecchini RS, White JR, Arthur DW, Julian TB, Rabinovitch RA, et al. Long-term primary results of accelerated partial breast irradiation after breast-conserving surgery for early-stage breast cancer: a randomised, phase 3, equivalence trial. *Lancet*. 2019;394(10215):2155-64.
32. Meattini I, Marrazzo L, Saieva C, Desideri I, Scotti V, Simontacchi G, et al. Accelerated Partial-Breast Irradiation Compared With Whole-Breast Irradiation for Early Breast Cancer: Long-Term Results of the Randomized Phase III APBI-IMRT-Florence Trial. *J Clin Oncol*. 2020;38(35):4175-83.
33. Orecchia R, Veronesi U, Maisonneuve P, Galimberti VE, Lazzari R, Veronesi P, et al. Intraoperative irradiation for early breast cancer (ELIOT): long-term recurrence and survival outcomes from a single-centre, randomised, phase 3 equivalence trial. *Lancet Oncol*. 2021.
34. Drost L, Yee C, Lam H, Zhang L, Wronski M, McCann C, et al. A Systematic Review of Heart Dose in Breast Radiotherapy. *Clin Breast Cancer*. 2018;18(5):e819-e24.
35. Yamazaki H, Takenaka T, Aibe N, Suzuki G, Yoshida K, Nakamura S, et al. Comparison of radiation dermatitis between hypofractionated and conventionally fractionated postoperative radiotherapy: objective, longitudinal assessment of skin color. *Sci Rep*. 2018;8(1):12306.
36. King MT, Link EK, Whelan TJ, Olivotto IA, Kunkler I, Westenberg AH, et al. Quality of life after breast-conserving therapy and adjuvant radiotherapy for

non-low-risk ductal carcinoma in situ (BIG 3-07/TROG 07.01): 2-year results of a randomised, controlled, phase 3 trial. *Lancet Oncol.* 2020;21(5):685-98.

37. Wan BA, Pidduck W, Zhang L, Nolen A, Drost L, Yee C, et al. Patient-reported fatigue in breast cancer patients receiving radiation therapy. *Breast.* 2019;47:10-5.

38. Choi KH, Ahn SJ, Jeong JU, Yu M, Kim JH, Jeong BK, et al. Postoperative radiotherapy with intensity-modulated radiation therapy versus 3-dimensional conformal radiotherapy in early breast cancer: A randomized clinical trial of KROG 15-03. *Radiother Oncol.* 2021;154:179-86.

39. Possanzini M, Greco C. Stereotactic radiotherapy in metastatic breast cancer. *Breast.* 2018;41:57-66.

40. Boyd S. On Oöphorectomy in the Treatment of Cancer. *Br Med J.* 1897;2(1918):890-6.

41. Huggins C, Hodges CV. Studies on prostatic cancer: I. The effect of castration, of estrogen and of androgen injection on serum phosphatases in metastatic carcinoma of the prostate. 1941. *J Urol.* 2002;168(1):9-12.

42. Huggins C, Bergenstal DM. Effect of Bilateral Adrenalectomy on Certain Human Tumors. *Proceedings of the National Academy of Sciences of the United States of America.* 1952;38(1):73-6.

43. Charles B. Huggins – Facts. *NobelPrize.org.* Nobel Media AB 2021.

44. Jensen EV, Desombre ER, Kawashima T, Suzuki T, Kyser K, Jungblut PW. Estrogen-binding substances of target tissues. *Science.* 1967;158(3800):529-30.

45. Paterni I, Granchi C, Katzenellenbogen JA, Minutolo F. Estrogen receptors alpha (ER α) and beta (ER β): subtype-selective ligands and clinical potential. *Steroids.* 2014;90:13-29.

46. Chang EC, Frasor J, Komm B, Katzenellenbogen BS. Impact of estrogen receptor beta on gene networks regulated by estrogen receptor alpha in breast cancer cells. *Endocrinology*. 2006;147(10):4831-42.
47. Rose C, Thorpe SM, Løber J, Daenfeldt JL, Palshof T, Mouridsen HT. Therapeutic effect of tamoxifen related to estrogen receptor level. *Recent Results Cancer Res*. 1980;71:134-41.
48. Rose C, Thorpe SM, Andersen KW, Pedersen BV, Mouridsen HT, Blichert-Toft M, et al. Beneficial effect of adjuvant tamoxifen therapy in primary breast cancer patients with high oestrogen receptor values. *Lancet*. 1985;1(8419):16-9.
49. Stewart HJ, Prescott R. Adjuvant tamoxifen therapy and receptor levels. *Lancet*. 1985;1(8428):573.
50. Controlled trial of tamoxifen as single adjuvant agent in management of early breast cancer. Analysis at six years by Nolvadex Adjuvant Trial Organisation. *Lancet*. 1985;1(8433):836-40.
51. Wilson R, Hanham IW, Mair G, Drake SR, Derry CD, McKenzie C, et al. Adjuvant hormono-chemotherapy in operable breast cancer. *Lancet*. 1978;1(8073):1101.
52. Effects of adjuvant tamoxifen and of cytotoxic therapy on mortality in early breast cancer. An overview of 61 randomized trials among 28,896 women. *N Engl J Med*. 1988;319(26):1681-92.
53. Fisher B, Costantino J, Redmond C, Poisson R, Bowman D, Couture J, et al. A randomized clinical trial evaluating tamoxifen in the treatment of patients with node-negative breast cancer who have estrogen-receptor-positive tumors. *N Engl J Med*. 1989;320(8):479-84.
54. Tamoxifen for early breast cancer: an overview of the randomised trials. Early Breast Cancer Trialists' Collaborative Group. *Lancet*. 1998;351(9114):1451-67.

55. Cuzick J, Forbes J, Edwards R, Baum M, Cawthorn S, Coates A, et al. First results from the International Breast Cancer Intervention Study (IBIS-I): a randomised prevention trial. *Lancet*. 2002;360(9336):817-24.
56. Cuzick J, Sestak I, Cawthorn S, Hamed H, Holli K, Howell A, et al. Tamoxifen for prevention of breast cancer: extended long-term follow-up of the IBIS-I breast cancer prevention trial. *Lancet Oncol*. 2015;16(1):67-75.
57. Smith IE, Dowsett M. Aromatase inhibitors in breast cancer. *N Engl J Med*. 2003;348(24):2431-42.
58. Powles TJ, Hickish T, Kanis JA, Tidy A, Ashley S. Effect of tamoxifen on bone mineral density measured by dual-energy x-ray absorptiometry in healthy premenopausal and postmenopausal women. *J Clin Oncol*. 1996;14(1):78-84.
59. ACOG committee opinion: Tamoxifen and endometrial cancer. *Int J Gynaecol Obstet*. 2001;73(1):77-9.
60. Fisher B, Costantino JP, Wickerham DL, Redmond CK, Kavanah M, Cronin WM, et al. Tamoxifen for prevention of breast cancer: report of the National Surgical Adjuvant Breast and Bowel Project P-1 Study. *J Natl Cancer Inst*. 1998;90(18):1371-88.
61. Santen RJ, Santner S, Davis B, Veldhuis J, Samojlik E, Ruby E. Aminoglutethimide inhibits extraglandular estrogen production in postmenopausal women with breast carcinoma. *J Clin Endocrinol Metab*. 1978;47(6):1257-65.
62. Smith IE, Fitzharris BM, McKinna JA, Fahmy DR, Nash AG, Neville AM, et al. Aminoglutethimide in treatment of metastatic breast carcinoma. *Lancet*. 1978;2(8091):646-9.
63. Miller WR, Dixon JM. Antiaromatase agents: preclinical data and neoadjuvant therapy. *Clin Breast Cancer*. 2000;1 Suppl 1:S9-14.
64. Aromatase inhibitors versus tamoxifen in early breast cancer: patient-level meta-analysis of the randomised trials. *Lancet*. 2015;386(10001):1341-52.

65. Regan MM, Neven P, Giobbie-Hurder A, Goldhirsch A, Ejlertsen B, Mauriac L, et al. Assessment of letrozole and tamoxifen alone and in sequence for postmenopausal women with steroid hormone receptor-positive breast cancer: the BIG 1-98 randomised clinical trial at 8·1 years median follow-up. *Lancet Oncol.* 2011;12(12):1101-8.
66. Ruhstaller T, Giobbie-Hurder A, Colleoni M, Jensen MB, Ejlertsen B, de Azambuja E, et al. Adjuvant Letrozole and Tamoxifen Alone or Sequentially for Postmenopausal Women With Hormone Receptor-Positive Breast Cancer: Long-Term Follow-Up of the BIG 1-98 Trial. *J Clin Oncol.* 2019;37(2):105-14.
67. Goss PE, Ingle JN, Pritchard KI, Robert NJ, Muss H, Gralow J, et al. Extending Aromatase-Inhibitor Adjuvant Therapy to 10 Years. *N Engl J Med.* 2016;375(3):209-19.
68. Francis PA, Pagani O, Fleming GF, Walley BA, Colleoni M, Láng I, et al. Tailoring Adjuvant Endocrine Therapy for Premenopausal Breast Cancer. *N Engl J Med.* 2018;379(2):122-37.
69. Balakrishnan A, Ravichandran D. Early operable breast cancer in elderly women treated with an aromatase inhibitor letrozole as sole therapy. *British journal of cancer.* 2011;105(12):1825-9.
70. Wink CJ, Woensdregt K, Nieuwenhuijzen GAP, van der Sangen MJC, Hutschemaekers S, Roukema JA, et al. Hormone treatment without surgery for patients aged 75 years or older with operable breast cancer. *Ann Surg Oncol.* 2012;19(4):1185-91.
71. Spring LM, Gupta A, Reynolds KL, Gadd MA, Ellisen LW, Isakoff SJ, et al. Neoadjuvant Endocrine Therapy for Estrogen Receptor-Positive Breast Cancer: A Systematic Review and Meta-analysis. *JAMA Oncol.* 2016;2(11):1477-86.
72. Graham JD, Yeates C, Balleine RL, Harvey SS, Milliken JS, Bilous AM, et al. Characterization of progesterone receptor A and B expression in human breast cancer. *Cancer Res.* 1995;55(21):5063-8.

73. Cui X, Schiff R, Arpino G, Osborne CK, Lee AV. Biology of progesterone receptor loss in breast cancer and its implications for endocrine therapy. *J Clin Oncol*. 2005;23(30):7721-35.
74. Bardou VJ, Arpino G, Elledge RM, Osborne CK, Clark GM. Progesterone receptor status significantly improves outcome prediction over estrogen receptor status alone for adjuvant endocrine therapy in two large breast cancer databases. *J Clin Oncol*. 2003;21(10):1973-9.
75. Allred DC. Issues and updates: evaluating estrogen receptor-alpha, progesterone receptor, and HER2 in breast cancer. *Mod Pathol*. 2010;23 Suppl 2:S52-9.
76. Goodman LS, Wintrobe MM, et al. Nitrogen mustard therapy; use of methyl-bis (beta-chloroethyl) amine hydrochloride and tris (beta-chloroethyl) amine hydrochloride for Hodgkin's disease, lymphosarcoma, leukemia and certain allied and miscellaneous disorders. *J Am Med Assoc*. 1946;132:126-32.
77. Gilman A, Philips FS. The Biological Actions and Therapeutic Applications of the B-Chloroethyl Amines and Sulfides. *Science*. 1946;103(2675):409-36.
78. Farber S, Diamond LK, Mercer RD, Sylvester RF, Wolff JA. Temporary Remissions in Acute Leukemia in Children Produced by Folic Acid Antagonist, 4-Aminopteroyl-Glutamic Acid (Aminopterin). *New England Journal of Medicine*. 1948;238(23):787-93.
79. Heidelberger C, Chaudhuri NK, Danneberg P, Mooren D, Griesbach L, Duschinsky R, et al. Fluorinated pyrimidines, a new class of tumour-inhibitory compounds. *Nature*. 1957;179(4561):663-6.
80. Johnson IS, Armstrong JG, Gorman M, Burnett JP, Jr. THE VINCA ALKALOIDS: A NEW CLASS OF ONCOLYTIC AGENTS. *Cancer Res*. 1963;23:1390-427.

81. Freireich EJ, Karon M, Frei III E, editors. Quadruple combination therapy (VAMP) for acute lymphocytic leukemia of childhood. *Proc Am Assoc Cancer Res*; 1964.
82. Fisher B, Carbone P, Economou SG, Frelick R, Glass A, Lerner H, et al. 1-Phenylalanine mustard (L-PAM) in the management of primary breast cancer. A report of early findings. *N Engl J Med*. 1975;292(3):117-22.
83. Bonadonna G, Brusamolino E, Valagussa P, Rossi A, Brugnatelli L, Brambilla C, et al. Combination chemotherapy as an adjuvant treatment in operable breast cancer. *N Engl J Med*. 1976;294(8):405-10.
84. Cameron D, Piccart-Gebhart MJ, Gelber RD, Procter M, Goldhirsch A, de Azambuja E, et al. 11 years' follow-up of trastuzumab after adjuvant chemotherapy in HER2-positive early breast cancer: final analysis of the HERceptin Adjuvant (HERA) trial. *Lancet*. 2017;389(10075):1195-205.
85. Reis-Filho JS, Pusztai L. Gene expression profiling in breast cancer: classification, prognostication, and prediction. *Lancet*. 2011;378(9805):1812-23.
86. Bartlett JM, Bayani J, Marshall A, Dunn JA, Campbell A, Cunningham C, et al. Comparing Breast Cancer Multiparameter Tests in the OPTIMA Prelim Trial: No Test Is More Equal Than the Others. *J Natl Cancer Inst*. 2016;108(9).
87. Turner NC, Ro J, André F, Loi S, Verma S, Iwata H, et al. Palbociclib in Hormone-Receptor-Positive Advanced Breast Cancer. *N Engl J Med*. 2015;373(3):209-19.
88. Esteva FJ, Hubbard-Lucey VM, Tang J, Pusztai L. Immunotherapy and targeted therapy combinations in metastatic breast cancer. *Lancet Oncol*. 2019;20(3):e175-e86.
89. Mina LA, Lim S, Bahadur SW, Firoz AT. Immunotherapy for the Treatment of Breast Cancer: Emerging New Data. *Breast Cancer* (Dove Med Press). 2019;11:321-8.

90. Slamon DJ, Clark GM, Wong SG, Levin WJ, Ullrich A, McGuire WL. Human breast cancer: correlation of relapse and survival with amplification of the HER-2/neu oncogene. *Science*. 1987;235(4785):177-82.
91. Pathologists RCo. Pathology reporting of breast disease in surgical excision specimens incorporating the dataset for histological reporting of breast cancer (high-res). . Ceullular pathology datasets. 2016.
92. Johnston SR. Targeting downstream effectors of epidermal growth factor receptor/HER2 in breast cancer with either farnesyltransferase inhibitors or mTOR antagonists. *Int J Gynecol Cancer*. 2006;16 Suppl 2:543-8.
93. Carter P, Presta L, Gorman CM, Ridgway JB, Henner D, Wong WL, et al. Humanization of an anti-p185HER2 antibody for human cancer therapy. *Proc Natl Acad Sci U S A*. 1992;89(10):4285-9.
94. Pegram M, Hsu S, Lewis G, Pietras R, Beryt M, Sliwkowski M, et al. Inhibitory effects of combinations of HER-2/neu antibody and chemotherapeutic agents used for treatment of human breast cancers. *Oncogene*. 1999;18(13):2241-51.
95. Pietras RJ, Fendly BM, Chazin VR, Pegram MD, Howell SB, Slamon DJ. Antibody to HER-2/neu receptor blocks DNA repair after cisplatin in human breast and ovarian cancer cells. *Oncogene*. 1994;9(7):1829-38.
96. Slamon DJ, Leyland-Jones B, Shak S, Fuchs H, Paton V, Bajamonde A, et al. Use of chemotherapy plus a monoclonal antibody against HER2 for metastatic breast cancer that overexpresses HER2. *N Engl J Med*. 2001;344(11):783-92.
97. Pietras RJ, Poen JC, Gallardo D, Wongvipat PN, Lee HJ, Slamon DJ. Monoclonal antibody to HER-2/neureceptor modulates repair of radiation-induced DNA damage and enhances radiosensitivity of human breast cancer cells overexpressing this oncogene. *Cancer Res*. 1999;59(6):1347-55.

98. von Minckwitz G, Procter M, de Azambuja E, Zardavas D, Benyunes M, Viale G, et al. Adjuvant Pertuzumab and Trastuzumab in Early HER2-Positive Breast Cancer. *N Engl J Med*. 2017;377(2):122-31.
99. Swain SM, Miles D, Kim SB, Im YH, Im SA, Semiglazov V, et al. Pertuzumab, trastuzumab, and docetaxel for HER2-positive metastatic breast cancer (CLEOPATRA): end-of-study results from a double-blind, randomised, placebo-controlled, phase 3 study. *Lancet Oncol*. 2020;21(4):519-30.
100. <https://smart.servier.com>.
101. Haybittle JL, Blamey RW, Elston CW, Johnson J, Doyle PJ, Campbell FC, et al. A prognostic index in primary breast cancer. *Br J Cancer*. 1982;45(3):361-6.
102. Galea MH, Blamey RW, Elston CE, Ellis IO. The Nottingham Prognostic Index in primary breast cancer. *Breast Cancer Res Treat*. 1992;22(3):207-19.
103. Giuliano AE, Edge SB, Hortobagyi GN. Eighth Edition of the AJCC Cancer Staging Manual: Breast Cancer. *Ann Surg Oncol*. 2018;25(7):1783-5.
104. Wesoła M, Jeleń M. A Comparison of IHC and FISH Cytogenetic Methods in the Evaluation of HER2 Status in Breast Cancer. *Adv Clin Exp Med*. 2015;24(5):899-903.
105. . Cancer research UK.
106. Perou CM, Sørlie T, Eisen MB, van de Rijn M, Jeffrey SS, Rees CA, et al. Molecular portraits of human breast tumours. *Nature*. 2000;406(6797):747-52.
107. Dai X, Li T, Bai Z, Yang Y, Liu X, Zhan J, et al. Breast cancer intrinsic subtype classification, clinical use and future trends. *American journal of cancer research*. 2015;5(10):2929-43.
108. Prat A, Adamo B, Cheang MC, Anders CK, Carey LA, Perou CM. Molecular characterization of basal-like and non-basal-like triple-negative breast cancer. *Oncologist*. 2013;18(2):123-33.

109. Cortazar P, Zhang L, Untch M, Mehta K, Costantino JP, Wolmark N, et al. Pathological complete response and long-term clinical benefit in breast cancer: the CTNeoBC pooled analysis. *Lancet*. 2014;384(9938):164-72.
110. Huang M, O'Shaughnessy J, Zhao J, Haiderali A, Cortés J, Ramsey SD, et al. Association of Pathologic Complete Response with Long-Term Survival Outcomes in Triple-Negative Breast Cancer: A Meta-Analysis. *Cancer Res*. 2020;80(24):5427-34.
111. Kumari M, Krishnamurthy PT, Sola P. Targeted Drug Therapy to Overcome Chemoresistance in Triple-negative Breast Cancer. *Curr Cancer Drug Targets*. 2020;20(8):559-72.
112. Sharom FJ. ABC multidrug transporters: structure, function and role in chemoresistance. *Pharmacogenomics*. 2008;9(1):105-27.
113. Ling X, Wu W, Fan C, Xu C, Liao J, Rich LJ, et al. An ABCG2 non-substrate anticancer agent FL118 targets drug-resistant cancer stem-like cells and overcomes treatment resistance of human pancreatic cancer. *J Exp Clin Cancer Res*. 2018;37(1):240.
114. Lee HE, Kim JH, Kim YJ, Choi SY, Kim SW, Kang E, et al. An increase in cancer stem cell population after primary systemic therapy is a poor prognostic factor in breast cancer. *Br J Cancer*. 2011;104(11):1730-8.
115. Dean M. ABC transporters, drug resistance, and cancer stem cells. *J Mammary Gland Biol Neoplasia*. 2009;14(1):3-9.
116. Bholá NE, Balko JM, Dugger TC, Kuba MG, Sánchez V, Sanders M, et al. TGF- β inhibition enhances chemotherapy action against triple-negative breast cancer. *J Clin Invest*. 2013;123(3):1348-58.
117. Krishna BM, Jana S, Singhal J, Horne D, Awasthi S, Salgia R, et al. Notch signaling in breast cancer: From pathway analysis to therapy. *Cancer Lett*. 2019;461:123-31.

118. Ng LF, Kaur P, Bunnag N, Suresh J, Sung ICH, Tan QH, et al. WNT Signaling in Disease. *Cells*. 2019;8(8):826.
119. Doheny D, Manore SG, Wong GL, Lo HW. Hedgehog Signaling and Truncated GLI1 in Cancer. *Cells*. 2020;9(9).
120. Gerweck LE, Vijayappa S, Kozin S. Tumor pH controls the in vivo efficacy of weak acid and base chemotherapeutics. *Mol Cancer Ther*. 2006;5(5):1275-9.
121. Cosse JP, Michiels C. Tumour hypoxia affects the responsiveness of cancer cells to chemotherapy and promotes cancer progression. *Anticancer Agents Med Chem*. 2008;8(7):790-7.
122. Ozretic P, Alvir I, Sarcevic B, Vujaskovic Z, Rendic-Miocevic Z, Roguljic A, et al. Apoptosis regulator Bcl-2 is an independent prognostic marker for worse overall survival in triple-negative breast cancer patients. *Int J Biol Markers*. 2018;33(1):109-15.
123. Seif F, Khoshmirsafa M, Aazami H, Mohsenzadegan M, Sedighi G, Bahar M. The role of JAK-STAT signaling pathway and its regulators in the fate of T helper cells. *Cell Communication and Signaling*. 2017;15(1):23.
124. Zhao TT, Jin F, Li JG, Xu YY, Dong HT, Liu Q, et al. TRIM32 promotes proliferation and confers chemoresistance to breast cancer cells through activation of the NF- κ B pathway. *J Cancer*. 2018;9(8):1349-56.
125. Fan Y, Dutta J, Gupta N, Fan G, G  linas C. Regulation of programmed cell death by NF-kappaB and its role in tumorigenesis and therapy. *Adv Exp Med Biol*. 2008;615:223-50.
126. Kerr JF, Wyllie AH, Currie AR. Apoptosis: a basic biological phenomenon with wide-ranging implications in tissue kinetics. *Br J Cancer*. 1972;26(4):239-57.
127. H  cker G. The morphology of apoptosis. *Cell Tissue Res*. 2000;301(1):5-17.

128. Majno G, Joris I. Apoptosis, oncosis, and necrosis. An overview of cell death. *Am J Pathol.* 1995;146(1):3-15.
129. Edinger AL, Thompson CB. Defective autophagy leads to cancer. *Cancer Cell.* 2003;4(6):422-4.
130. Komatsu M, Waguri S, Ueno T, Iwata J, Murata S, Tanida I, et al. Impairment of starvation-induced and constitutive autophagy in Atg7-deficient mice. *J Cell Biol.* 2005;169(3):425-34.
131. Degenhardt K, Mathew R, Beaudoin B, Bray K, Anderson D, Chen G, et al. Autophagy promotes tumor cell survival and restricts necrosis, inflammation, and tumorigenesis. *Cancer Cell.* 2006;10(1):51-64.
132. He C, Klionsky DJ. Regulation mechanisms and signaling pathways of autophagy. *Annu Rev Genet.* 2009;43:67-93.
133. Wazir U, Khanzada ZS, Jiang WG, Sharma AK, Kasem A, Mokbel K. The interaction between DAP1 and autophagy in the context of human carcinogenesis. *Anticancer Res.* 2014;34(1):1-8.
134. Wazir U, Jiang WG, Sharma AK, Mokbel K. The mRNA expression of DAP1 in human breast cancer: correlation with clinicopathological parameters. *Cancer Genomics Proteomics.* 2012;9(4):199-201.
135. Levin-Salomon V, Bialik S, Kimchi A. DAP-kinase and autophagy. *Apoptosis.* 2014;19(2):346-56.
136. Lin Y, Khokhlatchev A, Figeys D, Avruch J. Death-associated protein 4 binds MST1 and augments MST1-induced apoptosis. *J Biol Chem.* 2002;277(50):47991-8001.
137. Kimchi A. DAP genes: novel apoptotic genes isolated by a functional approach to gene cloning. *Biochim Biophys Acta.* 1998;1377(2):F13-33.
138. Liberman N, Marash L, Kimchi A. The translation initiation factor DAP5 is a regulator of cell survival during mitosis. *Cell Cycle.* 2009;8(2):204-9.

139. Kissil JL, Deiss LP, Bayewitch M, Raveh T, Khaspekov G, Kimchi A. Isolation of DAP3, a novel mediator of interferon-gamma-induced cell death. *J Biol Chem*. 1995;270(46):27932-6.
140. Kissil JL, Kimchi A. Assignment of death associated protein 3 (DAP3) to human chromosome 1q21 by in situ hybridization. *Cytogenet Cell Genet*. 1997;77(3-4):252.
141. Morgan CJ, Jacques C, Savagner F, Tourmen Y, Mirebeau DP, Malthiery Y, et al. A conserved N-terminal sequence targets human DAP3 to mitochondria. *Biochem Biophys Res Commun*. 2001;280(1):177-81.
142. Suzuki T, Terasaki M, Takemoto-Hori C, Hanada T, Ueda T, Wada A, et al. Proteomic analysis of the mammalian mitochondrial ribosome. Identification of protein components in the 28 S small subunit. *J Biol Chem*. 2001;276(35):33181-95.
143. Human Protein Atlas [Available from: <http://www.proteinatlas.org>.
144. Uhlen M, Zhang C, Lee S, Sjöstedt E, Fagerberg L, Bidkhor G, et al. A pathology atlas of the human cancer transcriptome. *Science*. 2017;357(6352).
145. Mukamel Z, Kimchi A. Death-associated protein 3 localizes to the mitochondria and is involved in the process of mitochondrial fragmentation during cell death. *J Biol Chem*. 2004;279(35):36732-8.
146. Miyazaki T, Shen M, Fujikura D, Tosa N, Kim HR, Kon S, et al. Functional role of death-associated protein 3 (DAP3) in anoikis. *J Biol Chem*. 2004;279(43):44667-72.
147. Harada T, Iwai A, Miyazaki T. Identification of DELE, a novel DAP3-binding protein which is crucial for death receptor-mediated apoptosis induction. *Apoptosis*. 2010;15(10):1247-55.
148. Lauricella M, Ciraolo A, Carlisi D, Vento R, Tesoriere G. SAHA/TRAIL combination induces detachment and anoikis of MDA-MB231 and MCF-7 breast cancer cells. *Biochimie*. 2012;94(2):287-99.

149. Li HM, Fujikura D, Harada T, Uehara J, Kawai T, Akira S, et al. IPS-1 is crucial for DAP3-mediated anoikis induction by caspase-8 activation. *Cell Death Differ.* 2009;16(12):1615-21.
150. Han J, An O, Hong H, Chan THM, Song Y, Shen H, et al. Suppression of adenosine-to-inosine (A-to-I) RNA editome by death associated protein 3 (DAP3) promotes cancer progression. *Sci Adv.* 2020;6(25):eaba5136.
151. Sui L, Ye L, Sanders AJ, Yang Y, Hao C, Hargest R, et al. Expression of Death Associated Proteins DAP1 and DAP3 in Human Pancreatic Cancer. *Anticancer Res.* 2021;41(5):2357-62.
152. Wazir U, Jiang WG, Sharma AK, Mokbel K. The mRNA expression of DAP3 in human breast cancer: correlation with clinicopathological parameters. *Anticancer Res.* 2012;32(2):671-4.
153. Wazir U, Sanders AJ, Wazir AM, Ye L, Jiang WG, Ster IC, et al. Effects of the knockdown of death-associated protein 3 expression on cell adhesion, growth and migration in breast cancer cells. *Oncol Rep.* 2015;33(5):2575-82.
154. Jia Y, Ye L, Ji K, Zhang L, Hargest R, Ji J, et al. Death-associated protein-3, DAP-3, correlates with preoperative chemotherapy effectiveness and prognosis of gastric cancer patients following perioperative chemotherapy and radical gastrectomy. *Br J Cancer.* 2014;110(2):421-9.
155. Sauvage F, Messaoudi S, Fattal E, Barratt G, Vergnaud-Gauduchon J. Heat shock proteins and cancer: How can nanomedicine be harnessed? *J Control Release.* 2017;248:133-43.
156. Hartl FU, Hayer-Hartl M. Molecular chaperones in the cytosol: from nascent chain to folded protein. *Science.* 2002;295(5561):1852-8.
157. Schmitt E, Gehrman M, Brunet M, Multhoff G, Garrido C. Intracellular and extracellular functions of heat shock proteins: repercussions in cancer therapy. *J Leukoc Biol.* 2007;81(1):15-27.
158. <https://www.picard.ch/downloads/Hsp90interactors.pdf>.

159. Li L, Wang L, You QD, Xu XL. Heat Shock Protein 90 Inhibitors: An Update on Achievements, Challenges, and Future Directions. *J Med Chem*. 2020;63(5):1798-822.
160. Zhang M, Wang D, Li P, Sun C, Xu R, Geng Z, et al. Interaction of Hsp90 with phospholipid model membranes. *Biochim Biophys Acta Biomembr*. 2018;1860(2):611-6.
161. Nagaraju GP, Mezina A, Shaib WL, Landry J, El-Rayes BF. Targeting the Janus-activated kinase-2-STAT3 signalling pathway in pancreatic cancer using the HSP90 inhibitor ganetespib. *Eur J Cancer*. 2016;52:109-19.
162. Szyller J, Bil-Lula I. Heat Shock Proteins in Oxidative Stress and Ischemia/Reperfusion Injury and Benefits from Physical Exercises: A Review to the Current Knowledge. *Oxid Med Cell Longev*. 2021;2021:6678457.
163. Loh CY, Arya A, Naema AF, Wong WF, Sethi G, Looi CY. Signal Transducer and Activator of Transcription (STATs) Proteins in Cancer and Inflammation: Functions and Therapeutic Implication. *Front Oncol*. 2019;9:48.
164. Xu Q, Tu J, Dou C, Zhang J, Yang L, Liu X, et al. HSP90 promotes cell glycolysis, proliferation and inhibits apoptosis by regulating PKM2 abundance via Thr-328 phosphorylation in hepatocellular carcinoma. *Mol Cancer*. 2017;16(1):178.
165. Giulino-Roth L, van Besien HJ, Dalton T, Totonchy JE, Rodina A, Taldone T, et al. Inhibition of Hsp90 Suppresses PI3K/AKT/mTOR Signaling and Has Antitumor Activity in Burkitt Lymphoma. *Mol Cancer Ther*. 2017;16(9):1779-90.
166. Hsieh CC, Shen CH. The Potential of Targeting P53 and HSP90 Overcoming Acquired MAPKi-Resistant Melanoma. *Curr Treat Options Oncol*. 2019;20(3):22.
167. Hall JA, Seedarala S, Zhao H, Garg G, Ghosh S, Blagg BS. Novobiocin Analogues That Inhibit the MAPK Pathway. *J Med Chem*. 2016;59(3):925-33.

168. Microarray KA.
http://www.kinexus.ca/ourServices/microarrays/antibody_microarrays/antibody_microarrays.html.
169. Jia Y, Ye L, Ji K, Toms AM, Davies ML, Ruge F, et al. Death associated protein 1 is correlated with the clinical outcome of patients with colorectal cancer and has a role in the regulation of cell death. *Oncol Rep*. 2014;31(1):175-82.
170. Weinstein JN, Collisson EA, Mills GB, Shaw KR, Ozenberger BA, Ellrott K, et al. The Cancer Genome Atlas Pan-Cancer analysis project. *Nat Genet*. 2013;45(10):1113-20.
171. Xiao L, Xian H, Lee KY, Xiao B, Wang H, Yu F, et al. Death-associated Protein 3 Regulates Mitochondrial-encoded Protein Synthesis and Mitochondrial Dynamics. *J Biol Chem*. 2015;290(41):24961-74.
172. Kim HR, Chae HJ, Thomas M, Miyazaki T, Monosov A, Monosov E, et al. Mammalian dap3 is an essential gene required for mitochondrial homeostasis in vivo and contributing to the extrinsic pathway for apoptosis. *Faseb j*. 2007;21(1):188-96.
173. Jia Y, Li Z, Cheng X, Wu X, Pang F, Shi J, et al. Depletion of death-associated protein-3 induces chemoresistance in gastric cancer cells through the β -catenin/LGR5/Bcl-2 axis. *J Investig Med*. 2019;67(5):856-61.
174. Miyata Y, Nakamoto H, Neckers L. The therapeutic target Hsp90 and cancer hallmarks. *Curr Pharm Des*. 2013;19(3):347-65.
175. Pillai RN, Fennell DA, Kovcin V, Ciuleanu TE, Ramlau R, Kowalski D, et al. Randomized Phase III Study of Ganetespib, a Heat Shock Protein 90 Inhibitor, With Docetaxel Versus Docetaxel in Advanced Non-Small-Cell Lung Cancer (GALAXY-2). *J Clin Oncol*. 2020;38(6):613-22.
176. Slovin S, Hussain S, Saad F, Garcia J, Picus J, Ferraldeschi R, et al. Pharmacodynamic and Clinical Results from a Phase I/II Study of the HSP90

Inhibitor Onalespib in Combination with Abiraterone Acetate in Prostate Cancer. Clin Cancer Res. 2019;25(15):4624-33.

177. Doi T, Kurokawa Y, Sawaki A, Komatsu Y, Ozaka M, Takahashi T, et al. Efficacy and safety of TAS-116, an oral inhibitor of heat shock protein 90, in patients with metastatic or unresectable gastrointestinal stromal tumour refractory to imatinib, sunitinib and regorafenib: a phase II, single-arm trial. Eur J Cancer. 2019;121:29-39.

178. Shah S, Luke JJ, Jacene HA, Chen T, Giobbie-Hurder A, Ibrahim N, et al. Results from phase II trial of HSP90 inhibitor, STA-9090 (ganetespib), in metastatic uveal melanoma. Melanoma Res. 2018;28(6):605-10.

179. Renouf DJ, Hedley D, Krzyzanowska MK, Schmuck M, Wang L, Moore MJ. A phase II study of the HSP90 inhibitor AUY922 in chemotherapy refractory advanced pancreatic cancer. Cancer Chemother Pharmacol. 2016;78(3):541-5.

180. Cavenagh J, Oakervee H, Baetiong-Caguioa P, Davies F, Gharibo M, Rabin N, et al. A phase I/II study of KW-2478, an Hsp90 inhibitor, in combination with bortezomib in patients with relapsed/refractory multiple myeloma. Br J Cancer. 2017;117(9):1295-302.

181. Jhaveri K, Wang R, Teplinsky E, Chandarlapaty S, Solit D, Cadoo K, et al. A phase I trial of ganetespib in combination with paclitaxel and trastuzumab in patients with human epidermal growth factor receptor-2 (HER2)-positive metastatic breast cancer. Breast Cancer Res. 2017;19(1):89.

182. Kong A, Rea D, Ahmed S, Beck JT, López López R, Biganzoli L, et al. Phase 1B/2 study of the HSP90 inhibitor AUY922 plus trastuzumab in metastatic HER2-positive breast cancer patients who have progressed on trastuzumab-based regimen. Oncotarget. 2016;7(25):37680-92.

183. Hulkko SM, Wakui H, Zilliacus J. The pro-apoptotic protein death-associated protein 3 (DAP3) interacts with the glucocorticoid receptor and affects the receptor function. Biochem J. 2000;349 Pt 3(Pt 3):885-93.

184. Tang T, Zheng B, Chen SH, Murphy AN, Kudlicka K, Zhou H, et al. hNOA1 interacts with complex I and DAP3 and regulates mitochondrial respiration and apoptosis. *J Biol Chem*. 2009;284(8):5414-24.
185. Hanahan D, Weinberg RA. Hallmarks of cancer: the next generation. *Cell*. 2011;144(5):646-74.
186. Oh YJ, Park SY, Seo YH. The targeted inhibition of Hsp90 by a synthetic small molecule, DPide offers an effective treatment strategy against TNBCs. *Oncol Rep*. 2018;39(4):1775-82.
187. Liu K, Chen J, Yang F, Zhou Z, Liu Y, Guo Y, et al. BJ-B11, an Hsp90 Inhibitor, Constrains the Proliferation and Invasion of Breast Cancer Cells. *Front Oncol*. 2019;9:1447.
188. Zhao Q, Wu CZ, Lee JK, Zhao SR, Li HM, Huo Q, et al. Anticancer effects of the Hsp90 inhibitor 17-demethoxy-reblastatin in human breast cancer MDA-MB-231 cells. *J Microbiol Biotechnol*. 2014;24(7):914-20.
189. Li H, Nie L, Huo Q, Zhao S, Ma T, Wu C, et al. [Effect of anacardic acid, a Hsp90 inhibitor, on proliferation, invasion and migration of breast cancer MDA-MB-231 cells]. *Nan Fang Yi Ke Da Xue Xue Bao*. 2015;35(3):355-9.
190. Koren J, 3rd, Blagg BSJ. The Right Tool for the Job: An Overview of Hsp90 Inhibitors. *Adv Exp Med Biol*. 2020;1243:135-46.
191. Woodford MR, Dunn D, Miller JB, Jamal S, Neckers L, Mollapour M. Impact of Posttranslational Modifications on the Anticancer Activity of Hsp90 Inhibitors. *Adv Cancer Res*. 2016;129:31-50.
192. Pazdur R, Kudelka AP, Kavanagh JJ, Cohen PR, Raber MN. The taxoids: paclitaxel (Taxol) and docetaxel (Taxotere). *Cancer Treat Rev*. 1993;19(4):351-86.
193. Crown J, O'Leary M, Ooi WS. Docetaxel and paclitaxel in the treatment of breast cancer: a review of clinical experience. *Oncologist*. 2004;9 Suppl 2:24-32.

194. Martins-Teixeira MB, Carvalho I. Antitumour Anthracyclines: Progress and Perspectives. *ChemMedChem*. 2020;15(11):933-48.
195. Yu KD, Ye FG, He M, Fan L, Ma D, Mo M, et al. Effect of Adjuvant Paclitaxel and Carboplatin on Survival in Women With Triple-Negative Breast Cancer: A Phase 3 Randomized Clinical Trial. *JAMA Oncol*. 2020;6(9):1390-6.
196. Gianni L, Mansutti M, Anton A, Calvo L, Bisagni G, Bermejo B, et al. Comparing Neoadjuvant Nab-paclitaxel vs Paclitaxel Both Followed by Anthracycline Regimens in Women With ERBB2/HER2-Negative Breast Cancer-The Evaluating Treatment With Neoadjuvant Abraxane (ETNA) Trial: A Randomized Phase 3 Clinical Trial. *JAMA Oncol*. 2018;4(3):302-8.
197. van Ramshorst MS, van der Voort A, van Werkhoven ED, Mandjes IA, Kemper I, Dezentjé VO, et al. Neoadjuvant chemotherapy with or without anthracyclines in the presence of dual HER2 blockade for HER2-positive breast cancer (TRAIN-2): a multicentre, open-label, randomised, phase 3 trial. *Lancet Oncol*. 2018;19(12):1630-40.
198. Jasra S, Anampa J. Anthracycline Use for Early Stage Breast Cancer in the Modern Era: a Review. *Curr Treat Options Oncol*. 2018;19(6):30.
199. Willson ML, Burke L, Ferguson T, Gherzi D, Nowak AK, Wilcken N. Taxanes for adjuvant treatment of early breast cancer. *Cochrane Database Syst Rev*. 2019;9(9):Cd004421.
200. Nedeljković M, Damjanović A. Mechanisms of Chemotherapy Resistance in Triple-Negative Breast Cancer-How We Can Rise to the Challenge. *Cells*. 2019;8(9):957.
201. Bardia A, Parton M, Kümmel S, Estévez LG, Huang CS, Cortés J, et al. Paclitaxel With Inhibitor of Apoptosis Antagonist, LCL161, for Localized Triple-Negative Breast Cancer, Prospectively Stratified by Gene Signature in a Biomarker-Driven Neoadjuvant Trial. *J Clin Oncol*. 2018;Jco2017748392.

202. Kim SB, Dent R, Im SA, Espié M, Blau S, Tan AR, et al. Ipatasertib plus paclitaxel versus placebo plus paclitaxel as first-line therapy for metastatic triple-negative breast cancer (LOTUS): a multicentre, randomised, double-blind, placebo-controlled, phase 2 trial. *Lancet Oncol.* 2017;18(10):1360-72.
203. Fekete JT, Győrffy B. ROCplot.org: Validating predictive biomarkers of chemotherapy/hormonal therapy/anti-HER2 therapy using transcriptomic data of 3,104 breast cancer patients. *Int J Cancer.* 2019;145(11):3140-51.
204. Zeng Y, Qin T, Flamini V, Tan C, Zhang X, Cong Y, et al. Identification of DHX36 as a tumour suppressor through modulating the activities of the stress-associated proteins and cyclin-dependent kinases in breast cancer. *Am J Cancer Res.* 2020;10(12):4211-33.
205. Liebmman JE, Cook JA, Lipschultz C, Teague D, Fisher J, Mitchell JB. Cytotoxic studies of paclitaxel (Taxol) in human tumour cell lines. *Br J Cancer.* 1993;68(6):1104-9.
206. Dimas DT, Perlepe CD, Sergentanis TN, Misitzis I, Kontzoglou K, Patsouris E, et al. The Prognostic Significance of Hsp70/Hsp90 Expression in Breast Cancer: A Systematic Review and Meta-analysis. *Anticancer Res.* 2018;38(3):1551-62.

ABBREVIATIONS:

5-FU 5-fluorouracil

A

ABC ATP-binding cassette
ABPI Accelerated partial breast irradiation
ACD Accidental cell death
AIs Aromatase inhibitors
AJCC American Joint Committee on Cancer
Akt AKT serine/threonine kinase
AKT/PKB Protein kinase B
AtNOA1 Arabidopsis thaliana nitric oxide-associated protein 1

B

bcl-2 b-cell lymphoma 2 protein
BCSCs Breast cancer stem cells
BVA Bovine serum albumin

C

CDK 4/6 Cyclin-dependent kinases 4/6
CRT Conformal radiation therapy

D

DAP-3 Death Associated Protein 3
DAPK Death associated protein kinase
DCIS Ductal carcinoma in situ
DD Death domain
DELE Death Ligand Signal Enhancer
DEPC Diethylpyrocarbonate
DFS Disease-free survival
DIBH Deep inspiration breath hold
DISC Death Induced Signalling Complex
DLL Delta like ligand
DMEM Dulbecco Modified Eagle Medium
DR Death receptor
Drp1 dynamin-related protein 1

E

ECIS	Electric cell-substrate impedance sensing
EFS	Event-free survival
EGFR	Epidermal growth factor receptor
EIF4G2	Eukaryotic Translation Initiation Factor 4 Gamma 2
ER	Oestrogen receptor
ERBB2 and 4	Erb-B2 Receptor Tyrosine Kinase 2 and 4
Erk1/2	Extracellular-related kinase 1 and 2
ER α	Oestrogen receptor alpha
ER β	Oestrogen receptor beta

F

FADD	Fas associated Death Domain
FAK	Focal Adhesion Kinase
FCS	Foetal calf serum
FISH	Fluorescent in situ hybridisation
FZD	Frizzled

G

G1-3	Grade 1-3
GAPDH	Glyceraldehyde 3-phosphate dehydrogenase
GLI1	Glioma-associated oncogene homolog 1
GRP94	Glucose-regulated protein 94

H

HCC	Hepatocellular carcinoma
HER2	Human epidermal growth factor 2
HH	Hedgehog
hNOA1	human homologue of Arabidopsis thaliana nitric oxide-associated protein 1
HSF1	Heat Shock Transcription Factor 1
HSP	Heat shock protein
HSP90	Heat Shock Protein 90

I

IHC	Immuno-histo-chemistry
IL13	Interleukin 13
IL4	Interleukin 4
IMRT	Intensity-modulated radiation therapy
IPS1	IFN- β promoter stimulator 1

J

JAK	Janus kinase
-----	--------------

K

KD Knock down

M

MAPK Mitogen activated protein kinase
MEK MAPK/ERK kinase
mTOR mammalian target of rapamycin

N

NECD Notch receptor extracellular domain
NF- κ B Nuclear factor kappa - light chain enhancer of activated B cells
NICD Notch receptor intracellular domain
NICE National Institute of Clinical Excellence
NPI Nottingham prognostic index

O

OS Overall survival

P

PBI Partial breast irradiation
PCD Programmed cell death
pCR pathologic complete response
PCR Polymerase chain reaction
PD-1 Programmed death 1
PD-L1 Programmed death ligand 1
PI3K Phosphoinositide 3-kinase
PKM2 Pyruvate kinase M2
PR Progesteron receptor
Protein-Kinase, Interferon-Inducible Double Stranded RNA Dependent
PRKRIR Inhibitor, Repressor Of (P58 Repressor)
PTCH1 Patched 1

R

Raf Proto-oncogene serine/threonine-protein kinase
Ras Rat sarcoma

S

SDS-PAGE Sodium dodecyl sulphate polyacrylamide gel electrophoresis
SEM Standard error of the mean
SERMs Selective oestrogen receptor modulators
SIB Simultaneous integrated boost
SMO Smoothened

STAT	Signal transducer and activator of transcription
SUFU	Suppressor of fused

T

TACE	TNF- α converting enzyme
TCGA	The cancer genome atlas
TEMED	Tetramethylethylenediamine
TGF- β	Transforming growth factor beta
TGF- β R	Transforming growth factor beta receptor
TNBC	Triple negative breast cancer
TNM	Tumour, node and metastasis

U

UICC	Union for International Cancer Control
------	--

W

WBI	Whole breast irradiation
WT	Wild type